IMMOBILIZATION OF HEAVY METALS IN SOLIDIFIED/STABILIZED CO-DISPOSED BITUMINOUS COAL FLY ASH AND CONCENTRATED FLUE GAS DESULFURIZATION WASTEWATER

A Dissertation
Presented to
The Academic Faculty

by

Jay Earl Renew

In Partial Fulfillment
of the Requirements for the Degree
Doctor of Philosophy in the
School of Civil and Environmental Engineering

Georgia Institute of Technology
May 2017

IMMOBILIZATION OF HEAVY METALS IN SOLIDIFIED/STABILIZED CO-DISPOSED BITUMINOUS COAL FLY ASH AND CONCENTRATED FLUE GAS DESULFURIZATION WASTEWATER

Approved by:

Dr. Ching-Hua Huang, Advisor
School of Civil and Environmental Engineering
Georgia Institute of Technology

Dr. Yongsheng Chen
School of Civil and Environmental Engineering
Georgia Institute of Technology

Dr. Susan Burns
School of Civil and Environmental Engineering
Georgia Institute of Technology

Dr. Yuanzhi Tang
School of Earth and Atmospheric Sciences
Georgia Institute of Technology

Dr. Sotira Yiacoumi
School of Civil and Environmental Engineering
Georgia Institute of Technology

Date Approved: April 4, 2017

Dedicated to Ashley, Afton, and Ryals.

ACKNOWLEDGEMENTS

I thank Dr. Ching-Hua Huang for her mentorship and guidance through this process. I thank her for giving me the chance to fulfill my dream of obtaining my Ph.D. I thank her for pushing me to excel in research. I thank her invaluable encouragement on this journey that began in the Fall of 2000.

I greatly thank Dr. Mark Berry and Dr. Bob Dahlin for their support and their invaluable encouragement in pursuit of my Ph.D without which I could not have pursued this goal.

I thank Kirk Ellison for his support and guidance in my graduate work.

I thank the Environmental Research and Education Foundation (EREF), Southern Company, and Georgia Power for research funding.

I thank Southern Research for their support and funding to allow me to pursue my Ph.D.

I thank Dr. David Kosson for his assistance and guidance in the modeling of the semi-dynamic tank leaching tests.

I thank Randy and Linda Lucente for their support and assistance with my family during this process.

TABLE OF CONTENTS

LIST OF TABLES

LIST OF FIGURES

LIST OF SYMBOLS AND ABBREVIATIONS

ABMet	Advanced Biological Metals Removal
AFm-Cl	Friedel's salt
AFt-SO_4	Ettringite
ASTM	American Society of Testing and Materials
BCFA	Bituminous coal fly ash
CCP	Coal combustion products
CCR	Coal combustion residuals
CFA	Coal fly ash
CSF	Chemical speciation fingerprint
C-S-H	Calcium silicate hydrate
DSEMF	Dynamic shear enhanced membrane filtration
EIA	Energy Information Administration
ELG	Effluent Limitation Guidelines
FGD	Flue gas desulfurization
FO	Forward osmosis
FS	$FeSO_4$
GE	General Electric
IMT	Intermittent mass transport
L/S	Liquid/solids ratio
L/SA	Liquid/surface area ratio

MCL	Maximum contaminant level
MD	Membrane distillation
MSWI	Municipal solid waste incineration
MVC	Mechanical vapor compression
NF	Nanofiltration
PC	Portland cement
PI	Principal investigator
RO	Reverse osmosis
SIT	Specific ion interaction theory
SCFA	Sub-bituminous coal fly ash
S/S	Solidification/stabilization or solidified/stabilized
TCLP	Toxicity characteristic leaching procedure
TDS	Total dissolved solids
U.S.	United States
USEPA	United States Environmental Protection Agency
XRD	X-ray diffraction
XRF	X-ray fluorescence
ZLD	Zero liquid discharge
ZVI	Zero valent iron

SUMMARY

Changes in the regulatory environment for the coal-fired power industry in the United States have driven the need to improve wastewater treatment and disposal practices, especially for wet flue gas desulfurization (FGD) systems. One option for treatment of FGD wastewater is the implementation of zero liquid discharge (ZLD). ZLD can be achieved through the coupling of brine concentrator or advanced membrane process with a solidification/stabilization (S/S) process. This S/S process could be achieved by co-disposing the concentrated FGD brines with coal fly ash (CFA) and Portland cement (PC).

The results of the study indicate that the proposed process can immobilize many toxic metals. S/S using bituminous CFA (BCFA) achieved good retainment (average 68−90%) of As^{V}, Cd^{II}, Hg^{II} and Se^{IV}, in the toxicity characteristic leaching procedure (TCLP); however, poor retainment was observed for Cr^{VI} and Se^{VI}. Sorption experiments using BCFA S/S solids showed good sorption of As^{V}, Cd^{II}, Hg^{II} and Se^{IV} (average 56−100%), but poor sorption of Cr^{VI} and Se^{VI}. Meanwhile, Cr^{VI} and Se^{VI} retainment could be enhanced by addition of $FeSO_4$ (FS) to the S/S mixture, likely due to the reduction of these metals to lower oxidation states.

Compared to BCFA, S/S using sub-bituminous CFA (SCFA) resulted in higher pH in the S/S solids and final TCLP leachate, which increased the retainment of As^{V}, Cd^{II} and Se^{VI}. Apart from the pH impact on the process, As^{V} retainment was likely improved by the high Ca content of SCFA and Se^{VI} retainment improved by the incorporation of SeO_4^{2-} in Friedel's salt (AFm-Cl) by exchange with Cl^{-}. Friedel's salt was positively identified in the X-ray diffraction (XRD) diffractogram for the SCFA S/S solids, but not for the BCFA S/S

solids. Even so, reduction of Se^{VI} with S/S is likely a better long-term strategy than SeO_4^{2-} substitution in the AFm phase because of higher stability under long-term landfill pH conditions. The main new contribution from this section of the Work to scientific literature is the definition of the different Se immobilization mechanisms in the BCFA S/S solids with FS addition and the SCFA S/S solids.

This work also evaluated the mass transport release of major elements (Ca^{2+}, Cl^-, Mg^{2+}, Na^+, and SO_4^{2-}) and heavy metal oxyanions (As, Cr, and Se) from monoliths of the S/S solids produced by the above described process. This study evaluated the impact of FS addition to the S/S mixture on the long-term leaching behaviors. FS addition to the S/S process decreased the solid's cumulative release and flux at shorter leaching times for the major components: Ca^{2+}, Cl^-, Mg^{2+}, Na^+, and SO_4^{2-}; however, the cumulative release appeared to converge for all five species at longer leaching times. FS addition significantly decreased release of oxyanions As, Cr, and Se. The results indicate that FS addition could increase the likelihood of successful long-term disposal of S/S solids of concentrated FGD brines containing these heavy metal oxyanions. Leach XS^{TM} modeling added additional evidence for the proposed leaching mechanisms for As and Se. The main new contribution from this section of the Work to scientific literature is the evaluation of the impact of a reductant on elemental release during a semi-dynamic tank leaching evaluation.

The coal-fired power industry will also encounter solid waste management challenges from materials that are characteristically unlike traditional CFA. The most challenging materials could contain significant salt concentrations in the form of Ca^{2+}, Mg^{2+}, Na^+, and Cl^- which could potentially enhance metal leaching from BCFA. This work showed that metal leaching from BCFA was enhanced with salt addition, but this effect

varied based on cation type and pH. Cationic metal (Cd^{II}, Cr^{III}, Mn^{II}, Pb^{II}, and Zn^{II}) leaching generally decreased with increasing pH. However, Cd and Zn did demonstrate amphoteric leaching patterns. Except for Pb due to Cl^- complexation, cationic metal leaching at low pH was not impacted by salt addition due to high metal solubility. Cd and Mn leaching was enhanced at medium pH primarily due to Cl^- complexation and Cr leaching increased primarily due to competitive cation exchange. Except for Mn, cationic metals were generally immobile due to low solubility even with salt addition at high pH. Mn leaching increased with $MgCl_2$ addition at high pH due to competitive cation exchange.

The leaching of AsO_4^{3-} was highest at medium pH while SeO_3^{2-} leaching increased with increasing pH. Salt addition did not impact Se leaching at low pH while As leaching increased primarily due to anion exchange with Cl^-. Leaching of both As and Se was increased with salt addition at medium and high pH primarily due to anion exchange with Cl^- (medium pH) and compression of the diffuse double layer (high pH); however, the results were also likely impacted by complexation and sorption with the cations to the CFA surface. A surface complexation model using PHREEQC was established to model As and Cd leaching at medium pH as these elements had the highest leaching increases with salt addition under the medium and high pH conditions which are environmentally relevant for BCFA landfills. The model demonstrated that As and Cd could be modeled utilizing the mechanisms described above. The main new contribution from this section of the Work to scientific literature is the evaluation of the impact of salt on metal leaching from BCFA.

CHAPTER 1. INTRODUCTION

1.1 SCOPE OF THIS WORK

This work evaluates the immobilization of heavy metals in co-disposed flue gas desulfurization (FGD) brines and coal fly ash (CFA) through solidification/stabilization (S/S) with Portland cement (PC). The proposed process is a zero liquid discharge (ZLD) strategy for FGD wastewater that includes the coupling of a brine concentrator or advanced membrane process for wastewater volume reduction followed by downstream S/S to produce a final solid material suitable for landfill disposal.

Metal leaching from the S/S materials was evaluated through batch equilibrium tests including the toxicity characteristic leaching procedure (TCLP) and tests that evaluate metal leaching versus final leachant pH. The impact of $FeSO_4$ (FS) addition to the S/S mixture to reduce Cr^{VI} and Se^{VI} mobility and also form Fe^{III} oxides for enhanced metal sorption was evaluated.

The produced S/S solids were characterized utilizing X-ray diffraction (XRD) and X-ray fluorescence (XRF) analysis. XRD analysis allowed for the elucidation of metal immobilization mechanisms especially for Se through evaluation of the crystalline phases formed.

The S/S solids were also subjected to semi-dynamic tank leaching tests which allowed for leaching to be evaluated for the solids as a monolith thereby taking into account diffusion in addition to solid-liquid partitioning. Based on the results of the semi-dynamic tank leaching tests, modeling by the LeachXS^{TM} model (Seignette et al. 2014) was utilized

to elucidate mechanisms of contaminant immobilization. The model was also used to predict leachate quality from the S/S solid over an extended 20 years period in regards to pH trend and leaching of major components (Ca^{2+}, Cl^{-} and Na^{+}) and toxic metal oxyanions (As^{V} and Se^{VI}).

The impact of salts on metal leaching from CFA was also evaluated, considering that more salts may be sent to industry landfills due to increases of unconventional wastes with high salt content. For instance, the ZLD strategies for FGD wastewater will likely greatly increase salts (in the form of Ca^{2+}, Mg^{2+}, Na^{+}, and Cl^{-}) in the landfill. Unless these materials are disposed of in a separate cell in the landfill and segregated from other waste materials, conventional coal combustion residuals (CCRs) such as CFA in the landfill will be exposed to higher salt concentrations. Significantly increased metal leaching from CFA could result as a consequence of the salt exposure, but the knowledge of such a processes is still lacking. To address the knowledge gap, the impact of exposure to $CaCl_2$, $MgCl_2$, and NaCl at various pH on the leaching of metals from CFA was evaluated using batch equilibrium tests. Leaching under the high salt conditions was modeled utilizing PHREEQC (Parkhurst et al. 1999) to assist in elucidating the mechanisms of increased mobilization for the metals (As and Cd) that exhibited the highest increase in leaching upon salt exposure at environmentally relevant conditions for landfill leachate at coal-fired power plants (near neutral and high pH). XRD analysis was conducted to evaluate the CFA before and after the leaching experiment to determine if the crystalline structure of the CFA was impacted.

1.2 OUTLINE OF THESIS

The five chapters of this thesis include a general introduction of the topics followed by three chapters that describe three different specific research focuses and conclusions for the overall work. Chapter 1 provides an overview of FGD wastewater and treatment, ZLD strategies, S/S, CFA, salt impact on metal leaching, leaching procedures, and geochemical modeling.

Chapter 2 assesses heavy metal immobilization in S/S solids produced through mixing simulated concentrated FGD brines with CFA, PC, and FS. Heavy metal (As, Cd, Cr, Hg, and Se) leaching was evaluated utilizing batch equilibrium leaching experiments including the TCLP (USEPA 1992a) and the USEPA Method 1313 (USEPA 2012). The produced S/S solids were also characterized utilizing XRD and XRF to determine the most likely Se immobilization phases.

Chapter 3 evaluates leaching from the solids as monoliths utilizing the USEPA Method 1315 (USEPA 2013). Semi-dynamic tank leaching tests were utilized to evaluate the mass transport releases of Ca^{2+}, Cl^{-}, Mg^{2+}, Na^{+}, As, Cr, and Se. The impact of FS addition to the S/S mixture on contaminant release was evaluated through these leaching tests. Modeling utilizing LeachXS^{TM} was conducted to enhance understanding of the release mechanisms for Ca^{2+}, Cl^{-}, Na^{+}, As and Se and to predict the leachate composition over 20 years.

Chapter 4 evaluates the impact of salts on the leaching of metals from bituminous CFA (BCFA). The USEPA Method 1313 (USEPA 2012) was utilized to evaluate metal leaching with modifications through the addition of $CaCl_2$, $MgCl_2$, or NaCl to the leachant.

The leaching evaluations for As and Cd were also modeled utilizing PHREEQC in the high salt environment.

Chapter 5 provides the overall conclusions from the work. The Chapter also provides recommendations for future research directions on the topic.

1.3 FLUE GAS DESULFURIZATION WASTEWATER

Wastewater disposal from wet FGD systems is a major concern for the coal-fired power industry. The USEPA determined that most of the high metal concentrations involved in waste from coal-fired power plants occur in FGD systems and hydraulic CFA transportation systems (USEPA 2009). Ca or Ca-Mg slurries are sprayed against the flue gas in wet FGD systems in order to remove SO_x. However, in addition to SO_x removal, heavy metals also partition from the gas phase (flue gas) to the aqueous phase and accumulate in FGD slurry (Huang et al. 2013a). FGD wastewater contains significant heavy metal (As, Cd, Cr, Hg, and Se) content and large salt (Ca^{2+}, Mg^{2+}, Na^{+}, SO_4^{2-}, and Cl^{-}) content (USEPA 2009).

FGD Modes of Operation. FGD scrubbers can operate in the modes of forced-oxidation, natural-oxidation, or inhibited-oxidation (Blythe et al. 2008, USEPA 2009). Figure 1.1 (USEPA 2009) shows a schematic for a forced-oxidation wet FGD system. Forced-oxidation FGDs are currently the more common type and the USEPA has stated their expectation that most new FGD systems will be forced-oxidation systems (USEPA 2009). In a forced-oxidation system (Figure 1.1), air is pumped through the FGD slurry in order to oxidize SO_3^{2-} to SO_4^{2-} which can then precipitate as $CaSO_4 \cdot 2H_2O$ (gypsum), a

beneficially utilized material that is incorporated in wallboard or utilized in agriculture (Blythe et al. 2008).

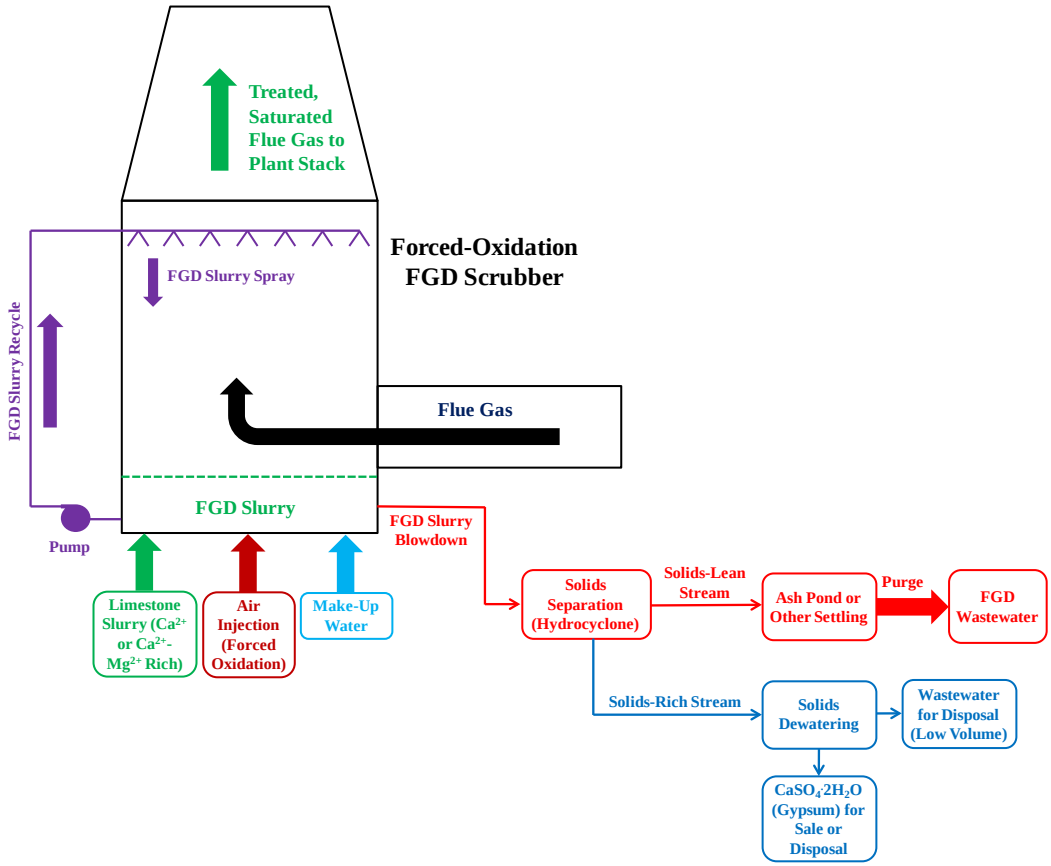

Figure 1.1. Schematic of a forced-oxidation FGD system (USEPA 2009).

Gypsum production is the major benefit of forced-oxidation FGD systems. Beneficial use of gypsum provides a revenue stream for the industry and also reduces waste disposal costs. However, one negative aspect of the forced-oxidation strategy is that Cr and Se can also be oxidized to their more mobile and toxic forms (Cr^{VI} and Se^{VI}) along with SO_3^{2-}, leading to more challenging FGD wastewater treatment problems. This work focuses particularly on the wastewater issues associated with forced-oxidation FGD systems.

In the less common inhibited-oxidation FGD systems, SO_3^{2-} is prevented from oxidizing through reductant addition (Blythe et al. 2008). These inhibited-oxidation FGD

systems produce an FGD sludge as the final product (Blythe et al. 2008). The produced sludge is usually mixed CFA and CaO or $Ca(OH)_2$ to form a solidified pozzolanic material that is landfill disposed (Blythe et al. 2008). Negative aspects of this process are (1) lack of beneficial use for the residual, (2) management of the wet FGD sludge, (3) all of the FGD sludge must be disposed of, and (4) cost of the solidification process. However, the process has a large benefit in that the process does not oxidize SO_3^{2-} and therefore does not likely generate Se and Cr in their more mobile and toxic states.

Bituminous versus Sub-bituminous FGD systems. Significant differences exist between the FGD wastewater from bituminous and sub-bituminous coal-fired power plants. In the U.S., total sulfur contents of 2.7% and 0.7% were reported by Edgar for bituminous coal and sub-bituminous coal, respectively (Edgar 1983). The USEPA has noted that the combustion of higher sulfur coals logically produces more SO_3 in the flue gas that FGD systems must remove which results in higher FGD blowdown volumes to be treated (USEPA 2009). As a result, a larger mass of salt and metals must be disposed from a bituminous coal power plant FGD system compared to a sub-bituminous power plant. Approximately 48% of the coal produced in the U.S. is bituminous and 44% is sub-bituminous, with 93% of the total coal produced utilized for energy production (USEIA 2015b).

FGD Wastewater Composition. Table 1.1 (USEPA 2009) demonstrates the complexity of FGD wastewaters. These example compositions are from four different FGD wastewater sources as part of a self-reporting study conducted by the USEPA (USEPA 2009); however, the Ca^{2+} value was obtained from a different source as one was not provided by the USEPA report (Chapman et al. 2007). FGD wastewater typically contains

high total dissolved solids (TDS) content. With regards to anions, the FGD wastewater is dominated by Cl^- with a significant amount of SO_4^{2-} present. Ca^{2+} and Mg^{2+} are dominant cations in the wastewater followed by Na^+. FGD wastewater also can contain significant concentrations of heavy metals including As, Cd, Cr, Hg, and Se as shown in Table 1.1.

Logically, concentrated FGD wastewater (from evaporator or advanced membrane process) will contain higher salt concentrations (e.g. Ca^{2+}, Mg^{2+}, Cl^-, etc.). The element concentrations shown in Table 1.1 could be increased by a factor of 10 to 15 after the concentration step. The final TDS could increase to an approximate range of 100,000-300,000 mg/L. Most of the SO_4^{2-} will likely be removed during the concentration step, through precipitation as $CaSO_4 \cdot 2H_2O$. Hence, the dominant anion in the concentrated FGD brine will still be Cl^-.

Heavy Metals. Presence of heavy metals in FGD wastewater is a concern because these elements are toxic and can result in negative environmental impacts upon release (USEPA 2009). Exposure to As, which is bioaccumulative, poses the following potential negative impacts: (1) human liver problems, (2) increased bladder cancer risk, and (3) deformities in fish development (USEPA 2009). Hg is known to be bioaccumulative and "human exposure at levels above the MCL for relatively short periods of time can result in kidney damage" (USEPA 2009). Of the heavy metals, Se, which is bioaccumulative, has the narrowest difference (360 µg/day) between acute toxicity in humans (400 µg/day) and human dietary requirement (40 µg/day) (USEPA 2009, Winkel 2012). Extended exposure for humans can "result in damage to the kidney, liver, and nervous and circulatory systems" (USEPA 2009).

Table 1.1. FGD wastewater compositions from four different sources (USEPA 2009).

Metal	Min. Conc. (µg/L)	Max. Conc. (µg/L)
Al	8,200	333,000
Sb	4.1	23
As	58	5,070
Ba	110	2,050
B	7,410	250,000
Ca[1]	Typical Conc. ~ 5,000,000	
Cd	ND (0.5)	302
Cr	1.7	350
Co	6.4	148
Cu	12.8	456
Fe	1,100	300,000
Pb	14.7	252
Mg	1,200,000	1,800,000
Mn	339	5,460
Hg	ND (0.1)	872
Mo	ND (2)	250
Ni	23.4	710
Se	400	21,700
Zn	33.1	1,060

Component	Min. Conc. (mg/L)	Max. Conc. (mg/L)
TDS	6,500	26,000
SO_4	780	4,100
Cl	1,100	13,000
Br	43	96
NO_3/NO_2	ND (10.0)	270

[1] – This value was obtained from (Chapman et al. 2007) outside of the USEPA study.

Se can be harmful to both birds and animals as exposure to high concentration of Se has been shown to be detrimental to bird egg hatching (Coefield 2009). The toxicity of Se was demonstrated in a famous Se contamination event occurred in the Kesterson Wildlife Refuge in California in the 1980s when a significant number of birds and fish died due to Se exposure from water (Coefield 2009).

Salts. Discharge of high TDS wastewaters can have negative environmental impacts including, but not limited to: osmotic imbalances, impacted cellular biochemistry of fish and macroinvertebrates, decreased ecosystem biodiversity, hypoxic salt layering within a lake, and increased metal leaching from sediments (Boelter 1992, Langen 2006, Nelson et al. 2009, Novotny 2010). In the past decade, state discharge limitations were implemented in Pennsylvania likely because of the activities of the upstream oil and gas industry (PSU 2009, Entrekin et al. 2011). A very high TDS level for a fresh surface water, 925 mg/L, was observed in the Monongahela River (Pennsylvania) in 2008 and this high TDS level was likely due to brine disposal associated with the upstream oil and gas industry (PSU 2009, Kargbo 2010). As a result of this high TDS level in the Monogahela River, a significant number of drinking water treatment plants (13) exceeded their secondary maximum secondary maximum contaminant levels (MCLs) for Cl^- (PSU 2009). The natural gas industry had to reconsider disposal options for their brines and the industry moved toward deep-well injection (depending on availability) or S/S followed by landfill disposal.

Potential for Water Reuse. FGD wastewater represents a potential source for water reclamation. It is well known that water scarcity and competition for water resources have become a significant issue for the thermoelectric power industry. Increased competition for freshwater sources is driven by (1) population growth, (2) increasing thermoelectric power demand, and (3) droughts and water shortages (Sovacool et al. 2009).

The United States Geological Survey (USGS) estimated that the thermoelectric power industry is responsible for approximately 39% of freshwater withdrawals in the U.S.; however, the USGS estimated that the industry is responsible for just 3% of US water

consumption (USGS 1998, USGS 2004). Much of the freshwater withdrawn passes through power plant cooling systems and is discharged back to surface water. The agriculture, mining, and manufacturing industries are beginning to compete with the thermoelectric power industry for limited water sites and water scarcity is beginning to impact thermoelectric power plant site selection in the US (USDOE 2006, Feeley Iii et al. 2008, Hightower et al. 2008, Koch et al. 2009, NETL 2009, Sovacool et al. 2009, Carter 2010, Fthenakis et al. 2010, Chandel et al. 2011, Macknick et al. 2012, Scanlon et al. 2013, USDOE 2013, Spang et al. 2014, USDOE 2014).

Sovacool et al. made predictions for projected population growth versus electrical demand in 2009 (Sovacool et al. 2009). Based on more recent data projections than Sovacool et al., the U.S. Census Bureau has estimated that U.S. population will increase significantly from 2015 (321 million) to 2030 (359 million) (USCB 2014). During a similar period, the U.S. Energy Information Administration (EIA) projects that electricity use will increase significantly from 2013 (3,836 billion kilowatt-hours) to 2040 (4,797 kilowatt-hours) (USEIA 2015a).

Increases in water demand from the thermoelectric power industry over the same period is difficult to estimate as it will depend on the thermoelectric power industries' (1) fuel mix (nuclear, coal-fired, concentrated solar, or natural gas), (2) cooling water technologies (wet, dry, or hybrid wet-dry), (3) water recovery efforts, and (4) power plant operational conditions.

At the same time that thermoelectric water demands and water scarcity is increasing, surface water storage capacity in the US has not grown significantly largely

due to negative environmental impacts associated with water reservoir construction (Hightower et al. 2008). All of the factors discussed above, work to make the thermoelectric power industry more vulnerable to water shortages and opposition to new power plant siting in water scarce areas. Any technology or strategy that enhances water reuse such as ZLD in power plants will be beneficial for the industry.

1.4 FLUE GAS DESUFURIZATION WASTEWATER TREATMENT

The USEPA recently released the proposed final revision to the Steam Electric Power Effluent Limitation Guidelines (ELG) which regulate FGD wastewater (USEPA 2015). The revised guidelines include strict discharge limits for existing FGD wastewater sources with maximum 30-day average limits of 8 µg/L, 356 ng/L, and 12 µg/L for As, Hg, and Se, respectively (USEPA 2015). Two potential pathways exist for FGD wastewater management - wastewater treatment and ZLD. Figure 1.2 shows a comparison of the two disposal pathways under the proposed revision to the ELG guidelines.

Proposed FGD wastewater treatment technologies include chemical precipitation coupled with reduction through biological or zero valent iron (ZVI) treatment. For purposes of the revised ELG, the USEPA defines the chemical precipitation process as "alkali-sulfide process including multi-stage chemical injections to achieve hydroxide precipitation, iron co-precipitation, and sulfide precipitation" (Layman 2013).

A hybrid-ZVI process successfully treated FGD wastewater for removal of As, Hg, Se^{IV}, and Se^{VI} (Huang et al. 2013a, Huang et al. 2013b). The solid residuals produced by this process, which were a thick Fe oxide based slurry, only failed the TCLP in a few instances for Cd (Huang et al. 2013b).

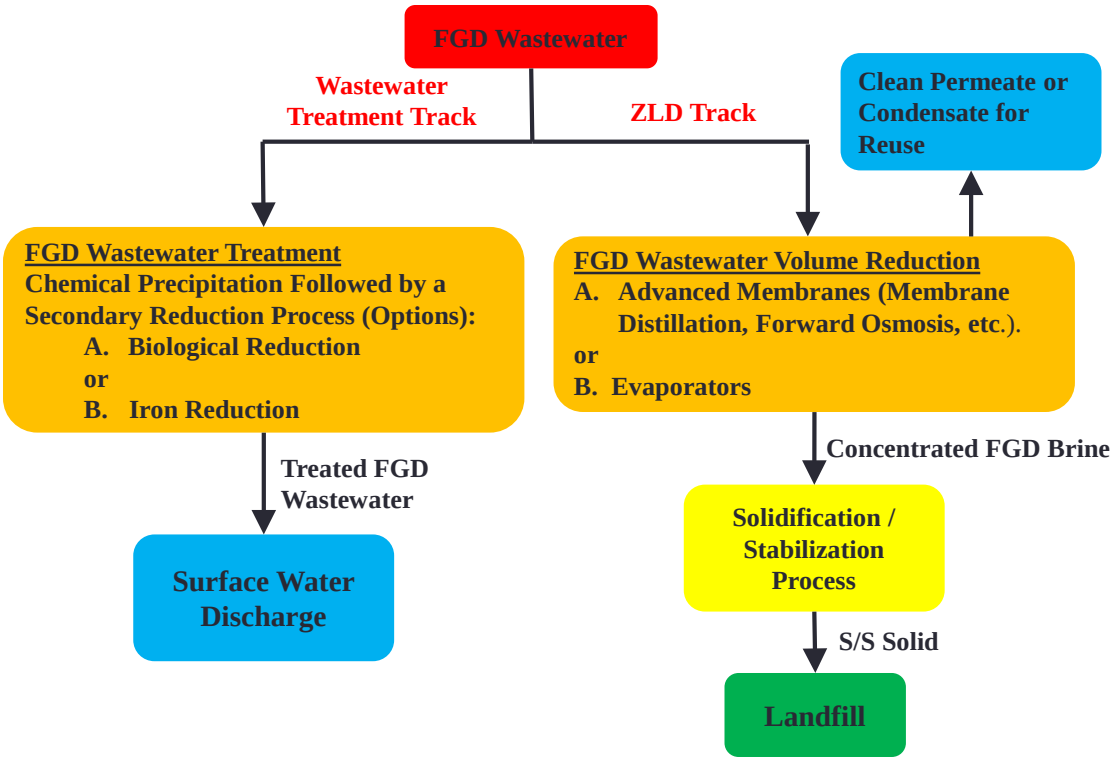

Figure 1.2. Disposal pathway comparison for FGD wastewater.

Biological reductive treatment processes such as General Electric's (GE) Advanced Biological Metals Removal (ABMet) successfully treated FGD wastewater for NO_3^{2-}, Se^{IV}, and Se^{VI} removal (Santos et al. 2015). Biological treatment processes are known to be relatively inexpensive methods to reduce Se^{IV} and Se^{VI} to Se^0 (Santos et al. 2015). Elemental Se produced by these biological processes is typically a small precipitate that is non-toxic and easily removed through filtration (Santos et al. 2015).

As shown in Figure 1.2, FGD wastewater treated through biological or ZVI processes would be discharged to surface water after treatment. Neither of these processes remove salts. Hence, high TDS waters will be discharged to the environment resulting in negative environmental impacts. In addition, these technologies do not offer the opportunity to reclaim water.

One of the major uncertainties regarding these two technologies (ZVI and biological reduction) is reliable performance under varied FGD wastewater conditions. FGD wastewater composition varies significantly by coal fuel type, water source, and facility operations. Regarding facility operations, a utility company may increase the cycles of concentration to their FGD systems to conserve water, subsequently increasing Cl^- concentrations up to potentially 40,000 mg/L. Doubt exists on whether these two FGD wastewater technologies will perform consistently under varied conditions.

1.5 ZERO LIQUID DISCHARGE STRATEGIES

Figure 1.2 shows the ZLD pathway for FGD wastewater. This pathway has gained interest in the coal-fired power industry due to reliability in meeting the new ELG limits, elimination of an environmental wastewater discharge, and maximization of water reuse in power plants. Tong et al. noted that the appeal (on an environmental basis) of ZLD is the balance between water efficiency (limiting freshwater utilization) and protection of aquatic environments from discharge of pollutants due to elimination of wastewater disharge (Tong et al. 2016). Industries other than the coal-fired power industry are interested in ZLD and Tong et al. noted that global investment in ZLD technologies is currently approximately $100 M-$200 M (Tong et al. 2016).

It is noted ZLD strategies for FGD wastewater do also pose long-term environmental risks for pollutant release to the environment (Tong et al. 2016). Solids stored in landfills can leach both metals and salts thereby negatively impacting the environment. A chance also exists of a large contaminant (heavy metals and salts) release during a period of inclement weather with heavy precipitation. This risk of a large

contaminant release does not exist on the same level of magnitude for the FGD wastewater treatment track. The ZLD process moves the disposal issue from a wastewater treatment problem to a long-term landfill disposal issue.

As shown in Figure 1.2, the likely first step of any ZLD process is volume reduction. FGD wastewater has a high scaling potential due to high Ca^{2+} and SO_4^{2-} content, as a result there are only a few volume reduction technologies that appear to be applicable for the proposed ZLD strategy. These volume reduction technologies include evaporators or advanced membrane processes such as dynamic shear enhanced membrane filtration (DSEMF), forward osmosis (FO), and membrane distillation (MD). All of these technologies are resistant to fouling and could potentially concentrate FGD wastewater to a level that make ZLD feasible.

Dynamic Shear Enhanced Membrane Filtration. DSEMF systems force the creation of strong shear forces at the membrane surface which decreases fouling potential (Luo et al. 2012, Luo et al. 2013). Several methods exist to create this "high shear rate on the membrane by using a rotating disk, or by rotating or vibrating the membranes" (Luo et al. 2013). As a result of these dynamic processes, the shear rate is not dependent on the feed rate to the membrane (Jaffrin 2008, Luo et al. 2013).

The high shear forces at the membrane surface decrease fouling due to particle deposition and allows for higher permeate fluxes to be maintained (Belfort et al. 1994, Luo et al. 2012, Luo et al. 2013). Through decreasing the accumulation of rejected solutes at the membrane surface, the concentration gradient is decreased between the membrane surface and bulk solution (Jaffrin 2008).

Several DSEMF technologies have reached commercial status including "DYNO filter (BOKELA), OptiFilter CR (Metso Paper), Rotary Membrane System (Spin TeK), single shaft disk filter (SSDF, Novoflow), vibratory shear-enhanced process (VSEP, New logic Research, Inc.), FMX vortex generating module (BKT Co. Ltd.)" (Luo et al. 2013). The VSEP system, which utilizes dynamic shear enhanced reverse osmosis (RO) for concentration, has been shown to successfully concentrate FGD wastewater on the pilot- and full-scale (Pakzadeh et al. 2014, Renew et al. 2016a). The BKT system, which utilizes dynamic shear enhanced nanofiltration (NF) combined with downstream conventional spiral wound RO, has been demonstrated to concentrate FGD wastewater on the pilot-scale (Pakzadeh et al. 2014).

DSEMF technologies cannot concentrate FGD wastewater to the same TDS level of evaporators, FO, and MD. However, the technology could concentrate the wastewater to a lower final brine TDS level, perhaps 50,000-80,000 mg/L. In addition, the technology could serve a pre-concentration step for evaporators, FO, or MD.

Evaporators. The utilization of thermal technologies such as evaporators and brine concentrators has a long history in utilization in ZLD strategies (Tong et al. 2016). ZLD has typically incorporated mechanical vapor compression (MVC) evaporators (Tong et al. 2016). Evaporators are energy intensive as Tong and Elimelech have noted energy consumption in the range of 20 to 39 kWh_e/m^3 (feedwater volume) (Tong et al. 2016). Evaporators could be utilized to concentrate FGD wastewater up to a very high level, perhaps 300,000 mg/L TDS.

Forward Osmosis. FO is a technology of interest for FGD wastewater concentration. The FO process is driven by a gradient of osmotic pressure between a hyper-saline solution and a wastewater separated by a membrane that is semi-permeable (Phillip 2010, Pérez-González et al. 2012, Hickenbottom et al. 2013, Shaffer et al. 2015). Some of the hyper-saline solutions (also known as draw solutions) that have been utilized for FO include "sulphur dioxide, aluminium sulfate, fructose, ammonium bicarbonate, etc." (Pérez-González et al. 2012). FO is known to be resistant to fouling that cannot be reversed that has been associated with high pressure processes such as RO (Mi et al. 2013, Tong et al. 2016). One of the negatives of FO is that the freshwater production requires draw solution regeneration (Hickenbottom et al. 2013, Stone et al. 2013). Regeneration of the draw solution requires RO or distillation which can be a costly processes (Hickenbottom et al. 2013, Stone et al. 2013). When distillation is utilized, the draw solution typically has a low boiling point to minimize energy use for solution recovery.

Oasys Water, an FO manufacturer, has one full-scale application in Zhejiang Province, China (2016). This installation includes complete softening followed by pre-concentration with RO and subsequent brine concentration with the FO unit (2016). The system concentrates FGD wastewater from "approximately 60,000 mg/L in the RO concentrate to 220,000 mg/L or higher" in the FO (2016). It should be noted that this system requires complete softening which is expensive for both chemical use and solids management. Most utilities want to avoid complete pre-softening to avoid these costs and introduction of complexity to the process.

FO has been successful in treating wastewaters other than FGD wastewater with high TDS content. In one study, a pilot FO unit successfully concentrated a produced water

(TDS = 73,000 ± 4,200 mg/L) from the oil and gas industry to a concentrated brine (TDS = 180,000 ± 19,000 mg/L) (McGinnis et al. 2013). It should be noted that there is a limit to the salinity of the wastewater for this technology because the TDS of the draw solution must be much higher than the wastewater or the osmotic pressure gradient cannot be maintained (McGinnis et al. 2013). As the difference in the salinity of the draw solution and the wastewater decreases, FO becomes less effective due to the decrease in chemical potential of the draw solution.

Membrane Distillation. MD is a technology of interest for FGD wastewater as a brine concentrator. Vapor pressure difference between a clean permeate and a concentrated brine (separated by a hydrophobic membrane) drive the distillation process (Alkhudhiri et al. 2012). Surface tension (due to pore size) prevents the direct transfer of water across the membrane (Alkhudhiri et al. 2012). Only water vapor crosses the semi-permeable membrane from the concentrated brine to the permeate (Alkhudhiri et al. 2012). The vapor pressure gradient is created through maintaining a temperature difference between the concentrated brine and the permeate (Martinez-Diez 2001, Gryta 2002, El-Bourawi 2006, Sirkar 2009, Camacho L.M. 2013, Gryta 2013). Minimal pressure gradients are required by the MD process unlike RO (El-Bourawi 2006, Gryta 2013). Heat would have to be added for an FGD application because the water cools readily upon discharge from the FGD system.

MD has been utilized to concentrate waters with high TDS contents. For example, in one research study, a NaCl solution was concentrated by MD from 34,000 mg/L to more than 240,000 mg/L (Gryta 2013). The brine was further concentrated to a TDS level of 300,000 mg/L; however a significant degradation in performance was observed (Gryta

2013). The main drawbacks to MD is a slow flux compared to RO (MD is not pressure driven) and variation in concentrate properties such as salinity and temperature can significantly negatively impact the process (Arthur 2005, Alkhudhiri et al. 2012).

Proposed ZLD Process. The concentrated brines from any of an evaporator or the advanced membrane processes could be S/S through mixing with a pozzolanic agent. The S/S process has a lower energy penalty than crystallization because it relies upon the pozzolanic reactions to consume the water content remaining in a wastewater following the volume reduction process. The S/S process also produces a less hygroscopic solid with better physical properties and enhanced chemical stabilization compared to a crystallized salt.

Figure 1.3 shows a flow diagram for the proposed process for FGD wastewater from a coal-fired power plant that burns bituminous coal and utilizes a forced-oxidation FGD system. The concentrated FGD brine will be mixed with BCFA, PC, and FS. FS is added to enhance immobilization of As, Cr, and Se. The final product is an S/S solid that is suitable for landfill disposal.

1.6 SOLIDIFICATION/STABILIZATION

S/S typically includes the mixing of wastes (liquids, sludges, brines, or solids) with PC, PC/CFA, CaO/CFA, or $Ca(OH)_2$/CFA (Kameswari et al. 2001, Keller 2002, Batchelor 2006, Qian et al. 2006, Singh 2006, Ramgobeen 2010). S/S utilizing PC was developed in the 1950s for stabilizing nuclear waste but the process was eventually expanded further for treating hazardous waste by the 1970s (Batchelor 2006). The process “has been identified

by the USEPA as the best demonstrated available technology for 57 regulated hazardous wastes" (Batchelor 2006).

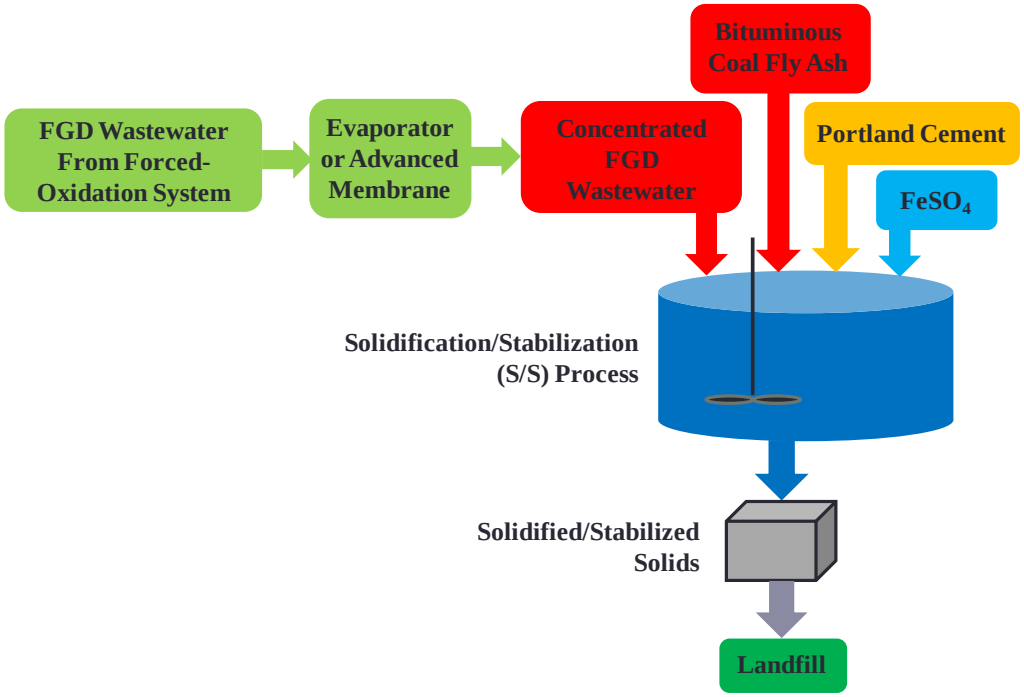

Figure 1.3. Proposed S/S technology.

S/S has been shown to be a viable treatment process for many heavy metal bearing solid wastes (Solem-Tishmack et al. 1995, Akhter et al. 1997, Mangialardi 1999, Kamon et al. 2000, Kameswari et al. 2001, Li et al. 2001, Pereira et al. 2001, Valls et al. 2002, Su et al. 2003, Yilmaz et al. 2003, Terzano et al. 2005, Batchelor 2006, Paria et al. 2006, Qian et al. 2006, Singh 2006, Kumpienem et al. 2007, Mickley 2008, Moon et al. 2009). S/S consists of two processes: solidification (improving physical properties of waste) and stabilization (converting contaminants to less mobile and toxic forms) (Batchelor 2006).

CFA has successfully replaced a portion of PC in several S/S mixture applications (Solem-Tishmack et al. 1995, Singh 1999, Pereira et al. 2001, Su et al. 2003, Terzano et al. 2005, Mahlaba 2006b, Mahlaba 2006a, Singh 2006, Kumpienem et al. 2007, Kaplan

2008, Mahlaba 2011c, Mahlaba 2011b, Mahlaba 2011a). Replacement of a portion of PC with CFA has been shown to increase the effectiveness of S/S mixtures through decreasing the permeability of the produced S/S solid (Connor et al. 1996, Batchelor 2006, Dhir 2006). CFA has been utilized in S/S mixtures to immobilize numerous waste streams which include significant heavy metal content including As, Cd, Cr, Hg, and Se (Solem-Tishmack et al. 1995, Akhter et al. 1997, Connor 1997, Kameswari et al. 2001, Pereira et al. 2001, Singh 2006, Kumpienem 2007). Cement-based S/S has been successfully utilized to treat municipal solid waste incineration (MSWI) fly ash (Lombardi 1998, Mangialardi 1999, Kamon et al. 2000, Keller 2002, Qian et al. 2006).

Solidification. Solidification is important for achieving a successful S/S process. Solidification can increase waste strength and improve microstructure (Batchelor 2006). S/S removes free liquids from waste through pozzolanic reactions and the S/S blocks will have a lower surface area/volume ratio compared to CFA thereby significantly decreasing the surface area exposure to water in the landfill (Batchelor 2006). The produced S/S solid will also be less permeable than other materials such as CFA in the landfill; hence, water is more likely to flow around instead of through the material thereby decreasing leaching potential (Batchelor 2006).

Stabilization. The goal of chemical stabilization is to decrease the mobility and toxicity of contaminants (Batchelor 2006). Contaminants in the dissolved phase are “free to diffuse down a pore to the external environment” (Batchelor 2006). Precipitation and adsorption are two important mechanisms of heavy metal immobilization in S/S (Batchelor 2006). In addition, CFA contains a significant amount of Fe^{III} and Al^{III} oxides which can provide active sites for heavy metal sorption (Cornelis et al. 2008a, Garrabrants 2010).

Oxyanions can also be chemically incorporated into mineral phases such as Friedel's salt or ettringite (Goñi et al. 2001, Baur et al. 2003b, Chrysochoou et al. 2006, Matschei et al. 2007, Wu et al. 2010). pH has a significant impact on all of the above mentioned immobilization mechanisms. Typically S/S solids will have high pH due to the high CaO content.

As^V. As^V can be stabilized in S/S through both precipitation and adsorption. Previous research has shown that Ca-As^V complex precipitation is involved in the As^V immobilization process with $NaCaAsO_4 \cdot 7.5H_2O$ being identified as the most likely dominant controlling phase (Akhter et al. 1997, Nishimura et al. 1998, Bothe Jr et al. 1999, Bothe et al. 1999, Moon et al. 2004, Cornelis et al. 2008a, Moon et al. 2008).

The presence of Fe^{III} in CFA can also could impact As^V immobilization through sorption. The Dzomback and Morel model showed that As^V sorbs readily to hydrous Fe^{III} oxides at a high pH range of cement-based S/S (Cornelis et al. 2008a). Addition of Fe^{II} and Fe^{III} to S/S mixtures has been shown to increase the immobilization of As^V (Miller et al. 2000). Any Fe^{II} added to a S/S mixture is likely readily oxidized to Fe^{III}.

Cd. S/S utilizing PC has been shown to immobilize Cd through precipitation of $Cd(OH)_2$ under high pH conditions (Akhter et al. 1990, Cartiedge et al. 1990). Previous researchers have also noted that $Cd(OH)_2$ may be protected through microencapsulation in a calcium-silicate-hydrate (C-S-H) and/or a $Ca(OH)_2$ matrix (Akhter et al. 1990, Cartiedge et al. 1990).

Cr^{VI}. S/S utilizing PC has been shown in previous research to be effective in immobilizing Cr^{III}, but not Cr^{VI} (Glasser 1997, Wang et al. 2000, Dermatas et al. 2003).

Cr^{III} is less soluble than Cr^{VI} under the high pH conditions of S/S (Richard et al. 1991, Glasser 1997). However, previous researchers have noted that $Cr(OH)_3$ precipitation is likely not the primary mechanism of Cr^{III} immobilization and incorporation of Cr^{III} in the Ca-Al^{III}-hydrate by replacing Al^{III} may be more important (Glasser 1997). Ca-Cr^{III}-hydrates have lower solubility than $Cr(OH)_3$ under S/S conditions (Glasser 1997). The Dzomback and Morel model has also shown that Cr^{III} is sorbs readily to hydrous Fe^{III} oxide under the pH conditions of S/S (Cornelis et al. 2008a).

Obviously, reduction of Cr^{VI} to Cr^{III} could enhance Cr immobilization. Fe^{II} has been shown to reduce Cr^{VI} to Cr^{III} (Dermatas et al. 2003, Su et al. 2005). Addition of FS to S/S mixtures greatly decreased Cr^{VI} leaching in previous research (Dermatas et al. 2003). Once Cr^{VI} is reduced to Cr^{III}, Cr^{III} can be incorporated in to the Ca-Al^{III}-hydrate phase, precipitated as $Cr(OH)_3$ or adsorb to Fe^{III} oxides.

Cr^{VI} has also been noted to be stabilized in certain S/S conditions due anion exchange for SO_4^{2-} in ettringite ($Ca_6Al_2(OH)_{12}(SO_4)_3 \cdot 26H_2O$) (Batchelor 2006). However, ettringite only forms under certain S/S conditions.

Hg. S/S has been shown effective in immobilizing Hg^{II} at concentrations levels below approximately 100 mg/kg which is within the scope of this work (Connor 1997). Previous researchers have noted that Hg^{II} can significantly sorb to Si^{IV} and Al^{III} oxides in CFA (Rio et al. 2003). It has also been noted that Hg^{II} can precipitate as HgO in cement-based S/S (McWhinney et al. 1990). It has also been hypothesized by other researchers that HgO precipitate can be microencapsulated in $CaCO_3$, thereby enhancing immobilization (McWhinney et al. 1990).

Se^{IV} and Se^{VI}. Se behaves differently based on the oxidation state (Se^{IV} versus Se^{VI}) in S/S matrices. The likely dominant immobilization phase for Se^{IV} is $CaSeO_3$ in S/S matrices as Baur and Johnson hypothesized that $CaSeO_3$ controls Se^{IV} solubility in cement materials where Ca^{2+} concentrations are on order of mM (Baur et al. 2003b). Reduction of Se^{VI} to Se^{IV} through the addition of chemical such as FS can enhance immobilization of Se as $CaSeO_3$.

The three most important cement minerals for heavy metal immobilization in S/S are monophase ($Ca_2(Al,Fe)(OH)_6 \cdot X \cdot xH_2O$), ettringite ($Ca_6Al_2(OH)_{12}(SO_4)_3 \cdot 26H_2O$), and C-S-H (Keller 2002). Monophases are denoted by the shorthand AFm-X in cement chemistry where X is an anion and ettringite is denoted by the shorthand AFt-SO_4 (Birnin-Yauri et al. 1998, Renaudina et al. 1999, Goñi et al. 2001, Matschei et al. 2007, Guerrero et al. 2009, Balonis et al. 2010, Wu et al. 2010).

Baur and Johnson studied the sorption of Se^{VI} to the AFm-SO_4, AFt-SO_4, and C-S-H by synthesizing these cement minerals and contacting them with Se^{VI} in aqueous solution (Baur et al. 2003b). Baur and Johnson observed no appreciable Se^{VI} sorption to C-S-H and weak/negligible Se^{VI} sorption to AFt-SO_4 (Rd = 0.03) (Baur et al. 2003b). The researchers did observe strong Se^{VI} sorption to AFm-SO_4 (Rd = 2.06) indicating that cement rich in AFm-SO_4 would likely stabilize Se^{VI} significantly (Baur et al. 2003b). In regards to AFm-Cl, one study demonstrated that AFm-Cl effectively uptook Se^{VI} from aqueous solutions through anion exchange by replacing Cl^- (Wu et al. 2010). In general, the AFm phases have been shown significant affinity for immobilizing oxyanions such as Se^{VI} through exchange for the anion (X) (Goñi et al. 2001, Chrysochoou et al. 2006, Matschei et al. 2007, Wu et al. 2010).

As mentioned previously, the AFm and AFt phases are similar in chemical formula and form readily in cement materials. Some of the properties that influence the formation of AFm phase over the AFt phase include the following – available Al_2O_3/SO_4 molar ratio, pH, and temperature (Chrysochoou et al. 2006). The AFm phase is generally promoted over the AFt phase formation when the Al_2O_3/SO_4^{2-} molar ratios is greater than 1.0 (Chrysochoou et al. 2006). The presence of SO_4^{2-} promotes the formation of AFt-SO_4 over the AFm phases (De Weerdt et al. 2011).

Cl^-. Formation of AFm-Cl has also been proposed to uptake Cl^- in high salt waste (Lampris et al. 2009, Ramgobeen 2010, Lampris 2013). In one study, MSWI fly ash with a Cl^- content of 130,000 to 220,000 ppm was S/S with the aim of immobilizing Cl^- through AFm-Cl formation (Lampris et al. 2009). Over a 72 day tank leaching test, Cl^- releases varied between 40% and 50% even with PC addition up to 50% (Lampris et al. 2009). The same author also reported general Cl^- releases of 60% to 80% in tank leaching tests over a number of mixes and conditions in 64 days (Lampris 2013).

$FeSO_4$ Addition. One S/S stabilization strategy is FS addition to the mixture as a reducing agent (Connor 1997). This strategy has been utilized to stabilize Cr^{VI} contaminated waste (Connor 1997). Fe^{II} will likely be oxidized to Fe^{III} in the S/S mixture and form Fe^{III} oxides that have been shown to strongly sorb oxyanions including As^V, and Cr^{VI} under the pH conditions of cement-based S/S (Connor 1997, Cornelis et al. 2008a).

Utilization of FS as the reductant in S/S has two distinct advantages: high solubility and availability as a waste product (Blanchard et al. 1981). FS is a waste product "produced in titanium dioxide manufacture and in steel pickling" (Blanchard et al. 1981). Hence, it is

likely that FS can be obtained at low cost. Even if waste FS is contaminated with heavy metals, FS is being utilized in a S/S process designed to immobilize heavy metals. The waste FS would be beneficially utilized and treated to a greater degree than its normal disposal process. Depending on how the proposed S/S technology is applied, the process could be considered the co-disposal of CFA, concentrated FGD wastewater, and waste FS.

The high solubility of FS allows for the reductant to be directly added to the S/S process. The dissolution of FS evenly distributes Fe^{II} throughout the S/S mixture. FS utilization does not require a separate reduction process upstream of S/S.

1.7 COAL FLY ASH

The U.S. produced approximately 48.4 million metric tons of CFA in 2013; however, approximately 21.2 million metric tons were beneficially utilized which left 27.2 million metric tons for landfill disiposal (ACAA 2013). 48% of the mined coal in the U.S. is bituminous and 44% of the mined coal is sub-bituminous (USEIA 2015b). There exists a significant amount of CFA in the U.S. available for S/S processes. Depending on coal source and type, CFA can contain significant concentrations of metals including “Ag, As, B, Ba, Cd, Co, Cr, Cu, Hg, Ni, Pb, Se, and Zn” (Wang 2007a).

CFA is one of the four coal combustion residuals (CCRs) (also including bottom ash, boiler slag-molten ash, and gypsum). CFAs are “spherical in shape” with a typical size “ranging in size from 0.01 to 100 μm” (Fatoba 2010). “Oxides Si, Al, Ca, and Fe” are the main inorganic components of CFA (Wang 2007a).

CFAs are classified as Class C or Class F by the American Society of Testing and Materials (ASTM) (ASTM 2012). Class F CFA is associated with "bituminous or anthracite coal" combustion while Class C CFA is associated with combustion of "sub-bituminous or lignite coals" (Basham et al. 2007).

CFA chemistry had a large impact on the S/S process. As mentioned above, sub-bituminous CFA (SCFA, Class C CFA) is more reactive than bituminous CFA (BCFA) (Basham et al. 2007). Regarding the greater reactivity of SCFA versus BCFA, the most obvious difference between the two CFAs is the higher CaO content SCFA. SCFAs with CaO contents >20% can be classified as cementitious material (Papadakis 2000). The chemical composition of SCFA is closer to the composition of PC than BCFA (Papadakis 2000). The high CaO content promotes pozzolanic reactions and increases the pH of the S/S mixture. CFA leachate pH is controlled by the dissolution of CaO and MgO which also occurs in the S/S process (Roy et al. 2011). Hence, SCFA will usually produce S/S solids with higher pH than BCFA.

With regards to heavy metals, previous researchers have noted that As is present in CFA primarily as the oxyanion AsO_4^{3-} (Goodarzi et al. 2001, Huggins et al. 2007, Goodarzi et al. 2008). As partitions to CFA from the flue gas majorly through sorption to Fe sites on BCFA and Ca sites for SCFA (Yudovich et al. 2005).

Cd is typically associated with the CFA surface and is believed to be associated with aluminosilicates and metal oxides surfaces in CFA, although it may also be precipitated as $Cd(OH)_2$ or $CaCO_3$ (Jones 1995). Its leaching is limited at high pH due to the low solubility of $Cd(OH)_2$.

The dominant Cr species in CFA is Cr^{III} with Huffman et al. finding greater than 95% Cr^{III} of total Cr (Huffman et al. 1994, Huggins et al. 1999, Goodarzi et al. 2001, Goodarzi et al. 2008). Cr has been identified as residing mainly in the amorphous glassy aluminosilicate slag portion of CFA on both the surface and the entire CFA particle (Huffman et al. 1994, Jones 1995, Kim et al. 2004).

Hg is present in flue gas as Hg^0, Hg^P (Hg on particulate), and Hg^{2+} (Berry et al. 2007, Feeley et al. 2009). Hg^P is easily removed through particulate collection devices (ESPs or baghouses) on the CFA. Hence, Hg^P is expected in the CFA (Feeley et al. 2009).

Previous research has shown that the dominant Se species in CFA is the oxyanion SeO_3^{2-} (Narukawa et al. 2005, Huggins et al. 2007, Wang et al. 2009). As with As^V, Se partitions to CFA from the flue gas majorly through sorption to Fe sites on BCFA and Ca sites for SCFA (Yudovich et al. 2005).

1.8 SALT IMPACT ON BITUMINOUS COAL FLY ASH METAL LEACHING

Implementation of the proposed S/S technology, or any known ZLD strategy, will greatly increase the salt mass disposed in coal-fired power industry landfills. If contact with salt increased metal leaching from CFA, negative environmental consequences would result. Little information exists on the impact of multiple cation Cl^- salts on CFA metal leaching.

Published scientific literature exists on impact of Cl^- salts on metal mobility in soils, sediments, dredged materials, and organic matter in rivers (Doner 1978, Tyler et al. 1982, Christensen 1984, Pickering 1986, Khattak et al. 1989, Amrheln 1992, Bauske et al. 1993,

Paalman et al. 1994, Lützenkirchen 1997, Lores et al. 1998, Norrström et al. 1998, Kabala et al. 2001, Keon et al. 2001, Hatje et al. 2003, Millward et al. 2003, Bäckström et al. 2004, Guevara-Riba et al. 2005, Norrström 2005, Usman et al. 2005, Du Laing et al. 2007, Du Laing et al. 2008, Du Laing et al. 2009a, Du Laing et al. 2009b, Nelson et al. 2009, Acosta et al. 2011). Research on the impact of Cl^- salts on metal mobility in the above referenced materials has centered on Cd, Cr, Cu, Ni, and Pb (Doner 1978, Tyler et al. 1982, Christensen 1984, Pickering 1986, Khattak et al. 1989, Amrheln 1992, Bauske et al. 1993, Paalman et al. 1994, Lützenkirchen 1997, Lores et al. 1998, Norrström et al. 1998, Kabala et al. 2001, Keon et al. 2001, Hatje et al. 2003, Millward et al. 2003, Bäckström et al. 2004, Guevara-Riba et al. 2005, Norrström 2005, Usman et al. 2005, Du Laing et al. 2007, Du Laing et al. 2008, Du Laing et al. 2009a, Du Laing et al. 2009b, Nelson et al. 2009, Acosta et al. 2011). In previous research on estuarine sediments, large increases in Cd leaching were observed due to Cl^- complexation and/or competitive ion exchange with Ca^{2+}, Mg^{2+}, and Na^+ (Du Laing et al. 2009b). Cl^- salt content also significantly increased the mobility of other metals including Cr and Cu (Du Laing et al. 2009b).

In the mining industry, hyper-saline solutions have been utilized to increase metal solubility through a Cl^- leach processes to recover Ag, Cd, Cu, Ge, Ni, Pb, Sb, and Zn (Jonte et al. 1952, Duke et al. 1958, Reynolds et al. 1981, Winand 1991, Sinadinovic 1997, Senanayake 1998, Reddy 2005). A significant volume of scientific literature exists on utilization of Cl^- hydrometallurgy to recover valuable metals from ores (Libuś et al. 1975, Pan et al. 1989, Bazarkina et al. 2010, Liu et al. 2011, Liu et al. 2012, Tian et al. 2012a, Tian et al. 2012b).

Cation Exchange. Competition for surface sorption sites between major cations (Ca^{2+}, Mg^{2+}, and Na^{+}) and trace metals can likely impact CFA leaching. Previous research has shown that zeolites, which have high Si/Al ratios similar to CFA, favor sorption of divalent cations with lower hydration energies to active sites (Wingenfelder et al. 2005, Teutli-Sequeira et al. 2009). This research shows that cations with lower hydration energy will preferentially exchange for higher energy cations on active sites on the zeolite surface (Wingenfelder et al. 2005, Teutli-Sequeira et al. 2009). Researchers have noted electrostatic forces along with energy bonding both play a role in the cation preference for sorption on hydrous oxides (Balistrieri et al. 1982, Paalman et al. 1994). Typically when comparing positively charged metals within the same valence state, typically the ion with the larger ionic radius will be preferentially sorbed to hydrous oxides (Paalman et al. 1994). It is apparent that the higher concentration of the major divalent cations (Ca^{2+} and Mg^{2+}) and the potential to form higher energy bonds with active surface sites can increase trace metal leaching.

Cl^- Complexation. In Cl^- hydrometallurgy, many cationic metals have been shown to complex with Cl^- (Winand 1991). Researchers developed the " following classification of strength of Cl^- acceptors - $AgCl > CuCl > PbCl_2 > ZnCl_2 > CuCI_2 > FeCl_3 > FeCl_2 > NiCl_2 >$ HCl, NaCl, KCl (C1- donors)" (Winand 1991). Cd is not in the classification because it is not a valuable recoverable metal. Cl^- complexation moves Cd speciation "shifts towards $CdCl^+$, $CdCl_2$, $CdCl_3^-$ and $CdCl_4^{2-}$" (Du Laing et al. 2008). Cl^- complexation reduces activity (i.e. effective concentration) of cations in the and can promote cation mobility (Du Laing et al. 2009b).

Anion Exchange for Oxyanions. A previous study hypothesized anion exchange with Cl^- for the increased mobilization of the oxyanion As from sediments during leaching tests with 1M $MgCl_2$ addition (Keon et al. 2001). This process mobilized the ionically bound As from the sediment (Keon et al. 2001).

1.9 LEACHING PROCEDURES

Toxicity Characteristic Leaching Procedure. The TCLP was utilized in this work. The TCLP is an equilibrium batch extraction test in which the initial pH of the leachant is defined (USEPA 1992a). The TCLP is a regulatory leaching test to determine whether a waste is non-hazardous or hazardous in the U.S. Acetic acid (CH_3COOH) is utilized to adjust the initial pH of the leachant to either 2.88 or 4.93 depending on the pH of the solid and the liquid/solids (L/S) ratio for the test is 20 (USEPA 1992a, Halim 2004). The solids and liquids are extracted for 18±2 hours (USEPA 1992a). The solids must be less than 9 mm in size or be reduced in size prior to extraction (USEPA 1992a, Halim 2004).

USEPA Method 1313. The USEPA Method 1313 (Liquid-Solid Partitioning as a Function of Extract pH for Constituents in Solid Materials using a Parallel Batch Extraction Procedure) is one of the methods within the leaching environmental assessment framework (LEAF) developed by Vanderbilt University (Garrabrants 2010). In contrast to the TCLP, the USEPA Method 1313 is a test defined by the final pH of the leachant not the initial pH of the leachant (Garrabrants 2010). The goal is to achieve a target pH in the leachant at the end of the extraction process (Garrabrants 2010). This target pH is achieved by adding inorganic HNO_3 or NaOH to the leachant prior to the experiment (Garrabrants 2010).

Preliminary titration tests are conducted with the solid material before the experiment to determine the amount of acid or base added to the leachant to achieve the desired final pH (USEPA 2012). The required L/S ratio for the method is also 10 and the extraction time is 24±2 hours (USEPA 2012).

USEPA Method 1315. In addition to the crushed solid, batch leaching tests (TCLP and USEPA Method 1313), S/S solids in this work were evaluated in the cylindrical monolith form in a semi-dynamic, mass transport-based leaching tests – the USEPA Method 1315 (Mass Transfer Rates of Constituents in Monolithic Materials Using a Semi-Dynamic Tank Leaching Procedure) (USEPA 2013). The batch leaching tests are important for evaluating solubility phases controlling leaching at a certain pH; however, the semi-dynamic, mass transport-based leaching tests can elucidate further understanding of contaminant release: (1) over a significant time period and (2) "the result of diffusion through a tortuous pore network with aqueous partitioning at the solid–liquid interface" (De Windt et al. 2007, Garrabrants et al. 2014).

In this method, solid monoliths are submerged in deionized water at a liquid to surface area (L/SA) ratio of 9 ± 1 mL/cm^2 (USEPA 2013). Elemental diffusion is driven this process through concentration gradients "between the bulk contacting solution and the pore solution at the core of the monolith" (Garrabrants et al. 2014). Results from the USEPA Method 1315 are usually modeled with Equation 1.1 for radial diffusion from a cylinder into an infinite bath (USEPA 2013).

$$M\left(\frac{mg}{m^2}\right) = 2\rho C_o \left[\frac{D^{OBS.} \cdot t}{\pi}\right]^{\frac{1}{2}} \qquad (1.1)$$

In Equation 1.1, M is the mass released during leaching interval i (mg/m^2); ρ is the density of the sample (kg/m^3); C_o is the contaminant concentration in the solid matrix (mg/kg); D^{OBS} is the observed diffusivity (m^2/s); and t is the leaching time (s) (USEPA 2013). To overcome the limitations of Equation 1.1, it is proposed to compare the results of the USEPA Method 1315 experiments to a geochemical model of the system. Geochemical modeling will benefit the work by enhancing understanding of leaching from the S/S solid regarding: (1) chemical processes (including inside tortuous pore network), (2) mass transfer processes, (3) "competition between different dynamic processes" (chemical and mass transfer) (Tiruta-Barna 2008).

1.10 GEOCHEMICAL MODELING

Geochemical Speciation Models. Geochemical modeling has been widely utilized in numerous applications from hydrothermal system to modeling leaching from hazardous waste (USGS 2014). Speciation calculations are made by these models utilizing thermodynamic and kinetic principals (USGS 2014). Geochemical models typically take into account the following processes "mineral dissolution and precipitation, aqueous inorganic speciation and complexation, solute adsorption and desorption, ion exchange, oxidation–reduction or redox transformations, gas uptake or production, organic matter speciation and complexation, evaporation, dilution, water mixing, reaction during fluid flow, reactions involving microbial activity, and photoactivity" (USGS 2014).

The USGS has developed several geochemical models including but not limited to WATEQ, SOMNEQ, and PHREEQC (Kharaka et al. 1973, Truesdell et al. 1973, USGS 2014). WATEQ was developed to model water systems with the temperature range of 0-

100 ºC while SOLMNEQ's temperature range extends up to 350 ºC (USGS 2014). WATEQ utilizes Debye-Huckel utilizes the ion association method for calculations while SOLEMNEQ can utilize both the ion association and Pitzer method for calculations (USGS 2014).

PHREEQC, developed by the USGS, was utilized in this work for modeling described in Chapter 4 (Parkhurst et al. 2013). PhreePlot was also utilized in order to optimize parameters and repeatedly and automatically run the program under a range of conditions (Parkhurst et al. 1999, Kinniburgh et al. 2010). In addition to the Pitzer method, the specific ion interaction theory (SIT) database is also included in PHREEQC. The SIT database was selected in this work's modeling efforts due to the high ionic strength of the leaching experiments (0-5.5 M). The SIT has typically been utilized for ionic strengths approaching 3.5-4.0 M and the Pitzer model has been applied at extreme ionic strengths up to the "saturation of most salts" (Xiong 2006). Xiong noted that errors in activity coefficients calculated by SIT versus Pitzer model "is usually less than 10% at ionic strength up to 6–10 m at 25°C" (Xiong 2006). Hyks et al. noted that insufficient thermodynamic data is available to model a complex leaching system (Hyks et al. 2009). Due to the same issue regarding limited thermodynamic data availability, it was decided to utilize the SIT database for the modeling described in Chapter 4.

Transport Models for Monolith Leaching. Geochemical models have been applied to evaluate leaching from S/S solids and cementitious materials including in semi-dynamic and dynamic leaching scenarios (Garrabrants et al. 2003, Halim et al. 2005, Tiruta-Barna et al. 2005, Malviya et al. 2006, De Windt et al. 2007, van der Sloot et al. 2007, Tiruta-Barna 2008, Schiopu et al. 2009, Voglar et al. 2011, Seignette et al. 2014). De Windt et al.

conducted geochemical and transport modeling for Pb release from a S/S monolith utilizing HYTEC (De Windt et al. 2007). Garrabrants et al. modeled 1-D leaching from a cement mortar utilizing an intermittent mass transport (IMT) model (Garrabrants et al. 2003). Malviya et al. utilized Visual MINTEQ Version 2.3 to calculate geochemical speciation only in S/S solids, but the modeling did not included transport component (Malviya et al. 2006). Hamlin et al., Schiopu et al., and Tiruta-Barna et al. modeled leaching from cementitious materials or waste utilizing PHREEQC (Halim et al. 2005, Tiruta-Barna et al. 2005, Tiruta-Barna 2008, Schiopu et al. 2009).

Applicable geochemical models can be divided into three categories as follows (Meeussen 2003, Tiruta-Barna et al. 2005, van der Sloot et al. 2007, Tiruta-Barna 2008, van der Sloot et al. 2012): speciation models with no transport capability – CHESS, EQ3/6, Geochemist's workbench, MINTEQA2, and WATEQ4F; combined speciation and transport models - HYTEC, LeachXS^{TM} (ORCHESTRA), and PHAST; and speciation models with limited transport capabilities – PHREEQC.

LeachXS^{TM}-Orchestra was developed by Vanderbilt University (Meeussen 2003, van der Sloot et al. 2012, Seignette et al. 2014). LeachXS^{TM} software calculates adsorption/desorption to Fe^{III} and Al^{III} oxides utilizing the Dzomback and Morel model (van der Sloot et al. 2012).

With regards to leaching from monoliths, the Leach XS^{TM} segments a solid monolith from the outside to the interior and calculates the local liquid and solid partitioning of each segment (Seignette et al. 2014). This same liquid-solid partitioning calculation is made at each time step due to changing conditions (Seignette et al. 2014).

The model simulates a well-mixed solution of a finite volume in contact with the monolith (Seignette et al. 2014).

CHAPTER 2. IMMOBILIZATION OF HEAVY METALS BY SOLIDIFICATION/STABILIZATION OF CO-DISPOSED FLUE GAS DESULFURIZATION BRINE AND COAL FLY ASH

2.1 ABSTRACT

Changes in the regulatory environment for the coal-fired power industry in the United States have driven the need to improve wastewater treatment and disposal practices, especially for wet flue gas desulfurization systems. One option for treatment of FGD wastewater is the implementation of zero liquid discharge (ZLD) treatment systems. ZLD can be achieved through the coupling of brine concentrator with a solidification/stabilization (S/S) process. This S/S process could be achieved by co-disposing the concentrated FGD brines with coal fly ash (CFA) and Portland cement. S/S using bituminous CFA (BCFA) achieved good retainment (average 68−90%) of As^{V}, Cd^{II}, Hg^{II} and Se^{IV}, in the toxicity characteristic leaching procedure (TCLP); however, poor retainment was observed for Cr^{VI} and Se^{VI}. Separate experiments showed good sorption of As^{V}, Cd^{II}, Hg^{II} and Se^{IV} (average 56−100%), but poor sorption of Cr^{VI} and Se^{VI}, to S/S solids. Meanwhile, Cr^{VI} and Se^{VI} retainment could be enhanced by addition of $FeSO_4$ to the S/S mixture, likely due to reduction of these metals to lower oxidation states. Compared to BCFA, S/S using sub-bituminous CFA (SCFA) resulted in higher pH S/S solids and final TCLP leachate, which increased retainment of As^{V}, Cd^{II} and Se^{VI}. Apart from the pH impact on the process, As^{V} retainment was likely improved by the high Ca content of SCFA and Se^{VI} retainment improved by the incorporation of SeO_4^{2-} in Friedel's salt (AFm-Cl) by exchange with Cl^{-}. Friedel's salt was positively identified in the X-ray diffraction (XRD)

diffractogram for the SCFA S/S solids, but not for the BCFA S/S solids. Even so, reduction of Se^{VI} plus S/S is likely a better long-term strategy than SeO_4^{2-} substitution in the AFm phase because of higher stability under long-term landfill conditions.

2.2 INTRODUCTION

Changes in the regulatory environment for the coal-fired power industry in the United States have driven the need to improve wastewater treatment and disposal practices, especially for wet flue gas desulfurization (FGD) systems. Per the United States Environmental Protection Agency (USEPA), most contaminant loadings associated with coal-fired power plants result from wet FGD and ash handling systems (USEPA 2009). In a typical wet FGD system, Ca^{2+} or Ca^{2+}-Mg^{2+} slurry is sprayed against the flue gas in order to remove SO_2. Along with SO_2, heavy metals are also removed from the flue gas and accumulate in the FGD slurry (Huang et al. 2013a). The resulting purge brines from FGD systems are complex wastewaters that contain significant concentrations of heavy metals including As, Ba, Cd, Cr, Hg, and Se (USEPA 2009), as well as high concentrations of salts in the forms of Ca^{2+}, Mg^{2+}, Na^{+}, SO_4^{2-}, and Cl^{-}. Because the majority of wet FGD systems utilize $Ca(OH)_2$ or $CaCO_3$ as an alkaline sorbent (Blythe et al. 2008), most FGD wastewaters are dominated by Ca^{2+} as the major cation. The major anion in the wastewater is Cl^{-} which is liberated during coal combustion.

The two commonly employed wet FGD systems are forced-oxidation and inhibited-oxidation systems. Forced-oxidation systems are more common and the USEPA expects the majority of new wet FGD systems installed in the future to be of this type (USEPA 2009). In forced-oxidation systems, air is bubbled through the FGD slurry to oxidize $CaSO_3$

to $CaSO_4 \cdot 2H_2O$ (gypsum), a product with commercial value. The oxidation of $CaSO_3$ can also oxidize heavy metals, including Se and Cr to their more mobile and toxic forms (Batchelor 2006). Treatment of FGD wastewater from forced-oxidation systems can be particularly difficult to optimize.

The USEPA recently released the proposed final revision to the Steam Electric Power Effluent Limitation Guidelines (ELG) which regulate FGD wastewater (USEPA 2015). The revised guidelines include stringent limits on As, Hg, and Se release to the environment from FGD wastewater, resulting in increased treatment requirements. Treatment options for FGD wastewater include biological processes, Fe-based reduction, and zero liquid discharge (ZLD) strategies. ZLD options are particularly attractive to the coal-fired power industry due to the elimination of an environmental wastewater discharge and to the ability to recycle and reuse water in power plants. Potential ZLD technologies for FGD wastewater include falling film evaporators and crystallizers, wastewater spray dryers, brine concentrators, and advanced membrane processes (forward osmosis, membrane distillation, etc.). The residuals from each of these systems contain heavy metals and high salt concentrations that can be solidified/stabilized (S/S) through mixing with coal fly ash (CFA) and a pozzolanic agent to produce a final cementitous S/S solid residual.

S/S consists of two processes: solidification (improving physical properties of waste) and stabilization (converting contaminants to less mobile and less toxic forms) (Batchelor 2006). S/S typically includes the mixing of wastes (sludges, brines, or solid waste) with Portland cement (PC), PC/CFA, CaO/CFA, or $Ca(OH)_2$/CFA (Batchelor 2006). The USEPA regards S/S as an established treatment technology for more than 57 wastes (Paria et al. 2006, Mickley 2008).

We propose the co-disposal of concentrated FGD brines (e.g., from a brine concentrator) and CFA through S/S utilizing PC, as a ZLD disposal option for FGD wastewater. This approach has the advantages of achieving the benefits of ZLD with a lower energy penalty compared to crystallization, while co-handling two abundant materials generated together at coal-fired power plants. The focus of this study was to evaluate heavy metal immobilization efficacy in the final S/S solid.

In this study, simulated concentrated FGD brines were prepared based on their expected composition from a bituminous coal-fired power plant that utilizes a forced-oxidation FGD system. Note that bituminous coal contains more sulfur compared to sub-bituminous coal. As a result, the bituminous coal-fired power plants generate flue gases that require more desulfurization than sub-bituminous power plants. As a result, the FGD wastewaters from bituminous power plants contain more heavy metals and salts and wastewaters from these plants are more challenging to treat.

Simulated concentrated FGD brines were mixed with two types of CFA (bituminous and sub-bituminous coal) along with PC. The resulting S/S solids were cured and then subjected to the toxicity characteristic leaching procedure (TCLP) (USEPA 1992a) to evaluate heavy metal (As^{V}, Cd^{II}, Cr^{VI}, Hg^{II}, Se^{IV}, and Se^{VI}) immobilization efficacy of the process. In some experiments, $FeSO_4$ (FS) was added as a reductant to the S/S process. In addition, experiments on the sorption of heavy metals to the S/S solids were conducted. The produced S/S solids from the study were characterized by x-ray diffraction (XRD) and x-ray fluorescence (XRF) in order to gain mechanistic insight into heavy metal immobilization in the process.

2.3 EXPERIMENTAL SECTION

2.3.1 Coal Fly Ashes

Bituminous CFA (BCFA) was obtained from a coal-fired power plant in the southeastern United States. Sub-bituminous CFA (SCFA) was obtained from a separate coal-fired power plant also in the southeastern United States. BCFA and SCFA metal concentrations were determined by completely digesting the solids and analyzing the liquids with inductively-coupled plasma mass spectrometry (ICP-MS) following USEPA Method 6020a (USEPA 2007).

2.3.2 Simulated Brines

All chemicals for preparation of the simulated brines were obtained from Fisher Scientific (Pittsburgh, PA) at reagent grade or higher. Simulated brines were produced by combining the following salts: $Ca_3As_2O_8$, $CaCl_2{\cdot}2H_2O$, $CdCl_2$, $HgCl_2$, $MgCl_2{\cdot}6H_2O$, $Mg(NO_3)_2{\cdot}6H_2O$, $MgSO_4{\cdot}7H_2O$, NaBr, NaCl, Na_2CrO_4, $Na_2HAsO_4{\cdot}7H_2O$, Na_2SeO_3, and Na_2SeO_4 in deionized water. The reagent grade deionized water was produced from a nanopure Millipore (Billerica, MA) water purification system. Simulated brines were prepared containing either Se^{IV} or Se^{VI}, but not both. Following mixing of the chemicals, the pH of the simulated brine was adjusted to 3.5 using HNO_3, because the pH of FGD wastewater was expected to decrease from its near neutral value to the acidic range during evaporation due to Mg^{2+} precipitation as $Mg(OH)_2$ or complexation as $MgOH^+$. Salts were allowed to dissolve completely before the experiment was initiated, and no solids were visible in the brines. Table 2.1 shows the range of simulated brine composition utilized in the experiments.

Table 2.1. Composition of simulated FGD Brines used for S/S experiments.

Composition	Range (mg/L)
TDS	140,000 - 264,000
Ca^{2+}	0 - 66,000
Mg^{2+}	4,000 - 12,000
Na^{+}	3,000 - 75,000
Cl^{-}	60,000 - 120,000
SO_4^{2-}	0 – 6,000
NO_3^{-}	375 - 85,000
As^{V}	1.0 - 20.8
Cd^{II}	0.4 - 23.5
Cr^{VI}	0.9 - 32.8
Hg^{II}	0.7 - 73.4
Se^{IV}	80.4 - 104.9
Se^{VI}	23.1 - 111.9
Density	1,104 - 1,192 (g/L)

TDS = total dissolved solids

Hg^{II}, Se^{IV}, and Se^{VI} concentrations were increased above what would be expected in a real concentrated FGD brine in order to evaluate the robustness of the process. Some simulated brines were prepared without heavy metal addition. S/S experiments were conducted utilizing these "metal-free" brines in order to determine the amount of heavy metals leaching from only CFA and PC in the high salt conditions.

2.3.3 Solidification/Stabilization

Samples were S/S by mixing simulated brine, CFA, and PC. Type I/II PC was obtained from Home Depot in Acworth, Georgia. Preliminary experiments determined that the optimum ratio for S/S was approximately 60% CFA, 30% simulated brine, and 10% PC by mass, and the same ratio was utilized in subsequent S/S experiments. This ratio was varied slightly when $FeSO_4 \cdot 7H_2O$ ($FS \cdot 7H_2O$) (from Fisher) was added to the mixture or

when simulated brine had a lower concentration of dissolved solids and the amount of water added (from the simulated brine) was decreased to control the water content.

During the S/S process, CFA, simulated brine, and FS were first added to a bench-scale mixer with a stainless steel bowl. The components were mixed for approximately 2 min to allow chemical reduction to take place, and after the initial 2 min, PC was added to the mixture and mixing was continued for an additional 18 min. The resulting slurry was then poured into 76 mm (diameter) × 152 mm (height) cylindrical plastic concrete forms. The slurry was then allowed to cure for 13−28 days in a humid environment at room temperature. S/S experiments were conducted mostly with BCFA and selectively with SCFA. Although SCFA is a self-cementing ash and does not require PC addition to initiate the pozzolanic reactions, PC was added in the S/S experiments with SCFA to compare the impact of SCFA versus BCFA chemistry in the process.

The formed S/S solids were crushed and subjected to the TCLP following the USEPA Method 1311 (USEPA 1992a). The TCLP leachate was digested and analyzed for heavy metal content according to the USEPA Method 200.8 utilizing an ICP-MS (USEPA 1994a). Two of the S/S solid samples were subjected to leaching by the USEPA Method 1313 (liquid-solid partitioning as a function of extractant pH using a parallel batch extraction procedure) (USEPA 2012). The TCLP and USEPA Method 1313 are both batch extraction procedures; however, USEPA Method 1313 differs from the TCLP in that it is a final extractant pH defined instead of an initial extractant pH defined. Preliminary titration tests were conducted to determine the amount of acid needed to adjust the final leachate pH to the desired level (targeted at 7.0 and 9.0 in this study) prior to the actual USEPA Method 1313 evaluation. Additional differences between the two leaching

methods included the use of an inorganic acid (HNO_3) for USEPA Method 1313 versus organic acid (CH_3COOH) for the TCLP, liquid-to-solid was lower for USEPA Method 1313 (10) than the TCLP (20), and extraction time for USEPA Method 1313 (24 ± 2 hours) was longer than that of TCLP (18 ± 2 hours). Generally, approximately 10 grams of solid was mixed with 100 mL of the extractant fluid with the amount of HNO_3 required to achieve the final leachate pH in the USEPA Method 1313 evaluation. The leachate was digested before ICP-MS analysis according to the USEPA Method 200.8 (USEPA 1994a).

2.3.4 Sorption Experiments

The adsorbent material for the experiments was S/S solids prepared from BCFA (60%), simulated brine (30%) without heavy metal addition (i.e., heavy metal-free brine), and PC (10%), following the same S/S procedures described above with 13 days of solid curing time. The formed solid was crushed and ground so that the particles passed through a 170 Mesh Sieve (88-µm openings).

Simulated brines were prepared at three different total dissolved solids (TDS) values as shown in Table 2.2. In addition to the simulated brines, sorption experiments were conducted utilizing deionized water for comparison and quality control. The pH of the brines and deionized water were adjusted to 3.5 with HNO_3 prior to initiation of the sorption experiments.

The sieved S/S solids (10 g) were contacted with 50 mL of the simulated brine or deionized water in 100-mL containers. Gentle stirring was provided by a magnetic stir bar. The S/S solids and the simulated brine were contacted for 48 h at room temperature.

Afterwards, the solid and liquid were separated by centrifugation. The supernatant was analyzed for heavy metals by the USEPA Method 200.8 (USEPA 1994a).

Table 2.2. Compositions of simulated brines for sorption experiments.

Composition	Level 1 (mg/L)	Level 2 (mg/L)	Level 3 (mg/L)
TDS	65,000	130,000	261,000
Ca^{2+}	9,000	18,000	37,000
Mg^{2+}	4,000	8,000	17,000
Na^{+}	6,000	11,000	23,000
Cl^{-}	25,000	50,000	100,000
NO_3^{-}	21,000	42,000	85,000
As^{V}	1.5 - 2.2	1.6 - 2.2	1.8 - 2.5
Cd^{II}	0.8 - 1.8	0.8 - 1.9	0.7 - 1.6
Cr^{VI}	5.1 - 6.1	5.4 - 5.9	5.6 - 5.8
Hg^{II}	23.7	17.6	15.3
Se^{IV}	88.3	91.5	84.1
Se^{VI}	87.4 - 95.2	85.1 - 91.8	84.0 - 93.6

2.3.5 X-Ray Diffraction and Fluorescence Analysis

BCFA S/S and SCFA S/S solids were crushed and ground to pass a 325 Mesh Sieve (45-µm openings). BCFA, SCFA, and PC were also passed through the same sieve. The crystalline phases of the CFAs, S/S solids, and PC were determined by powder X-ray diffraction (XRD) utilizing a PANalytical X-Pert Pro X-ray diffractometer (Almelo, The Netherlands) utilizing Cu-Kα radiation. The XRD was operated at a voltage of 40 kV and a current of 40 mA. 2Θ values ranging from 4º to 70º were evaluated. The XRD was operated at a voltage of 40 kV and a current of 40 mA. The step size was 0.02º and the time per step varied from 256-272 s/step. X-ray fluorescence (XRF) analysis was conducted for BCFA, SCFA, PC, and BCFA S/S solids utilizing a S8 Tiger Model from the Bruker Corporation (Karlsruhe, Germany).

2.4 RESULTS AND DISCUSSION

2.4.1 Solids Analysis

Table 2.3 shows metal composition of the solids examined in this study determined by total digestion. As shown in Table 2.3, BCFA had higher Al (120,308 ppm) and Fe (67,145 ppm) contents than SCFA and PC (3,622–23,320 ppm for Al; 22,321–39,981 ppm for Fe), but lower Ca content (13,299 ppm versus 172,634–517,288 ppm). After S/S, the BCFA S/S solid had relatively high Ca content (95,961 ppm) due to the addition of the simulated brine and PC to the S/S mixture. Note that the BCFA S/S solid showed a much higher Si content (171,524 ppm) than BCFA, SCFA and PC (13,815–28,146 ppm). It is unlikely that the other three solids' Si contents are as low as measured, but rather Si in the BCFA S/S solid was more easily mobilized during the digestion compared to the other three solids due to the BCFA S/S solid having undergone pozzolanic reactions.

The BCFA, SCFA, and BCFA S/S solid contained higher concentrations of heavy metals (As, Cd, and Se) than PC. Table 2.4 and Figure 2.1 shows the XRF analysis of the solids. The amorphous SiO_2 phase content was higher (38.5–54.3%) in BCFA, SCFA, and BCFA S/S solid than in PC (21.7%). The XRF results indicated that the SiO_2 contents were comparable for BCFA, SCFA and BCFA S/S solid, which differed from the total digestion results in Table 2.3, but was consistent with expectation. SCFA, PC, and BCFA S/S solid had a higher CaO content (28.1–63.8%) than BCFA (1.6%). The contrast in CaO content between SCFA and BCFA is one of the most important differences between the two CFAs for S/S. Figure 2.1 shows that BCFA, SCFA, and BCFA S/S solid had a higher Al_2O_3 content (18.2–25.2%) than PC (4.1%).

Table 2.3. Chemical composition of solids in this study.

(a) Bulk Elements

Composition	BCFA (ppm)	SCFA (ppm)	PC (ppm)	BCFA S/S Solid (ppm)
Al	120,308	23,320	3,622	98,313
Ca	13,299	172,634	517,288	95,961
Fe	67,145	39,981	22,321	35,079
Mg	2,653	16,592	5,359	6,953
K	16,228	<3,957	<3,804	12,357
Si	13,815	28,146	12,773	171,524

(b) Significant Elements (Concentrations > 100 ppm)

Composition	BCFA (ppm)	SCFA (ppm)	PC (ppm)	BCFA S/S Solid (ppm)
Ba	662	4,709	60	774
B	<193	537	<190	<200
Cu	152	184	30	128
Cr	141	63	104	127
Pb	100	34	7	51
Mn	219	226	433	163
Ni	129	56	27	83
Sr	31	155	<19	32
Ti	7,912	8,585	1,838	5,971
V	302	223	54	209
Zn	243	95	250	98

(c) Trace Elements (Concentrations < 100 ppm)

Composition	BCFA (ppm)	SCFA (ppm)	PC (ppm)	BCFA S/S Solid (ppm)
Sb	8	2	<1	4
As	88	19	6	61
Be	20	3	<1	15
Cd	1	2	<1	4
Co	50	23	5	41
Mo	16	<1	<1	<1
Se	7	14	<2	25
Ag	<1	<1	<1	<1
Tl	4	<1	<1	2
W	7	2	2	5
U	18	7	1	9

Table 2.4. XRF analysis of solids in this study.

Phase	BCFA	SCFA	PC	BCFA S/S Solid
SiO_2	54.3%	36.6%	21.7%	40.1%
CaO	1.6%	28.1%	63.8%	26.4%
Al_2O_3	25.2%	18.2%	4.1%	19.7%
Fe_2O_3	11.9%	6.4%	3.7%	6.4%
K_2O	2.6%	0.4%	0.5%	1.7%
Cl	0.2%	0.0%	0.1%	1.6%
TiO_2	1.6%	1.6%	0.4%	1.3%
MgO	0.8%	6.3%	0.9%	1.2%
Other	1.9%	2.4%	4.7%	1.7%

2.4.2 Heavy Metal Retainment

The effectiveness of the S/S process was evaluated by determining the % of mass of the heavy metal that was retained on the solid during the TCLP test using the equation (2.1):

$$\%\ \boldsymbol{Retainment} = \frac{MB-(ME-MFA)}{MB} * 100 \quad (2.1)$$

MB was the mass of heavy metal in the simulated brine added to the S/S mixture; ME was the mass of heavy metal detected in the TCLP extract; and MFA was the amount of heavy metal detected in the TCLP extract from the S/S samples made with the heavy metal-free brine when available. The typical final TCLP leachate pH varied from 5.1 to 7.8, depending on FS addition and brine composition.

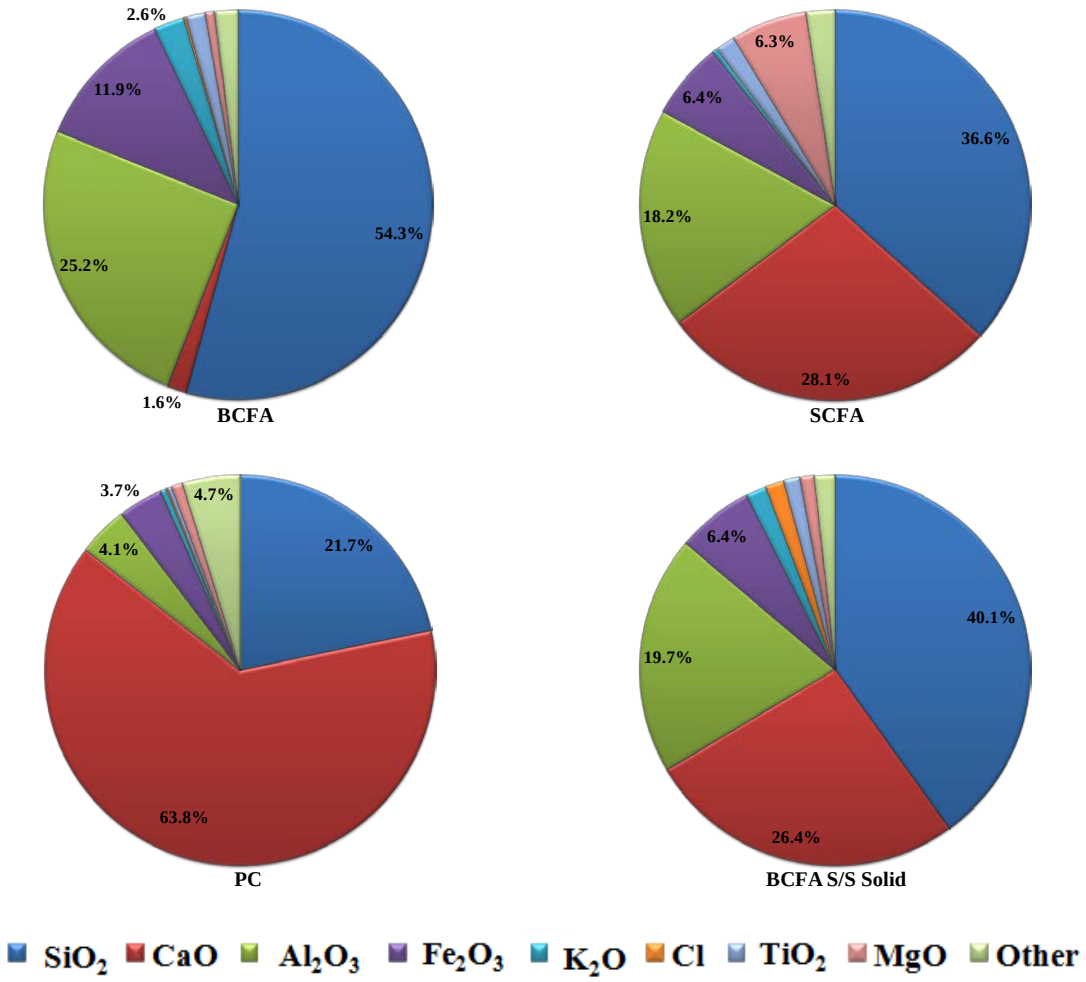

Figure 2.1. XRF analysis of solids in this study. Note: the S/S solid was prepared from brine, BCFA, and PC.

Figure 2.2 shows the typical heavy metal retainment by the S/S process. In general, good retainment was observed for As^{V}, Cd^{II}, Hg^{II}, and Se^{IV} (average 68−90%). The addition of FS increased the retainment of As^{V} from an average 77% to nearly 100%. The retainment for Cr^{VI} was inconsistent; however, the addition of FS to the S/S mixtures increased and stabilized the retainment of Cr^{VI} from average 59% to 99%. The addition of FS to the S/S mixtures increased the retainment of Se^{VI} from an average 16-46%. The retainment of each heavy metal is discussed individually below.

As^{V}. Previous research has shown S/S successful immobilizing As^{V} (Choi et al. 2009). Ca-As^{V} complex precipitation is the likely dominant immobilization mechanism as these complexes are at low solubility at neutral and high pH (Nishimura et al. 1998, Bothe Jr et al. 1999, Cornelis et al. 2008a, Moon et al. 2008). $NaCaAsO_4{\cdot}7.5H_2O$, $Ca_4(OH)_2(AsO_4)_2{\cdot}4H_2O$, $Ca_5(AsO_4)_3OH$ and $Ca_3(AsO_4){\cdot}3(2/3)H_2O$ have identified by previous researchers as important As^{V} precipitates in cement based S/S or waste mixed with lime with $NaCaAsO_4{\cdot}7.5H_2O$ as the likely most important phase (Akhter et al. 1997, Bothe et al. 1999, Moon et al. 2004, Moon et al. 2008).

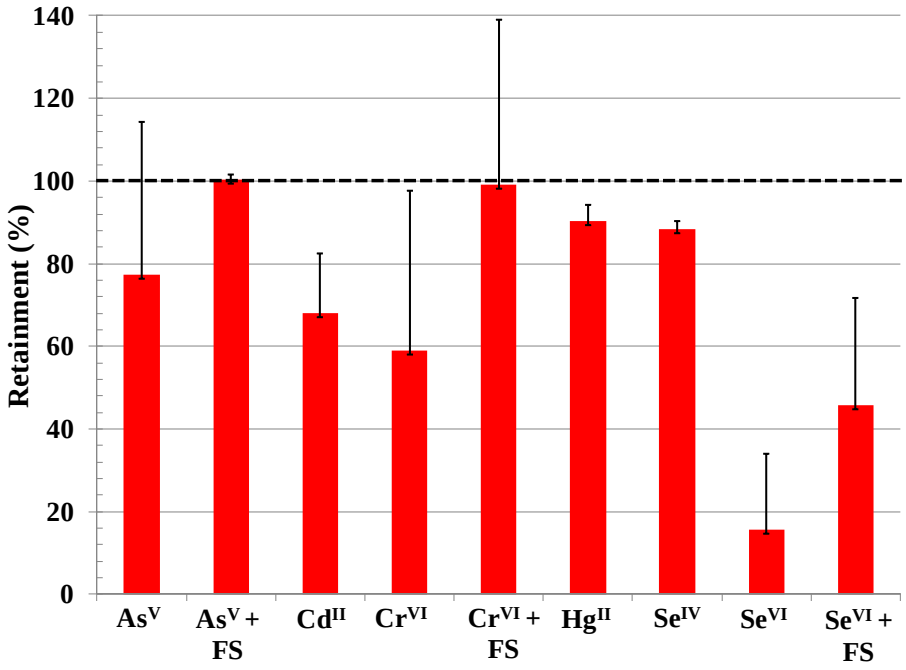

Figure 2.2. Typical retainment of heavy metals evaluated by TCLP in the S/S solids made from concentrated simulated brine, BCFA and PC at mass ratio of 3:6:1. Note: n = 22 for As^{V}, Cd^{II}, and Cr^{VI}; n = 20 for Hg^{II}; n = 15 for As^{V} + FS, Cr^{VI} + FS, and Se^{VI} +FS; n = 12 for Se^{VI}; n = 6 for Se^{IV}.

The Ca-As^{V} complex precipitation mechanism agrees with the results of good As^{V} retainment shown in Figure 2.2. Ca is abundant in the S/S mixture through the high CaO content of PC and the high dissolved Ca^{2+} concentration in the simulated brine. PC addition

to the S/S process mixture significantly increased the pH, which favors Ca-As^{V} complex precipitation.

Many Ca-As^{V} complex precipitates are not stable in the presence of atmospheric CO_2 and will react with CO_2 to form $CaCO_3$ and soluble As^{V} (Akhter et al. 1997). This mechanism may explain the variability in the Figure 2.2 As^{V} retainment results as differing amounts of Ca-As^{V} complex precipitates may have reacted with CO_2 to mobilize As^{V}, leading to the variable results.

Addition of Fe^{II} and Fe^{III} has been shown to increase the As^{V} retainment in S/S solids (Palfy et al. 1999, Miller et al. 2000, Choi et al. 2009). The Dzombak and Morel model indicated that As^{V} sorbs readily to hydrous Fe^{III} oxides at a pH range in common with in common with cement-based S/S (Cornelis et al. 2008a). Miller et al. conducted a cement-based S/S treatment study for As^{V} contaminated soils with FS and $Fe_2(SO_4)_3$ addition (Miller et al. 2000). Addition of both Fe^{II} and Fe^{III} in this study enhanced As^{V} immobilization in S/S with PC (Miller et al. 2000). In the current study, it is likely that Fe^{II} (from FS) was oxidized to Fe^{III} in the S/S mixture enhancing As^{V} immobilization through sorption on the generated Fe^{III} oxides, leading to better retainment (Figure 2.2).

Cd^{II}. Cement-based S/S has been shown effective immobilizing Cd^{II} (Akhter et al. 1990, Cartiedge et al. 1990). The dominant immobilization mechanism for Cd^{II} is precipitation of $Cd(OH)_2$ under high pH conditions (Akhter et al. 1990, Cartiedge et al. 1990). Previous researchers suggested that $Cd(OH)_2$ precipitate can form the nuclei of crystallization for the mineral calcium silicate hydrate (C-S-H) (Akhter et al. 1990, Cartiedge et al. 1990). It is believed that $Cd(OH)_2$ is protected by microencapsulation in C-

S-H and/or $Ca(OH)_2$ (crystalline portlandite) matrix (Akhter et al. 1990, Cartiedge et al. 1990). The $Cd(OH)_2$ precipitate would have some protection against the lower pH conditions of the TCLP leachant. The mechanism described above agrees with the good Cd^{II} retainment results shown in Figure 2.2.

Cr^{VI}. Cement-based S/S has been shown to be effective immobilizing Cr^{III}, but not Cr^{VI} (Glasser 1997, Wang et al. 2000, Dermatas et al. 2003). Cr^{III} stabilizes more readily than Cr^{VI} due to the lower solubility of Cr^{III} under the high pH conditions of S/S and a chemical incorporation process occurring during S/S (Richard et al. 1991, Glasser 1997). Glasser noted that $Cr(OH)_3$ precipitation alone cannot account for Cr^{III} immobilization in S/S matrices (Glasser 1997). Glasser indicated that chemical incorporation of Cr^{III} in the Ca-Al^{III}-hydrate phase by replacing Al^{III} could play a larger role in Cr^{III} immobilization in S/S than $Cr(OH)_3$ precipitation (Glasser 1997). The solubility of Ca-(Cr^{III}, Al^{III})-hydrates is lower than $Cr(OH)_3$ under S/S conditions (Glasser 1997). In addition, results from the Dzombak and Morel model indicate that Cr^{III} readily sorbed to hydrous Fe^{III} oxides in the high pH conditions of S/S (Cornelis et al. 2008a).

Fe^{II} has can reduce Cr^{VI} to Cr^{III} (Dermatas et al. 2003, Su et al. 2005). Addition of FS to S/S mixtures greatly decreased Cr^{VI} leaching in previous research (Dermatas et al. 2003) as well as in the current study (Figure 2.2). Thus, the mechanism of Cr^{VI} reduction by FS to Cr^{III} is likely responsible for the improved Cr^{VI} retainment. The Fe^{II} from the FS will be oxidized to form Fe^{III} oxides in the S/S solid which could enhance Cr^{III} retainment. In some cases, Cr^{VI} retainment was increased above 100% with FS addition (Figure 2.2); this situation likely results from: (i) Cr^{VI} from the BCFA being reduced to Cr^{III}, which could be incorporated in the Ca-Al^{III}-hydrate phase, precipitate as $Cr(OH)_3$, or adsorb to

Fe^{III} oxides (existing and new) and (ii) some of the Cr^{III} originally from the BCFA could also be incorporated in the Ca-Al^{III}-hydrate phase or adsorb to newly formed Fe^{III} oxides.

Hg^{II}. S/S has been shown effective in immobilizing Hg^{II} at concentrations below 100 mg/kg (Connor 1997). Hg^{II} concentrations (primarily from the simulated concentrated wastewater) in the S/S solids in this Work were quite low at 6.9-19.0 mg/kg. The Hg^{II} contributed from BCFA and PC to the S/S mixture was negligible (<0.2 mg/kg).

Rio and Delebarre noted that Hg^{II} can sorb significantly to Si^{IV} and Al^{III} oxides in CFA (Rio et al. 2003). In fact, the researchers indicated that the release of CaO from CFA in aqueous solution could enhance sorption by increasing the number of active sites for Hg^{II} to sorb (Rio et al. 2003). It is known CaO is released from CFA (particularly SCFA) in the cement hydration process (Detwiler 1997). However, as shown in Figure 2.1, BCFA contains only a 1.6% CaO compared to 28.1% CaO for SCFA, so not as many active sites would become available for BCFA as for SCFA.

McWhinney et al. noted that Hg^{II} can precipitate as HgO in cement-based S/S (McWhinney et al. 1990). In addition, precipitated HgO could be protected from water contact through microencapsulation with $CaCO_3$, thereby enhancing Hg^{II} immobilization (McWhinney et al. 1990). A combination of the HgO precipitation and sorption to CFA mechanisms described above likely account for the good Hg^{II} retainment results shown in Figure 2.2.

Se^{IV} and Se^{VI}. Se^{IV} and Se^{VI} behave differently in S/S (Cornelis et al. 2008a, Cornelis et al. 2008b). $CaSeO_3$ precipitation is the likely dominant Se^{IV} immobilization mechanism in S/S. Baur and Johnson hypothesized that $CaSeO_3$ controls porewater Se^{IV}

solubility in cement materials where Ca^{2+} concentrations are on the mM level (Baur et al. 2003b). While evaluating the sorption of Se^{IV} and Se^{VI} to cement minerals, Baur and Johnson observed that $CaSeO_3$ precipitated in solutions at Se^{IV} concentrations above 2.5×10^{-4} M and pH 9.01–9.33 (Baur et al. 2003b). Wang et al. demonstrated that Se^{IV} leaching from CFA can be decreased by $Ca(NO_3)_2$ addition, which likely resulted in $CaSeO_3$ precipitation (Wang et al. 2009). The data produced by Wang et al. implies that CFA Se^{IV} leaching is controlled by $CaSeO_3$ under high Ca^{2+} conditions (Wang et al. 2009).

The likely dominant Se^{VI} immobilization mechanism in S/S is chemical incorporation of SeO_4^{2-} in the structure of the cement hydration products: ettringite ($Ca_6Al_2(OH)_{12}(SO_4)_3\cdot26H_2O$) or monophase ($Ca_2(Al,Fe)(OH)_6)\cdot X\cdot xH_2O$) (Zhang et al. 2003, Cornelis et al. 2008a, Moon et al. 2009, Wang et al. 2009, Wu et al. 2010). Monophases are denoted in cement chemistry by the shorthand AFm-X where X is an anion which could include CO_3^{2-}, Cl^-, OH^-, or SO_4^{2-} and ettringite is denoted by AFt-SO_4 (Birnin-Yauri et al. 1998, Renaudina et al. 1999, Goñi et al. 2001, Matschei et al. 2007, Guerrero et al. 2009, Balonis et al. 2010, Wu et al. 2010). AFm-X in cement typically includes more Al^{III} than Fe^{III} in the structure (Matschei et al. 2007). AFm-Cl is known as Friedel's salt (Matschei et al. 2007). The AFm phase structure consists of positively charged $Ca_2[Al(OH)_6]^+$ layers, producing a net charge imbalance (Goñi et al. 2001, Matschei et al. 2007). Anions (X) collect in the area between the $Ca_2[Al(OH)_6]^+$ layers to balance the mineral's charge (Goñi et al. 2001, Matschei et al. 2007). The exchange of interlayer anions with external anions is typically highly favored (Goñi et al. 2001, Matschei et al. 2007).

Baur and Johnson studied the sorption of Se^{VI} to AFm-SO_4, AFt-SO_4, and calcium silicate hydrate (C-S-H) through mineral synthesis and contact with Se^{VI} in aqueous solution (Baur et al. 2003b). The researchers observed no significant Se^{VI} sorption to C-S-H and weak Se^{VI} sorption to AFt-SO_4 (Rd = 0.03) (Baur et al. 2003b). The researchers observed strong Se^{VI} sorption to AFm-SO_4 (Rd = 2.06) indicating that cement rich in AFm-SO_4 would significantly immobilize Se^{VI} (Baur et al. 2003b). Through XRD analysis, Baur and Johnson determined that Se^{VI} sorption increased $Ca_2[Al(OH)_6]^+$ layer spacing likely due to Se^{VI} replacing SO_4^{2-} (Baur et al. 2003b). Wu et al. demonstrated that AFm-Cl effectively and rapidly removed Se^{VI} from aqueous solutions through Se^{VI} exchanging for Cl^- in the interlayers (Wu et al. 2010). In general, AFm phases have shown significant affinity for immobilizing oxyanions through anion exchange (Goñi et al. 2001, Chrysochoou et al. 2006, Matschei et al. 2007, Wu et al. 2010).

AFt-SO_4^{2-} and AFm-X stabilities are both pH sensitive (Chrysochoou et al. 2006). AFt-SO_4 can form in the pH range of 11.0 to 13.0 (Chrysochoou et al. 2006), and begins to dissolve into $CaSO_4 \cdot 2H_2O$ and $Al(OH)_3$ when pH drops below 10.5 (Chrysochoou et al. 2006). AFm phases can form at pH values above 12.0 (Chrysochoou et al. 2006), and can dissolve when pH drops below 11.0 (Chrysochoou et al. 2006).

In general, the experimental results for BCFA S/S in this study (Figure 2.2) agree with the existing scientific literature on Se^{IV} and Se^{VI} immobilization mechanisms in cement-based S/S. Good retainment was seen for Se^{IV} but poor retainment for Se^{VI}. If any Se^{VI} were incorporated in the AFt or AFm phases in the BCFA S/S solids, a majority was probably dissolved in the lower pH conditions of the TCLP extractant.

FS addition increased Se^{VI} retainment. As mentioned, the components were mixed for 2 minutes prior to PC addition so that the simulated brine could react with Fe^{II} at lower pH conditions. Reduction of Se^{VI} (to Se^{IV}) by Fe^{II} was thermodynamically favorable in the simulated brine pH conditions. It is believed that the dominant mechanism for enhanced Se^{VI} retainment is reduction of Se^{VI} to Se^{IV} followed by precipitation as $CaSeO_3$ in the high Ca and high pH conditions of the process. Adsorption to the generated hydrous Fe^{III} oxides might contributed slightly to the overall immobilization of Se^{VI} and Se^{IV} (Cornelis et al. 2008a).

2.4.3 Impact of $FeSO_4$ Addition

Figure 2.3 shows the impact of FS dose added to the S/S mixture on the retainment of As^{V}, Cr^{VI} and Se^{VI}. A general trend of increasing heavy metal retainment was observed with increasing FS addition and the resulting mechanisms are likely the same as those discussed in the previous sections.

Notably, the addition of even a small quantity of FS increased the As^{V} retainment to nearly 100% (Figure 2.3). FS addition above 1% increased Cr^{VI} retainmnet to approximately 100% (Figure 2.3). The Figure shows that maximum Se^{VI} retainment was achieved with the addition of 2% to 6% FS. Note that FS addition decreased the strength of the solid and this effect became pronounced when FS addition exceeded 3%. Thus, FS addition should be optimized to minimize Se^{VI} leaching while maintaining the S/S solid strength.

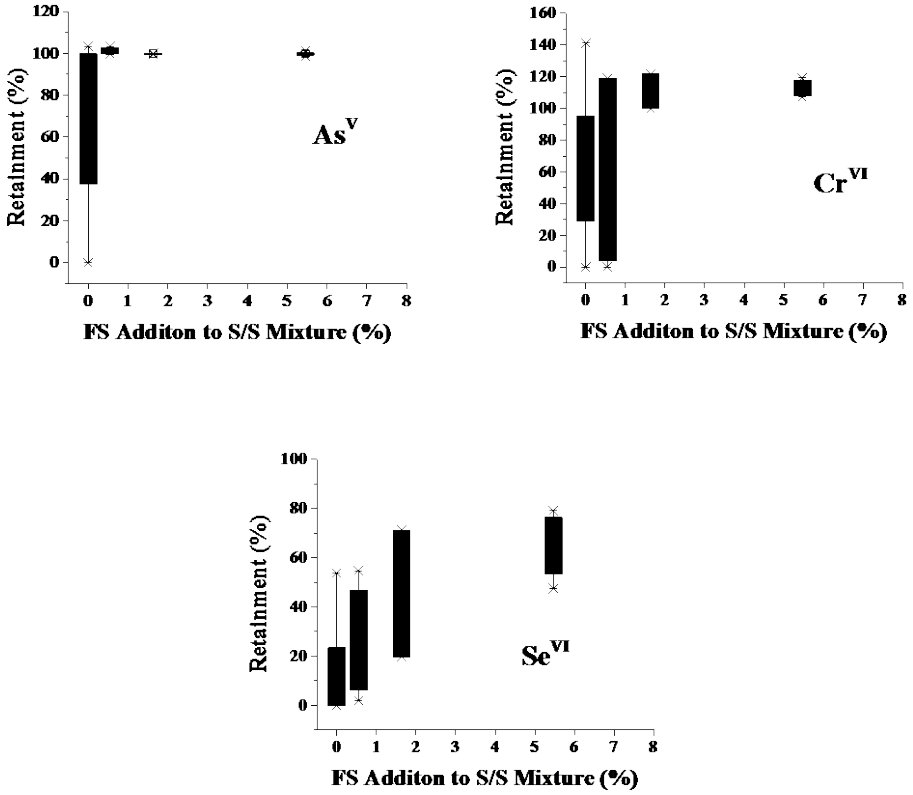

Figure 2.3. Impact of FS addition to S/S mixture on heavy metal retainment. S/S was conducted on concentrated simulated brines, BCFA, and PC.

2.4.4 Sorption Experiments

To obtain insight on the propensity of heavy metals to sorb to S/S solids, separate sorption experiments were conducted. S/S solids for the sorption experiments were prepared using a heavy metal-free simulated brine, BCFA, and PC. The ground and sieved S/S solids were contacted with simulated brines containing heavy metals. The TDS of the simulated brines was varied from 65,000 to 261,000 mg/L. No FS was added to the sorption experiments. Equation 2.2 was utilized to calculate the percent heavy metal sorption to the solid:

$$\%\,\boldsymbol{Sorption} = \left[1 - \frac{MD-MF}{MB}\right] * 100 \qquad (2.2)$$

MB was the mass of heavy metal in the brine solution in the sorption experiment; MD was the mass of heavy metal detected in the supernatant after the sorption experiment; and MF was the mass of heavy metal detected in the supernatant of the suspension with the heavy metal free simulated brine.

As Figure 2.4 shows, the sorption experimental results were similar to the S/S experimental results, i.e., good removal was seen for As^{V}, Cd^{II}, Hg^{II}, and Se^{IV} (average 56−100%) whereas poor removal was seen for Se^{VI} and Cr^{VI}. These results were similar to the results of S/S without FS addition, indicating that the same main immobilization mechanisms described in the earlier section are likely operative in the observed results in Figure 2.2.

Notably, Figure 2.4 shows a clear trend of decreasing Hg^{II} sorption with increasing TDS content of the simulated brine. This decrease in adsorption potential was likely due to Cl^{-}-complexation of Hg^{II} at the higher TDS values, which decreased the effective concentration thereby promoting Hg^{II} mobility to the liquid phase (Zhang et al. 2002). Comparatively, no similar trend of decrease in Hg^{II} retainment was seen for increasing TDS in the simulated brine in the S/S process (Figure 2.2). Zhang et al. found that increasing Cl^{-} did not impact the efficacy of a S/S process for a Hg-containing brine utilizing activated carbon (AC) and cement (Zhang et al. 2002). The authors suggested that the S/S process efficacy was not affected due to formation of a gel membrane during the cement hydration process on the outside of AC pores preventing mobilization of Hg (Zhang et al. 2002). While the current experiments did not include AC, McWhinney et al. indicated that precipitated HgO could potentially be protected from water (and therefore Cl^{-}) contact in S/S solids due to microencapsulation with $CaCO_3$ (McWhinney et al. 1990).

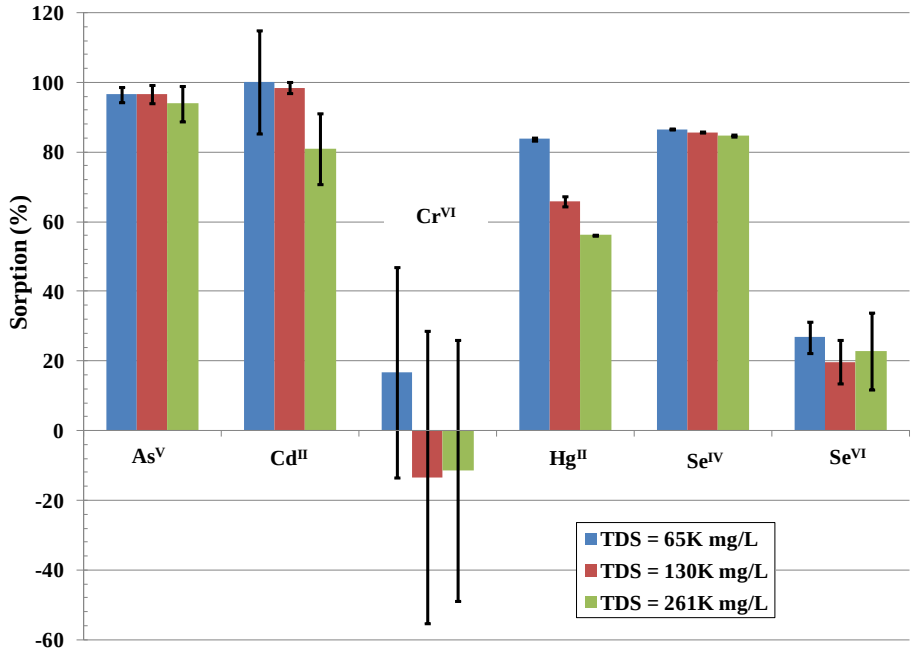

Figure 2.4. Sorption of heavy metals from brine solutions (TDS = 65K-261K mg/L) to the S/S solid. S/S solid was prepared from heavy metal-free simulated brine, BCFA and PC at mass ratio of 3:6:1. Note: For each TDS level, n = 6 for As^{V}, Cd^{II}, and Cr^{VI}; n = 4 for Se^{VI}; n = 2 for Hg^{II} and Se^{IV}.

2.4.5 Comparison of BCFA and SCFA in S/S

BCFA and SCFA S/S were conducted to compare the impact of CFA chemistry on the process (Figure 2.5). The S/S experiments were conducted utilizing the same simulated brine but slightly different S/S recipes. The BCFA S/S mixtures were 30% simulated brine, 60% BCFA, and 10% PC (ratio varied slightly to accommodate FS addition). The SCFA S/S mixture was 25% simulated brine, 65% SCFA, and 10% PC (ratio also varied slightly with FS addition). The recipe was adjusted because the initial SCFA S/S mixture appeared to have a water content that was too high. It is also noted that, although SCFA is a self-cementing CFA, PC was added in the S/S mixture so that the impact of CFA chemistry on the S/S process could be compared. Figure 2.5 shows the final TCLP leachate pH for the S/S solids.

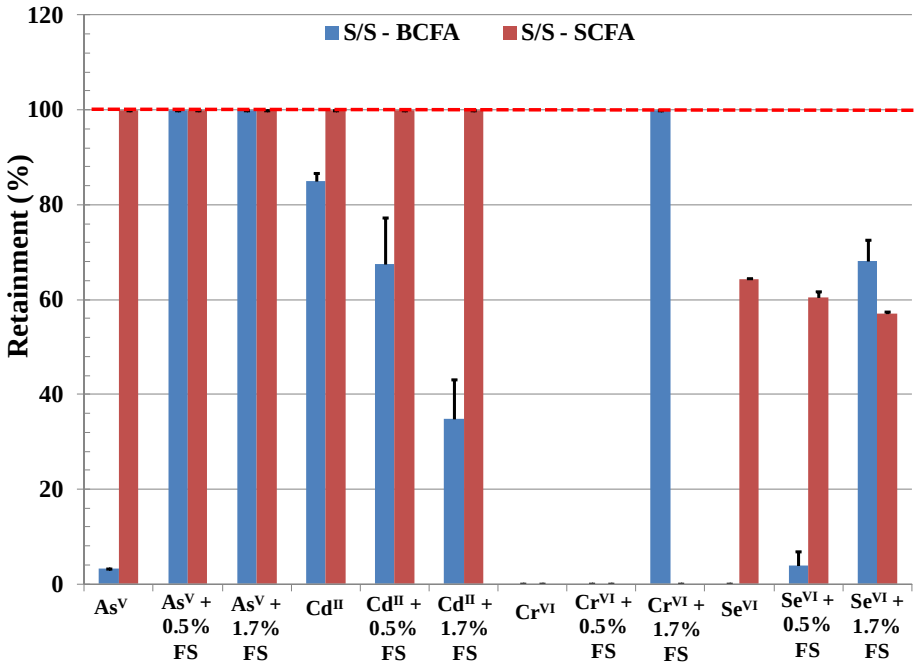

Figure 2.5. TCLP evaluation of heavy metal retainment by S/S with BCFA versus with SCFA. S/S was conducted by mixing simulated brine, BCFA and PC at mass ratio of 3:6:1, or by mixing simulated brine, SCFA and PC at mass ratio of 2.5:6.5:1. The ratio was slightly varied when FS addition was included.

The results show that SCFA S/S was more effective than BCFA S/S immobilizing As^V without FS addition (Figure 2.5). Note that As^V retainment results in BCFA S/S in this set of experiments was atypically low (average 3.3%) compared to the typical retainment values observed (17.6-103.3%); nevertheless, the trend of SCFA S/S being more effective was still valid. The better performance of SCFA S/S was likely due to the higher SCFA CaO content compared to BCFA (28.1% versus 1.6%) which increased the pH. The final TCLP leachate pH for SCFA S/S solid was higher than the BCFA S/S solid (9.7 versus 7.8) (Figure 2.6). Ca-As^V complexes are less soluble at the higher pH. In addition, more Ca was added to the S/S mixture with SCFA which also promoted Ca-As^V complex precipitation. With the addition of only 0.5% FS, As^V retainment increased to approximately 100% for the BCFA S/S likely due to As^V sorption to produced Fe^{III} oxides.

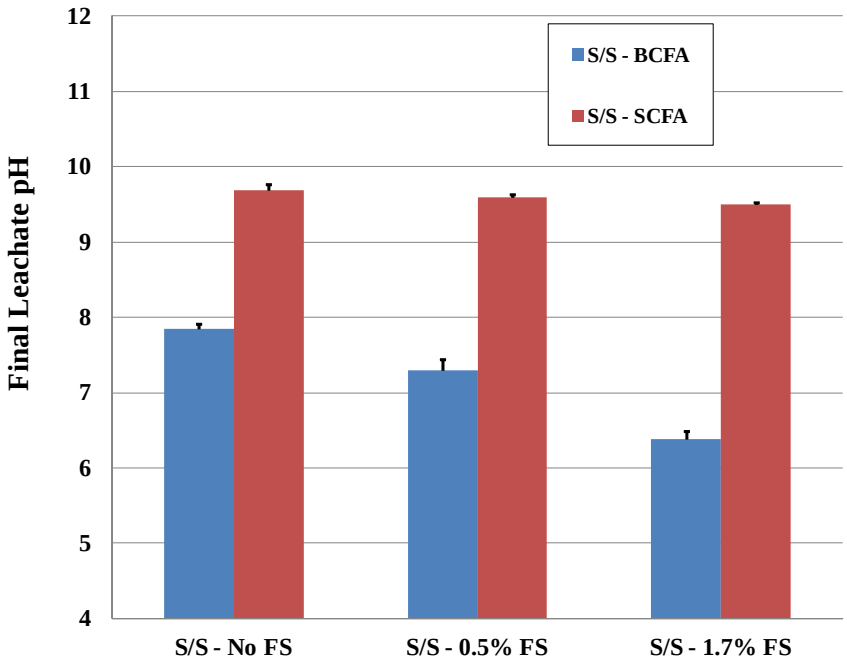

Figure 2.6. Final TCLP leachate pH of S/S solids made with BCFA versus with SCFA. The S/S samples were the same as those shown in Figure 2.4.

SCFA S/S was more effective than BCFA S/S immobilizing Cd^{II} (Figure 2.5). The better performance of SCFA S/S was likely due to the higher pH of SCFA S/S, as Cd^{II} is insoluble as $Cd(OH)_2$ at high pH conditions. Note the decreasing trend of final TCLP leachate pH with increasing FS addition for both CFA S/S processes, with the trend more pronounced for BCFA S/S than for SCFA S/S (Figure 2.5). As a result of this trend, Cd^{II} retainment decreased with increasing FS addition for more for BCFA S/S, from 85% (final leachate pH = 7.8) with no FS addition to 35% (final leachate pH = 6.4) with 1.7% FS addition.

Figure 2.5 shows that neither the BCFA nor SCFA S/S was effective immobilizing Cr^{VI}. However, BCFA S/S with the addition 1.7% FS completely stabilized Cr^{VI} likely due to Cr^{VI} reduction to Cr^{III} followed by Cr^{III} incorporation into the Ca-Al^{III}-hydrate phase, sorption to produced Fe^{III} oxides, or precipitation of $Cr(OH)_3$. FS addition did not enhance

Cr^{VI} immobilization in SCFA S/S. As mentioned previously, during the first 2 min of the S/S process, the CFAs, FS, and simulated concentrated wastewater were mixed prior to PC addition. The S/S mixture pH during the first 2 min period was much higher for SCFA versus BCFA S/S. The higher pH for SCFA S/S during this initial period hindered the ability of FS to reduce Cr^{VI} (Connor 1997).

Figure 2.5 shows that SCFA S/S was more effective than BCFA S/S immobilizing Se^{VI}. We propose that two mechanisms likely contributed to these results. The first mechanism was Se^{VI} incorporation into AFm phase structure. As mentioned, AFm-X can effectively immobilize Se^{VI} by exchanging for the anion (X) in the interlayer structure. Since AFm phases form at higher pH values, the higher SCFA S/S conditions likely enhanced AFm phase formation and Se^{VI} retainment (Chrysochoou et al. 2006). Although the AFm-Se^{VI} may begin to dissolve at the lower pH conditions of the TCLP test (Chrysochoou et al. 2006), it is possible that the phase did not completely dissolve during the TCLP test, thus exhibiting significant Se^{VI} retainment. Figures 2.5 and 2.6 shows that as the final TCLP leachate pH decreased for the SCFA S/S solids so did the Se^{VI} retainment likely due to more AFm phase dissolving and releasing Se^{VI}.

The second proposed Se^{VI} immobilization mechanism was Se^{VI} reduction by FS. Figure 2.5 shows that FS addition increased the Se^{VI} immobilization for BCFA S/S. This result was observed although the final TCLP leachate pH decreased with increasing FS addition (Figure 2.6). Thus, the likely dominant Se^{VI} immobilization mechanism was reduction to Se^{IV} followed by $CaSeO_3$ precipitation. With the addition of 1.7% FS to the BCFA S/S process, Se^{VI} retainment was at the highest level, approximately 68%, for either CFA S/S process.

Further evidence for these two proposed immobilization mechanisms is provided by the results of the USEPA Method 1313 evaluation (USEPA 2012). The solids evaluated by this method included BCFA S/S solids with 1.7% FS addition and SCFA S/S solids with no FS addition. These were the solids with the highest Se^{VI} retainment for each of the CFA S/S processes. By adjusting the final leachate pH for both S/S solids to be similar (both near 7.0 or 9.0), the impact of the Se^{VI} controlling phases on retainment can be more directly compared. Note that the final leachate pH for one of the target pH 9.0 samples drifted slightly lower to 8.0; however, this sample is included as this pH is within range of interest (Figure 2.7).

Figure 2.7 shows that Se^{VI} retainment by the BCFA S/S solid was hardly impacted by lowering the final leachate pH from 9.0 to 7.0. In contrast, Se^{VI} retainment by the SCFA S/S solid showed considerable decrease (59% to an average of 54.5%) with decreasing leachate pH. These results strongly suggest that Se release is controlled by two different phases in the SCFA S/S solid and BCFA S/S solid.

The Figure 2.7 data supports AFm-Se^{VI} solubility controlling Se release from the SCFA S/S solid and $CaSeO_3$ solubility controlling Se release from the BCFA S/S solid. AFm-Se^{VI} solubility is more pH sensitive than $CaSeO_3$ in the pH range relevant to the USEPA Method 1313 evaluation (Page et al. 1983, Suryavanshi et al. 1996b, Glass et al. 2000a, Glass et al. 2000b, Reddy et al. 2002, Baur et al. 2003a, Nishimura et al. 2007, Nishimura et al. 2009).

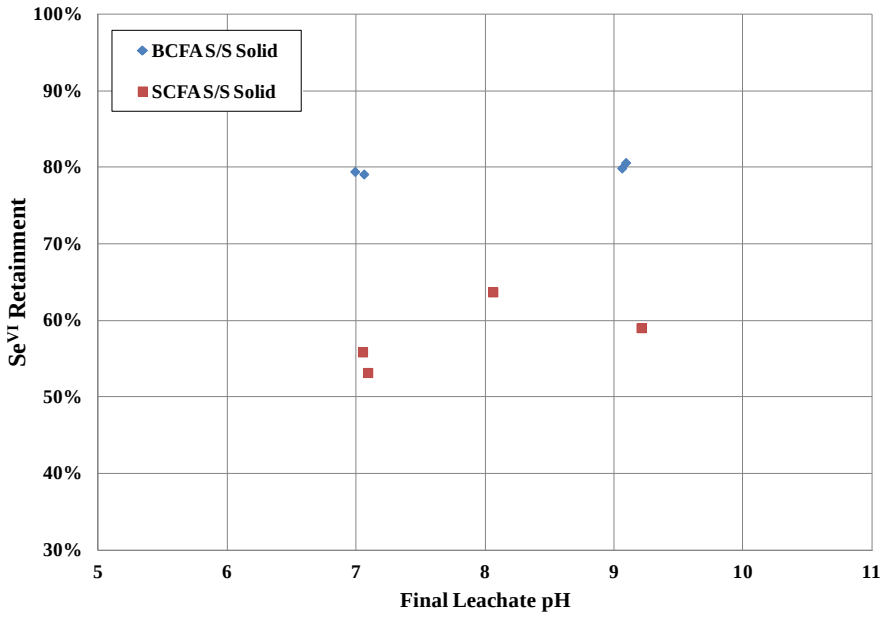

Figure 2.7. Se^{VI} retainment by S/S with BCFA versus with SCFA evaluated using the USEPA Method 1313. The BCFA S/S solid was prepared by mixing simulated brine, BCFA, PC and $FS{\cdot}7H_2O$ at mass ratio of 9.3:19.7:3.3:1.0. The SCFA S/S solid was prepared by mixing simulated brine, SCFA and PC at mass ratio of 2.5:6.5:1.0 without FS addition.

Comparison between $CaSeO_3$ solubility (experimental) versus pH graphs by Nishimura and Hata and AFm-Se^{VI} solubility (thermodynamically modeled) versus pH graphs calculated by Baur and Johnson indicate that AFm-Se^{VI} solubility increases at a higher rate with decreasing pH than $CaSeO_3$ (Nishimura et al. 2007, Nishimura et al. 2009). Moreover, previous research has shown that Cl^--containing minerals in cement such as AFm-Cl significantly release Cl^- as pH decreases due to dissolution (Page et al. 1983, Suryavanshi et al. 1996b, Glass et al. 2000a, Glass et al. 2000b, Reddy et al. 2002). Reddy et al. observed that essentially 100% of the acid-soluble Cl^- present in a cement material was released as the pH dropped from an initial value of 12.75 to 11.0 over 10 days; much of the acid-soluble Cl^- in the cement material was expected to be present in AFm-Cl which would likely have a similar solubility to AFm-Se^{VI} (Reddy et al. 2002).

2.4.6 X-Ray Diffraction Analyses

Figure 2.8 shows the XRD patterns for BCFA, BCFA S/S solid, SCFA, and SCFA S/S solid. The XRD pattern of PC is shown in Figure 2.9. The recipe for the BCFA S/S solid was 24.4% simulated brine, 62.0% BCFA, 10.0% PC, and 3.7% FS. The recipe for the SCFA S/S solid was 25.0% simulated brine, 65.0% SCFA, and 10.0% PC.

Figure 2.8 shows that the largest difference between the SCFA and SCFA S/S XRD diffractograms is the presence of Friedel's salt (AFm-Cl) in the SCFA S/S solid. The presence of AFm-Cl was confirmed by the peaks at 2Θ values of 11.3, 22.7, and 23.4, which match with the AFm-Cl XRD patterns in the databases of the International Center for Diffraction Data (Table 2.5) and in multiple previous studies (Renaudina et al. 1999, Goñi et al. 2001, Balonis et al. 2010). AFm phase formation in the SCFA S/S solid is logical. SCFA S/S mixture contains large quantities of the necessary chemical components for AFm phase formation-CaO and Al_2O_3. Both SCFA and PC contain a large CaO component as shown in the XRF analysis (Figure 2.1) and the XRD diffractogram (Figure 2.8). In addition, the SCFA S/S solid pH is high due to the higher than BCFA due to this CaO content (Chrysochoou et al. 2006). Figure 2.8 shows that SCFA contains significant amount of tricalcium aluminate ($3CaO{\cdot}Al_2O_3$ or C_3A), and cements high in C_3A are known to promote AFm phase formation due to high reactive Al_2O_3 content (Suryavanshi et al. 1996a). The high Cl^- content added from the simulated brine would promote Cl^- as the major anion in the AFm phase as addition of NaCl and $CaCl_2$ has been shown to enhance AFm-Cl fomation in cements (Suryavanshi et al. 1996a).

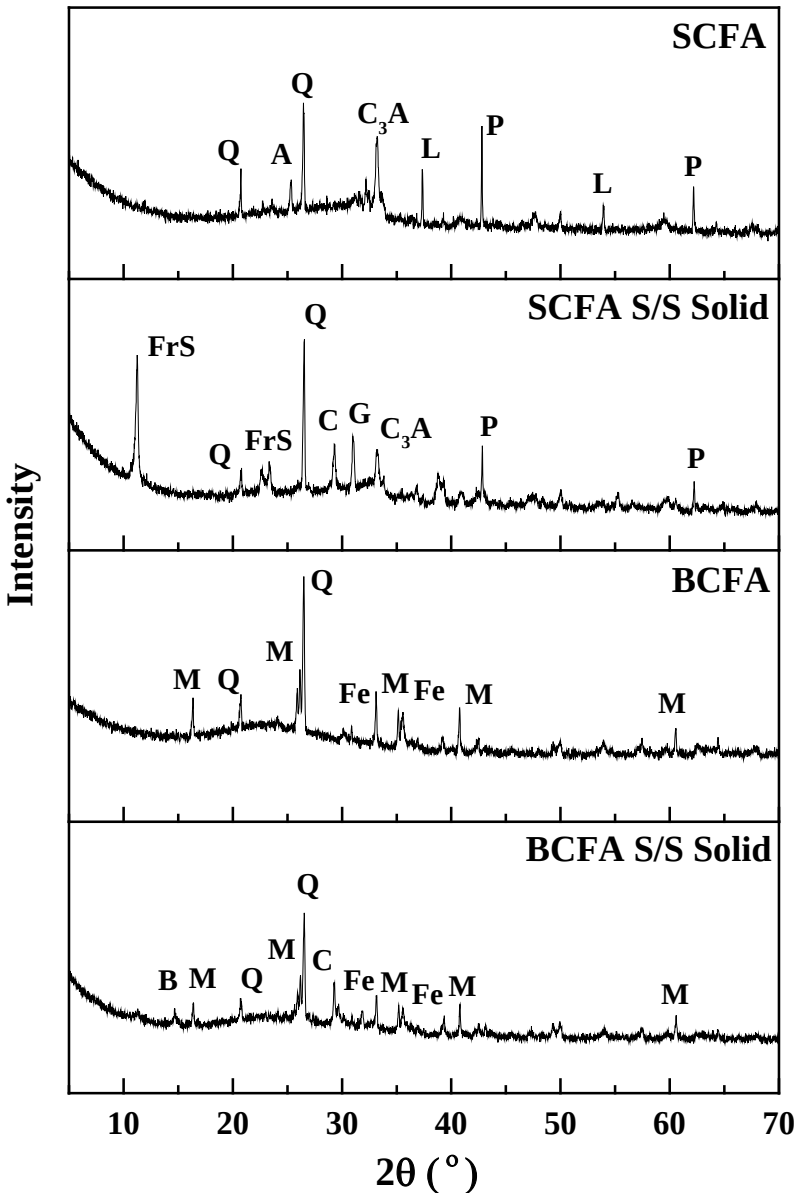

Figure 2.8. XRD patterns of SCFA, SCFA S/S solid, BCFA, and BCFA S/S solid. The SCFA S/S solid was made by simulated brine, SCFA and PC at mass ratio of 2.5:6.5:1. The BCFA S/S solid was made by simulated brine, BCFA, PC and FS at mass ratio of 2.44:6.2:1:0.37. A, anhydrite; B, bassanite; C, calcium carbonate; C_3A, tricalcium aluminate, Fe, iron oxide (Fe_2O_3); FrS, Friedel's salt; G, gypsum; L, lime; M, mullite; P, periclase; Q, quartz.

The main crystalline phases of SCFA included CaO (lime), $CaSO_4$ (anhydrite), C_3A, MgO (periclase) and SiO_2 (quartz). The main crystalline phases for the SCFA S/S solids included AFm-Cl, $CaCO_3$ (calcium carbonate), C_3A, $CaSO_4.2H_2O$ (gypsum), MgO and SiO_2 (Figure 2.8 and Table 2.5). The results indicate that a portion of the CaO in the

SCFA is consumed during the cement hydration process as expected. In addition, a portion of the $CaSO_4$ hydrated to form $CaSO_4.2H_2O$.

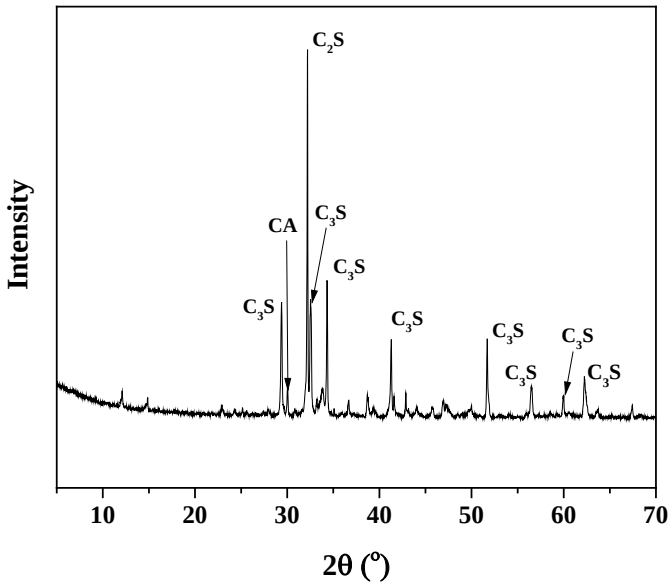

Figure 2.9. XRD diffractogram for PC. CA, calcium aluminate; C_2S, dicalcium silicate; and C_3S, tricalcium silicate.

The main mineral phases for BCFA were $3Al_2O_3 \cdot 2SiO_2$ (mullite), SiO_2 (quartz) and Fe_2O_3 (iron oxide). The main mineral phases for the BCFA S/S solid were the same as for the BCFA with the addition of $CaSO_4 \cdot 0.5H_2O$ (bassanite) and $CaCO_3$ (Figure 2.8 and Table 2.5). More Fe_2O_3 was observed in the BCFA S/S solid versus the BCFA; the increased presence of Fe_2O_3 is likely due to FS addition to the S/S mixture. A very small amount of AFm-Cl could be present in the BCFA S/S XRD diffractogram, but the peak at 11.3 was not intense enough for positive identification.

Table 2.5. Peaks utilized to identify minerals in XRD diffractograms.

(a) SCFA

Mineral	2Θ for Identified Peaks (°)	Reference PDF No.
A	25.3	00-037-1496
C_3A	33.2	00-038-1429
L	37.3 and 53.9	00-037-1496
P	42.8 and 62.2	00-004-0829
Q	20.7 and 26.5	00-033-1161

(b) SCFA S/S Solid

Mineral	2Θ for Identified Peaks (°)	Reference PDF No.
C	29.3	00-005-0586
C_3A	33.2	00-038-1429
FrS	11.3, 22.7, and 23.3	00-078-1219
G	31.0	00-021-0816
P	42.9 and 62.2	00-004-0829
Q	20.8 and 26.5	00-033-1161

(c) BCFA

Mineral	2Θ for Identified Peaks (°)	Reference PDF No.
Fe	33.1 and 35.6	01-072-6226
M	16.4, 26.1, 35.2, 40.8, and 60.5	00-015-0776
Q	20.7 and 26.5	00-033-1161

(d) BCFA S/S Solid

Mineral	2Θ for Identified Peaks (°)	Reference PDF No.
B	14.7	01-074-2787
C	29.3	00-005-0586
Fe	33.1 and 35.6	01-072-6226
M	16.4, 26.2, 35.2, 40.8, and 60.6	00-015-0776
Q	20.7 and 26.5	00-033-1161

Note - Reference XRD diffractograms are from the database of the International Center for Diffraction Data.

Fewer differences exist between the XRD diffractograms of BCFA and the BCFA S/S solid, compared to SCFA and the SCFA S/S solid (Figure 2.8). The most obvious difference between the two CFAs is the higher CaO content of SCFA. In addition, although BCFA has a larger total Al_2O_3 content (amorphous and crystalline) (Figure 2.1), SCFA could have larger reactive Al_2O_3 content due to most of the crystalline Al_2O_3 being present as C_3A in SCFA versus inert, non-reactive mullite in BCFA. The greater SCFA reactive Al_2O_3 content promotes cement hydration reactions and AFm phase formation.

2.4.7 Environmental Relevance

The advantage of the AFm-Se^{VI} solubility controlling mechanism is that no reductant addition is necessary. However, the AFm-Se^{VI} mechanism may not be as robust under a landfill disposal scenario as the FS reduction mechanisms because landfill leachate pH will decrease over time. For alkaline CFA, the initial landfill leachate pH can range for 10.5 to 11.0; however, geochemical controls can cause the leachate pH to decrease to a typical range of 8.0 to 9.0 over time due to the exhaustion of Ca and Mg oxides (Talbot et al. 1978, Roy et al. 2011). CaO will also be exhausted from the S/S solids over time and the pH will decrease and as leachate pH decreases, a significant amount of the AFm-Se^{VI} may dissolve releasing Se^{VI} to the environment. A better long-term disposal strategy for the S/S process may be Se^{VI} reduction to Se^{IV} followed by $CaSeO_3$ precipitation which is less soluble than AFm-Se^{VI} at environmentally relevant neutral pH conditions due to it's higher thermodynamic stability.

2.5 CONCLUSIONS

Overall, the evaluated S/S process achieved good retainment (average of 68−90%) for As^{V}, Cd^{II}, Hg^{II}, and Se^{IV}. The addition of FS could enhance the retainment of As^{V}, Cr^{VI}, and Se^{VI}. The addition of even a very small amount of FS increased the retainment of As^{V} to approximately 100% likely due to formation of Fe^{III} oxides that are good absorbents for As^{V}. FS addition reduced brine's Cr^{VI} to Cr^{III}, which enhanced immobilization by incorporation of Cr^{III} into Ca-Al^{III}-hydrate phase, sorption of Cr^{III} to Fe^{III} oxides, and precipitation of $Cr(OH)_3$. Some of the Cr^{VI} from the CFA was also reduced and immobilized likely via the same mechanisms. The mechanism of enhanced immobilization of Se^{VI} by FS addition was likely reduction to Se^{IV} and $CaSeO_3$ precipitation.

The S/S results generally agreed well with the sorption experiment results, in which good sorption to the S/S solid was seen for As^{V}, Cd^{II}, Hg^{II}, and Se^{IV} (average of 56−100%) while poor sorption was seen for Cr^{VI} and Se^{VI}. The sorption experiments also revealed a decrease in Hg^{II} sorption with increasing TDS content of the brine due to the Cl^{-}-complexation of Hg^{II}.

Comparison between BCFA and SCFA S/S indicated that SCFA S/S solids had greater retainment of As^{V}, Cd^{II}, and Se^{VI} compared to BCFA S/S solids. As^{V} retainment was likely enhanced by the higher pH and CaO content, Cd^{II} by better $Cd(OH)_2$ stability at the higher pH condition, and Se^{VI} by SeO_4^{2} substitution in the AFm phase produced at the higher pH, CaO content, and reactive Al_2O_3 content of SCFA S/S. Support for this proposed mechanism was provided by identification of AFm-Cl in the SCFA S/S solid

utilizing XRD. XRD diffractograms showed that SCFA was more reactive in the S/S process than BCFA.

However, utilization of thm-SeO_4 stabilization mechanism may not be sustainable for safe long-term landfill disposal. Reduction of Se^{VI} plus S/S may be a better long-term strategy than AFm substitution under environmentally relevant pH conditions.

CHAPTER 3. MASS TRANSPORT RELEASE OF HEAVY METAL OXYANIONS FROM SOLIDIFIED/STABILIZED CO-DISPOSED FLUE GAS DESULFURIZATION BRINE AND COAL FLY ASH MONOLITHS

3.1 ABSTRACT

The United States (US) coal-fired power industry is facing increasing pressure to improve wastewater disposal practices. One of the most pressing waste disposal issues is the treatment of flue gas desulfurization (FGD) wastewater. Zero liquid discharge (ZLD) strategies are gaining significant interest in the industry and can include the coupling of a brine concentrator and solidification/stabilization (S/S) process. This current project evaluated the mass transport release of major components (Ca^{2+}, Cl^{-}, Mg^{2+}, Na^{+}, and SO_4^{2-}) and heavy metal oxyanions (As, Cr, and Se) from solids produced by this process utilizing a United States Environmental Protection Agency (USEPA) Method 1315 evaluation. This study evaluated the impact of $FeSO_4$ (FS) addition to the S/S mixture on the process. FS addition to the S/S process decreased the solid's cumulative release and flux at shorter leaching times for the major components: Ca^{2+}, Cl^{-}, Mg^{2+}, Na^{+}, and SO_4^{2-}; however, this impact was only transient. FS addition significantly decreased release of oxyanions As, Cr, and Se. The results indicate that FS addition could increase the likelihood of successful long-term disposal of S/S solids of concentrated FGD brines containing these heavy metal oxyanions. Leach XS^{TM} modeling added additional evidence for the proposed leaching mechanisms for As and Se.

3.2 INTRODUCTION

The United States (US) coal-fired power industry is facing increasing pressure to improve wastewater treatment and disposal practices. One of the industry's most important waste disposal issues concerns flue gas desulfurization (FGD) wastewater. The US Environmental Protection Agency (USEPA) recently released the proposed revision to the Steam Electric Power Effluent Limitation Guidelines (ELG) which regulate FGD wastewater treatment and includes limits for As, Hg, NO_2^-/NO_3^-, and Se (USEPA 2015).

FGD wastewater is a complex and difficult to treat water matrix with significant heavy metal content (As, Cd, Cr, Hg, and Se) and large salt content (Ca^{2+}, Mg^{2+}, Na^+, SO_4^{2-}, and Cl^-) (USEPA 2009). Concern exists that currently proposed conventional treatment technologies may not reliably meet the proposed ELG limits. Zero liquid discharge (ZLD) strategies are gaining significant interest due to the certainty of meeting ELG limits, elimination of an environmental wastewater discharge, and potential water reuse maximization in coal-fired power plants.

Any ZLD strategy for FGD wastewater will likely include volume reduction as a first step utilizing an advanced membrane or an evaporation process. The produced concentrated FGD brine from the volume reduction step will then likely be solidified/stabilized (S/S). S/S consists of two processes: solidification (producing a solid product with improved physical properties) and stabilization (converting a contaminant to its less mobile and less toxic forms) (Batchelor 2006). S/S typically includes mixing of wastes (liquids, sludges, brines or solid waste) with Portland cement (PC), PC/coal fly ash (CFA), CaO/CFA, or $Ca(OH)_2$/CFA (Kameswari et al. 2001, Keller 2002, Batchelor 2006,

Qian et al. 2006, Singh 2006, Ramgobeen 2010). The process "has been identified by the USEPA as the Best Demonstrated Available Technology for 57 regulated hazardous wastes" (Batchelor 2006). It should be noted that although ZLD strategies have the advantage of producing no liquid discharge, this strategy greatly increases solid waste challenges as the FGD wastewater metals and salts must be successfully stabilized for the long term in an industry landfill.

We previously demonstrated the promising success of this ZLD strategy producing stabilized S/S solids with low heavy metal leaching potential (Renew et al. 2016b). This work evaluated metal leaching through the toxicity characteristic leaching procedure (TCLP) (USEPA 1992a) and USEPA Method 1313 (liquid-solid partitioning as a function of extract pH using a parallel batch extraction procedure) (USEPA 2012). Our previous work demonstrates that S/S using bituminous coal fly ash (BCFA) can achieve good retainment (68-90%) for As^{V}, Cd^{II}, Hg^{II} and Se^{IV}; however, good retainment for Cr^{VI} and Se^{VI} oxyanions requires addition of a reductant such as $FeSO_4$ (FS). FS reduces Se^{VI} to Se^{IV}, which is immobilized by forming $CaSeO_3$ precipitate in the S/S solids; however, it's challenging to increase the retainment efficiency above 60% without a significant addition of FS (>2% by weight) (Renew et al. 2016b).

The current study focuses on leaching of the major components and heavy metal oxyanions from the S/S solids utilizing USEPA Method 1315 (Mass Transfer Rates of Constituents in Monolithic or Compacted Granular Materials Using a Semi-Dynamic Tank Leaching Procedure) (USEPA 2013). Unlike batch extraction methods (TCLP and USEPA Method 1313), USEPA Method 1315 can elucidate further understanding of contaminant release: (1) over a significant time period and (2) "the result of diffusion through a tortuous

pore network with aqueous partitioning at the solid–liquid interface" (De Windt et al. 2007, Garrabrants et al. 2014). Leaching from solid monoliths rather than crushed solids are evaluated in this method which more closely resembles a leaching scenario for an actual S/S solid disposal process (USEPA 2013). Deionized water is the leachate for this method which results in pH conditions closer to an actual S/S disposal scenario compared to the TCLP which is designed to replicate a municipal solid waste disposal scenario (Garrabrants et al. 2014).

The objective of this study was to evaluate the mass transport release of the major components (Ca^{2+}, Cl^-, Mg^{2+}, Na^+, and SO_4^{2-}) and the heavy metal oxyanions (As, Cr, and Se) utilizing USEPA Method 1315. Little Cd leaching was observed in the experiments so Cd was not included in the study. The impact of FS addition on the mass transport release of the elements was evaluated. Parallel to the leaching experiments, Ca^{2+}, Cl^-, Na^+, As, and Se leaching from the S/S solids was modeled utilizing the LeachXS^{TM} software which provided insight into leaching mechanisms (Seignette et al. 2014).

The S/S solids were produced by mixing BCFA, PC, and simulated concentrated FGD brine with increasing amounts of FS. This scenario chosen for these experiments represents the most challenging FGD brine disposal scenario for power plants that (1) utilize bituminous coal and (2) have forced-oxidation scrubbers. Because bituminous coal contains more sulfur than sub-bituminous coal, power plants that use this coal generate a larger volume of FGD wastewater with higher concentrations of heavy metals and salts (USEPA 2009). Approximately 48% of the coal produced in the US is bituminous and 44% is sub-bituminous (USEIA 2015b). As the name implies, forced-oxidation FGD systems bubble air through the FGD slurry to oxidize $CaSO_3$ to $CaSO_4 \cdot 2H_2O$ (gypsum), a product

with commercial value. This process can also oxidize heavy metals, including Se and Cr to their more mobile and toxic forms making the produced brine more difficult to treat or manage.

3.3 EXPERIMENTAL SECTION

3.3.1 Materials

CFA was obtained from a bituminous coal-fired power plant in the southeastern United States. PC was obtained from Home Depot (Cartersville, Georgia). Simulated concentrated FGD brine was obtained from a power company, and the composition is detailed Table 3.1. The simulated brine was analyzed for metals utilizing inductively coupled plasma-mass spectrometry (ICP-MS) (Series 7700, Agilent Technologies, Santa Clara, California) through a combination of USEPA Methods 200.8 and 6020a (USEPA 1994a, USEPA 2007). The brine sample was digested by adding 5% HNO_3/5%HCl and heating the sample for 1 h at approximately 95 ^oC. After cooling, the samples were analyzed utilizing ICP-MS. Anions were analyzed utilizing USEPA Method 300.0 by ion chromatography (IC) (Dionex ICS-5000 DP, ThermoFisher, Waltham, Massachusetts) (USEPA 1993). Ferrous sulfate ($FeSO_4 \cdot 7H_2O$, FS) was obtained from Fisher Scientific (Pittsburgh, PA).

Table 3.1. Simulated FGD brine composition.

(a) Bulk Elements

Element	Concentration (µg/L)
Ca	33,664,945
Mg	3,312,244
Na	2,187,124
K	745,440
Si	110,445
Sr	195,860

(b) Trace Elements

Element	Concentration (µg/L)
Sb	101
As^{V}	1,916
Ba	2,872
B	4,676
Cd	9,163
Cr^{VI}	863
Cu	292
Fe	2,581
Pb	28
Hg	1,060
Mo	16
Se^{VI}	17,971
Ag	36
Ti	45

(c) Anions

Element	Concentration (mg/L)
Br^{-}	1.3
Cl^{-}	80,270
F^{-}	< 0.5
NO_2^{-} (as N)	581
NO_3^{-} (as N)	50
SO_4^{2-}	245
PO_4^{3-} (as P)	< 0.5

The simulated brine whose chemical content is shown in Table 3.1 contained high Ca^{2+}, Mg^{2+}, and Na^{+} concentrations (2,000-34,000 mg/L). The anion with the highest concentration was Cl^{-} (80,000 mg/L). The brine also contained significant As^{V}, Cd^{II}, Cr^{VI}, Hg^{II}, and Se^{VI} content with concentrations varying from 900-18,000 µg/L. As, Cr, and Se were added to the simulated brine at the highest oxidation state to simulate forced-oxidation FGD scrubber conditions.

3.3.2 Solids Analysis

CFA and PC were digested utilizing a modified version of the USEPA Method 3052 (USEPA 1996b). In this modified method, 0.2 grams of the solid were digested in a 10 mL mixture of 10%HF-20%HCl-20%HNO_3-50%H_2O. After the first stage of heating in the microwave assisted digester, 40 mL of water was added to the closed vessel and the mixture was heated again. Digestates were analyzed utilizing a combination of the USEPA Methods 200.8 and 6020a (USEPA 1994a, USEPA 2007).

3.3.3 Solidification/Stabilization

BCFA was mixed with the simulated brine and FS (if applicable) for 2 min in a benchtop mixer. Table 3.2 shows the formulations of the 4 mixtures in the project. After 2 min, PC was added to the mixture and the mixture was homogenized for an additional 18 min. The resulting cement slurry mixture was then poured into 7.62-cm diameter × 15.24-cm (cut to a height of 9.52-12.54 cm) plastic forms. The S/S solid was allowed to cure for 58-62 days. Table 3.3 shows the mass, surface area, and leachate interval volume for the monolith samples during the USEPA Method 1315 evaluation.

3.3.4 USEPA Method 1315

Samples were placed in containers and on stands according to the requirements of USEPA Method 1315 (USEPA 2013). The leachant was deionized water. The monolith surface area to leachant volume for all samples was approximately 10.0 mL/cm^2. The leachant was refreshed at cumulative leaching times of 0.08, 1.04, 2, 7, 14, 35, 49, 78, and 119 days except that leaching for Mixture B was stopped after 49 days due to loss of a sample.

Table 3.2. S/S mixtures.

Mixture	Simulated Brine	BCFA	$FS{\cdot}7H_2O$	PC
A	26.20%	63.8%	0.0%	10.0%
B	25.30%	62.9%	1.8%	10.0%
C	24.40%	62.0%	3.7%	10.0%
D	23.50%	61.0%	5.5%	10.0%

Table 3.3. S/S solid mass, surface area, and interval leachate volume.

Mixture	Mass (grams)	Surface Area (cm^2)	Leachate Volume (mL)	Leachate Volume/Surface Area (mL/cm^2)
A	717	319	3,190	10.0
B	860	342	3,420	10.0
C	812	384	3,830	10.0
D	834	391	3,910	10.0

These leachate refreshment intervals differ somewhat from those suggested by USEPA Method 1315. Leachate samples were taken at the end of each interval through filtration utilizing 0.45-µm mixed cellulose ester (MCE) filters (Fisher Scientific). The conductivity, oxidation reduction potential (ORP), and pH of the leachate samples were immediately measured after filtration. The filtered leachate was also analyzed for metals utilizing a combination of the USEPA Methods 200.8 and 6020a or USEPA Method 200.8

with ICP-MS (USEPA 1994a, USEPA 2007). The filtered leachate samples for analysis by the combination of USEPA Methods 200.8 and 6020a were digested as described for the brine sample in Section 3.3.1 before ICP-MS analysis. When a few amount of the samples were measured by USEPA Method 200.8 only, the filtered leachate samples were digested and prepared per USEPA Method E200.2 (USEPA 1994b). The leachate samples were analyzed for Cl^- and SO_4^{2-} utilizing the USEPA Method 300.0 with IC (USEPA 1993).

3.3.5 USEPA Method 1313

The S/S solid samples were also subjected to leaching by the USEPA Method 1313 at a target pH of 2.0±0.5 (USEPA 2012). This method was applied to determine the element concentration available for leaching. Preliminary titration tests were conducted to determine the amount of HNO_3 needed to adjust the final leachate pH to 2.0±0.5. Approximately 2 g of solid was mixed with 20 mL of deionized water with HNO_3 addition. Samples were tumbled for 24 hours. After filtering with a 0.45-µm MCE filter, the leachate was analyzed for metals utilizing ICP-MS through a combination of the USEPA Methods 200.8 and 6020a (USEPA 1994a, USEPA 2007) and for anions utilizing the USEPA Method 300.0 with IC (USEPA 1993). Prior to ICP-MS analysis the filtered leachate samples were digested as described for the brine in Section 3.3.1.

3.3.6 Establishment of LeachXS™ Model

LeachXS™ Version 2.0.87 (Seignette et al. 2014) was utilized to model Ca^{2+}, Cl^-, Na^+, As, and Se release from the S/S solid for Mixture A during the USEPA Method 1315 evaluation. As and Se were selected for the model because these two heavy metals along with Hg are most associated with FGD wastewater and are part of the proposed final

revision to the ELGs. Cl^- was selected as it is an important contaminant for FGD wastewater disposal due to it's high content in FGD wastewater and high solubility. Ca^{2+} and Na^+ were included in the model for calibration purposes and their high content in FGD wastewater.

LeachXS^{TM}-ORCHESTRA, developed by the Vanderbilt University (Meeussen 2003, van der Sloot et al. 2012, Seignette et al. 2014). Table 3.4 shows the geometric and physical parameters of the S/S solid that were input into the model.

The S/S monolith column was divided into 20 sections that extended into the column structure. The existing mineral phases already present in the LeachXS^{TM} model did not yield an acceptable match between observed and modeled data for As; hence, a new phase was added for As. A candidate phase, $NaCaAsO_4 \cdot 7.5H_2O$, was selected for modeling purposes as this phase has been identified by previous researchers as the dominant As^V mobility in an As-contaminated soil S/S with cement kiln dust (CKD), in CFA spiked with As salts, and in kaolinite slurries treated with lime (Akhter et al. 1997, Bothe et al. 1999, Moon et al. 2004, Moon et al. 2008). No Log K values for $NaCaAsO_4 \cdot 7.5H_2O$ was found in literature so the Log K value was modeled utilizing Equation 3.1.

$$NaCaAsO_4 \cdot 7.5H_2O = Na^+ + Ca^{2+} + AsO_4^{3-} + 7.5H_2O \quad (3.1)$$

Through modeling, the Log K value for the above equation was varied until the modeled results closely matched the experimental results. The Log K value was found to be approximately 8.0. Although modeling does not prove that $NaCaAsO_4 \cdot 7.5H_2O$ was the controlling phase for As release, modeling verifies that the phase or phases controlling As release will have a similar solubility to the modeled solubility of $NaCaAsO_4 \cdot 7.5H_2O$.

Table 3.4. Geometric and physical parameters for Mixture A S/S solid.

Section Number	Leach Surface Area (cm^2)	Skeletal Density (g/cm^3)	Depth (cm)	Thickness (cm)	Volume (cm^3)
1	319.1	2.3	0.020	0.020	6.2
2	316.1	2.3	0.050	0.030	9.4
3	311.5	2.3	0.084	0.034	10.6
4	306.2	2.3	0.124	0.040	12.0
5	300.2	2.3	0.169	0.046	13.5
6	293.4	2.3	0.221	0.052	15.2
7	285.6	2.3	0.282	0.060	16.9
8	276.8	2.3	0.351	0.069	18.8
9	266.9	2.3	0.430	0.080	20.8
10	255.6	2.3	0.522	0.092	22.8
11	243.0	2.3	0.627	0.105	24.8
12	228.9	2.3	0.748	0.121	26.8
13	213.2	2.3	0.888	0.139	28.5
14	195.9	2.3	1.048	0.160	29.9
15	176.8	2.3	1.232	0.184	30.6
16	156.1	2.3	1.444	0.212	30.7
17	133.8	2.3	1.687	0.243	29.6
18	110.3	2.3	2.300	0.613	51.8
19	61.0	2.3	3.000	0.700	28.0
20	22.0	2.3	3.810	0.810	7.3

With regards to leaching from monoliths, the Leach XS^{TM} segments a solid monolith from the outside to the interior and calculates the local liquid and solid partitioning of this segment (Seignette et al. 2014). This same liquid solid partitioning

calculation is made at each time step due to changing conditions (Seignette et al. 2014). A well-mixed solution of a finite volume in contact with the external surface of the monolith is simulated in the model (Seignette et al. 2014). Model input included available element content, solid physical specifications (dimensions, surface area, skeletal density, porosity, tortuosity factor), refresh solution specifications (volume, chemical composition, and refreshment schedule), global aqueous Fickian diffusion coefficient, and any adjustments to the model's mineral set.

The porosity was estimated (not directly measured) by measuring the S/S solid mass for Mixture A after drying for 24 hours at 95 ^{o}C and immediately and also after submerging for 30 min under water. The porosity was estimated by comparing these two mass measurements to be approximately 35%. Tortuosity was utilized to calibrate the model and was set to 7. Tortuosity was varied to match the observed Cl^- release as much as possible. Cl^- was utilized for this calibration process due to it's nonreactive and conservative nature.

The chemical composition and volume (3,190 mL) for the extractant fluid, deionized water, was also specified in the model according to the models preset leachant composition which contained very little elemental composition ($<3x10^{-5}$ µg/L for all elements). The refreshment schedule was specified to match the actual refreshment schedule for the leaching experiment. The global aqueous Fickian Diffusion coefficient ($2.25x10^{-10}$ m^2/s) input into the model was the maximum D^{OBS} for nonreactive Cl^- in the leaching experiments.

3.4 RESULTS AND DISCUSSION

3.4.1 Elemental Content of Solids

Table 3.5 shows metal composition of the solids examined in this study determined by digestion followed by ICP-MS analysis. The BCFA had a higher Al (114,000 versus 20,000 mg/kg), Fe (77,000 versus 23,000 mg/kg), K (17,000 versus 4,000 mg/kg), Si (30,000 versus 5,000 mg/kg), and Ti (7,000 versus 1,000 mg/kg) than PC. PC had a higher Ca (427,000 versus 12,000 mg/kg) and Mg (18,000 versus 5,000 mg/kg) than BCFA. The Ca content is higher in PC due to the high CaO content typical of PC. BCFA and PC contained similar concentrations of Cd (1 mg/kg) and Cr (156-174 mg/kg). BCFA contained significantly higher concentrations of As (69 versus 7 mg/kg) and Se (10 versus 1 mg/kg) than PC.

Table 3.6 shows the total element composition of the S/S solids. The total element composition was calculated based on the mixture formula and the composition of the components shown in Tables 3.1 and 3.5. As expected, the solids have a high Ca (60,000-61,000 mg/kg), Cl^- (18,000-20,000 mg/kg), and SO_4^{2-} (56-62 mg/kg).

The SO_4^{2-} concentration was likely underestimated due to SO_4^{2-} not being measured in the BCFA and PC and these components could have contained Ca-SO_4 precipitates. The solids contained significant oxyanion concentrations of As (46-48 mg/kg), Cr (128-133 mg/kg), and Se (11-12 mg/kg).

Table 3.5. BCFA and PC chemical composition.

(a) Bulk Elements

Element	BCFA (mg/kg dry)	PC (mg/kg dry)
Al	113,617	20,269
Ca	11,852	427,361
Fe	76,948	22,687
K	16,965	4,134
Mg	4,715	17,514
Si	29,571	5,420
Ti	6,569	1,294

(b) Significant Elements

Element	BCFA (mg/kg dry)	PC (mg/kg dry)
Ba	762	87
Cr	174	156
Cu	116	94
Mn	134	1,200
Ni	118	40
Zn	196	726

(c) Trace Elements

Element	BCFA (mg/kg dry)	PC (mg/kg dry)
Ag	0.3	1.3
As	69.3	7.3
Be	16.2	< 0.6
Cd	1.1	0.9
Co	44.4	6.3
Mo	24.7	7.1
Pb	73.6	16.5
Sb	5.9	3.9
Se	10.2	0.6
Tl	4.4	0.3

Table 3.6. Total elemental content of the S/S solids.

(a) Bulk Elements

Element	Mixture A (mg/kg dry)	Mixture B (mg/kg dry)	Mixture C (mg/kg dry)	Mixture D (mg/kg dry)
Al	78,356	77,246	76,147	75,050
B	164	162	159	157
Ca	61,197	60,822	60,377	59,966
Mg	5,835	5,761	5,685	5,611
Na	2,623	2,576	2,528	2,481
K	12,005	11,833	11,662	11,491
Si	20,436	20,147	19,860	19,573
Sr	504	497	490	482

(b) Trace Elements

Element	Mixture A (mg/kg dry)	Mixture B (mg/kg dry)	Mixture C (mg/kg dry)	Mixture D (mg/kg dry)
Sb	4.4	4.3	4.3	4.2
As	47.7	47.1	46.4	45.7
Ba	520.8	513.4	506.0	498.6
Cd	3.2	3.1	3.0	2.9
Cr	133.1	131.4	129.8	128.1
Cu	87.5	86.4	85.2	84.1
Pb	51.1	50.4	49.7	49.0
Mo	17.3	17.1	16.8	16.6
Se	11.5	11.2	11.0	10.7
Ag	0.3	0.3	0.3	0.3
Ti	4,542.9	4,478.7	4,415.2	4,351.8

(c) Anions

Element	Mixture A (mg/kg dry)	Mixture B (mg/kg dry)	Mixture C (mg/kg dry)	Mixture D (mg/kg dry)
Cl^-	20,326	19,636	18,921	18,214
SO_4^{2-}	62.1	60.0	57.8	55.6

3.4.2 Available Elemental Content Determined by the USEPA Method 1313

The available elemental content is the mass concentration of the element that is available to leach under realistic conditions (typically pH 2-13, L/S ratio = 10 mL/g-dry) (Kosson et al. 2014). Some of the element will be present in recalcitrant phases that are not available to leach under realistic conditions (Kosson et al. 2014). Table 3.7 shows the

available elemental content of the S/S solids as determined by the USEPA Method 1313 at pH 2.0±0.5. The available element content was calculated according to Equation 3.2:

$$Available\ Element\ Content\ (\frac{mg}{kg}) = \frac{LC \times LV}{SM} \qquad (3.2)$$

LC is the leached concentration detected in the leachate in µg/L; LV is the leachate volume in L; and SM is the dry solid mass in g. Due to the nature of the cement materials which generally form under high pH and dissolve at lower pH, it was assumed that the highest availability for most elements would be at low pH (2.0±0.5). It is noted that the final leachate pH for the USEPA Method 1313 evaluations were all within the required method pH range of 2.0±0.5. The final leachate pHs for Mixtures No. A-D were 2.1, 1.6, 2.3, and 2.0, respectively. For bulk elements, Table 3.7 shows that the available Al content varied from around 5,000-10,000 mg/kg among the four Mixtures which represents 6-13% of the total Al Content (Table 3.6). Most of the Al content in the S/S solids was likely from BCFA as BCFA had a much higher Al content than PC (Table 3.5).

Our previous research has shown that much of the crystalline Al in the BCFA and its S/S solid was present as mullite ($2Al_2O_3{\cdot}SiO_2$), which is difficult to break down except at low pH (Renew et al. 2016b). While the significant amount of Al was available at low pH as shown in the USEPA Method 1313 evaluation, it is not believed that much of the Al would be available under the higher pH conditions of the USEPA Method 1315 evaluation.

Table 3.7. Available elemental content of the S/S solids as determined by the USEPA Method 1313.

(a) Bulk Elements

Element	Mixture A (mg/kg dry)	Mixture B (mg/kg dry)	Mixture C (mg/kg dry)	Mixture D (mg/kg dry)
Al	4,715	9,898	7,619	7,193
B	145	130	110	111
Ca	31,517	62,991	62,883	59,083
Fe	1,604	7,688	4,459	4,728
Mg	2,218	3,597	3,766	3,714
Na	1,037	1,080	1,160	1,205
K	1,261	2,285	2,050	2,162
Si	6,751	18,215	12,371	10,600
Sr	140	205	191	202

(b) Trace Elements

Element	Mixture A (mg/kg dry)	Mixture B (mg/kg dry)	Mixture C (mg/kg dry)	Mixture D (mg/kg dry)
Sb	1.8	2.7	1.5	1.5
As	17.0	44.3	20.1	6.2
Ba	17.5	22.7	17.3	9.8
Cd	3.4	3.3	2.7	3.0
Cr	21.6	37.5	33.9	33.0
Cu	19.8	27.2	27.2	26.0
Pb	5.5	14.1	6.9	7.2
Mo	4.2	10.5	3.8	0.7
Se	7.4	8.7	4.5	1.2
Ag	0.0	0.1	0.1	0.1
Ti	78.2	407.7	174.9	85.5

(c) Anions

Element	Mixture A (mg/kg dry)	Mixture B (mg/kg dry)	Mixture C (mg/kg dry)	Mixture D (mg/kg dry)
Cl^-	21,783	22,215	20,374	21,474
SO_4^{2-}	6,731	15,248	16,029	18,783

Note – Final leachate pH for Mixtures A, B, C, and D were 2.1, 1.6, 2.3, and 2.0, respectively.

Available Ca content was high and varied from around 32,000-63,000 mg/kg representing 52-100% of the total Ca in the S/S solid. The high Ca availability is due to the high Ca content of both the simulated brine and PC. Our previous work has shown through X-ray fluorescence (XRF) that most of the Ca is present in the S/S solids as CaO which is available for reactions (Renew et al. 2016b). Ca is also present in CFA and S/S materials as calcium-silicate-hydrate (C-S-H), $Ca(OH)_2$, ettringite, monosulfate, $CaSO_4$, $CaSO_4 \cdot 2H_2O$ as noted by other researchers (De Windt et al. 2007, Izquierdo et al. 2012). Cement phases such as ettringite and monosulfate are both pH sensitive (Chrysochoou et al. 2006). Ettringite starts to dissolve when pH drops below 10.5 and monosulfate can dissolve when pH drops below 11.0 (Chrysochoou et al. 2006).

Available Fe content varied from approximately 2,000-8,000 mg/kg with a general trend of increasing with FS addition (Table 3.2) to the Mixture except for Mixture B. The available Fe from Mixture B was unexpectedly higher than those of Mixtures C and D, likely due to the particularly lower pH of the leachate for Mixture B.

For trace elements, the available As content varied from 6-44 mg/kg which represents 14-94% of the total As content. Mixture B had the highest As availability (94% of total As content) compared to the other Mixtures (14-43% of total As content) likely due to the lower leachate pH conditions. The available Cd and Cr content was 3 mg/kg (90-100% of total Cd content) and 22-38 mg/kg (16-29% of total Cr content), respectively. The available Se content varied from 1-9 mg/kg (11-78% of total Se content) with decreasing availability with increasing FS addition except for the lower final pH conditions of Mixture B.

For major anions, the Cl^- available content (100% of total Cl^- content) was similar for all Mixtures (20,000-22,000 mg/kg). The available SO_4^{2-} content varied from around 7,000-19,000 mg/kg with the logical increase in availability with increasing FS addition.

3.4.3 Leachate pH

Figure 3.1 shows the leachate pH as a function of cumulative leaching time (t). The minimum pH measured for all Mixtures occurred at 0.08 days with values between 7.4-8.0. The pH increased with t to a maximum for most Mixtures at 35 days with values between 10.6-10.7. It is likely that the pH increased from 0.08-35 days due to increasing CaO dissolution according to Equation 3.3 (Roy et al. 2011):

$$CaO + H_2O = Ca^{2+} + 2OH^- \quad (3.3)$$

The dissolution of other Ca oxides in cement phases could also impact pH. After 35 days, the pH decreased slightly with values of 10.0-10.7 at 119 days. This decrease was likely due to a decrease in available CaO content. The results indicate that an alkaline pH was maintained throughout the evaluation and FS addition did not appear to significantly impact leachate pH.

3.4.4 Leaching of Major Components

Calcium. Figure 3.2 shows the Ca^{2+} flux in $mg/m^2 \cdot s$ and Figures 3.3a-d show the nonaccumulated leached concentration (mg/L), cumulative mass release per solid surface area (mg/m^2), D^{OBS} (m^2/s) versus Fe^{II} addition at 1.04 and 49 days, and the leached concentration versus pH.

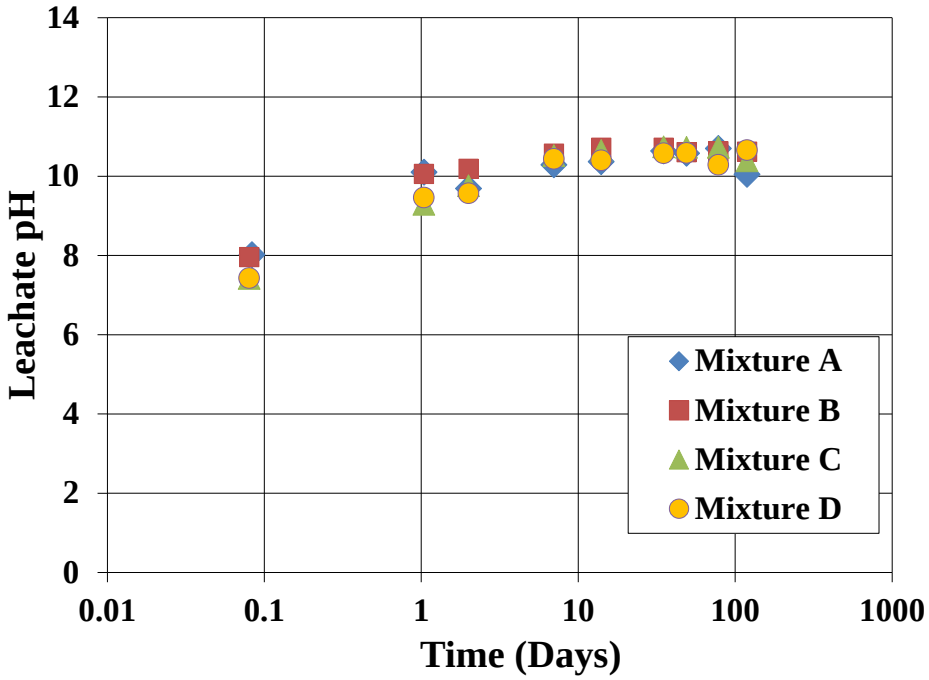

Figure 3.1. Leachate pH results.

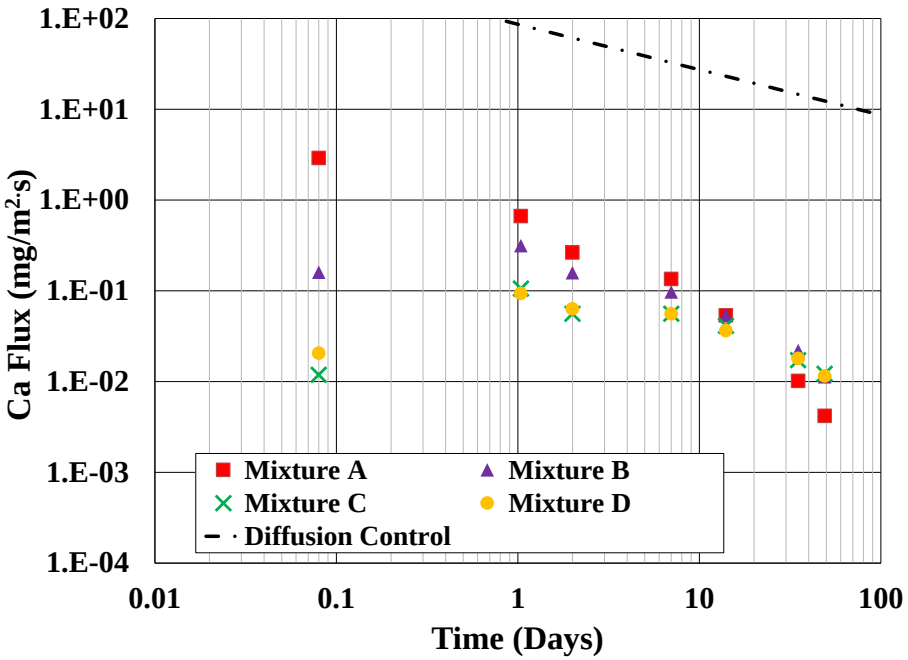

Figure 3.2. Ca^{2+} flux.

Figure 3.2 shows that the flux varied from approximately 2.9-4.2×10^{-3}, 0.31-1.1 × 10^{-2}, 0.11-1.2×10^{-2}, and 9.4×10^{-2}-1.1 × 10^{-2} mg/m^2·s for Mixtures A-D, respectively. It is known that, when diffusion mainly controls element release from a cylindrical monolith, the cumulative release and flux are proportional to that of the radial diffusion from a cylinder in an infinite bath (USEPA 2013). Equation 3.4 calculates mass release due to radial diffusion from a cylinder in an infinite bath (USEPA 2013).

$$M\left(\frac{mg}{m^2}\right) = 2\rho C_o\left[\frac{D^{OBS}.t}{\pi}\right]^{\frac{1}{2}} \quad (3.4)$$

M is the mass release during the interval in mg/m^2; ρ is the density of the cylinder in kg/m^3; C_o is the available leaching content for the contaminant in mg/kg; D^{OBS} is the observed diffusivity for the component in m^2/s; and t is cumulative leaching time in seconds. For flux, Equation 3.4 is divided by the interval t with the resulting Equation 3.5 (USEPA 2013).

$$F\left(\frac{mg}{m^2 \cdot s}\right) = 2\ \rho\ C_o\left[\frac{D^{OBS}}{\pi \cdot t}\right]^{\frac{1}{2}} \quad (3.5)$$

F is the flux in mg/m^2·s. Elemental flux primarily controlled by diffusion will be proportional to the flux as calculated by Equation 3.5 for radial diffusion from a cylinder in an infinite bath (USEPA 2013). For all cumulative release and flux graphs in this study, lines (labeled “Diffusion Control”) are shown to represent the cumulative release and flux under diffusion control as calculated by Equations 3.4 and 3.5 for Mixture A. For this calculation, the D^{OBS} value was the highest value calculated for the element which always

occurred at t=1.08 days**.** D^{OBS} can be calculated from Equation 3.4 for a known mass release.

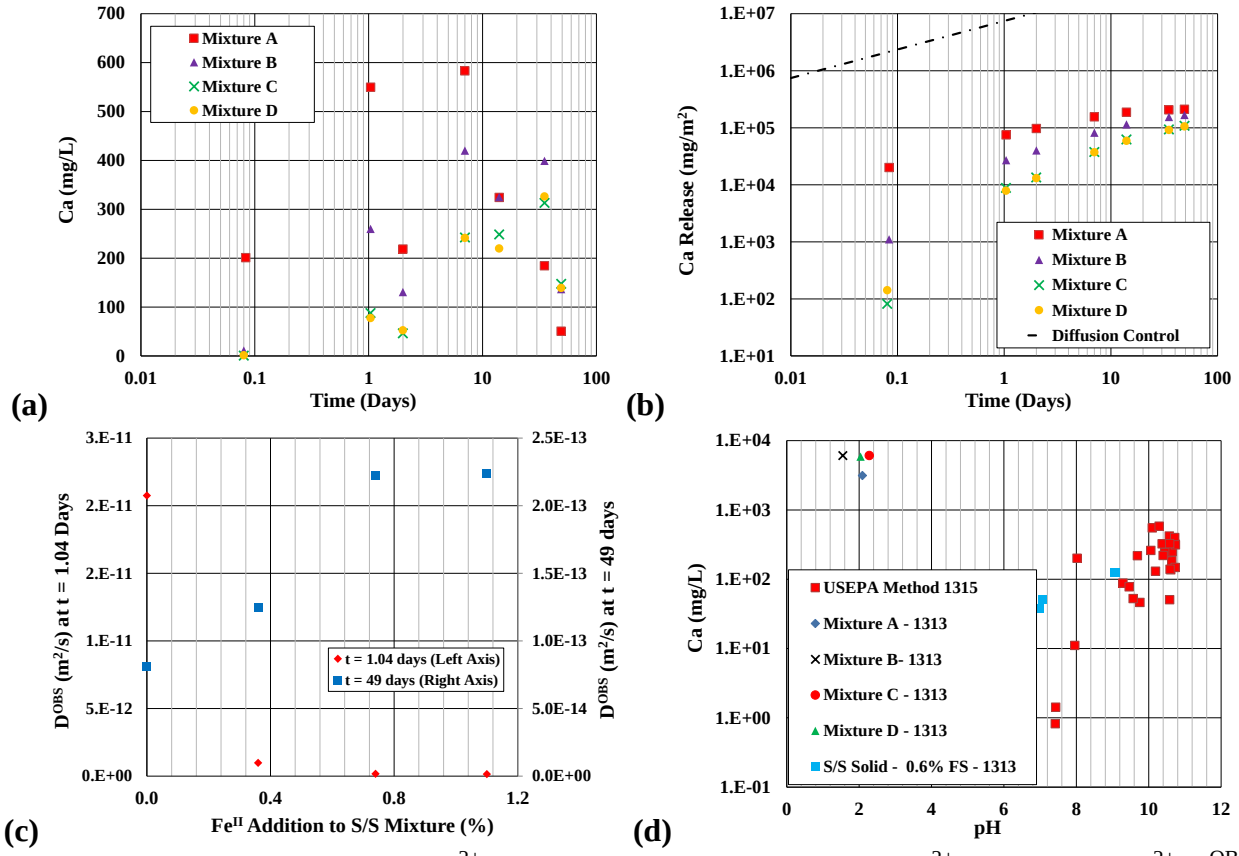

Figure 3.3. (a) Leached Ca^{2+} concentrations, (b) cumulative Ca^{2+} release, (c) Ca^{2+} D^{OBS} versus Fe^{II} addition at 1.04 and 49 days, and (d) leached Ca^{2+} concentrations versus pH.

Figure 3.2 shows that the Ca^{2+} flux for Mixture A decreased at a higher rate than the diffusion control line. This trend could indicate that Ca^{2+} phase (calcium-silicate-hydrate (C-S-H), CaO, $Ca(OH)_2$, $CaSO_4$, $CaSO_4{\cdot}2H_2O$, etc.) aqueous solubility controlled release. The solid phase controls leaching of solubility controlled species through solid-liquid partitioning (Garrabrants et al. 2012). Figure 3.3b also shows that the cumulative release pattern for Mixture A did not support diffusion-controlled Ca^{2+} release as the slope of the cumulative release pattern deviated from the diffusion control line. Figure 3.3d shows that the leached Ca^{2+} concentrations determined by USEPA Method 1313 and 1315

evaluations at similar pH had similar leached concentrations. This provides evidence that Ca^{2+} is near it's solubility limit in the USEPA Method 1315 evaluation and therefore aqueous solubility is controlling release. The USEPA Method 1313 results for the BCFA S/S solid with 0.6% FS as described in Figure 2.7 of Chapter 2 (Renew et al. 2016b). It is noted that FS addition impacts the leaching and availability of the elemental species. However, it was believed that leaching from the S/S solids with 0.6% FS addition (described in Figure 2.7) does provide a useful general comparison to the samples in this study.

Figure 3.2 shows that the flux for the Mixtures with FS addition were significantly less than Mixture A at t<1 days. At t>1 day, the Ca^{2+} flux for the Mixtures began to converge. As discussed below, Figure 3.9c shows that SO_4^{2-} flux increased simultaneously with Ca^{2+} flux for the Mixtures with FS addition, which supports the hypothesis that Ca-SO_4 precipitates controlled Ca^{2+} release at low leaching times. Figure 3.3c shows that the D^{OBS} decreased with increasing Fe^{II} addition at t=1.04 days; however, this trend is reversed at t=49 days with D^{OBS} increasing with increasing Fe^{II} addition. As Ca-SO_4 precipitates decrease in concentration due to dissolution, the impact of FS addition to the S/S mixture on Ca^{2+} release may significantly decrease. Figure 3.3b shows that Mixtures with FS addition have significantly lower cumulative release at lower leaching times; however, the cumulative release appeared to converge at higher leaching times. For Mixture A, approximately 31% of the available Ca^{2+} was released at 49 days.

Chloride. Figure 3.4 shows that Cl^- flux varied from approximately 6.1-6.8×10^{-4}, 0.4-2.4×10^{-2}, 0.3-6.8×10^{-3}, and 0.2-6.9×10^{-3} mg/m^2·s for Mixtures A-D, respectively. The

flux results indicate that Cl^- behaved as a highly soluble species. Cl^- flux was very high for Mixture A at t<2 days and began to decrease significantly at t>2 days due to decreasing available Cl^- content. A similar trend is shown for cumulative release in Figure 3.5b with Cl^- rapidly releasing from Mixture A at lower leaching time but not at longer leaching time. The slope of the cumulative release pattern significantly decreased at larger leaching times. This rapid decrease is due to the depletion of available Cl^-. Approximately 100% of the available Cl^- has been released from Mixture A at t = 119 days.

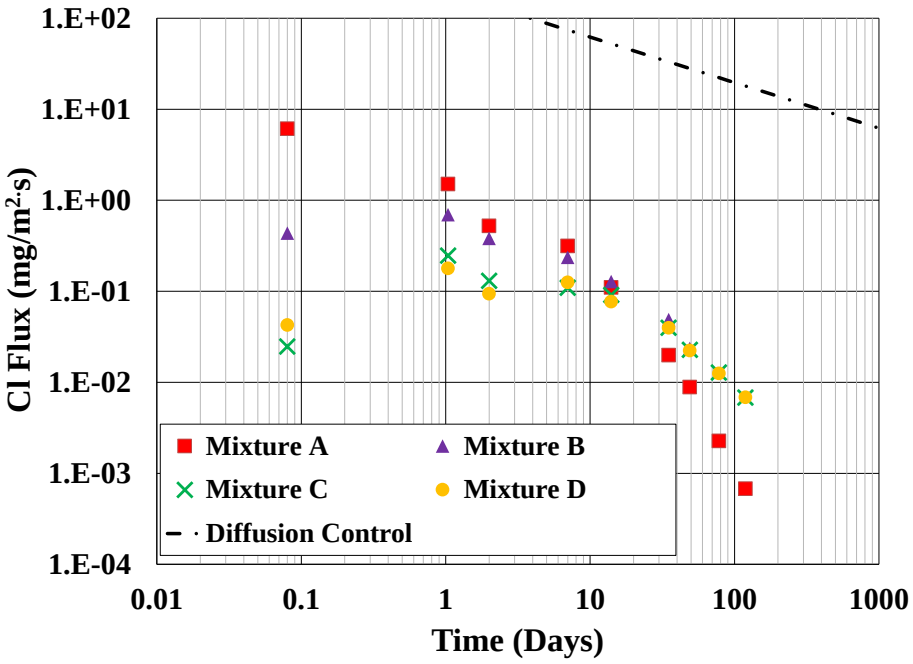

Figure 3.4. Cl^- flux.

Figure 3.4 shows that the Cl^- fluxes for the Mixtures with FS addition were lower than Mixture A at t<10 days, and appeared to converge with Mixture A at higher leaching times. Figure 3.5c shows that the D^{OBS} decreased with increasing Fe^{II} addition at t=1.04 days; however, this trend is reversed at t=49 days with D^{OBS} increasing with increasing Fe^{II} addition. Figure 3.5b shows that although the cumulative Cl^- release was less for Mixtures with FS addition, the cumulative Cl^- release for all Mixtures appeared to converge at high

leaching times. The impact of FS addition on Cl^- release was only transient and greatly decreased at longer leaching times.

Magnesium. Figure 3.6c shows that the Mg^{2+} flux significantly decreased over time for all Mixtures. The Figure shows that the flux pattern generally decreased at a slightly higher rate than the slope of the diffusion control line. Mg^{2+} leaching from CFA is known to be controlled by hydroxide and carbonate phases (Izquierdo et al. 2012). However, Figure 3.6e shows that the USEPA Method 1315 leached Mg^{2+} concentrations are significantly less than the USEPA Method 1313 leached concentrations at approximately the same pH which indicates that Mg^{2+} is not at it's maximum solubility in the USEPA Method 1315 evaluation. Hence, it is likely diffusion does play some role in Mg^{2+} release. Figure 3.6b shows that cumulative Mg^{2+} release pattern decreases at a slightly lower rate than the diffusion control line. For Mixture A, approximately 16% of the available Mg^{2+} was released at 49 days.

Figure 3.6c shows that the Mg^{2+} flux was lower for Mixtures with FS addition at low leaching times. However, the fluxes began to converge at higher leaching times. A similar trend is shown for the cumulative Mg^{2+} release in Figure 3.6b. Figure 3.6d shows that at t=1.04 days, the D^{OBS} decreases significantly with increasing Fe^{II} addition; however, this same trend is not seen when t=49 days. Hence, FS addition appears to only enhance Mg^{2+} stabilization at lower leaching times.

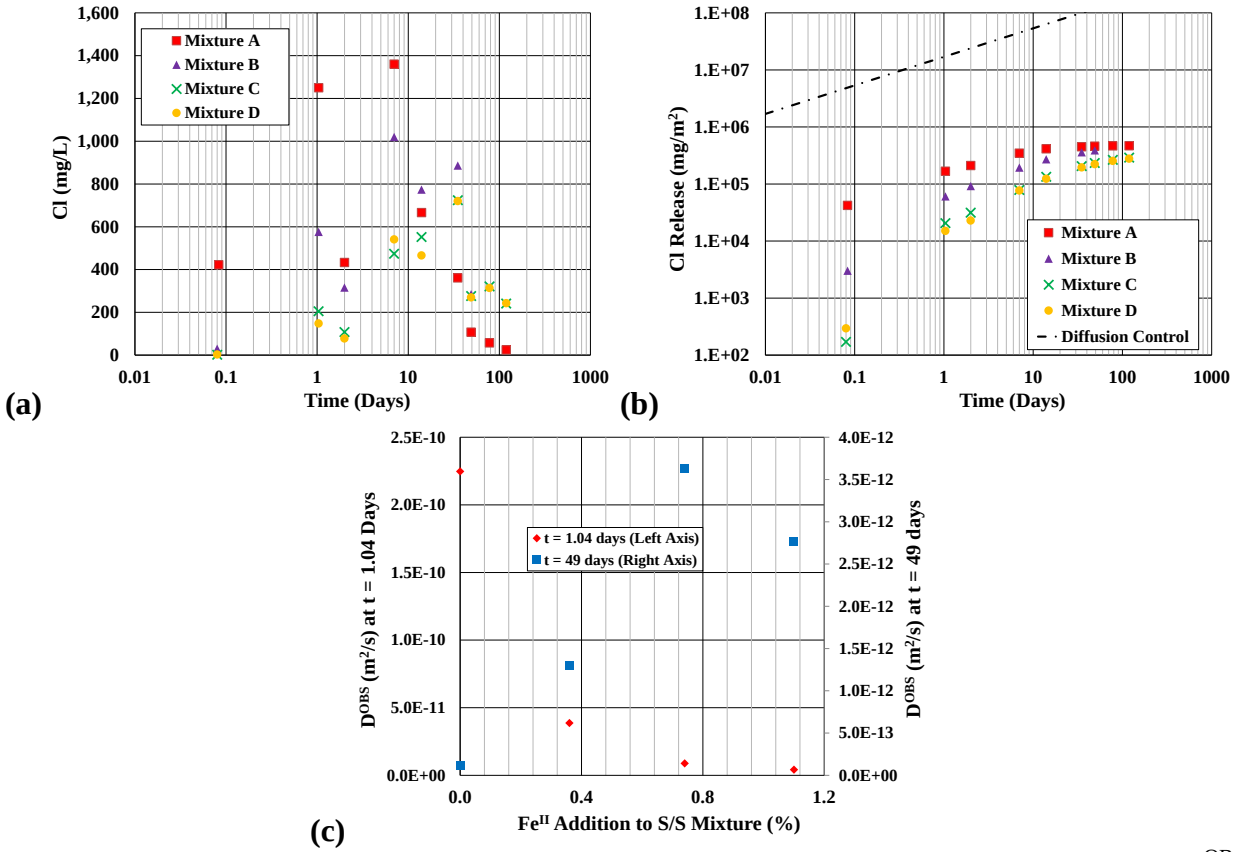

Figure 3.5. (a) Leached Cl^- concentrations, (b) cumulative Cl^- release, and (c) Cl^- D^{OBS} versus Fe^{II} addition at 1.04 and 49 days.

Sodium. Figure 3.7 shows that Na^+ flux varied from approximately 0.25-1.7×10^{-4}, 4.1x10^{-2}-6.2×10^{-4}, 1.5x10^{-2}-9.1×10^{-4}, and 1.2x10^{-2}-8.2×10^{-4} mg/m^2·s for Mixtures A-D, respectively. This rapid decrease in flux suggests highly soluble species behavior. A similar trend is shown for cumulative release in Figure 3.8b. The cumulative release pattern slope significantly decreased at higher leaching times likely due decrease in available Na^+. For Mixture A, approximately 60% of the available Na^+ was from the solid when t = 49 days. Figure 3.8d provides further evidence for the highly soluble species hypothesis as the USEPA Method 1315 Na^+ leached concentrations are less than the USEPA Method 1313 leached concentrations at the same approximate pH range which indicates that Na^+ is not at it's maximum solubility in the USEPA Method 1315 evaluation.

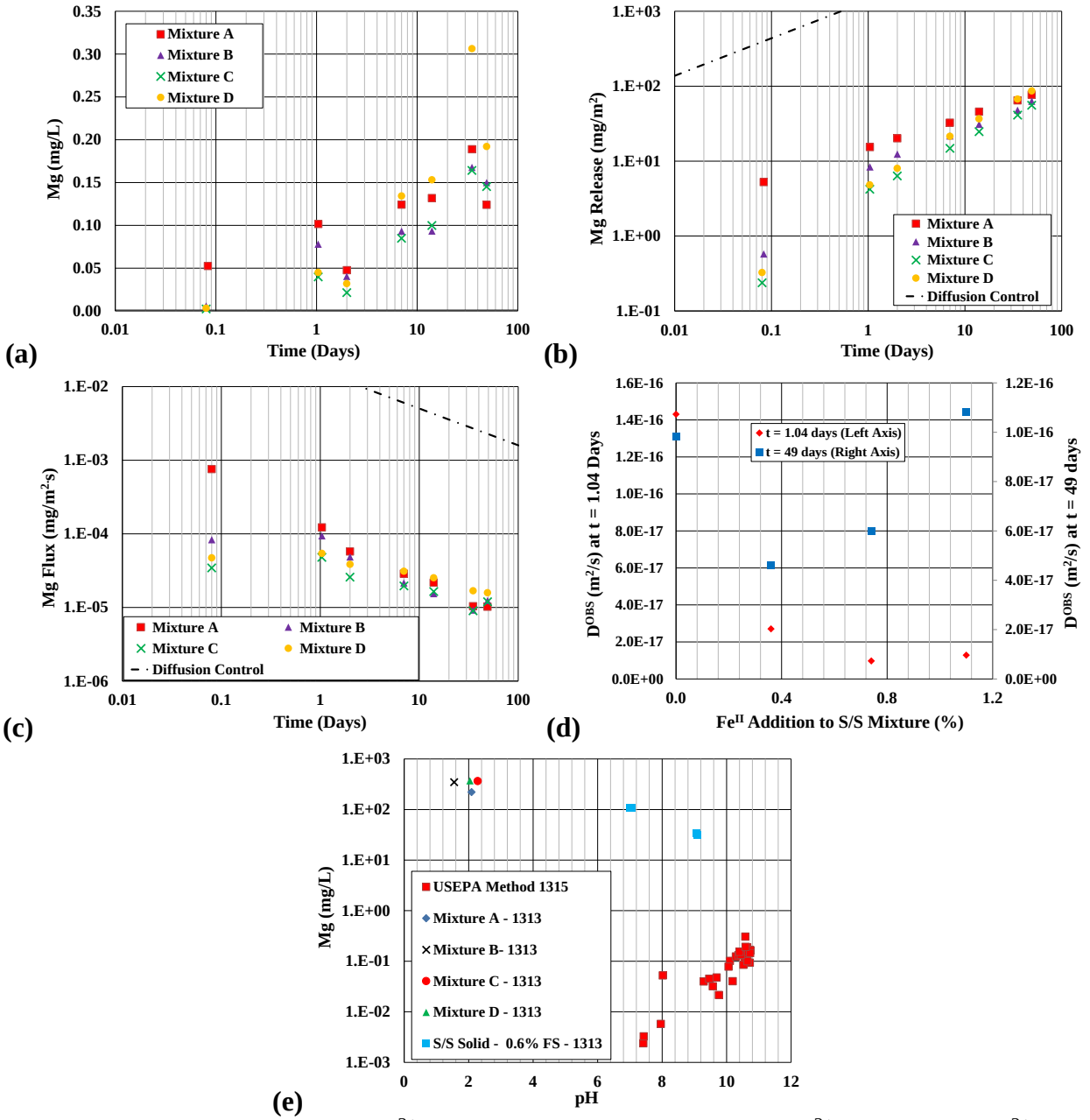

Figure 3.6. (a) Leached Mg^{2+} concentrations, (b) cumulative Mg^{2+} release, (c) Mg^{2+} flux, (d) Mg^{2+} D^{OBS} versus Fe^{II} addition at 1.04 and 49 days, and (e) leached Mg^{2+} concentrations versus pH.

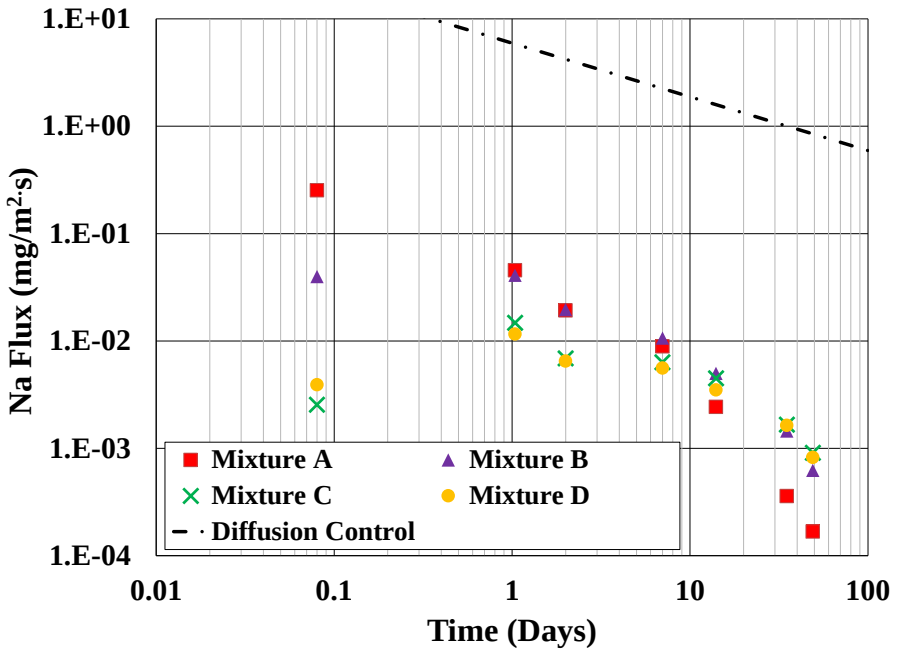

Figure 3.7. Na^+ flux.

Figure 3.8c shows that the Na^+ flux was lower for Mixtures with FS addition at lowt leaching times; however, the fluxes began to converge at higher leaching times. A similar trend is shown for the cumulative Na^+ release in Figure 3.8b. Figure 3.8c shows that at t=1.04 days, the D^{OBS} decreases significantly with increasing Fe^{II} addition; however, this same trend is not seen when t=49 days as D^{OBS} increases with increasing Fe^{II} addition. Hence, FS addition appears to only enhance Na^+ stabilization at shorter leaching times.

Sulfate. Figure 3.9c shows that SO_4^{2-} flux varied from approximately $3.7x10^{-2}$-2.3×10^{-4}, $2.1x10^{-2}$-7.5×10^{-4}, $1.1x10^{-2}$-3.2×10^{-4}, and $1.3x10^{-2}$-4.0×10^{-4} $mg/m^2{\cdot}s$ for Mixtures A-D, respectively. As mentioned above, $CaSO_4$ and $CaSO_4{\cdot}2H_2O$ dissolution generally control SO_4^{2-} release from CFA (Izquierdo et al. 2012). Figure 3.9c shows that the flux pattern generally decreased at a higher rate than the diffusion control line especially at higher leaching times which suggests solubility controlled release. In addition, Figure 3.9b shows that the slope of the cumulative release pattern for Mixture A was generally less

than the diffusion control line which provides evidence solubility controlled release. For Mixture A, approximately only 7% of the available SO_4^{2-} was released at 119 days.

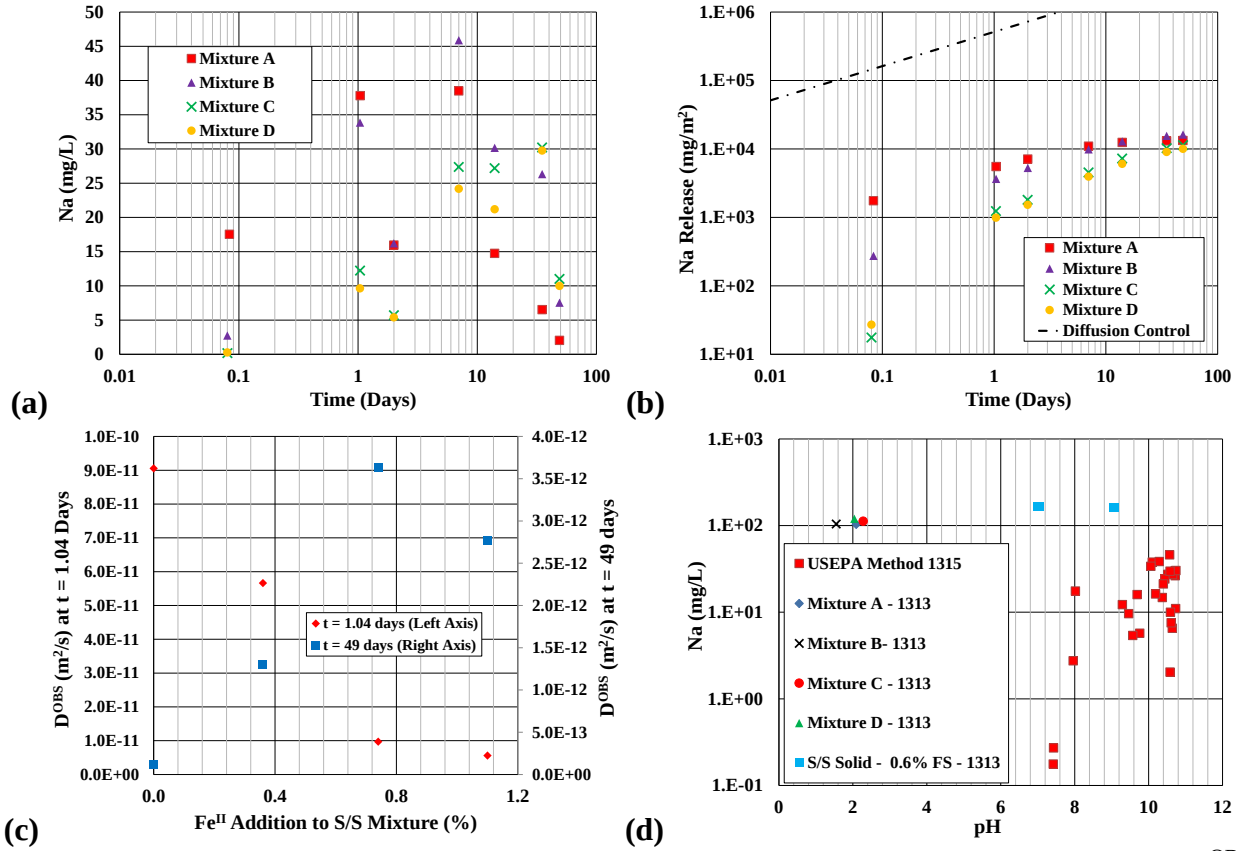

Figure 3.8. (a) Leached Na^+ concentrations, (b) cumulative Na^+ release, and (c) Na^+ D^{OBS} versus Fe^{II} addition at 1.04 and 49 days, and (d) leached Na^+ concentrations versus pH.

Figure 3.9c shows that for t<1 day the SO_4^{2-} flux was greater for Mixture A than the Mixtures with FS addition. This trend likely resulted from SO_4^{2-} addition (in FS) promoting the precipitation of $CaSO_4$ or $CaSO_4{\cdot}2H_2O$ and therefore decreasing SO_4^{2-} release. This trend was overcome at t>1 day as the flux for all Mixtures approached similar values. The convergence of the fluxes was likely due to a lower portion of the SO_4^{2-} being in the form of Ca-SO_4 precipitates at t>1, thereby decreasing the impact of the FS addition. Figure 3.9d shows that there is decrease in D^{OBS} with increasing Fe^{II} addition at t=1.04 days; however, there is a significant difference t=49 days with D^{OBS} increasing with

increasing Fe^{II} addition. The evidence from cumulative release pattern indicates that the impact of FS addition decreased over time. Figure 3.9b shows SO_4^{2-} release is higher for Mixture A than the other Mixtures at t<1 day; however, cumulative release for all Mixtures approached the same value at t>1 day likely for the same reason as described for the flux convergence. It appears that FS only had a slight impact on SO_4^{2-} release and that impact decreased significantly at larger leaching times.

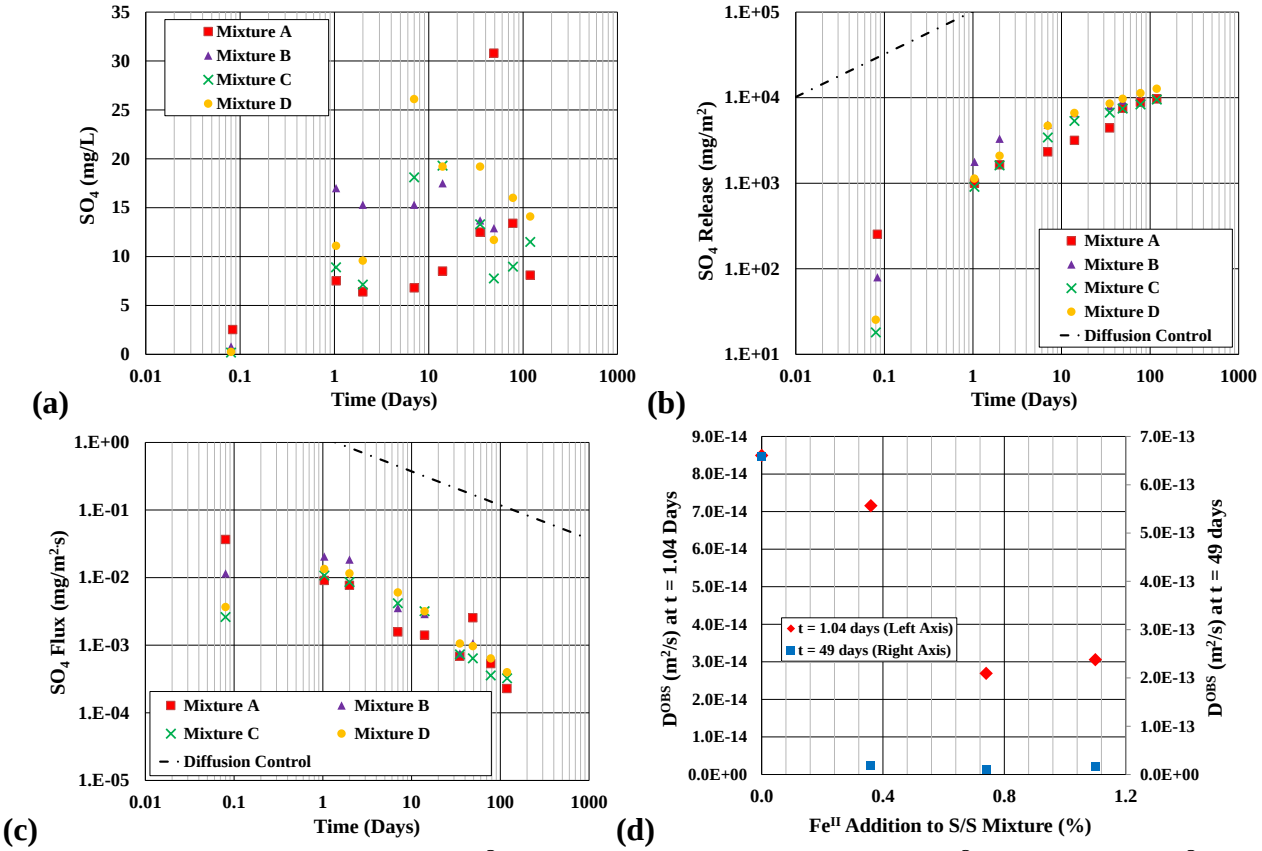

Figure 3.9. (a) Leached SO_4^{2-} concentrations, (b) cumulative SO_4^{2-} release, (c) SO_4^{2-} flux, and (d) SO_4^{2-} D^{OBS} versus Fe^{II} addition at 1.04 and 49 days.

3.4.5 Leaching of Oxyanions

Arsenic. The vast majority of As present in the S/S solids was expected to be As^V (AsO_4^{3-}) because only As^V was added to the simulated FGD brine and previous research has shown that As is present in CFA primarily as the oxyanion AsO_4^{3-} (Goodarzi et al.

2001, Huggins et al. 2007, Goodarzi et al. 2008). PC only contained 7 mg/kg dry of As and was only 10% of the S/S mixtures. Previous research has shown that Ca-As^{V} complex precipitation is the likely dominant S/S immobilization mechanism as these complexes have low solubility at neutral and high pH with $NaCaAsO_4 \cdot 7.5H_2O$ being the expected dominant phase in S/S (Nishimura et al. 1998, Bothe Jr et al. 1999, Cornelis et al. 2008a, Moon et al. 2008).

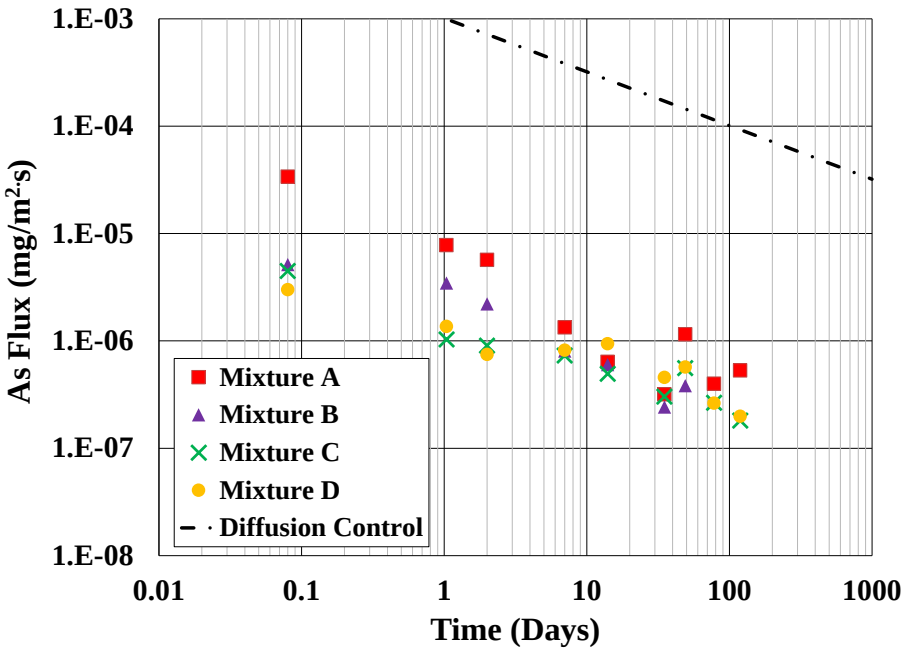

Figure 3.10. As flux.

Figure 3.10 shows that the As flux varied from approximately 3.4×10^{-5}-3.2×10^{-7}, 5.1×10^{-6}-2.4×10^{-7}, 4.5×10^{-6}-1.8×10^{-7}, and 3.0×10^{-6}-2.0×10^{-7} mg/m^2·s for Mixtures A-D, respectively. The As flux pattern slope for Mixture A was generally less than the diffusion control line which implies solubility controlled release. Figure 3.11b shows that cumulative release pattern also implies solubility controlled release as the slope of the cumulative release for Mixture A was generally less than the diffusion control line. Further, Figure

3.11d shows that the leached As concentrations determined by USEPA Method 1313 and 1315 evaluations at the same approximate pH range were similar which implies that As is near it's solubility limit in the USEPA Method 1315 experiment. For Mixture A, approximately only 2% of the available As was released at 119 days.

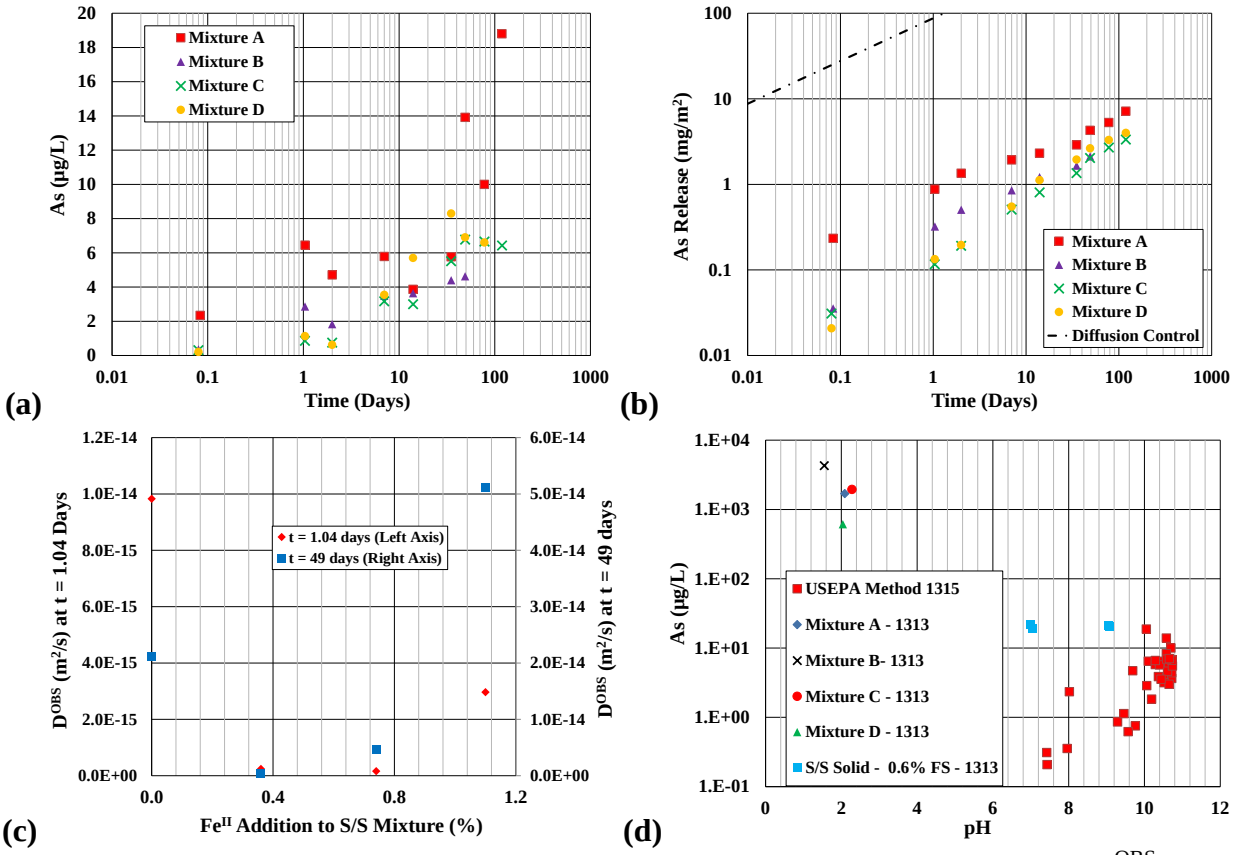

Figure 3.11. (a) Leached As concentrations, (b) cumulative As release, (c) As D^{OBS} versus Fe^{II} addition at 1.04 and 49 days, and (d) leached As concentrations versus pH.

Figure 3.10 shows that the flux was lower for Mixtures with FS addition especially at shorter leaching times. The same trend was seen in the cumulative As release pattern (Figure 3.11b) with higher cumulative As release for Mixture A versus those with FS addition. Although the likely primary As immobilization mechanism was Ca-As^{V} complex precipitation, the addition of FS likely enhanced As stabilization through sorption to produced hydrous Fe^{III} oxides. The addition of Fe^{II} and Fe^{III} has been shown to increase

the As^{V} retainment in S/S solids (Palfy et al. 1999, Miller et al. 2000, Choi et al. 2009). The Dzombak and Morel model indicates that As^{V} sorbs readily to hydrous Fe^{III} oxides at a pH range in common with cement-based S/S (Cornelis et al. 2008a). Most of Fe^{II} from the added FS was likely quickly oxidized to Fe^{III} in the S/S matrix. The addition of FS could also have reduced some of the As^{V} to As^{III}; however, As reduction was not expected to significantly impact the leaching results as As^{III} has been shown to sorb at least as readily as As^{V} to hydrous Fe^{III} oxides at above neutral pH conditions (Dixit et al. 2003).

As the leaching time increased the difference in the flux between the Mixtures with and without FS addition decreased. Figure 3.11c shows that the D^{OBS} decreased with increasing Fe^{II} addition at t=1.04 days; however, this trend is reversed at t=49 days with D^{OBS} increasing with increasing Fe^{II} addition.

It is clear that FS addition significantly decreased As release likely due to sorption to formed hydrous Fe^{III} oxides. However, at longer leaching times, this impact was somewhat reduced though not as much for the major components.

***Chromium*.** Cr^{VI} was added in the simulated brine in the experiments. Research has reported that the dominant Cr species in CFA is Cr^{III}, with Huffman et al. finding greater than 95% Cr^{III} in CFA samples (Huffman et al. 1994). Cr^{VI} is much more mobile than Cr^{III}; hence, the Cr^{VI} from the brine is likely to be much more mobile than Cr^{III} from the CFA. The PC also contained a significant amount of Cr (156 mg/kg dry).

Previous researchers demonstrated cement-based S/S to be effective in immobilizing Cr^{III}, but not Cr^{VI} (Glasser 1997, Wang et al. 2000, Dermatas et al. 2003). Cr^{III} has a lower solubility than Cr^{VI} under the high pH conditions expected in S/S (Richard

et al. 1991, Glasser 1997). In addition, Glasser noted that chemical incorporation of Cr^{III} in the Ca-Al^{III}-hydrate phase by replacing Al^{III} likely plays the most important role in Cr^{III} immobilization in Cr immobilization in S/S (Glasser 1997).

Figure 3.12 shows that the Cr flux varied over time from approximately 4.8×10^{-6}-2.4×10^{-7}, 1.6×10^{-6}-2.0×10^{-7}, 1.6×10^{-6}-6.7×10^{-8}, and 1.6×10^{-6}-7.4×10^{-8} mg/m^2·s for Mixture A-D, respectively. Cr flux for Mixture A appeared to decrease essentially proportional to the diffusion control line. Figure 3.13b shows that cumulative release pattern for Mixture A increased essentially proportional to the diffusion control line. Figure 3.13d shows that the leached Cr concentrations determined by USEPA Method 1313 were slightly higher than the USEPA Method 1315 evaluations at a similar pH range indicating that Cr is not at it's maximum solubility. For Mixture A, approximately only 0.8% of the available Cr was released at 119 days.

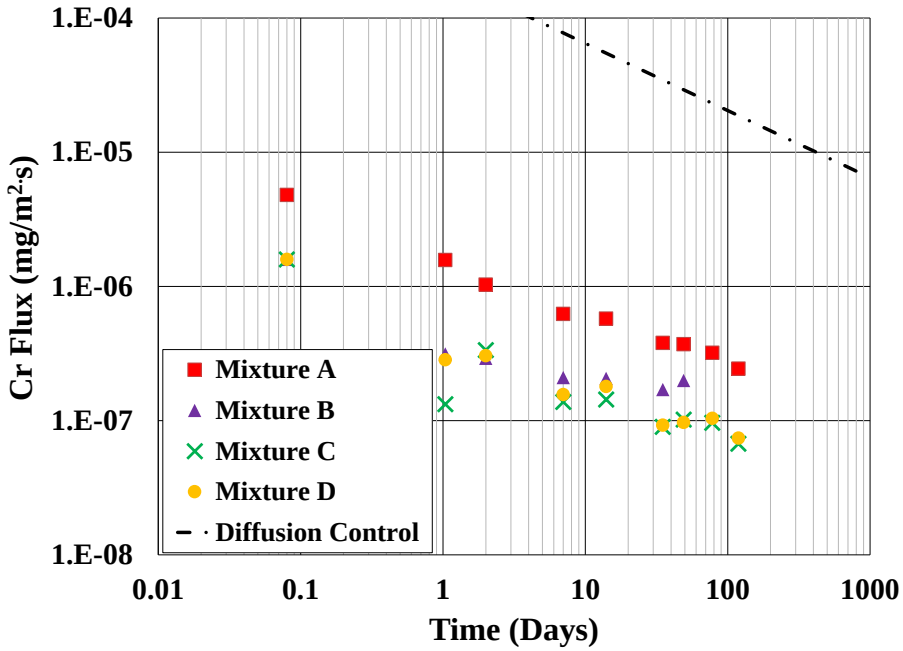

Figure 3.12. Cr flux.

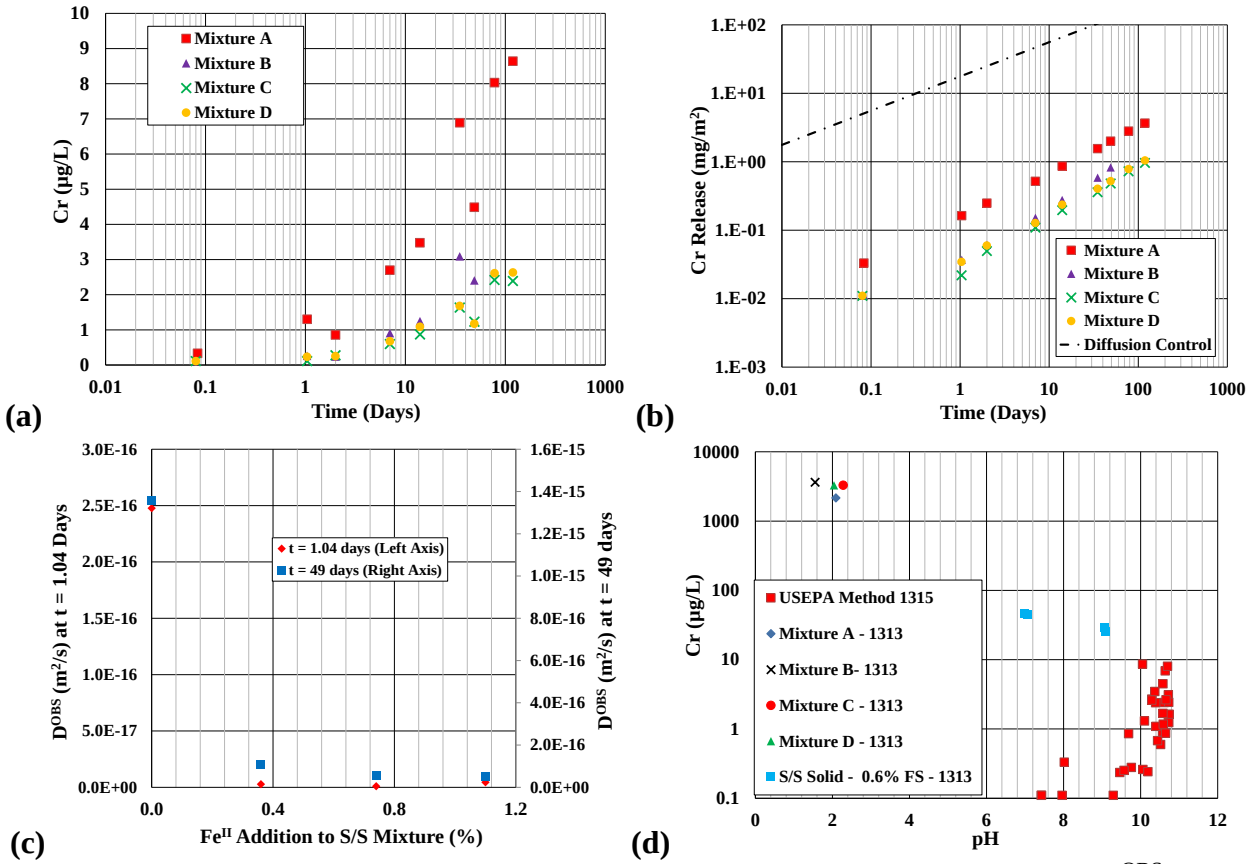

Figure 3.13. (a) Leached Cr concentrations, (b) cumulative Cr release (c) Cr D^{OBS} versus Fe^{II} addition at 1.04 and 49 days, and (d) leached Cr concentrations versus pH.

Figures 3.12 shows that Cr flux was lower for Mixtures with FS addition. Unlike for As, the Cr fluxes for the Mixtures did not significantly converge at larger leaching times. Figure 3.13c shows that the D^{OBS} greatly decreased with increasing Fe^{II} addition at t=1.04 days ($2.5x10^{-16}$-$9.2x10^{-19}$ m^2/s) and this trend continued at t=49 days with D^{OBS} decreasing ($1.4x10^{-15}$-$5.1x10^{-17}$ m^2/s) with increasing Fe^{II} addition.

Figure 3.13b shows that the cumulative Cr release was also lower for the Mixtures with FS addition for all leaching times. Fe^{II} can reduce Cr^{VI} to Cr^{III}, (Dermatas et al. 2003, Su et al. 2005) and thus FS addition to S/S mixtures greatly decreased Cr^{VI} leaching in previous research (Dermatas et al. 2003, Renew et al. 2016b). The mechanism of Cr^{VI} reduction by FS to Cr^{III} is likely responsible for the reduced flux and cumulative release

for Mixtures B-D. The likely mechanism is: (i) Cr^{VI} in the S/S solid was reduced to Cr^{III}, which could be incorporated in the Ca-Al^{III}-hydrate phase, precipitated as $Cr(OH)_3$, and/or adsorb to Fe^{III} oxides (existing and new); and (ii) some of the Cr^{III} originally from the BCFA and PC could also be incorporated in the Ca-Al^{III}-hydrate phase or adsorb to newly formed Fe^{III} oxides. FS addition shows significant promise for enhancing Cr stabilization in the S/S of concentrated FGD brines.

***Selenium*.** Se added to the mixture from the brine will be present as Se^{VI} (as SeO_4^{2-}) as it was added in that form to concentrated brine. Previous research indicates that Se^{IV} is generally present in CFA (Narukawa et al. 2005, Huggins et al. 2007, Wang et al. 2009).

Se behaves differently based on oxidation state (Se^{IV} versus Se^{VI}) in S/S matrices. The likely dominant immobilization phase for Se^{IV} is $CaSeO_3$ in S/S matrices. Baur and Johnson hypothesized that $CaSeO_3$ solubility controls Se^{IV} release in cementitous materials where Ca^{2+} concentrations are significant (Baur et al. 2003b).

Se^{VI} immobilization in S/S matrices is more complex. Baur and Johnson studied the sorption of Se^{VI} to the monosulfate (AFm-SO_4), ettringite (AFt-SO_4) and observed only strong Se^{VI} sorption to AFm-SO_4 (Rd = 2.06) (Baur et al. 2003b). However, our previous work did not detect AFm in S/S solids produced with bituminous CFA at significant quantities with XRD (Renew et al. 2016b). Therefore, these two phases probably do not dominate Se^{VI} leaching in the S/S solids in this study. It could be that the more readily soluble $CaSeO_4$ (Log K_{sp} = 4.77) is the most important phase for Se^{VI} leaching (Séby et al. 2001).

Figure 3.14 shows that the Se flux decreased from 2.2×10^{-5}-6.0×10^{-7}, 8.0×10^{-7}-4.6×10^{-7}, 7.9×10^{-7}-1.3×10^{-7}, and 7.9×10^{-7}-1.2×10^{-7} mg/m^2·s for Mixtures A-D, respectively. The Se flux pattern for Mixture A appeared to be proportional to the diffusion control line showing the characteristics of a highly soluble species as would be expected for the available Se^{VI}. Figure 3.15b shows that the cumulative Se release pattern for Mixture A increased proportionally to the diffusion control line, providing further evidence for diffusion-controlled Se^{VI} release and highly soluble species behavior. Figure 3.15d shows that at similar pH the Se leached concentrations for the USEPA Method 1313 evaluation are significantly higher than the USEPA Method 1315 evaluation which implies that Se is not at it's solubility limit. For Mixture A, approximately only 7% of the available Se was released at 119 days.

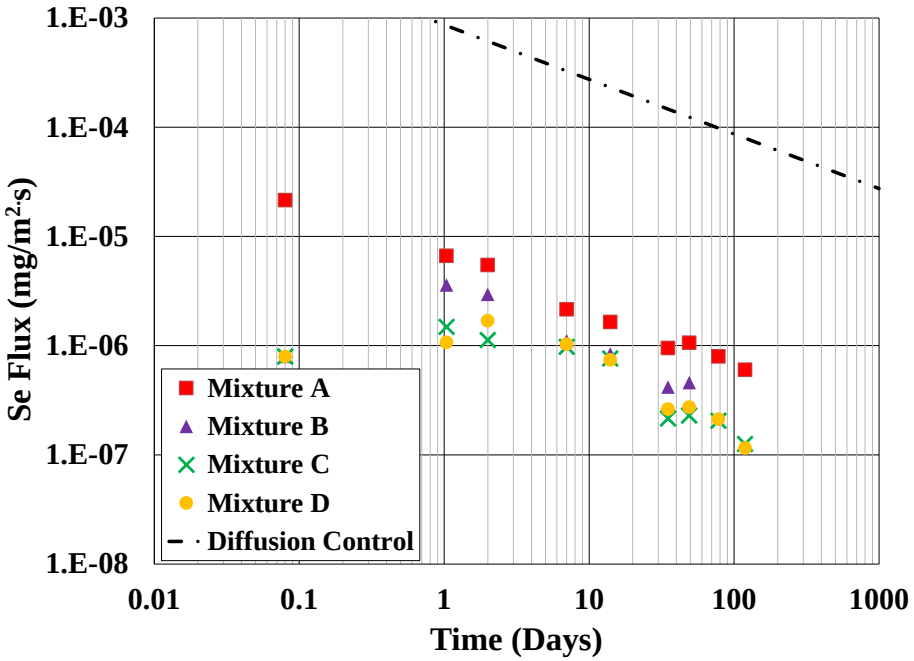

Figure 3.14. Se flux.

The Se flux for Mixtures with FS addition were not proportional to the diffusion control line at t<10 days and the flux actually increased 0.08<t<2.0 days for Mixtures B, C, and D. The flux for all mixtures was generally proportional to the diffusion control line at t>2.0 days. The flux was less for Mixtures with FS addition likely due to the reduction of a portion of Se^{VI} to Se^{IV} followed by precipitation as $CaSeO_3$. As leaching time increased, the difference in the flux between Mixture A and the Mixtures with FS addition became less, likely because the Se speciation differences between the Mixtures became less as the amount of available Se^{VI} was decreased. Figure 3.15c shows that D^{OBS} generally decreased with increasing Fe^{II} addition at t=1.04 days; however, at the highest Fe^{II} addition, the D^{OBS} was higher than with no addition. At t=49 days, D^{OBS} generally increased with increasing Fe^{II} addition. Figure 3.15b shows that the Se cumulative release was lower for the Mixtures with FS addition than Mixture A for the entire leaching experiment.

The results from this leaching experiment indicate that Se behaved as a highly soluble species and was readily released with diffusion as the primary limiting factor. FS addition did decrease Se release from the S/S solids over the long term.

3.4.6 LeachXS™ Modeling

Figure 3.16a shows the modeled and observed pH results for Mixture A generally agreed. The observed pH values varied between 8.0-10.7 while the modeled pH values varied between 9.4-10.9. Both modeled and observed results shows that the pH remains alkaline throughout the entire leaching evaluation.

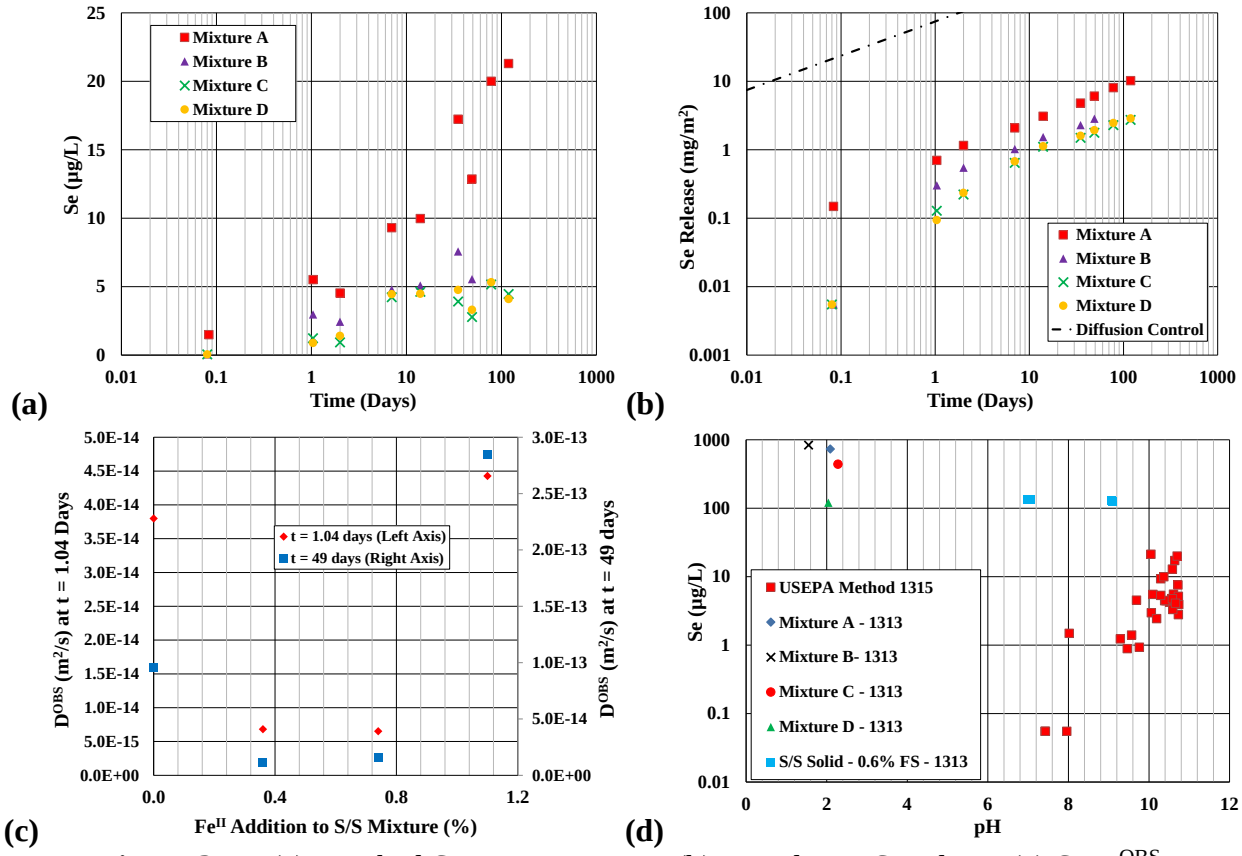

Figure 3.15. (a) Leached Se concentrations, (b) cumulative Se release (c) Se D^{OBS} versus Fe^{II} addition at 1.04 and 49 days, and (d) leached Se concentrations versus pH.

Figures 3.16b-d show the modeled cumulative release for Ca^{2+}, Cl^-, Na^+, As, and Se, respectively. The results show that the model is more successful in obtaining good agreement between the observed and modeled results for the major components (Ca^{2+}, Cl^-, and Na^+) at longer leaching times. It appears that an initial "washing off" effect occurs for these major components that is difficult to model at short leaching times. These elements are present in the S/S solid with very high availability (Ca^{2+}-31,517 mg/kg, Na^+-1,037 mg/kg, and Cl^--21,783 mg/kg).

Good agreement is observed between the modeled and observed As. As was input into the model as AsO_4^{3-} and reduction was not considered because no FS (reductant) was

added. $NaCaAsO_4 \cdot 7.5H_2O$ was modeled as the phase controlling As leaching as shown in Equation 3.1.

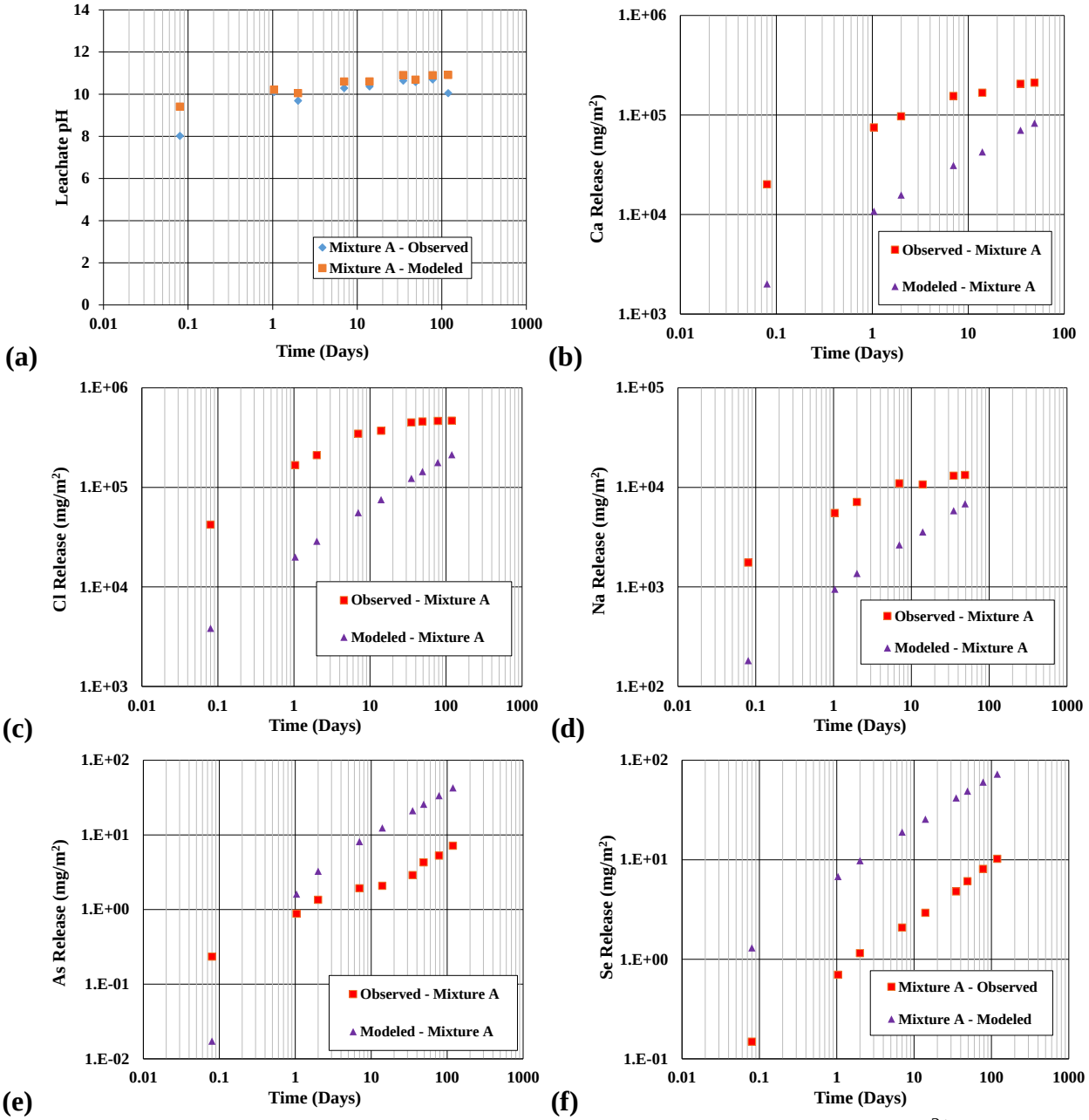

Figure 3.16. Comparison of modeled and observed results (a) pH, (b) Ca^{2+}, (c) Cl^-, (d) Na^+, (e) As, and (f) Se.

The modeled Log K value of 8.0 for $NaCaAsO_4 \cdot 7.5H_2O$ was input in the model. Other Ca-As^V phases already present in the Leach XS™ model with available Log K values

were also utilized in an attempt to model As leaching, including but not limited to $Ca_3(AsO_4)_2 \cdot 2.25H_2O$ (Log K = 21.1), $Ca_3(AsO4)_2 \cdot 3H_2O$ (Log K = 21.4), $Ca_4(OH)_2(AsO4)_2 \cdot 4H_2O$ (Log K = -0.5), $Ca_5(OH)(AsO_4)_3$ (Log K = 26.1).

Inclusion of these phases did not provide a satisfactory fit between the observed and modeled values. As mentioned above, the developed model does not confirm that $NaCaAsO_4 \cdot 7.5H_2O$ is the controlling As phase. The model confirms that phase or phases are controlling As solubility with an As solubility similar to that modeled for $NaCaAsO_4 \cdot 7.5H_2O$ in this study.

The LeachXS^{TM} model also included modeling for As^V-substituted ettringite as a solid solution (Log K = 26.8). Modeling this phase did not provide an acceptable fit to the experimental results. The high available Al value (Table 3.7) for Mixture A drove the formation of ettringite-As^V in the model. However, no ettringite was detectable in the bituminous CFA S/S solids analyzed with XRD in our previous work (Renew et al. 2016b). Our previous research showed that much of the crystalline Al in the S/S solids was present as mullite ($2Al_2O_3 \cdot SiO_2$) which is difficult to break down except at low pH (Renew et al. 2016b). Hence, although a significant amount of Al is available at low pH, it is unlikely that a significant amount of Al would be available under the higher pH conditions of the leaching evaluation (8.0-10.7, Figure 3.1). Hence, the available Al was decreased to near 0 mg/kg in the model.

The available Se was entered into the model in the form of SeO_4^{2-}. One of the phases added in the model was $CaSeO_4$ (Log K = 4.77) (Séby et al. 2001). As shown in the experimental results, Se behaved primarily as a highly soluble species and release was

primarily limited only by diffusion in both the observed and modeled results. Note that a portion of the available Se is likely present as Se^{IV} in addition to Se^{VI} which may explain some of the differences in the modeled and observed results.

Real Scenario Application. The developed model was utilized to evaluate long-term leaching from a 10 cm × 10 cm × 10 cm depth monolith over 20 years as depicted in Figure 3.17. The block had the chemical composition of Mixture A. A conservative effective infiltration rate of 15 mm/year was assumed as contacting the solid. It should be noted that the scenario includes a low liquid to surface area (L/SA) ratio 0.005 L/100 cm^2. One-dimension diffusion was assumed for this model. The model results of leachate pH, Ca^{2+}, Cl^-, Na^+, As, and Se are shown in Figures 3.18a-f.

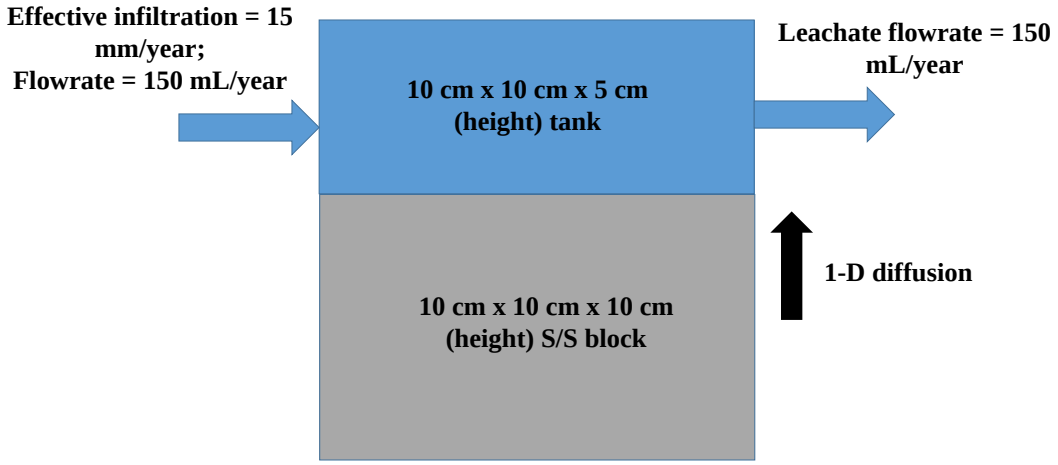

Figure 3.17. Real scenario application.

The model indicated that leachate pH would rapidly increase to a maximum of 10.9 then slowly decrease to 9.8 at the end of 20 years. Hence, over 20 years the leachate would remain alkaline, which is positive for the success of the S/S process as many cationic metals are less soluble at higher pH.

All elements shown in Figure 3.18 rapidly increased to a maximum concentration immediately and then slowly decreased to minimum stabilized concentration over 20 years. The leachate concentration for Ca^{2+}, Cl^{-}, Na^{+}, As, and Se varied from 187-217 mg/L, 31-368 mg/L, 1-17 mg/L, 5-63 µg/L, and 10-125 µg/L, respectively.

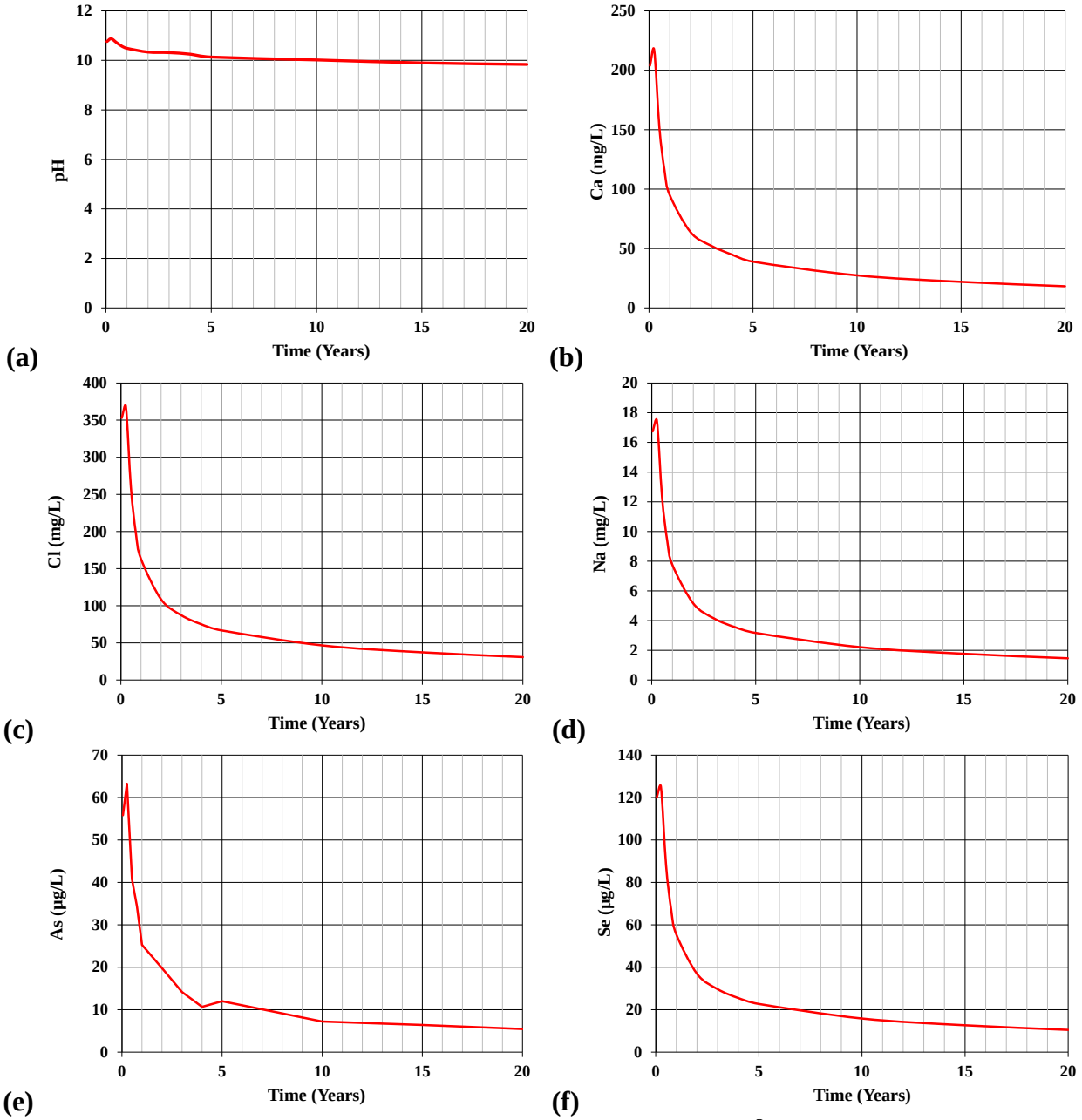

Figure 3.18. Long-term modeling of leachate (a) pH, (b) Ca^{2+}, (c) Cl^{-}, (d) Na^{+}, (e) As, and (f) Se.

Figure 3.19 show the solid concentration profiles for these elements after 20 years. The Figure shows how the elements are depleted from the solid over 20 years. The results show that precipitation significantly impacted the As profile. It should be noted that if a higher L/SA was utilized, the blocks could be even more depleted of the elements.

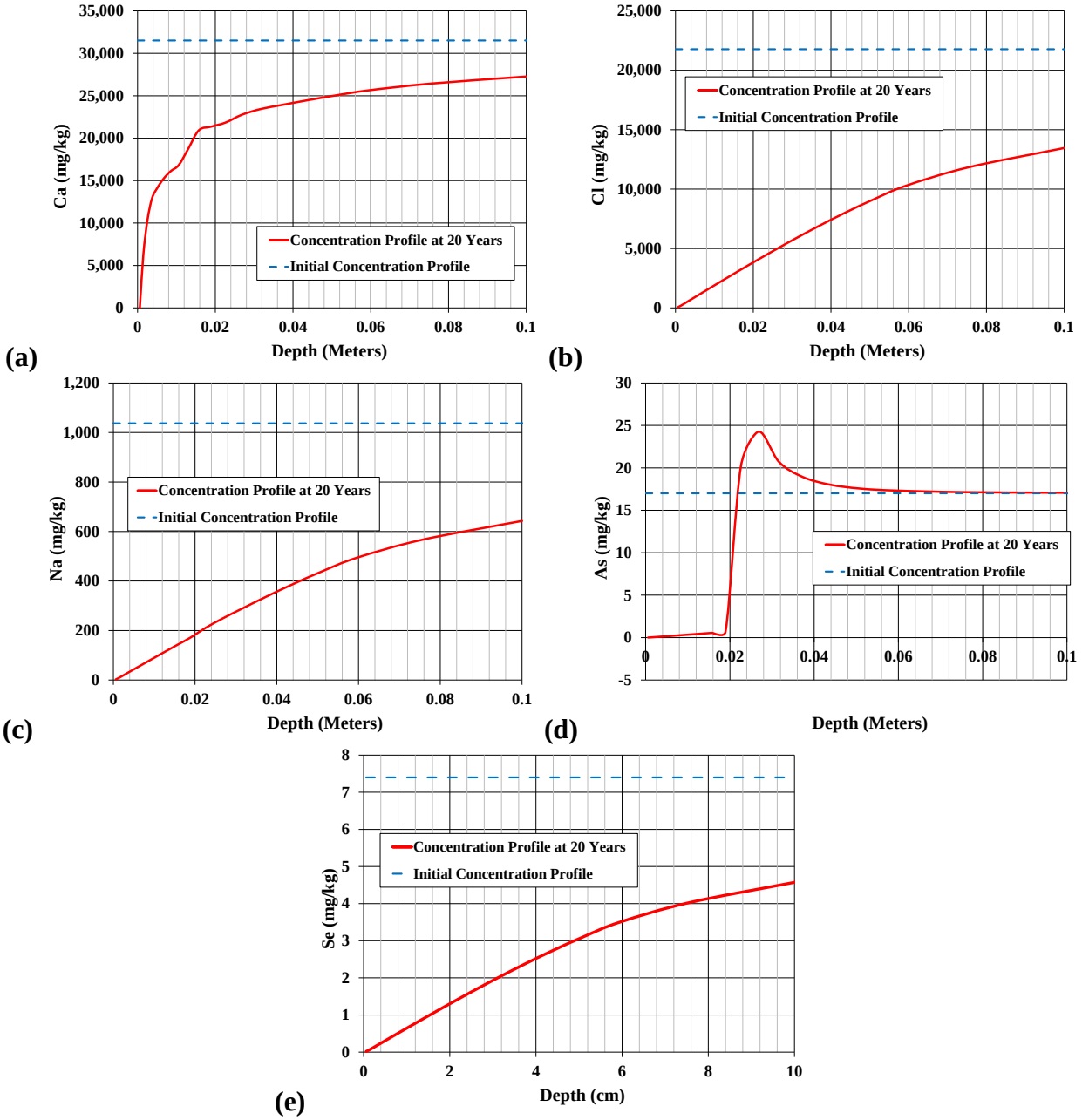

Figure 3.19. Modeled solid concentration profiles at 20 years (a) Ca, (b) Cl, (c) Na, (d) As, and (e) Se.

The results from the long-term modeling provide important insights for the coal-fired power industry. The results indicate that the highest release of all elements will be immediate. Hence, any leachate treatment system for a landfill should be able to treat leachate with a high contaminant content immediately after installation. Addition of FS (not modeled) to the S/S mixture could also decrease As and Se leaching in the early period. Alkaline pH can be expected over the first 20 years.

3.5 CONCLUSIONS

This study provided insight on the mass transport release of major components and heavy metal oxyanions from S/S solids of concentrated FGD brines through a USEPA Method 1315 evaluation. Ca^{2+} and SO_4^{2-} demonstrated the characteristics of solubility controlled release while Cl^- and Na^+ demonstrated characteristics of highly soluble species release. For oxyanions, As^V demonstrated the characteristics of solubility-controlled release while Se^{VI} demonstrated the characteristics of high soluble species release. Diffusion appeared to control Cr^{VI} release, but only a small fraction of the available Cr was released.

FS addition to the S/S process decreased the solid's cumulative release and flux at shorter leaching times for Ca^{2+}, Cl^-, Mg^{2+}, Na^+, and SO_4^{2-}, although the cumulative release and flux appeared to converge at longer leaching times. Hence, the impact of FS on the release of these major components was only transient. FS addition significantly decreased oxyanion (As^V, Cr^{VI}, and Se^{VI}) release. FS addition can increase likelihood of successful long-term disposal of S/S solids containing significant concentrations of oxyanions including As^V, Cr^{VI} and Se^{VI}. Leach XS™ modeling added additional evidence for the

proposed leaching mechanisms for As^{V} and Se^{VI} without FS addition. As^{V} leaching was successfully modeled utilizing $NaCaAsO_4 \cdot 7.5H_2O$ as the immobilization phase. Although the model does not confirm that $NaCaAsO_4 \cdot 7.5H_2O$ was the dominant phase, it confirms that a phase or phases with similar solubility as that modeled for $NaCaAsO_4 \cdot 7.5H_2O$ control As release.

Model utilization in a real scenario for the S/S solid over 20 years indicated that the leachate pH could remain alkaline (pH>9.0). Ca^{2+}, Cl^{-}, Na^{+}, As, and Se reached their highest leachate concentrations immediately.

CHAPTER 4. SALT IMPACT ON METAL LEACHING FROM A BITUMINOUS COAL FLY ASH

4.1 ABSTRACT

The coal-fired power industry is encountering solid waste management challenges from materials that are characteristically unlike traditional coal fly ash (CFA). The most challenging materials could contain significant salt concentrations in the form of Ca^{2+}, Mg^{2+}, Na^{+}, and Cl^{-}. Meanwhile, new flue gas desulfurization (FGD) wastewater regulations may lead to implementation of zero liquid discharge (ZLD) approaches which could increase the mass of salt sent to industry landfills. Salt addition to industry landfills could have negative consequences including increased metal leaching from CFA. This study evaluated the impact of salts ($CaCl_2$, $MgCl_2$, and NaCl) on the leaching of metals (As, Cd, Cr, Mn, Pb, Se, and Zn) from a bituminous CFA (BCFA) at low to high pH conditions. The evaluation was accomplished by adding salts to the extraction fluid in the modified USEPA Method 1313 leaching tests of BCFA.

In the presence of extra salts, metal leaching was enhanced, but this effect varied based on cation type and pH. With regards to the cationic metals, competitive cation exchange was the dominant mechanism for increased Cr and Mn leaching at medium pH. Cl^{-} complexation appeared to be the dominant mechanism of increased leaching with salt addition for Pb and Mn at medium pH. For the oxyanions, salt addition increased As and Se leaching at medium and high pH conditions. At low pH, As leaching significantly increased at low pH with salt addition, while Se leaching did not significantly increase. The increased As leaching with increasing salt addition at medium pH could be modeled

based on: (1) competition between Cl^- and AsO_4^{3-} for hydrous Fe^{III} oxide sorption sites; or (2) complexation and sorption of the cations (Ca^{2+}, Mg^{2+}, and Na^+) with AsO_4^{3-} to CFA surface sites. Modeling of Cd leaching increase by salt addition at neutral pH indicated that Cd leaching was controlled by (1) Cl^- complexation, and (2) competitive cation exchange for active sites with Ca^{2+}, Mg^{2+}, and Na^+.

4.2 INTRODUCTION

The coal-fired power industry is facing increasing solid waste management challenges from materials that are characteristically unlike traditional coal fly ash (CFA). The most challenging materials include those that contain significant concentrations of salts. These materials may include CFAs impacted by new air emission controls such as injection of $CaBr_2$, $Ca(OH)_2$, Na-based sorbents, and $Na_2CO_3 \cdot NaHCO_3 \cdot 2H_2O$ (trona). Previous work by the Electric Power Research Institute (EPRI) has indicated that trona injection for SO_x control will increase CFA mass in landfills and the landfill leachate pH (Blythe et al. 2008). The CFA mass collected and potentially landfilled could increase by approximately 4-12% due to the presence of Na_2SO_4 and Na_2CO_3 mixed in with the fly ash (Blythe et al. 2008). Similar mass and and potentially pH increases can be expected with other Na-based sorbents. Dry sorbent injection of $Ca(OH)_2$ for SO_x control could potentially impact CFA disposal by increasing the mass through the addition of $CaSO_4$, $Ca(OH)_2$, $CaCO_3$, and $CaSO_3$ (Blythe et al. 2008).

In addition, new flue gas desulfurization (FGD) wastewater regulations may lead to implementation of zero liquid discharge (ZLD) strategies which could increase the mass of salt sent to industry landfills. The FGD wastewater contains significant quantities of

heavy metals including As, Cd, Cr, Hg, and Se, and high concentrations of salts in the majority form of Ca^{2+}, Mg^{2+}, Na^{+}, and Cl^{-} (USEPA 2009, Huang 2013). The ZLD strategies for FGD wastewater will likely include a concentration step that will produce thick brines, at ~100,000 to 300,000 mg/L of total dissolved solids (TDS), from the wastewater by an advanced membrane or evaporation process. The produced concentrated brines could be solidified and stabilized with a polozolanic agent (e.g. CaO, $Ca(OH)_2$, Portland cement (PC), etc.) to produce a final solid for landfill disposal (Renew et al. 2014, Renew et al. 2016b).

The addition of large quantities of soluble salts either through the generation of CFA impacted by Na- or Ca-sorbent injection or by the ZLD implementation of FGD wastewater could potentially increase leachate metal content at industry landfills. Depending on coal source and type, CFA can contain significant concentrations of metals including “Ag, As, B, Ba, Cd, Co, Cr, Cu, Hg, Ni, Pb, Se, and Zn” (Wang 2007a). The cations and anions of salts could potentially increase metal leaching from CFA as these ions percolate through the landfill. Associated negative consequences may include increased leachate treatment costs and release of toxic metals to the aquatic environment. Thus, it is important for the coal-fired power industry to better understand the environmental impact of disposal of high salt materials into industry landfills before these materials are widely introduced.

Previous research has shown that high salinity conditions can increase metal mobility from estuarine sediments, soils and organic matter (Pickering 1986, Lores et al. 1998, Kabala et al. 2001, Du Laing et al. 2009b, Nelson et al. 2009). Research into metal leaching from estuarine sediments has shown that metal mobility can be increased by both

Cl^- complexation and competitive cation exchange (Du Laing et al. 2009b). For example, Cd-Cl complexes, which are stable, can decrease the activity dissolved Cd^{2+}, thereby promoting desorption from sediments (Du Laing et al. 2009b). The increased Cd^{2+} mobility with increasing salinity could also result from the effect of competitive cation exchange (Du Laing et al. 2009b). With regards to competitive cation exchange, Ca-salt addition was shown to promote metal mobilization more than Na-salt addition due to more effective competitive cation exchange for sorption sites (Du Laing et al. 2009b). In addition, one study found that Cd, Cr, and Cu leaching from marsh sediments increased with increasing salinity while Ni and Pb mobility did not increase (Du Laing et al. 2009b). Another study showed that road salts significantly impacted the mobility of Cd and Cu from roadside soils in Eastern Washington, and addition of Mg-salts increased Cd mobility more than Na-salts (Nelson et al. 2009). Furthermore, increasing salinity was shown to decrease sorption potential for Zn, Cd, and Cr to dissolved organic matter (Lores et al. 1998). Comparatively, minimal research has been conducted on the impact of high salinity on metal leaching from CFAs. A couple of studies have noted that Cl^- can increase Cd leaching from CFA likely due to Cl^- complexation (Jones 1995, Izquierdo et al. 2012). However, relevant data concerning this issue is still scarce, and there is a lack of understanding of the associated mechanisms overall.

To date, unfortunately no commercial solidification/stabilization (S/S) technology has been developed for effective limitation of salt mobility, especially Cl^-, in industry landfills with a practical pozzolonic agent addition level (Lampris et al. 2009, Ramgobeen 2010, Lampris 2013). Previous researchers noted that the formation of Friedel's salt ($CaO{\cdot}Al_2O_3{\cdot}CaCl_2{\cdot}10H_2O$), represented by AFm-Cl in cement chemistry shorthand, can

uptake Cl^- in cement through chemical incorporation (Fu 1996, Renaudina et al. 1999, Rapin et al. 2002, Ramgobeen 2010). Lampris et al. reported the S/S of a municipal solid waste incineration (MSWI) fly ash containing a Cl^- content from 130,000 to 220,000 ppm using PC with the aim of Cl^- immobilization through AFm-Cl formation (Lampris et al. 2009). In their 72-day tank leaching tests, the authors observed Cl^- releases at 40% to 50% even with PC addition up to 50% of the S/S mixture (Lampris et al. 2009). Reddy et al. observed that approximately 100% of the available Cl^- present in a cement material leached when the pH dropped from an initial value of 12.75 to 11.00 over 10 days; much of the available Cl^- in the cement material was in the form of AFm-Cl (Reddy et al. 2002). Thus, one may expect that a significant portion of the soluble salts in the disposed new types of CFA and/or S/S mixtures may leach in industry landfills, which can increase salt exposure of existing materials in landfills and potentially impact their metal leaching.

The objective of this study was to obtain a better understanding of the impact of various salts ($CaCl_2$, $MgCl_2$, and NaCl) on metal leaching from a bituminous CFA (BCFA), with both the impacts of the cations and Cl^- being considered. BCFA was selected for this study over sub-bituminous CFA (SCFA) because: (1) bituminous coal plants are expected to produce a larger mass of high-salt residuals compared to sub-bituminous coal plants; (2) BCFA contains more trace metals than sub-bituminous CFA; (3) more BCFA is produced in the U.S.; and (4) BCFA has less beneficial reuse potential than SCFA. In the U.S., Edgar reported total sulfur values 2.7% and 0.7% for bituminous coal and sub-bituminous coal, respectively (Edgar 1983). The USEPA has noted that the combustion of higher sulfur coals logically produces more SO_3 that FGD systems must remove resulting in higher FGD blowdown volumes (USEPA 2009). As a result, a larger mass of salt and metals must be

disposed from a bituminous coal power plant FGD system compared to a sub-bituminous power plant. As a result, a larger mass of salt and metals must be disposed from a bituminous coal power plant FGD system compared to a sub-bituminous coal power plant. Additionally, compared to sub-bituminous coal, bituminous coal contained higher concentrations of several metals including As (25 versus 3 ppm), Cd (1.6 versus 0.2 ppm), Cr (15 versus 7 ppm), Pb (22 versus 5 ppm), Se (4.6 versus 1.3 ppm), and Zn (53 versus 0 ppm) (Edgar 1983). Higher trace metal content in the coal would result in higher trace metal content in the associated CFA. Approximately 48% of the coal produced in the U.S. is bituminous and 44% is sub-bituminous (USEIA 2015b). When also considering that bituminous coal has a higher ash content (6.6-17.4%) than sub-bituminous coal (6.6%), it is clear that more BCFA than SCFA is produced in the U.S (Edgar 1983). BCFA is also more likely to be landfilled than SCFA because SCFA has greater beneficial reuse potential in cementitious applications due to its stronger pozzolanic properties resulting from a high CaO content (Papadakis 2000).

The evaluation was accomplished by adding the salts at different concentrations to the extraction fluid used in the USEPA Method 1313 (USEPA 2012) for the leaching tests. The study included leaching evaluations for As, Cd, Cr, Mn, Pb, Se, and Zn. In addition, the leaching of As and Cd was modeled utilizing the geochemical program PHREEQC to facilitate the understanding of the leaching mechanisms (Parkhurst et al. 1999).

4.3 EXPERIMENTAL SECTION

4.3.1 Materials and Chemicals

CFA samples were obtained from a bituminous coal-fired power plant in the southeastern United States on two occasions (CFA-I and CFA-II). $CaCl_2 \cdot 2H_2O$, $MgCl_2 \cdot 6H_2O$, and NaCl were obtained from Fisher (Pittsburgh, PA). All salts were of American Chemical Society (ACS) grade. Trace metal grade HNO_3 was obtained from Fisher.

4.3.2 Solids Analysis

CFA-I was digested utilizing the USEPA Method 3050B (USEPA 1996a). CFA-II was digested utilizing a modified version of the USEPA Method 3052 (USEPA 1996b). In this modified method, 0.2 grams of the solid were digested in a 10 mL mixture of 10%HF-20%HCl-20%HNO_3-50%H_2O. After the first stage of heating in the microwave assisted digester, 40 mL of water was added to the closed vessel and the mixture was heated again. Salts were digested utilizing USEPA Method 3050B. Digestates were analyzed utilizing the USEPA Method 6020A (USEPA 2007) or a combination of the USEPA Methods 6020A and 200.8 (USEPA 1994a).

4.3.3 Leaching Procedures

A modified version of the USEPA Method 1313 (USEPA 2012) was the basis of the experimental approach to evaluate metal leaching. Prior to the leaching tests, the first step was to develop the required HNO_3 doses to be added for the extractant fluid to achieve the target pH.

Based upon the pre-test titration results, samples were prepared by mixing 200 mL of extractant fluid (with necessary amounts of HNO_3 added) with varied amounts of salt ($CaCl_2$, $MgCl_2$, or NaCl) in a high density polyethylene (HDPE) bottle. For each salt addition level, samples with a final target pH of low (~4.0), medium (~7.0), or high (~10.0) level were prepared for CFA-I. Some difficulty was encountered maintaining the high pH samples with $CaCl_2$ and $MgCl_2$ addition likely due to precipitation of $Ca(OH)_2$ or $Mg(OH)_2$ or complexation of Ca^{2+} and Mg^{2+} with OH^-. Only medium (~7.0) target pH samples were prepared for CFA-II. The three different salts were added at varied concentrations (0-2.2 M) based on the cation concentration. The mixed samples were tumbled for 24 hours at room temperature. After tumbling, the solids and the liquids were separated utilizing 0.7-µm, pre-acid-washed toxicity characteristic leaching procedure (TCLP) filters (Environmental Express, Charleston, SC). The filtrate was collected in a HDPE bottle and analyzed for metals. Prior to ICP-MS analysis, the filtered leachate from CFA-I samples was digested per USEPA Method SW3005A (USEPA 1992b). Filtered leachate from CFA-II was digested by adding 5% HNO_3/5%HCl and heating the sample for 1 h at approximately 95 ^oC. Both methods would sufficiently digest any metals in the solid phase in the filtrate.

4.3.4 X-Ray Diffraction

Quantitative crystallographic analysis was performed on a CFA sample from the same plant that CFA-I and CFA-II were collected using powder X-ray diffraction (XRD). The internal standard utilized was 10% corundum (Al_2O_3) which was mixed with the CFA sample. The CFA sample was placed on a zero background holder. The sample was analyzed in a Bruker (Billerica, MA) D2 Phase with Cu radiation (30 kV/10mA). The range

of the scan was 8º -70º with a step size of 0.0152º and a counting time of 1.5 s/step. Once the pattern was obtained, the data was analyzed using EVA software (Bruker) for the qualitative analysis and TOPAS software of quantitative analysis.

In addition, qualitative XRD analysis was conducted on CFA-II from samples collected on the TCLP filters after the USEPA Method 1313 extraction procedure with and without salt addition**.** The sample powders were analyzed using a PANalytical X-Pert Pro XRD (Almelo, The Netherlands). The XRD was operated at a voltage of 40 kV and a current of 40 mA. The range of the scan was 4º -70º with a step size of 0.02º and a time per step of 225 s/step.

4.3.5 Surface Complexation Modeling

PHREEQC Interactive Version 3.3.7 was utilized to develop surface complexation models for As and Cd leaching from CFA-I at near neutral pH. The specific ion interaction theory (SIT) database was utilized for thermodynamic information. PhreePlot was utilized to assist in parameter optimization and to repeatedly run the PHREEQC model utilizing a range of salt concentrations (Kinniburgh et al. 2010).

The SIT database was selected in this work's modeling efforts due to the high ionic strength of the leaching experiments (0-5.5 M). The SIT has typically been utilized for ionic strengths approaching 3.5-4.0 M and the Pitzer model has been applied at extreme ionic strengths up to the "saturation of most salts" (Xiong 2006). Xiong noted that errors in activity coefficients calculated by SIT versus Pitzer model "is usually less than 10% at ionic strength up to 6–10 m at 25°C" (Xiong 2006). Hyks et al. noted that insufficient thermodynamic data is available to model a complex leaching system (Hyks et al. 2009).

Due to the same issue regarding limited thermodynamic data availability, it was decided to utilize the SIT database for the modeling described this Chapter.

Leaching Model for Arsenic. Tables 4.1 and 4.2 show additions that were made to the SIT database to develop the surface complexation models. The As^{V} surface complexation model was influenced by the work of van Der Hoek et al., who modeled As leaching based on Fe (hydr)oxide (van der Hoek et al. 1996). The As leaching results from this study seemed to be closer those in the study by van Der Hoek et al. with significant As leaching at near neutral pH more than the CFA leaching models developed by Wang et al., who based all leaching from three acid surface sites and had essentially no leaching at near neutral pH (van der Hoek et al. 1996, Wang 2007a, Wang et al. 2008).

As sorption to weak hydrous ferric oxide (Hfo_wOH) sites is modeled. In order to simplify modeling, the Log K values for the Reaction (1) and (2) were assumed to be the same value in order to reduce the number of constants that needed to be modeled similar to the approach taken by Su and Wang (Su et al. 2011). The Log K values of these reactions were interpolated based on pH from values provided by van Der Hoek et al (van der Hoek et al. 1996). Reaction (4) hypothesizes that Cl^{-} will compete for surface sites with As. Reactions (5) through (10) model complexation of Ca^{2+}, Mg^{2+}, and Na^{+} with As and sorption onto surface sites. Wang et al. noted that AsO_4^{3-} is known to complex with Ca^{2+} and can potentially sorb to surface sites (especially as neutral species) (Wang 2007a). The proposed model hypothesizes that As^{V} will also complex with Mg^{2+} and Na^{+} and sorb to the surface of the CFA. In order to simplify the modeling process, the Log Ks for Reactions Nos. 5 and 6, 7 and 8, and 9 and 10 were assumed to have the same value. Modeled Log K values for the sorption of $CaHAsO_4$ and $Ca_{1.5}(AsO_4)$ to two CFAs by Wang were close in

value (1.9 versus 2.6, versus 2.1 and 3.0), hence, it was felt acceptable to assume this simplification step (Wang 2007a).

Table 4.1. Changes of surface association reactions made to in SIT database.

No.	Reaction	Log K	Reference
	As Model		
1	$Hfo\_wOH + AsO_4^{3-} + 3H^+ = Hfo\_wH_2AsO_4 + H_2O$	4.53	(van der Hoek et al. 1996)
2	$Hfo\_wOH + AsO_4^{3-} + 2H^+ = Hfo\_wHAsO_4^- + H_2O$	4.53	(van der Hoek et al. 1996)
3	$Hfo\_wOH + AsO_4^{3-} = Hfo\_wOHAsO_4^{3-}$	6.85	Modeled
4	$Hfo\_wOH + Cl^- = Hfo\_wCl + OH^-$	-5.20	Modeled
5	$Surface\_OH + Ca^{2+} + AsO_4^{3-} = Surface\_CaAsO4 + OH^-$	2.40	Modeled
6	$Surface\_OH + Ca^{2+} + H^+ + AsO_4^{3-} = Surface\_CaHAsO_4^+ + OH^-$	2.40	Modeled
7	$Surface\_OH + Mg^{2+} + AsO_4^{3-} = Surface\_MgAsO_4 + OH^-$	0.45	Modeled
8	$Surface\_OH + Mg^{2+} + H^+ + AsO_4^{3-} = Surface\_MgHAsO_4^+ + OH^-$	0.45	Modeled
9	$Surface\_OH + Na^+ + AsO_4^{3-} = Surface\_NaAsO_4^- + OH^-$	0.18	Modeled
10	$Surface\_OH + Na+ + H^+ + AsO_4^{3-} = Surface\_NaHAsO_4 + OH^-$	0.18	Modeled
	Cd Model		
11	$\beta\_OH = \beta\_O^- + H+$	-8.11	(Wang 2007b, Su et al. 2011)
12	$\beta\_O^- + Cd^{2+} = \beta\_OCd^+$	12.13	Modeled
13	$\beta\_O^- + Ca^{2+} = \beta\_OCa^+$	9.80	Modeled
14	$\beta\_O^- + Mg^{2+} = \beta\_OMg^+$	9.00	Modeled
15	$\beta\_O^- + Na^+ = \beta\_ONa$	7.60	Modeled

Table 4.2. Surface sites and properties of CFA for sorption modeling.

Surface Site	Site Densities (moles/g)	Surface Area (m^2/g)
As Model		
Hfo_wOH	$1.25x10^{-6}$	1.27
Surface_OH	$1.00x10^{-4}$	1.27
Cd Model		
β_OH	$1.80x10^{-5}$	1.27

The maximum amount of Fe leached by CFA-I was assumed to be the amount of adsorbable Fe which was utilized to calculate the Hfo_wOH site density shown in Table 4.2. The surface site density for Surface_OH was unknown, but a large site density was assumed as shown in Table 4.2. The main purpose of the Reactions (5) through (10) is to demonstrate the differences in complexation and sorption with Ca^{2+}, Mg^{2+}, and Na^{+}, respectively. The CFA surface area was adopted from Yeboah et al., who had determined the surface area to be around 1.27 m^2/g for CFA from the same coal-fired power plant where CFA-I and CFA-II were collected (Yeboah et al. 2014).

The As model was operated under oxidizing conditions by fixing the pe of the reaction at a positive value so no reduction occurred. The available As^{V} (0.61 μg As^{V}/g CFA) in the model was calculated from the highest leaching value measured in the leaching experiment under neutral conditions in this study. Both As and Cd modeling assumed equilibrium conditions and the leachant pH was the same as experimentally observed.

Leaching Model for Cadmium. The Cd leaching model was significantly influenced by modeling work by Wang et al. on Cd^{II} leaching from CFA (Wang et al. 2004, Wang et al. 2006, Wang 2007b, Wang et al. 2007, Wang et al. 2008, Wang et al. 2009, Su

et al. 2011). This work found that there were three acid surface sites that were associated with CFA leaching – α, β, and γ (Wang 2007b). The β sites are associated with Cd leaching (Wang et al. 2004, Wang et al. 2006, Wang 2007b, Wang et al. 2007, Wang et al. 2008, Wang et al. 2009, Su et al. 2011). The surface complexation reactions for the model are shown in Table 4.1. The model hypothesizes that Ca^{2+}, Mg^{2+}, and Na^{+} can compete with Cd^{2+} for β sites as observed for estuarine sediments (Du Laing et al. 2009b). The number of β site density was assumed to be similar to that measured for a Class F CFA by Wang et al. (Table 4.2) (Wang et al. 2004). The available Cd (0.52 µg Cd/g CFA) in the model was calculated from the highest leached Cd concentration measured under neutral pH conditions in this study.

4.4 RESULTS AND DISCUSSION

4.4.1 Analysis of CFA Solids

Figure 4.1 shows the quantitative XRD results for a CFA sample that was collected from the same plant as CFA-I and CFA-II. Although it was collected at a different time than CFA-I and CFA-II, it was unlikely that the crystalline phases of the material changed over time since the coal fuel did not change. The main phases detected were indicative of bituminous CFA. The CFA was mostly amorphous (78.2%), and the crystalline phases from the highest to the lowest content by mass were quartz (SiO_2), hematite (Fe_2O_3), diopside ($MgCaSi_2O_6$), trona, mullite ($Al_6Si_2O_{13}$), and anyhydrite ($CaSO_4$).

Table 4.3 shows the metal analysis for the digested CFA-I, CFA-II, and dissolved salts in this study. It is noted that CFA-II was digested by a much stronger digestion method as described in the Experimental Section. Both CFA-I and CFA-II contained a similar

amount of Ca. The concentrations of Al, Fe, K, and Mg are higher in CFA-II than in CFA-I. CFA-II also contained higher concentrations of trace metals (As, Ba, Cd, Cr, Mn, Pb, Se, and Zn). The presented results indicate that both CFAs had metal contents indicative of BCFA.

The metal content results for the salts showed that the $CaCl_2 \cdot 2H_2O$ salt contained slight contamination of Pb and As. Thus, the amounts of Pb and As added to the leaching experiments from this salt addition were subtracted in all calculations and graphs of leached concentrations in this study.

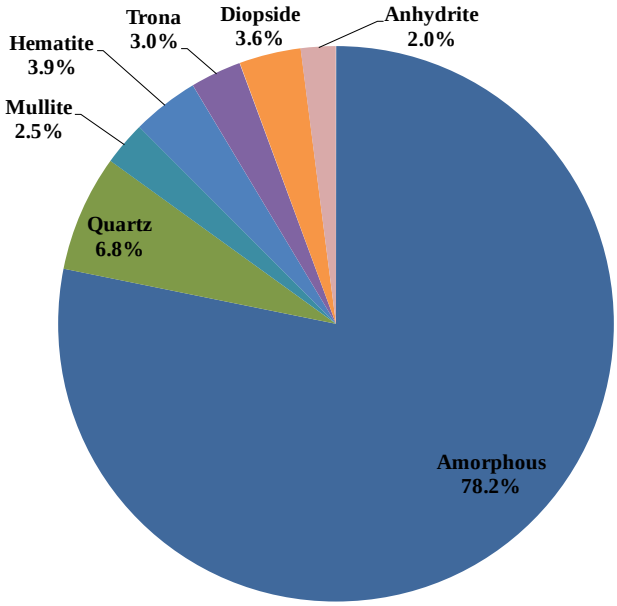

Figure 4.1. Quantitative XRD analysis of CFA.

Table 4.3. Metal composition analysis for digested CFA-I, CFA-II, and salts.

(a) Bulk Elements

Composition	CFA-I (mg/kg dry)	CFA-II (mg/kg dry)	$CaCl_2 \cdot 2H_2O$ (mg/kg dry)	$MgCl_2 \cdot 7H_2O$ (mg/kg dry)	NaCl (mg/kg dry)
Al	29,200	113,617	< 34.4	< 34.4	< 27.9
Ca	15,600	11,852	--	47.6	< 50.0
Fe	28,800	76,948	< 19.4	8.0	20.2
K	2,580	16,965	5.6	< 5.7	52.4
Mg	1,710	4,715	31.4	--	< 102.0

(b) Significant Elements

Composition	CFA-I (mg/kg dry)	CFA-II (mg/kg dry)	$CaCl_2 \cdot 2H_2O$ (mg/kg dry)	$MgCl_2 \cdot 7H_2O$ (mg/kg dry)	NaCl (mg/kg dry)
Ba	320	762	1.0	10.8	< 1.0
Cr	71	174	< 0.3	< 0.3	< 1.3
Cu	37	116	< 0.2	< 0.2	< 0.7
Mn	72	134	< 0.2	< 0.2	< 0.7
Ni	29	118	< 0.2	< 0.3	< 0.8
Pb	31	73	0.1	< 0.3	< 1.4
Zn	53	196	< 0.8	< 0.9	< 3.8

(c) Trace Elements

Composition	CFA-I (mg/kg dry)	CFA-II (mg/kg dry)	$CaCl_2 \cdot 2H_2O$ (mg/kg dry)	$MgCl_2 \cdot 7H_2O$ (mg/kg dry)	NaCl (mg/kg dry)
Ag	0.1	0.3	< 0.01	< 0.01	< 0.04
As	25.6	69.3	0.13	< 0.07	< 0.3
Be	6.3	16.2	< 0.7	< 0.8	< 0.6
Cd	0.8	1.1	< 0.3	< 0.3	< 0.2
Co	24.6	44.4	< 0.2	< 0.2	< 0.7
Mo	24.3	24.7	< 0.4	< 0.5	< 1.9
Sb	1.2	5.9	< 30.9	< 0.6	< 2.5
Se	5.5	10.2	< 0.1	< 0.2	< 0.7
Tl	0.8	4.4	< 0.19	< 0.2	< 0.8

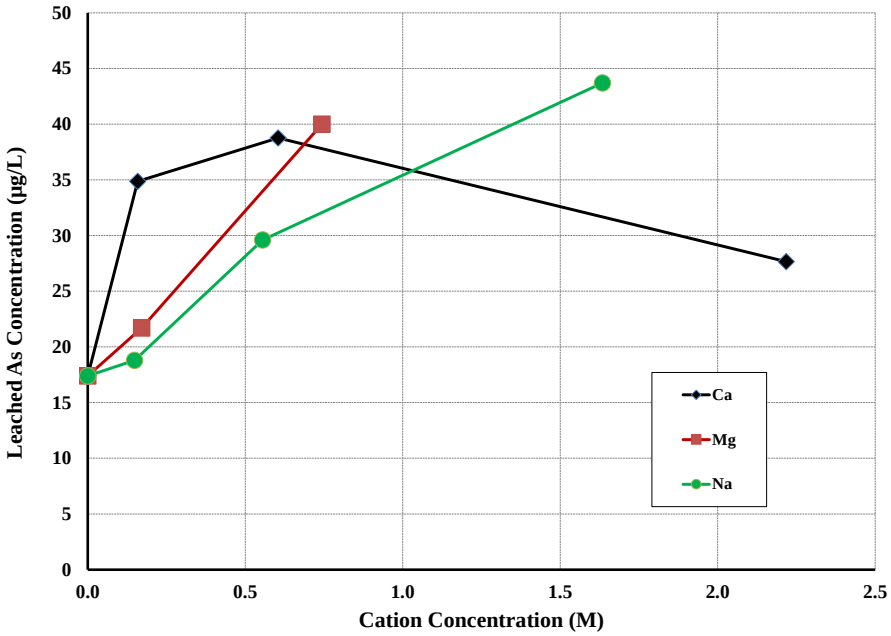

Figure 4.2. As leaching from CFA-I at low pH. Note: Ca = $CaCl_2$ addition, Mg = $MgCl_2$ addition, and Na = NaCl addition. The sample pHs with $CaCl_2$, $MgCl_2$, or NaCl added were 3.6-4.5, 4.1-4.5, and 4.2-4.5, respectively.

4.4.2 Leaching Results

Arsenic. Figure 4.2 shows that all salts increased As leaching from CFA-I at low pH, similarly from a minimum concentration of 17 µg/L to maximum concentrations of 39, 44, and 40 µg/L for $CaCl_2$, NaCl, and $MgCl_2$, respectively. At near neutral pH (Figure 4.3a), As leaching from CFA-I increased from an initial concentration of 30 µg/L to maximum concentrations of 46 and 60 µg/L with NaCl and $MgCl_2$, respectively, whereas $CaCl_2$ addition decreased As leaching.

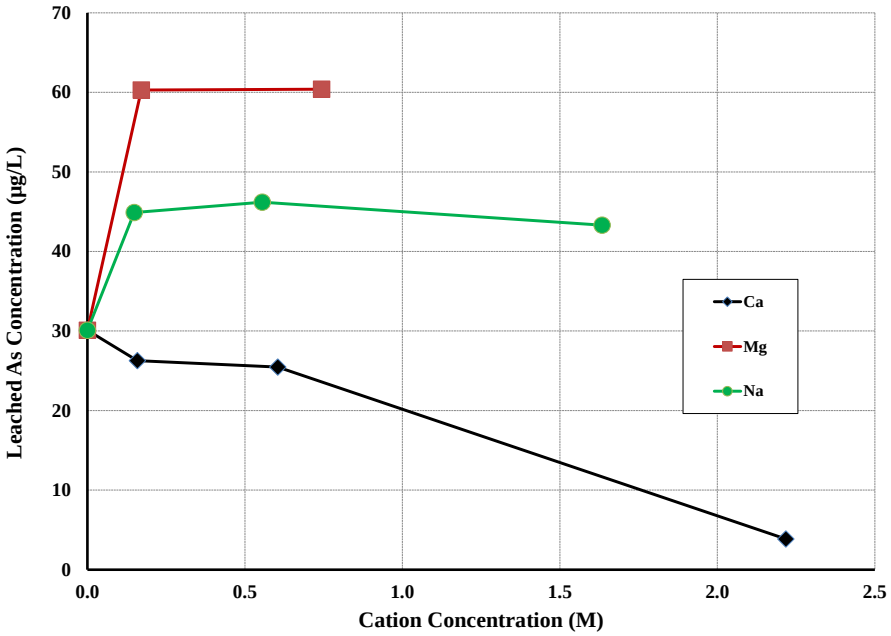

(a)

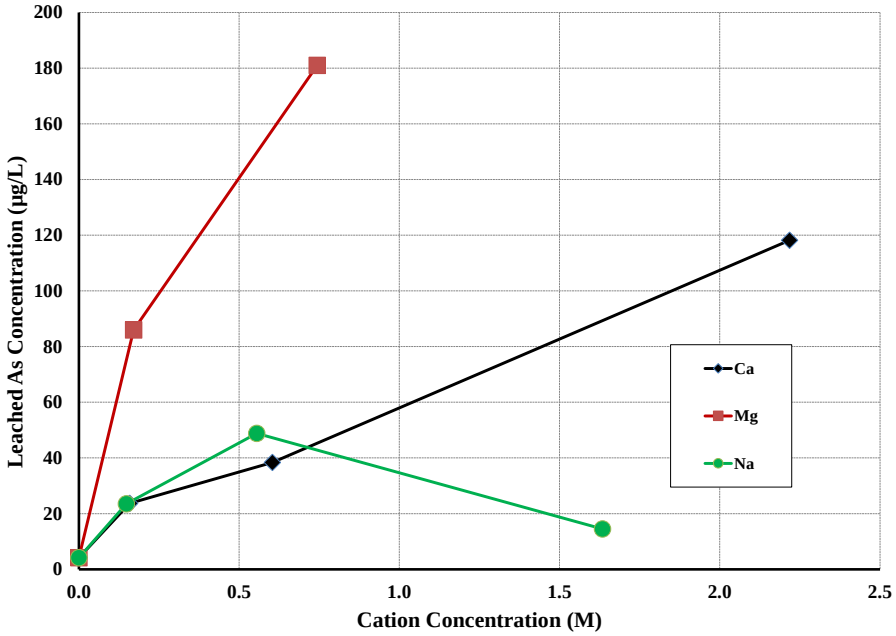

(b)

Figure 4.3. As leaching from CFA-I at (a) medium pH and (b) high pH conditions. Note: Ca = $CaCl_2$ addition, Mg = $MgCl_2$ addition, and Na = NaCl addition. Medium pH: pH 6.7-7.6 ($CaCl_2$), 6.8-7.6 ($MgCl_2$), and 7.1-7.6 (NaCl). High pH: pH 8.0-9.9 ($CaCl_2$), 8.1-9.9 ($MgCl_2$), and 9.9-10.1 (NaCl).

Figure 4.4 shows similar results for CFA-II with As leaching increasing from 4 µg/L to a maximum concentration of 7 µg/L with $MgCl_2$ addition, while $CaCl_2$ addition

decreased As leaching. At high pH (Figure 4.3b), As leaching from CFA-I increased from minimal leaching to approximately maximum leached concentrations of 118, 181, and 49 µg/L with $CaCl_2$, $MgCl_2$, and NaCl, respectively.

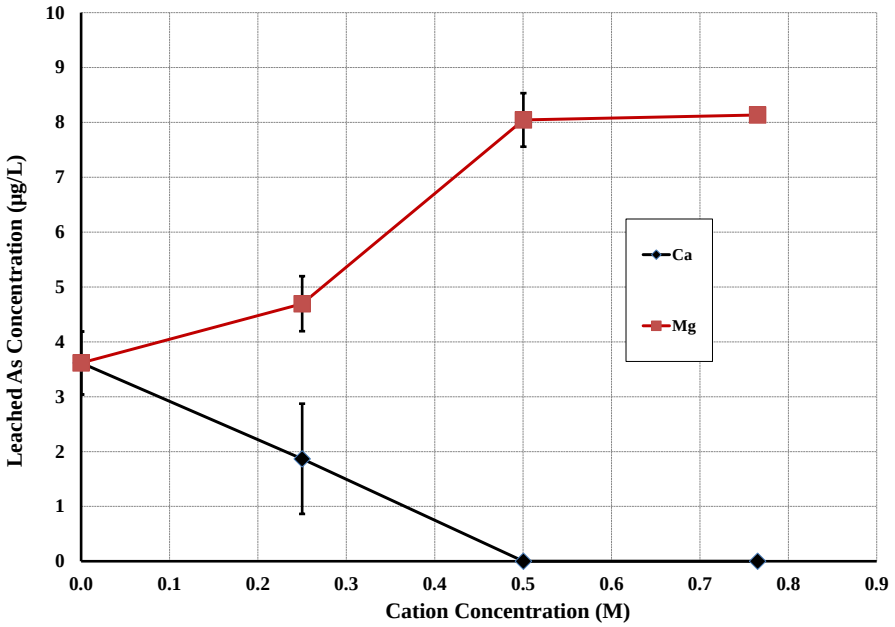

Figure 4.4. As leaching results from CFA-II at medium pH. Note: Ca = $CaCl_2$ addition and Mg = $MgCl_2$ addition. The sample pHs with $CaCl_2$ and $MgCl_2$ added were 6.7-7.5 and 6.7-7.4, respectively.

With regards to heavy metals, previous researchers have noted that As is present in CFA primarily as the oxyanion AsO_4^{3-} (Goodarzi et al. 2001, Huggins et al. 2007, Goodarzi et al. 2008). As partitions to CFA from the flue gas majorly through sorption to Fe sites on BCFA and Ca sites for SCFA (Yudovich et al. 2005). In general, As leaching from bituminous CFA is controlled by adsorption/desorption from Fe hydroxides and is heavily dependent on As speciation (Wang et al. 2009).

Anion-exchange could drive AsO_4^{3-} mobilization at low and medium pH. Keon et al. hypothesized anion exchange with Cl^- as the main mechanism of enhanced As

mobilization during batch equilibrium leaching tests with $MgCl_2$ addition in the range of 1 M (Keon et al. 2001). The researchers noted that $MgCl_2$ likely mobilized the ionically bound As (Keon et al. 2001).

Anion exchange may not play a large role at higher pH, as the CFA surface becomes deprotonated and more negatively charged. While the XRF analysis in this study showed a major percentage of amorphous phase in CFA, our previous work on a BCFA sample showed SiO_2, Al_2O_3 and Fe_2O_3 to be the major phases (Renew et al. 2016b). Considering the typical point of zero charges (pzc) for SiO_2 (~2.2-3.5), Al_2O_3 (~9.5-10.0), and Fe_2O_3 (~7.0), the CFA in this study is estimated to have a pzc around 5-6 (Mohapatra et al. 1997). While there may be a significant amount of positively charged sites for AsO_4^{3-} to sorb to at low and medium pH, the number of these sites decreases as pH increases. The low pH results indicate that anion exchange for Cl^- was likely the main mechanism of mobilization as leaching increased with increased Cl^- concentration regardless of which type of cation addition.

The medium pH results show that although anion exchange for Cl^- may drive the process, other factors may be influencing the results as well. Wang noted that Ca^{2+} could potentially form complexes with AsO_4^{3-} and these complexes could sorb to the CFA surface (Wang 2007a). Hence, it is possible that Ca^{2+} addition could limit leaching of As through this process This process could explain why Ca^{2+} addition at near neutral pH actually decreased As mobilization. It should be noted that per the pzc value for CFA, there are less positively-charged sites at medium pH compared to at low pH. Hence, this complexation process may be more important where less positively-charged sites exist for As to sorb. Keon et al. hypothesized that AsO_4^{3-} could also potentially complex with Mg^{2+} (Keon et

al. 2001). Although little information is available in literature on this topic, it is possible that Mg^{2+} and Na^{+} could also potentially complex with AsO_4^{3-} and sorb to active sites. Differences in the affinity of Ca^{2+}, Mg^{2+}, and Na^{+} in complexing with As^{V} and the resulted complexes sorbing to the active sites could explain the differences in As leaching shown in Figure 4.3a. Furthermore, Ca-As^{V} precipitation could also play a role as these complexes begin to decrease in solubility under alkaline conditions (Masue et al. 2007). Nishimura and Robins reported Ca-As^{V} solubilities for $CaHAsO_4 \cdot H_2O$ (average Log K_{SP} = 3.23, pH = 5.35-6.46), $Ca_3(AsO_4)_2 \cdot H_2O$ (average Log K_{SP} = 5.58, pH = 7.51-9.58), and $Ca_2AsO_4OH \cdot 2H_2O$ (average Log K_{SP} = 1.29, pH = 12.02-12.48) (Nishimura et al. 1998). Less information is available in literature on the correlation between $Mg_3(AsO4)_2$ solubility and pH.

As mentioned above, the CFA surface becomes increasingly negatively charged due to deprotonation in the high pH range. As a result, anion exchange may not play as large a role at high pH due to repulsive forces between the anions and the CFA surface. Iyer proposed that elements leaching from the CFA surface must traverse the diffuse double layer (DDL) to reach the bulk solution with resistance present in the DDL (Iyer 2002). High ionic strength can compress the DDL around CFA and has been shown to increase leaching for at least some elements (Stanmore et al. 1992, Iyer 2002). It is possible that DDL compression due to high salinity conditions increased AsO_4^{3-} leaching with divalent ions obviously compressing the DDL more than monovalent ions. This process could be the reason that addition of the divalent $MgCl_2$ increased As leaching more than the monovalent NaCl. The reason that $CaCl_2$ did not increase leaching as much as $MgCl_2$ could

be because of the reasons described for the medium pH with Ca^{2+} addition limiting As leaching either through complexation and sorption or Ca-As^{V} phase precipitation.

Cadmium. Figure 4.5 shows that salt addition did not significantly increase Cd leaching from CFA-I from an initial concentration of 56 µg/L under low pH conditions. At near neutral pH conditions for CFA-I (Figure 4.6a), all salts significantly increased Cd leaching from an initial concentration <method detection limit (MDL, 12.2 µg/L, graphed as 25% MDL) to maximum concentrations of 49 µg/L, 50 µg/L, and 44 µg/L with $CaCl_2$ $MgCl_2$ and NaCl, respectively. Similarly, $CaCl_2$ and $MgCl_2$ addition both increased Cd leaching from CFA-II at near neutral pH as shown in Figure 4.7.

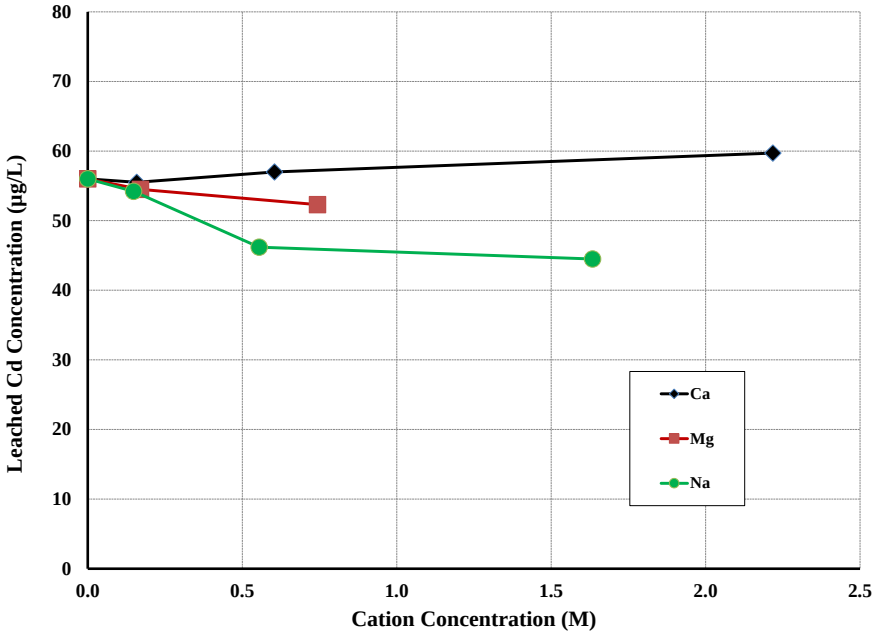

Figure 4.5. Cd leaching from CFA-I at low pH. Note: Ca = $CaCl_2$ addition, Mg = $MgCl_2$ addition, and Na = NaCl addition. The sample pHs with $CaCl_2$, $MgCl_2$, or NaCl added were 3.6-4.5, 4.1-4.5, and 4.2-4.5, respectively.

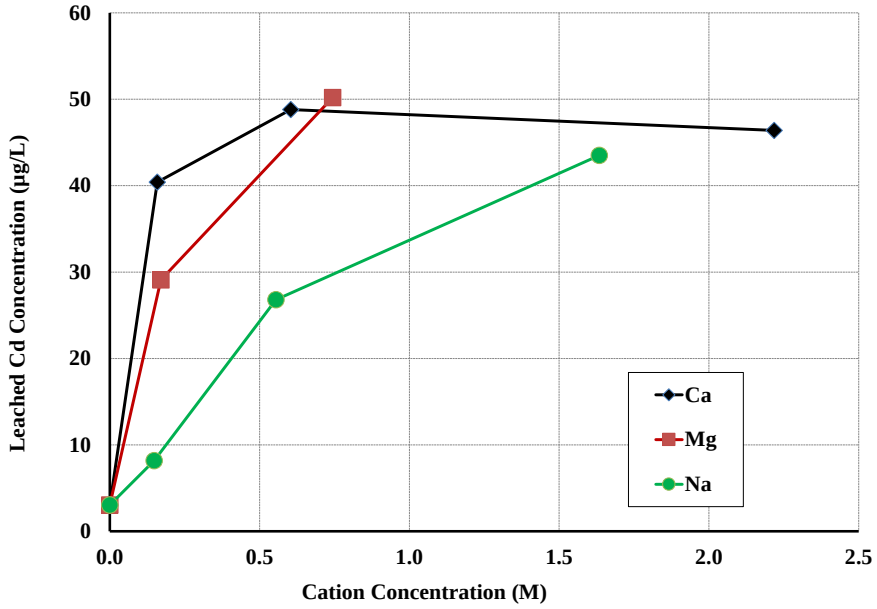

(a)

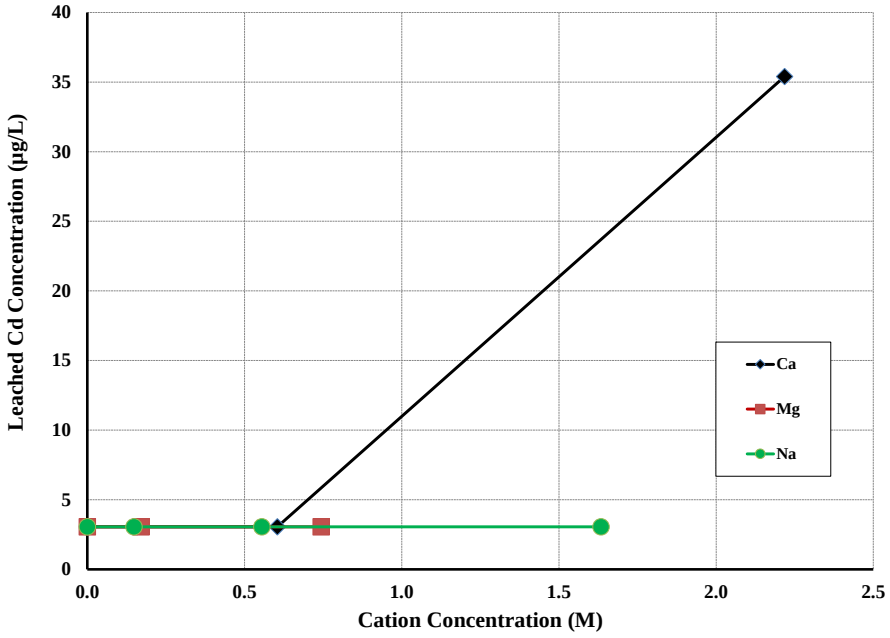

(b)

Figure 4.6. Cd leaching from CFA-I at (a) medium pH and (b) high pH conditions. Note: Ca = $CaCl_2$ addition, Mg = $MgCl_2$ addition, and Na = NaCl addition. Medium pH: pH 6.7-7.6 ($CaCl_2$), 6.8-7.6 ($MgCl_2$), and 7.1-7.6 (NaCl). High pH: pH 8.0-9.9 ($CaCl_2$), 8.1-9.9 ($MgCl_2$), and 9.9-10.1 (NaCl).

However, Cd leaching increases by the salts for CFA-II were not as dramatic as for CFA-I perhaps due to the larger Cd leached concentration for CFA-II versus CFA-I (38

µg/L versus <MDL) without salt addition. At high pH (Figure 4.6b), Cd leaching from CFA-I was not increased with salt addition except for the highest salt addition with $CaCl_2$ where the leached Cd concentration increased to 35 µg/L.

Cd which is typically associated with the CFA surface is believed to be associated with aluminosilicates and metal oxides surfaces in CFA although it may also be precipitated as $Cd(OH)_2$ or $CaCO_3$ (Jones 1995). It's leaching is limited at high pH due to the low solubility of $Cd(OH)_2$. As typical for leaching of cationic metals from CFA, Cd leaches readily at low pH, but not at high pH (Izquierdo et al. 2012). At low pH, Cd leaching was not impacted by salt addition due to the high solubility of Cd^{2+}. Essentially all of the Cd available to leach at low pH readily leached regardless of salt addition.

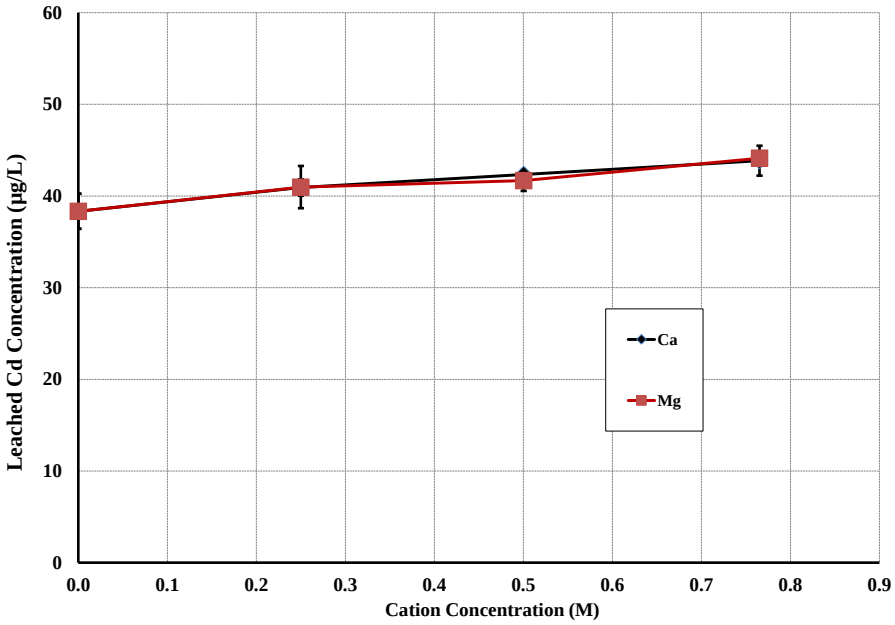

Figure 4.7. Cd leaching results from CFA-II at medium pH. Note: Ca = $CaCl_2$ addition and Mg = $MgCl_2$ addition. The sample pHs with $CaCl_2$ and $MgCl_2$ added were 6.7-7.5 and 6.7-7.4, respectively.

At near neutral pH, it is apparent that Cl^- complexation significantly increased Cd leaching. Cd leaching increased with Cl^- concentration regardless of the cation type. As

mentioned earlier, Cd-Cl complexes are stable (Du Laing et al. 2009b). Cl^- complexation moves Cd speciation "shifts towards $CdCl^+$, $CdCl_2$, $CdCl_3^-$ and $CdCl_4^{2-}$" (Du Laing et al. 2008). Cl^- complexation reduces activity (i.e. effective concentration) of cations in the and can promote cation mobility (Du Laing et al. 2009b).

A high pH, salt addition did not significantly increase Cd leaching due to the low solubility of $Cd(OH)_2$ in this region. Izquierdo noted that Cd is essentially completely stabilized on CFA under alkaline conditions (Izquierdo et al. 2012). Only the highest Cl^- addition overcame the insolubility of $Cd(OH)_2$ under high pH conditions and increased leaching likely due to Cl^- complexation.

Chromium. Figure 4.8 shows that salt addition did not significantly increase Cr leaching from CFA-I under low pH conditions from an initial concentration of 119 µg/L. At near neutral pH conditions (Figure 4.9a), $CaCl_2$ increased Cr leaching from CFA-I from an initial concentration of 11 µg/L to a maximum concentration of 60 µg/L, $MgCl_2$ mildly increased Cr leaching to 18 µg/L , and NaCl had negligible effect. Figure 4.10 shows that for CFA-II under near neutral pH conditions, $CaCl_2$ and $MgCl_2$ addition increased Cr leaching from an initial value of 2.7 µg/L to maximum concentrations of 6.3 and 4.5 µg/L, respectively. Under high pH conditions for CFA-I (Figure 4.9b), only the highest $CaCl_2$ addition significantly increased Cr leaching from an initial concentration of approximately 111 µg/L to a maximum concentration of 447 µg/L.

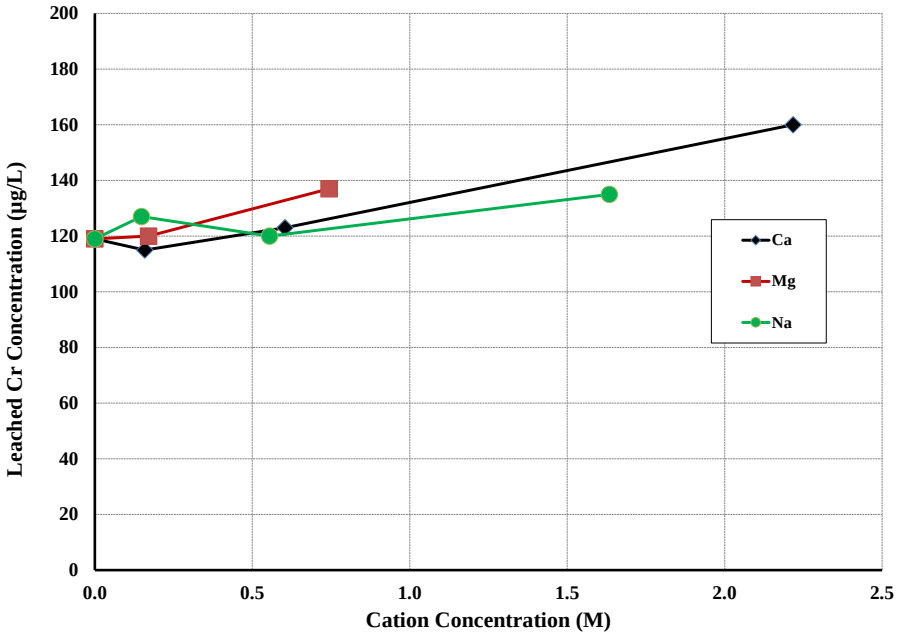

Figure 4.8. Cr leaching from CFA-I at low pH. Note: Ca = $CaCl_2$ addition, Mg = $MgCl_2$ addition, and Na = NaCl addition. The sample pHs with $CaCl_2$, $MgCl_2$, or NaCl added were 3.6-4.5, 4.1-4.5, and 4.2-4.5, respectively.

The dominant Cr species in CFA is Cr^{III} with Huffman et al. finding greater than 95% Cr^{III} of total Cr (Huffman et al. 1994, Huggins et al. 1999, Goodarzi et al. 2001, Goodarzi et al. 2008). Cr has been identified as residing mainly in the amorphous glassy aluminosilicate slag portion of CFA on both the surface and the entire CFA particle (Huffman et al. 1994, Jones 1995, Kim et al. 2004).

It is apparent that the under low pH conditions, salt addition had no significant impact on Cr leaching because that element leaches readily at low pH as has been reported in literature (Izquierdo et al. 2012). All of the Cr available to leach readily did so regardless of salt addition.

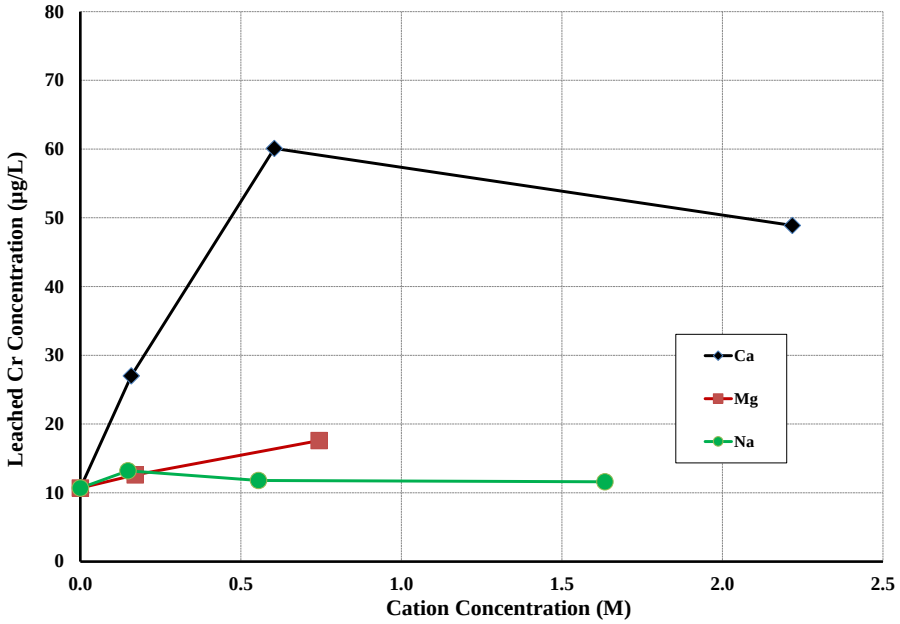

(a)

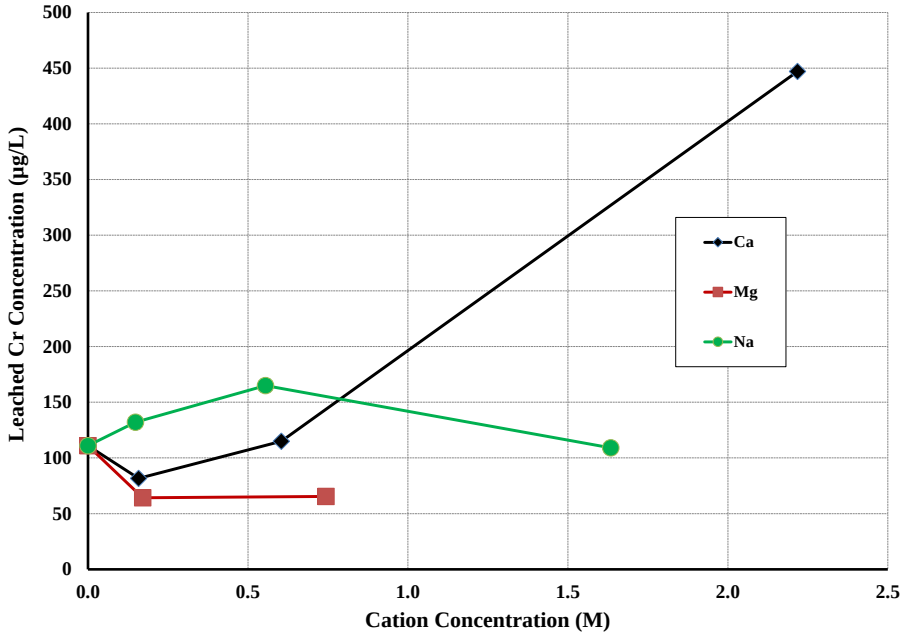

(b)

Figure 4.9. Cr leaching from CFA-I at (a) medium pH and (b) high pH conditions. Note: Ca = $CaCl_2$ addition, Mg = $MgCl_2$ addition, and Na = NaCl addition. Medium pH: pH 6.7-7.6 ($CaCl_2$), 6.8-7.6 ($MgCl_2$), and 7.1-7.6 (NaCl). High pH: pH 8.0-9.9 ($CaCl_2$), 8.1-9.9 ($MgCl_2$), and 9.9-10.1 (NaCl).

Under near neutral pH, Cr leaching increased significantly with $CaCl_2$ addition likely due to competitive cation exchange. It is apparent that the solubility of Cr^{III} is low

enough that salt addition can make a difference. Competition for surface sorption sites between major cations (Ca^{2+}, Mg^{2+}, and Na^{+}) and trace metals can likely impact metal leaching from CFA.

Previous research has shown that zeolites, which have high Si/Al ratios similar to CFA, favor sorption of divalent cations with lower hydration energies to active sites (Wingenfelder et al. 2005, Teutli-Sequeira et al. 2009). This research shows that cations with lower hydration energy will preferentially exchange for higher energy cations on active sites on the zeolite surface (Wingenfelder et al. 2005, Teutli-Sequeira et al. 2009). Researchers have noted electrostatic forces along with energy bonding both play a role in the cation preference for sorption on hydrous oxides (Balistrieri et al. 1982, Paalman et al. 1994). Typically when comparing positively charged metals within the same valence state, typically the ion with the larger ionic radius will be preferentially sorbed to hydrous oxides (Paalman et al. 1994).

It is apparent that the higher concentration of the major divalent cations (Ca^{2+} and Mg^{2+}) and the potential to form higher energy bonds with active surface sites can increase trace metal leaching. It is apparent that the higher concentration of the major divalent cations (Ca^{2+} and Mg^{2+}) and the potential to form higher energy bonds with active surface sites can increase trace metal leaching. Table 4.4 lists the ionic radius and Gibbs free energy of hydration for each of the cationic metals of interest in this study (Marcus 1991). The ionic radius of Cr^{III} is low (0.062 nm) and the Gibbs free energy of hydration is high (-4,010 KJ/mol) compared to Ca^{2+} (0.100 nm; -1,505 KJ/mol) (Marcus 1991). It is reasonable to hypothesize that Ca^{2+} would have high affinity for replacing Cr^{III} as shown in the medium pH results.

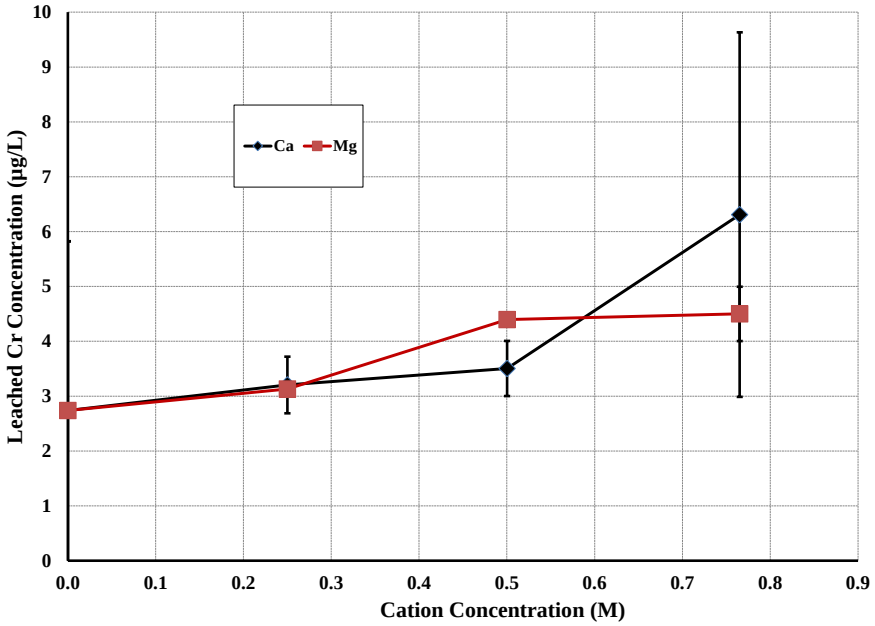

Figure 4.10. Cr leaching results from CFA-II at medium pH. Note: Ca = $CaCl_2$ addition and Mg = $MgCl_2$ addition. The sample pHs with $CaCl_2$ and $MgCl_2$ added were 6.7-7.5 and 6.7-7.4, respectively.

Table 4.4. Ionic radius and Gibbs free energy of hydration for cations. (Marcus 1991)

Cation	Ionic Radius (nm)	Gibbs Free Energy of Hydration (-KJ/Mol)
Ca^{2+}	0.100	-1,505
Cd	0.095	-1,755
Cr^{III}	0.062	-4,010
Mg^{2+}	0.072	-1,830
Mn^{II}	0.083	-1,760
Na^{+}	0.102	-365
Pb	0.118	-1,425
Zn	0.075	-1,955

At high pH, there did not appear to be a clear trend of Cr leaching with regard to salt addition. Since nearly the same initial leached concentration was observed at high pH as observed at low pH, it is hypothesized that Cr^{III} leaching increased at the highest $CaCl_2$ addition perhaps because of the breakdown of some amorphous glassy aluminosilicate

layer increasing the quantity of Cr^{III} available to leach. The harsher conditions at higher pH and with high salt addition could have resulted in this breakdown of the glassy phase. Cl^- complexation at the very high Cl^- addition could also have played a role.

Manganese. Figure 4.11 shows that salt addition did not significantly increase Mn leaching from CFA-I under low pH conditions from an initial concentration of 2,000 µg/L. At near neutral pH conditions (Figure 4.12a), all salts increased Mn leaching from CFA-I with respect to Cl^- concentration from an initial concentration of 455 µg/L. The Mn leached concentration reached maximums of 1,510, 1,310, 1,320 µg/L with $CaCl_2$, $MgCl_2$, and NaCl, respectively. For CFA-II under near neutral pH conditions (Figure 4.13), Mn leaching increased from an initial concentration of 774 µg/L to maximum concentrations of 924 and 1,038 µg/L with $CaCl_2$ and $MgCl_2$ addition, respectively. Under high pH conditions for CFA-I (Figure 4.12b), only $MgCl_2$ addition significantly increased Mn leaching to a maximum concentration of 267 µg/L.

Mn is associated with the amorphous glassy aluminosilicate or the ferromagnetic portion of CFA (Izquierdo et al. 2012). Mn is known to be enriched on both the CFA surface and the overall CFA particle (Jones 1995). Similar to other cationic metals, Mn leaches at low pH and does not readily leach at medium and higher pH (Izquierdo et al. 2012). Salt addition did not increase Mn leaching at low pH because all of the metal available to leach readily leached regardless of salt addition.

Regarding Mn leaching at medium pH, Mn leaching increased similarly with increasing Cl^- concentration regardless of the type of cation (Figure 4.12a). Previous research reported that Mn leaching from soils increased with salt addition through

competitive cation exchange (Khattak et al. 1989). However, previous research also showed that Mn formed Cl^- complexes although they are known to be weak (Winand 1991, Du Laing et al. 2008). Our results strongly suggested that Cl^- complexation likely played a significant role in increasing Mn leaching at medium pH. Even though Mn leaching with 1.6 M Cl^- addition by NaCl decreased compared to that with 0.6 M addition of Cl^- (Figure 4.12a), this result might be due to issues with detection of Mn by ICP-MS under highly saline conditions. Results with CFA-II also showed increased Mn leaching similarly with $CaCl_2$ or $MgCl_2$ addition, although the increase was not as pronounced as that for CFA-I (Figure 4.13). It should be noted that the initial Mn leaching concentration of CFA-II was higher than that of CFA-I (774 versus 455 µg/L).

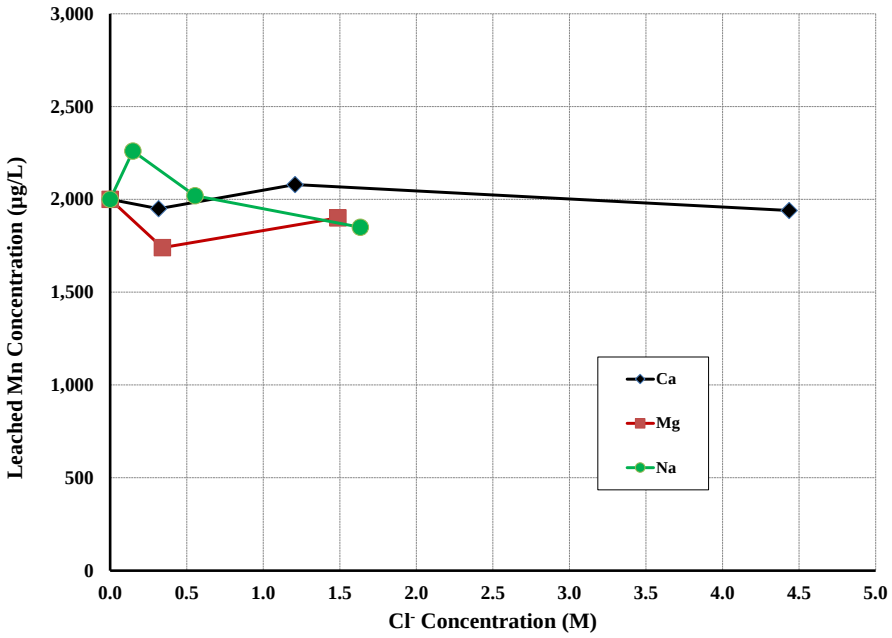

Figure 4.11. Mn leaching from CFA-I at low pH. Note: Ca = $CaCl_2$ addition, Mg = $MgCl_2$ addition, and Na = NaCl addition. The sample pHs with $CaCl_2$, $MgCl_2$, or NaCl added were 3.6-4.5, 4.1-4.5, and 4.2-4.5, respectively.

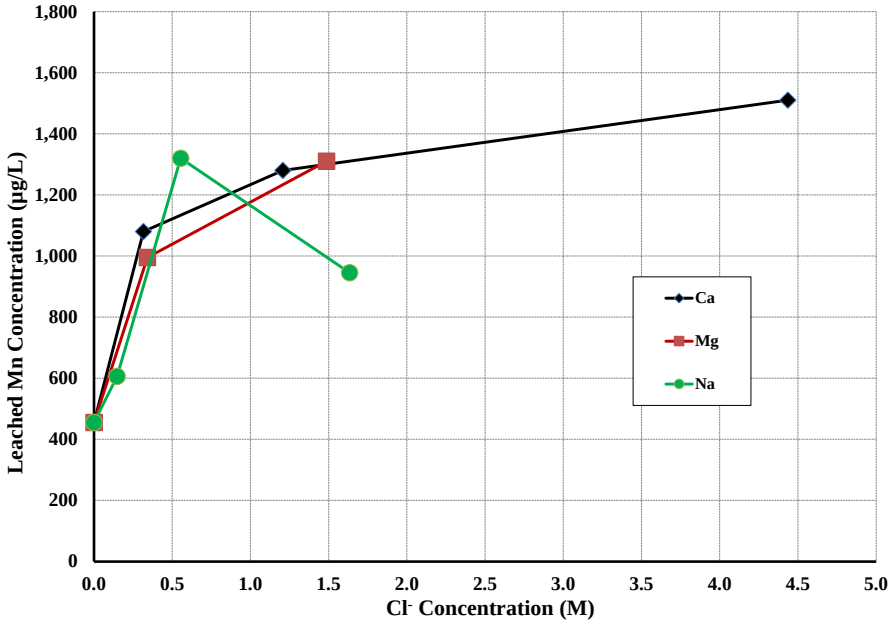

(a)

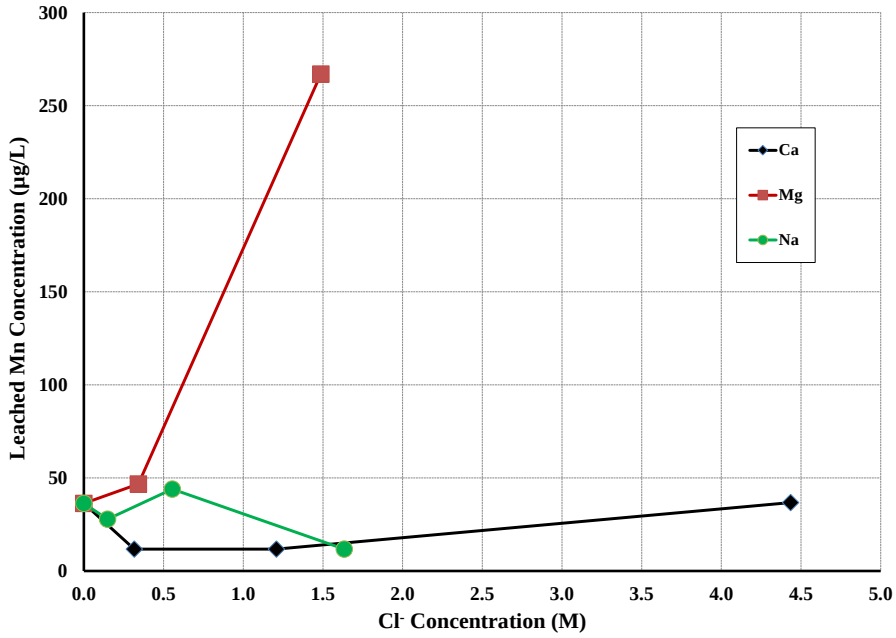

(b)

Figure 4.12. Mn leaching from CFA-I at (a) medium pH and (b) high pH conditions. Note: Ca = $CaCl_2$ addition, Mg = $MgCl_2$ addition, and Na = NaCl addition. Medium pH: pH 6.7-7.6 ($CaCl_2$), 6.8-7.6 ($MgCl_2$), and 7.1-7.6 (NaCl). High pH: pH 8.0-9.9 ($CaCl_2$), 8.1-9.9 ($MgCl_2$), and 9.9-10.1 (NaCl).

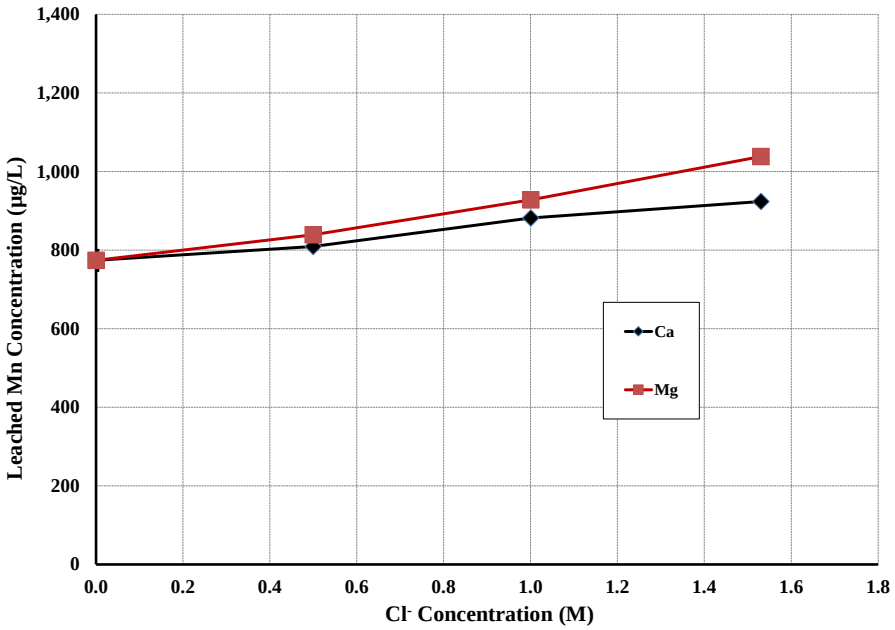

Figure 4.13. Mn leaching results from CFA-II at medium pH. Note: Ca = $CaCl_2$ addition and Mg = $MgCl_2$ addition. The sample pHs with $CaCl_2$ and $MgCl_2$ added were 6.7-7.5 and 6.7-7.4, respectively.

At high pH, Mg^{2+} addition enhanced Mn mobility through competitive cation exchange more than Ca^{2+} and Na^{+} from CFA-I. The Gibbs free energy of hydration for Mn is -1,760 KJ/mol which is higher than Ca^{2+}, but lower than Mg^{2+} (Marcus 1991, Wingenfelder et al. 2005). However, the ionic radius of Mg^{2+} (0.072 nm) is smaller than that of Ca^{2+} (0.100 nm) and closer in size to that of Mn (0.083 nm) (Marcus 1991, Wingenfelder et al. 2005). It could be that Mg^{2+} can compete with Mn more effectively at high pH than Ca^{2+} for sorption sites due to the smaller size of Mg^{2+} compared to Ca^{2+}. It is also noted that lower Mn leaching occurred at high pH compared to medium pH. It could be that competitive cation exchange was more important when less of the metal was available for leaching.

Lead. Figure 4.14 shows that addition of $CaCl_2$, $MgCl_2$, and NaCl significantly increased Pb leaching from CFA-I from a minimal concentration to maximum

concentrations of 439, 248, and 324 µg/L, respectively. At near neutral pH (Figure 4.15a), only $CaCl_2$ addition increased Pb leaching from CFA-I from a minimal concentration to a maximum concentration of 237 µg/L, and this increase only occurred at the maximum $CaCl_2$ addition concentration.

Salt addition did not increase Pb leaching from CFA-II under near neutral pH conditions up to a Cl^- concentration of 1.5 M which was less than the highest Cl^- addition for CFA-I (data not shown). At high pH conditions for CFA-I (Figure 4.15b), $CaCl_2$, $MgCl_2$, and NaCl addition all decreased Pb leaching from an initial concentration of 43 µg/L.

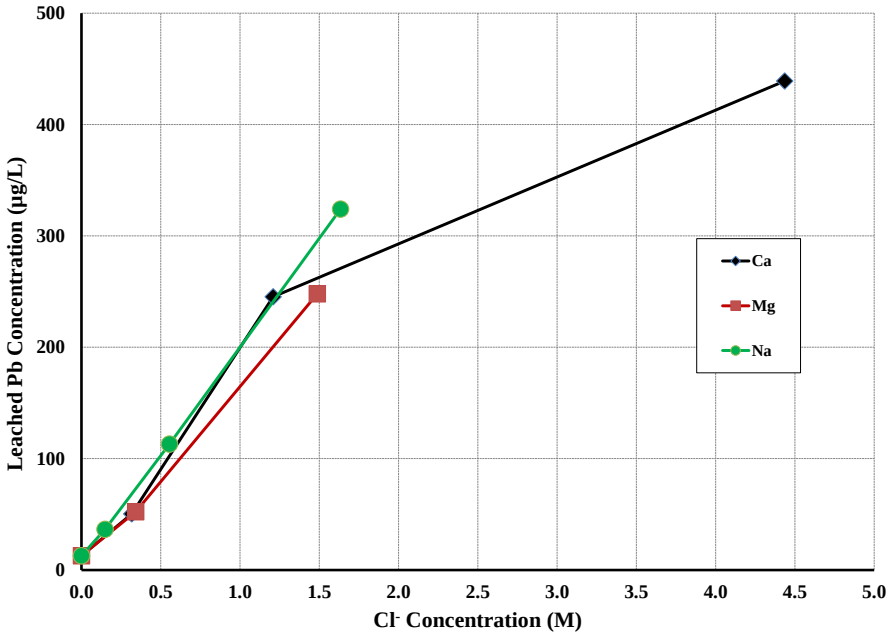

Figure 4.14. Pb leaching from CFA-I at low pH. Note: Ca = $CaCl_2$ addition, Mg = $MgCl_2$ addition, and Na = NaCl addition. The sample pHs with $CaCl_2$, $MgCl_2$, or NaCl added were 3.6-4.5, 4.1-4.5, and 4.2-4.5, respectively.

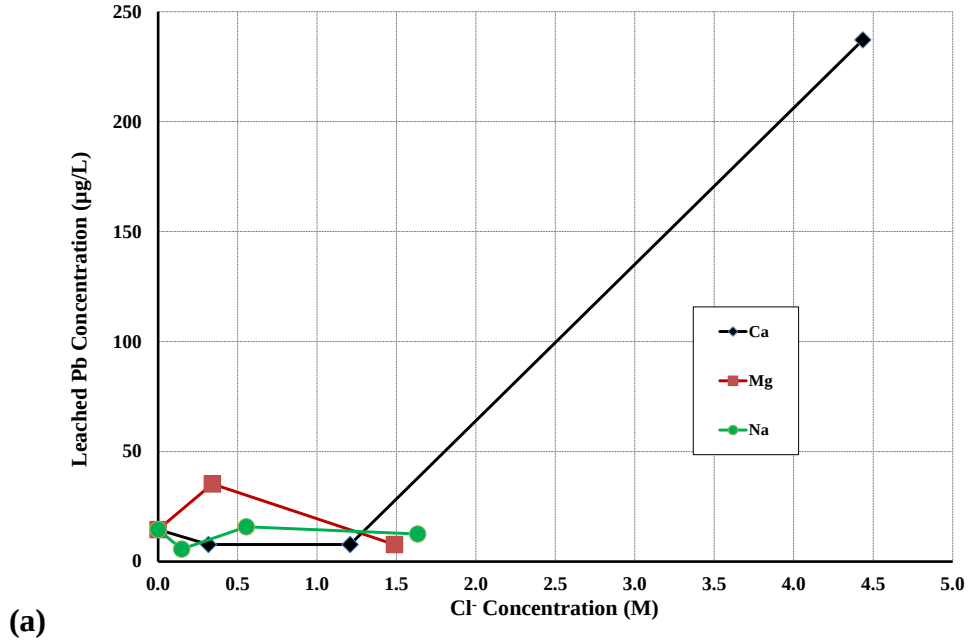

(a)

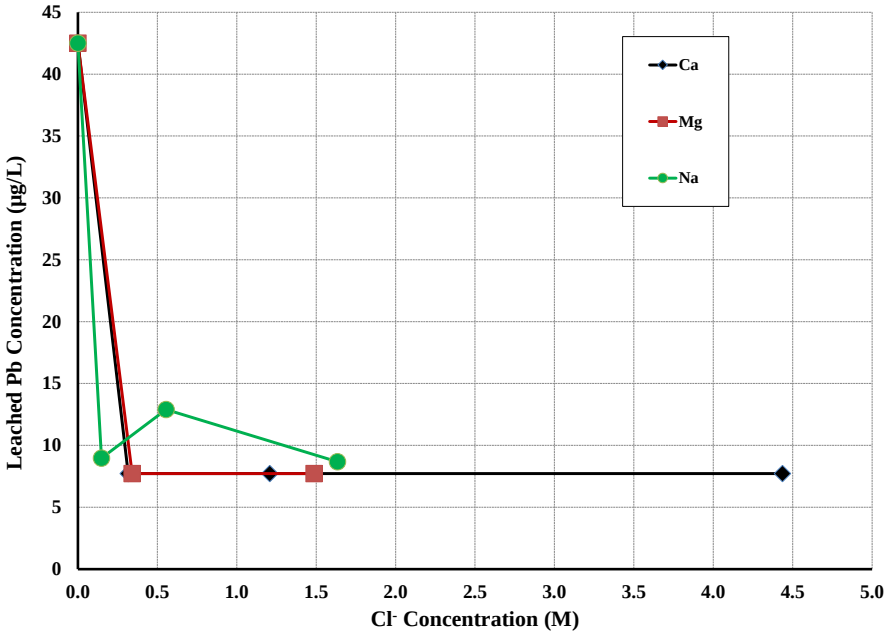

(b)

Figure 4.15. Pb leaching from CFA-I at (a) medium pH and (b) high pH conditions. Note: Ca = $CaCl_2$ addition, Mg = $MgCl_2$ addition, and Na = NaCl addition. Medium pH: pH 6.7-7.6 ($CaCl_2$), 6.8-7.6 ($MgCl_2$), and 7.1-7.6 (NaCl). High pH: pH 8.0-9.9 ($CaCl_2$), 8.1-9.9 ($MgCl_2$), and 9.9-10.1 (NaCl).

Pb is known to reside in the surface of CFA and is known leach sparingly over a wide pH range (Izquierdo et al. 2012). Cl^- complexation is likely responsible for the dramatic increase of Pb leaching from CFA-I with increasing Cl^- concentration (regardless of cation) under low pH conditions. Pb has been shown to strongly complex with Cl^- in other studies (Winand 1991, Sinadinovic 1997). Previous research indicated that competitive cation exchange played a role in Pb mobilization from soils (Pickering 1986, Acosta et al. 2011). However, the previous study included salt additions only up to an ionic strength of 0.3 M which was much lower than in this study (up to 5.5 M), and thus could be the reason for the different major leaching mechanisms between the two studies.

At medium pH conditions, Cl^- addition minimally influenced Pb leaching from CFA-I for all three salts ($CaCl_2$, $MgCl_2$, and NaCl) except at the highest Cl^- addition likely due to decreased $PbCl_2$ solubility. $PbCl_2$ solubility dramatically decreases in the pH range of 6.7-10.5 compared to at low pH (Pierrard et al. 2002). The addition of Cl^- when the Pb solubility is low likely decreases Pb mobility through the common ion effect with $PbCl_2$ precipitation according to Le Châtelier's principle per Equation 4.1.(Winand 1991)

$$PbCl_{2(s)} = Pb^{2+} + 2Cl^- \qquad (4.1)$$

Only at the very highest Cl^- addition for the medium pH samples did the impact of Cl^- complexation (decreased Pb^{2+} solution activity) likely overcame the decreased solubility of $PbCl_2$. Pb leaching was below the MDL (<~3 µg/L) for CFA-II at medium pH with Cl^- addition up to 1.5 M (data not shown).

Under high pH conditions, Pb leaching decreased with all salt additions. This decrease in Pb leaching is likely due to precipitation as shown in Equation 4.1. This

precipitation effect was not overcome even at the highest Cl^- addition unlike for the medium pH conditions.

Selenium. Figure 4.16 shows that salt addition did not appreciably increase Se leaching from an initial concentration of 42 µg/L. At near neutral pH for CFA-I (Figure 4.17a), $MgCl_2$ significantly increased Se leaching from an initial concentration of 63 µg/L to a maximum value of 111 µg/L. NaCl addition increased Se leaching to a maximum of 85 µg/L while $CaCl_2$ addition decreased Se leaching to 55 µg/L. For CFA-II at near neutral conditions (Figure 4.18), $MgCl_2$ addition increased Se leaching from an initial value of 16 µg/L to a maximum concentration of 40 µg/L while $CaCl_2$ addition only increased Se leaching to a maximum concentration of 26 µg/L.

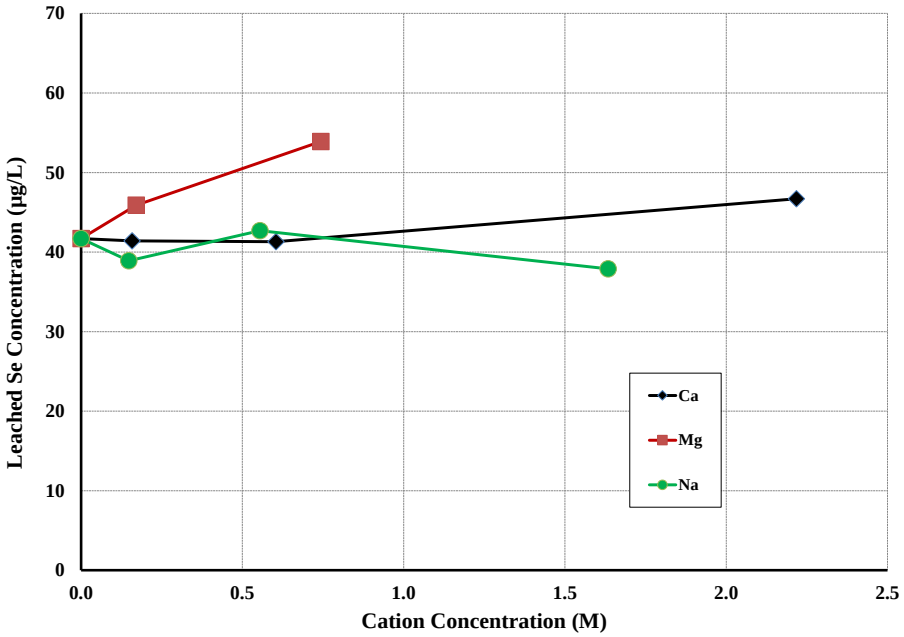

Figure 4.16. Se leaching from CFA-I at low pH. Note: Ca = $CaCl_2$ addition, Mg = $MgCl_2$ addition, and Na = NaCl addition. The sample pHs with $CaCl_2$, $MgCl_2$, or NaCl added were 3.6-4.5, 4.1-4.5, and 4.2-4.5, respectively.

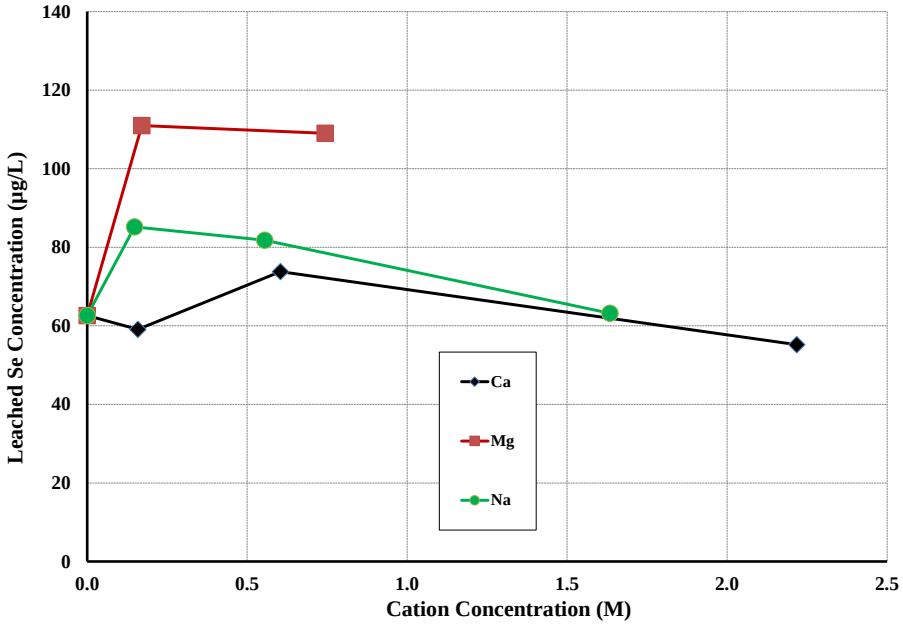

(a)

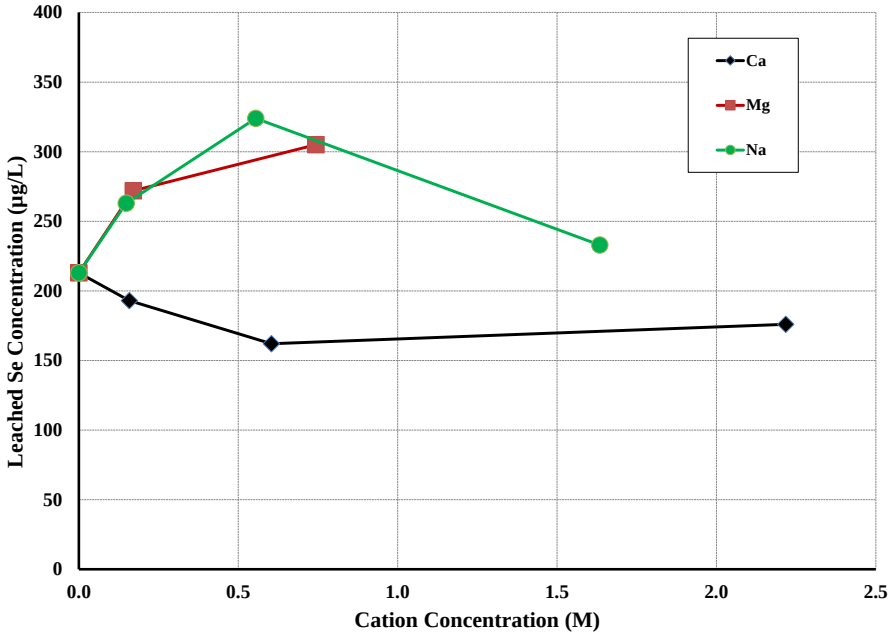

(b)

Figure 4.17. Se leaching from CFA-I at (a) medium pH and (b) high pH conditions. Note: Ca = $CaCl_2$ addition, Mg = $MgCl_2$ addition, and Na = NaCl addition. Medium pH: pH 6.7-7.6 ($CaCl_2$), 6.8-7.6 ($MgCl_2$), and 7.1-7.6 (NaCl). High pH: pH 8.0-9.9 ($CaCl_2$), 8.1-9.9 ($MgCl_2$), and 9.9-10.1 (NaCl).

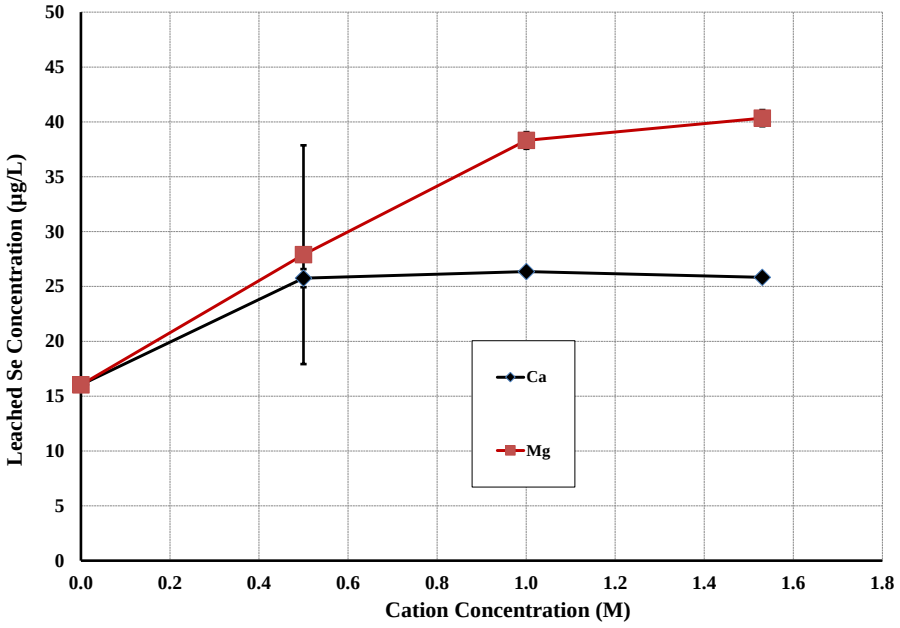

Figure 4.18. Se leaching results from CFA-II at medium pH. Note: Ca = $CaCl_2$ addition and Mg = $MgCl_2$ addition. The sample pHs with $CaCl_2$ and $MgCl_2$ added were 6.7-7.5 and 6.7-7.4, respectively.

Under high pH conditions for CFA-I (Figure 4.17b), $MgCl_2$ addition increased Se leaching from an initial concentration of 213 µg/L to a maximum concentration of 305 µg/L while NaCl addition increased Se leaching to a maximum concentration of 324 µg/L. $CaCl_2$ addition actually decreased Se leaching to minimum concentration of 162 µg/L.

Previous research has shown that the dominant Se species in CFA is the oxyanion SeO_3^{2-} (Narukawa et al. 2005, Huggins et al. 2007, Wang et al. 2009). As with As, Se partitions to CFA from the flue gas majorly through sorption to Fe sites on BCFA and Ca sites for SCFA (Yudovich et al. 2005).

Previous research has shown that SeO_3^{2-} leaching is controlled by adsorption/desorption from Fe hydroxides in BCFA and is heavily dependent on Se speciation (Wang et al. 2009). The pKa values of H_2SeO_3 are 2.64 and 8.36 (Wang et al.

2007). Wang et al. hypothesized that Se leaching from BCFA increases when the pH drops below 2.6 because Se is present primarily as the H_2SeO_3 which does not sorb strongly to the positively-charged Fe hydroxides sites due to being present as a neutral compound (Wang et al. 2007).

Wang et al. further noted that Se leaching from BCFA is typically at it's lowest point between pH 2.6 and 7.0 due to Se being present as the charged $HSeO_3^-$ and SeO_3^{2-} which can strongly sorb to the positively-charged Fe hydroxides (Wang et al. 2007). When the pH is increases to be above 7.0, the surface sites of BCFA become deprotonated and more of the negatively-charged $HSeO_3^-$ and SeO_3^{2-} readily leach from the surface (Wang et al. 2007).

The leaching results for the oxyanions SeO_3^{2-} are somewhat similar to the results for the oxyanion AsO_4^{3-}. It is believed that anion-exchange for Cl^- could be important for Se mobilization as Keon et al. hypothesized that anion exchange with Cl^- was a main mechanism of enhanced As mobilization in leaching tests with $MgCl_2$ addition (Keon et al. 2001).

No significant Se leaching increases by salts were observed at the low pH (3.6-4.5) experiments because Se was probably strongly sorbed to Fe hydroxides as Se was in the charged species $HSeO_3^-$. Therefore, it was likely difficult for Cl^- to compete with Se for Fe active sites due to Se species being charged.

At medium pH, the results show that anion exchange for Cl^- may drive the enhanced Se leaching with other factors influencing the results. It may be that SeO_3^{2-} can complex with Ca^{2+} as Wang noted that Ca^{2+} can form complexes with AsO_4^{3-} (Wang 2007a).

Although little information is available in literature, it is possible that Mg^{2+} and Na^{+} can potentially complex with SeO_3^{2-} and sorb to active site. As with As, differences in the affinity of Ca^{2+}, Mg^{2+}, and Na^{+} in complexing with Se^{IV} and the resulted complexes sorbing to the active sites could explain the differences in Se leaching as shown in Figure 4.17a. It should also be noted that $CaSeO_3$ precipitation could also play a role as these complexes begin to decrease in solubility under alkaline conditions (Masue et al. 2007). Differences in the solubility of $MgSeO_3$(s) (log K = 5.9 to 8.99) and $CaSeO_3$(s) (Log K = 5.53 to 7.65) could also play a role in the different leaching results (Séby et al. 2001). Both phases have a significant range of published Log K values so there could be a difference in their solubility under the experimental conditions.

The Se leaching results at high pH are likely driven by the same mechanisms as described for As. As mentioned above, the CFA surface becomes increasingly deprotonated with negative charge at higher pH and repels anions. The DDL compression due to high salinity is more significant with divalent ions than with monovalent ions. Both of the above effects increase SeO_3^{2-} leaching. However, there is a complicating factor that the pH of the $MgCl_2$ samples was less than the NaCl samples likely due to the precipitation of $Mg(OH)_2$ or complexation of $MgOH^{+}$. Hence, it is believed that although the greater compression of the DDL likely made it easier for Se to leach more with the addition of $MgCl_2$ than NaCl, the lower final leachate pH with $MgCl_2$ addition compared to NaCl addition likely decreased Se leaching in the $MgCl_2$ samples compared to the NaCl samples as Se leaching increases win increasing pH in this region due to increasing negative charge of the CFA surface. Thus, it is possible that these two factors worked simultaneously and resulted in the similarly increased Se leaching with $MgCl_2$ and NaCl addition. The reason

that $CaCl_2$ did not increase leaching at high pH could be because of the reasons described for the medium pH results either through complexation and sorption or $CaSeO_3$ precipitation.

Zinc. Figure 4.19 shows that salt addition (regardless of cation) did not significantly impact Zn leaching from an initial concentration of 1,380 µg/L. At neutral pH for CFA-I (Figure 4.20a), Zn leaching was decreased from an initial concentration of 584 µg/L with all salt additions except at the highest $CaCl_2$ addition where the leached Zn concentration reached a maximum of 885 µg/L at an added Cl^- concentration of 4.4 M. $CaCl_2$ and $MgCl_2$ addition also decreased Zn leaching from CFA-II under near neutral pH conditions from an initial leaching concentration of 722 µg/L with Cl^- additions up to 1.5 M (Figures 4.21). Under high pH conditions (Figure 4.20b), all salts decreased Zn leaching from CFA-I from an initial leached Zn concentration of 633 µg/L.

Zn is known to be primarily present on the CFA surface (Jones 1995). As shown in our results, Zn typically has an amphoteric leaching pattern with relation to pH but with generally higher leaching at low pH (Izquierdo et al. 2012). At low pH, Zn leaching was not affected by salt addition. This may be due to that (1) all of the Zn available to leach readily does so, and (2) Zn oxide, hydroxides, and hydroxychlorides are at their maximum solubility at high pH (Peulon et al. 1998).

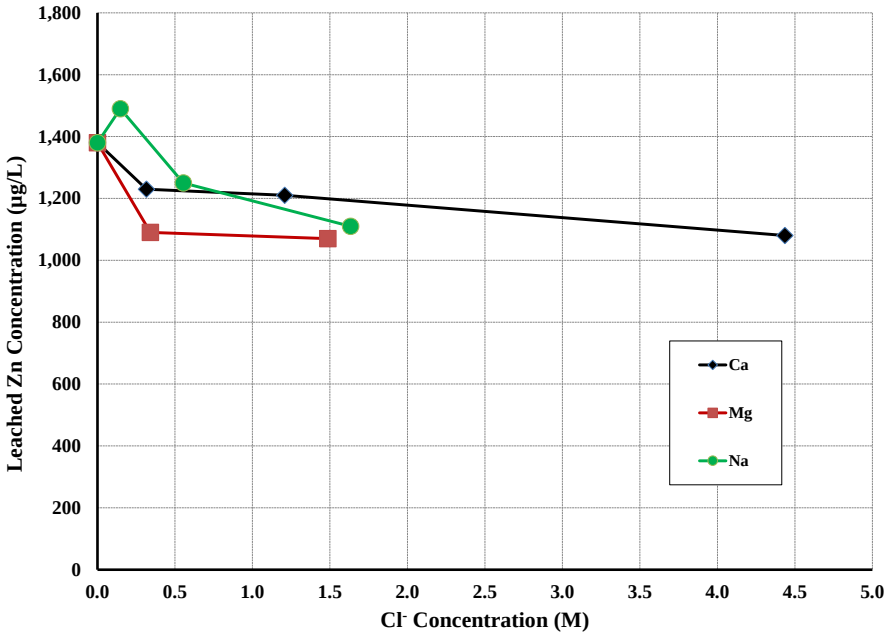

Figure 4.19. Zn leaching from CFA-I at low pH. Note: Ca = $CaCl_2$ addition, Mg = $MgCl_2$ addition, and Na = NaCl addition. The sample pHs with $CaCl_2$, $MgCl_2$, or NaCl added were 3.6-4.5, 4.1-4.5, and 4.2-4.5, respectively.

The results that moderate salt additions at moderate pH conditions decreased Zn mobility could be related to the lower solubility of Zn oxide, hydroxides, and hydroxychlorides at neutral to high pH (Reichle et al. 1975, Peulon et al. 1998). Zn hydroxychlorides can form according to Equation 4.2 (Peulon et al. 1998).

$$Zn + xOH + yCl^- = Zn(OH)_xCl_y \qquad (4.2)$$

Zn hydroxychlorides have been shown to have Log K values between -13.4 and -14.92 (Peulon et al. 1998). Under neutral to alkaline conditions, the solubility of these compounds could be exceeded under the conditions of this study. Per the common ion effect, Cl^- addition from all three salts moved the reaction to the right in precipitating $Zn(OH)_xCl_y$.

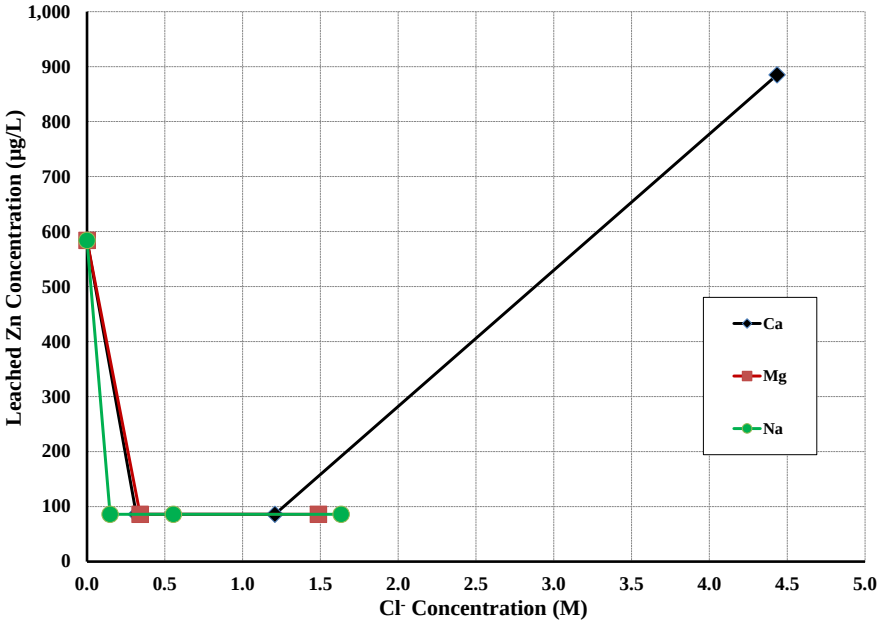

(a)

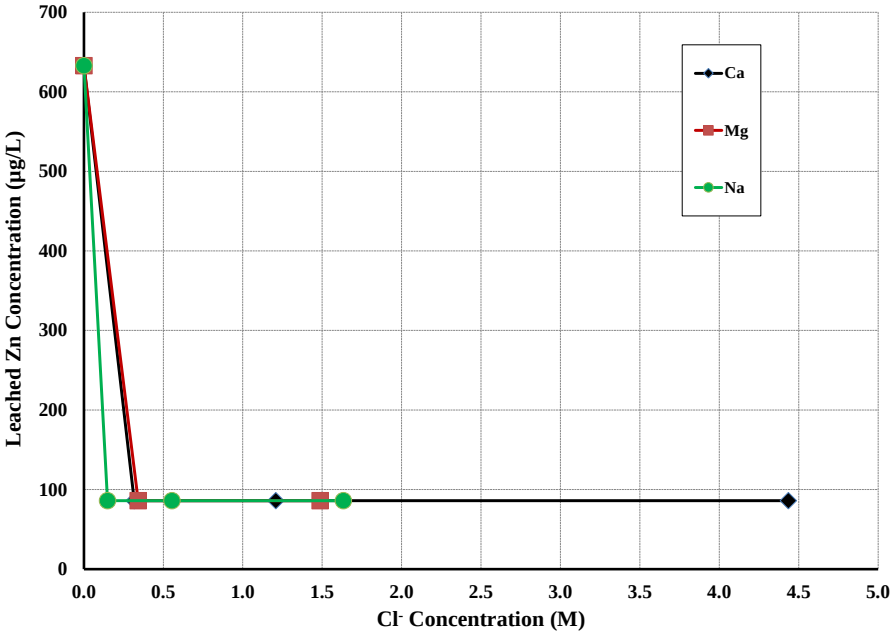

(b)

Figure 4.20. Zn leaching from CFA-I at (a) medium pH and (b) high pH conditions. Note: Ca = $CaCl_2$ addition, Mg = $MgCl_2$ addition, and Na = NaCl addition. Medium pH: pH 6.7-7.6 ($CaCl_2$), 6.8-7.6 ($MgCl_2$), and 7.1-7.6 (NaCl). High pH: pH 8.0-9.9 ($CaCl_2$), 8.1-9.9 ($MgCl_2$), and 9.9-10.1 (NaCl).

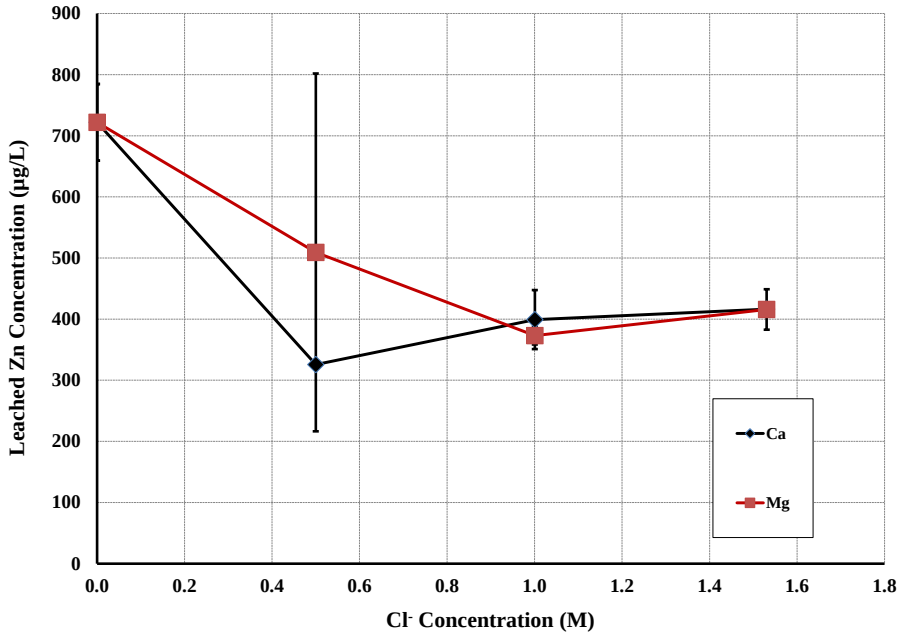

Figure 4.21. Zn leaching results from CFA-II at medium pH. Note: Ca = $CaCl_2$ addition and Mg = $MgCl_2$ addition. The sample pHs with $CaCl_2$ and $MgCl_2$ added were 6.7-7.5 and 6.7-7.4, respectively.

However, Zn does form Cl^- complexes which would increase Zn solubility (by reducing free Zn^{2+} activity in solution) (Winand 1991, Peulon et al. 1998). A very high Cl^- concentration (4.5 M) could overcome the common ion effect as shown by the results for the highest $CaCl_2$ addition in Figure 4.20a.

The same Zn leaching trend for the medium pH samples was also observed in the high pH experiments for CFA-I (Figure 4.20b), and there was no increased Zn leaching at the highst Cl^- addition, likely due to even lower solubility of Zn oxide, hydroxides, and hydroxychlorides at high pH.

Comparison of Metals. Figure 4.22 shows a summary of the leaching results in this study with 0.6 M of $CaCl_2$ added to the extractant fluid. The composition of concentrated FGD wastewater brines is expected to be dominated by $CaCl_2$. The Cl^- concentration of 0.6

M is approximately 25% to 50% of the concentration that would be expected in a concentrated FGD wastewater brine. The results indicate that the metal leaching increases of most concern under environmentally relevant conditions (medium and high pH as expected in the landfill leachate of a coal-fired power plant landfill) include As, Cd, and Cr. As and Cd had the most striking leaching increases under environmentally relevant conditions.

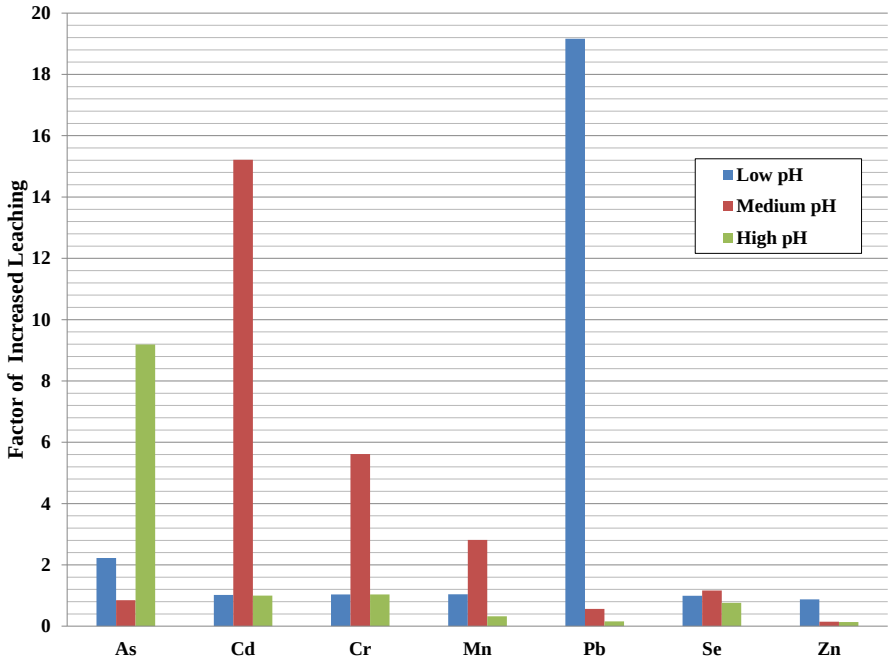

Figure 4.22. Factor of increased metal leaching from CFA-I for the addition of 1.21 M of Cl^- as $CaCl_2$. Note: When the concentration was less than the MDL, the concentration was assumed to be 25% of the MDL.

4.4.3 Modeling Results

Very limited information is available in literature on modeling the leaching behavior of metals in the presence of high salt concentrations. Modeling has previously been conducted on As and Cd leaching from CFA at different pHs and normal, low ionic strength conditions (van der Hoek et al. 1996, Wang et al. 2004, Wang et al. 2006, Wang

2007a, Wang 2007b, Wang et al. 2007, Wang et al. 2008, Wang et al. 2009, Su et al. 2011). However, no modeling efforts have been made to evaluate metal leaching from CFA with increasing salt concentrations. The closest similar modeling effort was conducted by Hyks et al. on contaminant leaching from municipal solid waste incineration (MSWI) air pollution control residues, in which the authors modeled results from column percolation tests for pH, alkalinity, and Al, Ba Ca, S, Si, and Zn releases from a high salt material (with 122,000-173,000 mg/kg Cl^-) (Hyks et al. 2009). The Cl^- leachate concentrations reached as high as 100,000 mg/L (Hyks et al. 2009). However, no modeling of toxic metals such as As and Cd was made in this study.

In this study, the modeling approaches done by the previous research on As and Cd leaching from CFA were adopted and modified to apply to the employed experimental conditions. The modeling results are shown in Figures 4.23 and 4.24.

The modeled results show that an adequate fit with the experimental results could be achieved based on two assumed simultaneous mechanisms driving As leaching with increasing salt addition (Figure 4.23).

The two mechanisms are: (1) competition between Cl^- and AsO_4^{3-} for hydrous Fe^{III} active sorption sites, and separately (2) complexation of the cations (Ca^{2+}, Mg^{2+}, and Na^+) with AsO_4^{3-} and their adsorption to CFA surface sites. Although this model is a simple surface complexation model, the model identified that the proposed hypotheses are feasible.

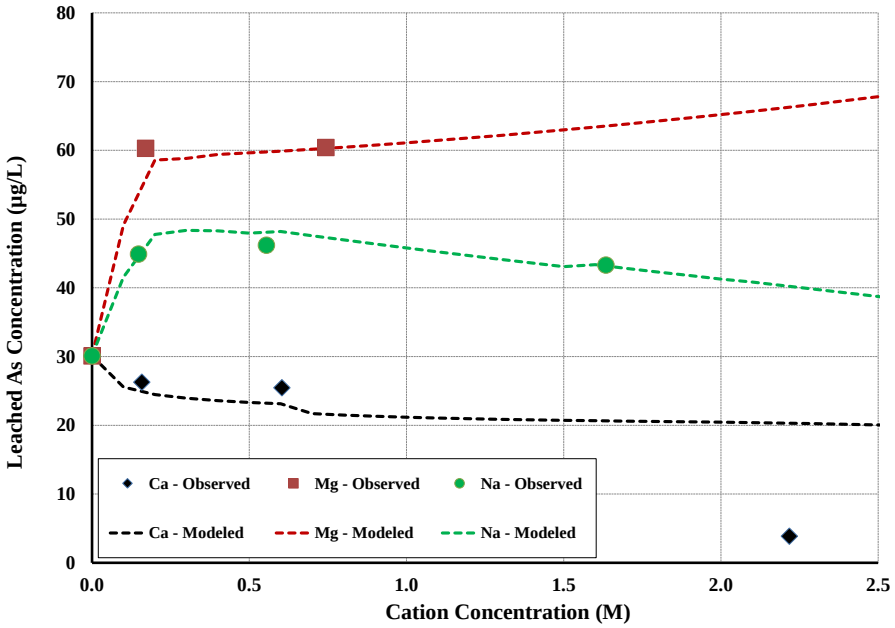

Figure 4.23. As modeling leaching from CFA-I under medium pH conditions. Note: Ca = $CaCl_2$ addition, Mg = $MgCl_2$ addition, and Na = NaCl addition. pH 6.7-7.6 ($CaCl_2$), 6.8-7.6 ($MgCl_2$), and 7.1-7.6 (NaCl).

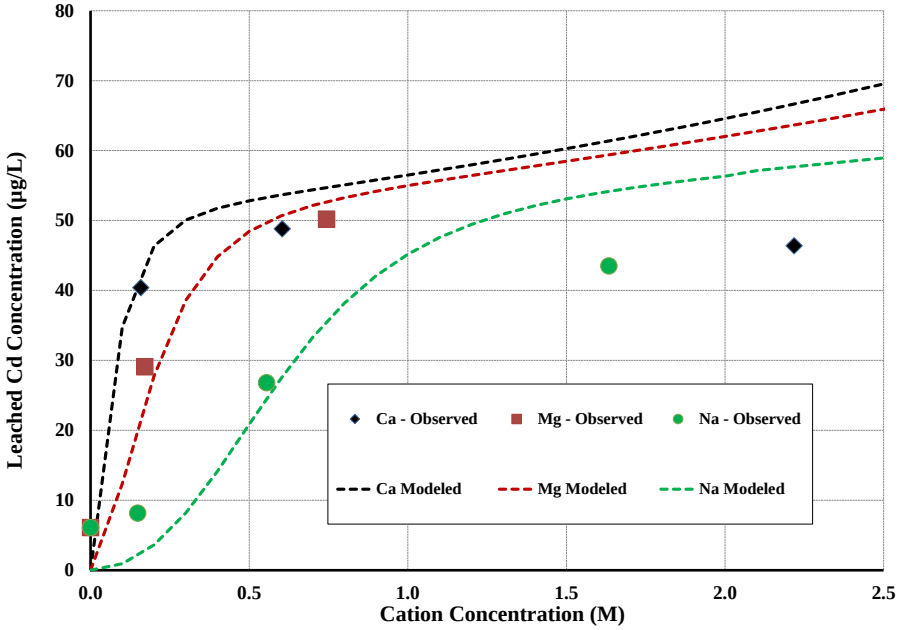

Figure 4.24. Cd modeling leaching from CFA-I under medium pH conditions. Note: Ca = $CaCl_2$ addition, Mg = $MgCl_2$ addition, and Na = NaCl addition. pH 6.7-7.6 ($CaCl_2$), 6.8-7.6 ($MgCl_2$), and 7.1-7.6 (NaCl).

The results also showed the potential differences in the complexation of AsO_4^{3-} with the different cations (Ca^{2+}, Mg^{2+}, and Na^{+}) and sorption the CFA active surface sites. The results showed the following preference for this process based on cation: Ca^{2+} (Log K = 2.4) >> Mg^{2+} (Log K = 0.45) > Na^{+} (Log K = 0.18) as shown in Table 4.1.

Figure 4.24 shows that modeling of Cd leaching can achieve an adequate fit with the experimental results based on two simultaneous mechanisms. The model shows that Cd leaching is controlled by (1) Cl^{-} complexation, and (2) competitive cation exchange for active sites with Ca^{2+}, Mg^{2+}, and Na^{+}. Cl^{-} complexation is the more important mechanism as there are fairly small differences for the active sites with the following preference as follows: Ca^{2+} (Log K = 9.8) > Mg^{2+} (Log K = 9.0) > Na^{+} (Log K = 7.8). However, competitive cation exchange definitely plays a role. The model shows that for an addition of 2 M NaCl, 0.07% of the dissolved Cd is speciated as Cd^{2+} versus 97.5% without salt addition. Similarly for 1 M addition of $CaCl_2$, 0.05% of the dissolved Cd is speciated as Cd^{2+}.

4.4.4 XRD Analysis

Figure 4.25 shows the XRD patterns for the CFA-II solids after leaching (final leahate pH = 6.7-7.5). The main mineral phases were $3Al_2O_3 \cdot 2SiO_2$ (mullite), SiO_2 (quartz) and Fe_2O_3 (iron oxide). The results show that exposure to the salts did not break down the mineralogy of the solids. This observation adds support that surface processes anion exchange, cation exchange, and Cl^{-} complexation are the likely mechanisms of increased metal leaching, not the breakdown of crystalline CFA phases by salt attack.

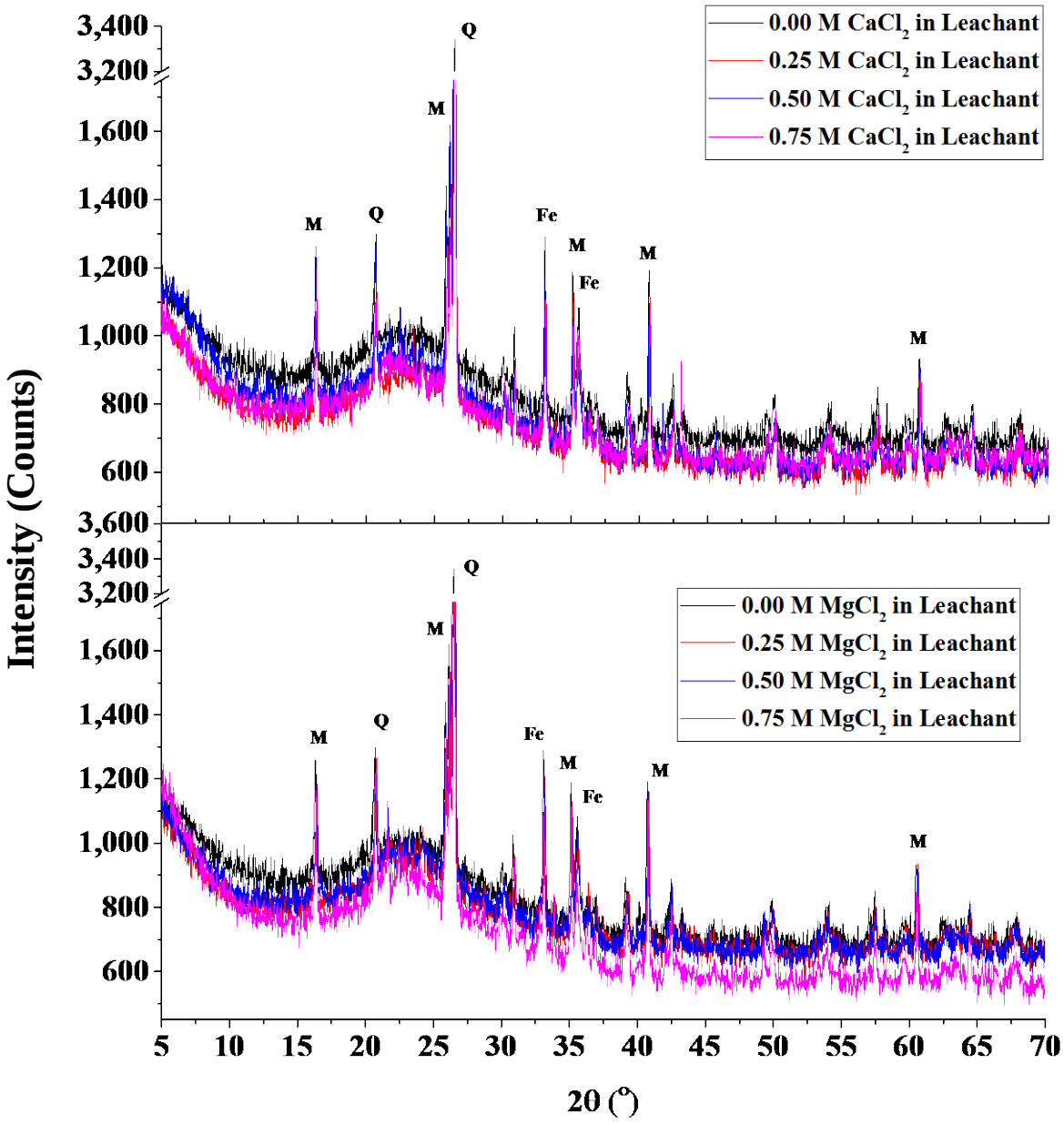

Figure 4.25. XRD patterns for CFA-II impacted by leaching with $CaCl_2$ and $MgCl_2$.

4.5 CONCLUSIONS

Contact of bituminous CFA with high salinity waste brines could increase metal leaching, and the effect could vary depending on the metals, pH and salt composition and concentration. With regards to cationic metal (Cd^{II}, Cr^{III}, Mn^{II}, Pb^{II}, and Zn^{II}) leaching from

BCFA without salt addition, Cd and Mn leaching significantly decreased with increasing pH. Cd and Zn demonstrated amphoteric leaching patterns in regards to pH. Although Zn did demonstrate a slight amphoteric pattern, Zn leaching was higher at low pH compared to high pH. Pb demonstrated low leaching at low and medium pH conditions and moderate leaching at high pH conditions.

Increasing salt addition did not impact Cd, Cr, Mn, and Zn leaching from BCFA at low pH because essentially all of the available cationic metal readily leached regardless of salt addition. Salt addition did significantly increase Pb leaching at low pH due to Cl^- complexation.

Under medium pH conditions, salt addition increased Cd and Mn leaching from BCFA due to Cl^- complexation. $CaCl_2$ addition increased Cr leaching due to competitive cation exchange with Ca^{2+}, while $MgCl_2$ and NaCl did not significantly increase Cr leaching. Moderate salt addition decreased Zn and did not impact Pb leaching at medium pH due to the low solubility of $PbCl_2$ and Zn hydroxychlorides. For Pb and Zn, leaching only increased at medium pH at the very highest salt addition due Cl^- complexation overcoming the low solubility of $PbCl_2$ and Zn hydroxychlorides.

At high pH conditions, salt addition did not increase Cd and Cr leaching from BCFA except at the highest salt addition. The low solubility of Cd and Cr hydroxides at high pH prevented leaching increases with salt addition. However, high Cl^- addition overcame the low solubilities of Cd and Cr hydroxides through Cl^- complexation. Mn leaching increased at high pH only with $MgCl_2$ addition through competitive cation

exchange with Mg^{2+}. Pb and Zn leaching decreased at high pH due to increasing precipitation of $PbCl_2$ and Zn hydroxychlorides with increasing Cl^- addition.

In regards to oxyanions, AsO_4^{3-} leaching was highest at medium pH and lower at low and high pH while SeO_3^{2-} leaching increased with increasing pH. Increasing salt concentrations did no impact Se leaching at low pH likely because of the oxyanion being strongly sorbed to Fe^{III} oxide sorption sites at low pH due to being present as negatively charged species. As leaching did increase at low pH due to anion exchange with Cl^-.

At medium pH, salt addition increased both As and Se leaching due to anion exchange with Cl^-. However, As and Se leaching was also likely impacted by complexation and sorption with the cations (Ca^{2+}, Mg^{2+}, and Na^+) which resulted in $MgCl_2$ addition increasing leaching more than $CaCl_2$ and NaCl addition. Precipitation of As and Se with the cations may also have played a role.

At high pH, both As and Se leaching increased with salt addition. As the BCFA surface becomes more negatively charged at high pH, it is believed that salt addition could enhance As and Se leaching mainly through compressing the diffuse double layer (DDL) around the BCFA making it easier for the two oxyaions to leaching. The leaching results at this pH are also likely impacted by complexation and sorption with the cations as leaching is impacted differently with the addition of the $CaCl_2$, $MgCl_2$, and NaCl.

A surface complexation model was established to model As and Cd leaching at medium pH as these elements has the highest leaching increases with salt addition under the low and high pH conditions which are environmentally relevant for BCFA landfill. The increased As leaching with salt addition at medium pH could be modeled based on: (1)

competition between Cl^- and AsO_4^{3-} for hydrous Fe^{III} oxide sorption sites; and (2) complexation and sorption of the cations (Ca^{2+}, Mg^{2+}, and Na^+) with AsO_4^{3-} to CFA surface sites. Modeling of Cd leaching with increasing salt addition at neutral pH indicated that Cd leaching was controlled by (1) Cl^- complexation, and (2) competitive cation exchange for active sites with Ca^{2+}, Mg^{2+}, and Na^+ with Cl^- complexation being the more important process.

CHAPTER 5. CONCLUSIONS AND RECOMMENDATIONS

5.1 CONCLUSIONS

The results of the work show that the proposed process can successfully immobilize heavy metals (including Se^{VI}) in a co-disposal process for FGD wastewater and bituminous coal fly ash (CFA) through solidification/stabilization (S/S). Bach equilibrium based leaching experiments showed that the S/S solids achieved good retainment (average of 68−90%) for As^{V}, Cd^{II}, Hg^{II}, and Se^{IV}. Immobilization of As^{V}, Cr^{VI}, and Se^{VI} in the S/S solids could be enhanced through the addition of $FeSeO_4$ (FS). The addition of even a very small amount of FS increased the retainment of As^{V} to approximately 100% likely due to formation of Fe^{III} oxides that are good absorbents for As^{V}. FS addition reduced the brine's Cr^{VI} to Cr^{III}, which enhanced immobilization by incorporation of Cr^{III} into Ca-Al^{III}-hydrate phase, sorption of Cr^{III} to Fe^{III} oxides, and/or precipitation of $Cr(OH)_3$. Some of the Cr^{VI} from the CFA was also likely reduced and immobilized via the same mechanisms. The mechanism of enhanced immobilization of Se^{VI} by FS addition was likely reduction to Se^{IV} and $CaSeO_3$ precipitation.

Comparison between bituminous CFA (BCFA) and sub-bituminous CFA (SCFA) S/S indicated that SCFA S/S solids had greater retainment of As^{V}, Cd^{II}, and Se^{VI} compared to BCFA S/S solids. As^{V} retainment was likely enhanced by the higher pH and CaO content, Cd^{II} by better $Cd(OH)_2$ stability at the higher pH conditions, and Se^{VI} by SeO_4^{2} substitution in the AFm phase produced at the higher pH, CaO content, and reactive Al_2O_3 content of SCFA S/S. Support for this proposed mechanism was provided by identification of AFm-Cl in the SCFA S/S solid utilizing XRD. XRD diffractograms showed that SCFA

was more reactive in the S/S process than BCFA. However, it is not practical to utilize SCFA instead of BCFA in the S/S process due to the most difficult wastewater problems being present at bituminous coal-fired power plants. It would be expensive to transport the large SCFA quantity required for the S/S process to a bituminous coal-fired power plant. In addition, utilization of the AFm-SeO_4 stabilization mechanism may not be sustainable for safe long-term landfill disposal. Reduction of Se^{VI} with FS plus S/S may be a better long-term strategy than AFm substitution under environmentally relevant pH conditions.

Semi-dynamic tank leaching tests also showed that FS significantly decreased As^{V}, Cr^{VI}, and Se^{VI} cumulative release over the long term. FS addition increases the likelihood of successful long-term disposal of S/S concentrated FGD brines containing these toxic oxyanions. The results of these experiments also showed that FS addition decreased the cumulative release of the salts Ca^{2+}, Cl^{-}, Mg^{2+}, Na^{+}, and SO_4^{2-}; however, cumulative release is only decreased at shorter leaching times. At longer leaching times, the cumulative release for these salts from S/S mixtures with and without FS addition converge. It is clear that while FS addition can enhance immobilization of the toxic heavy metal oxyanions over the long term, FS addition does not decrease the release of the salts Ca^{2+}, Cl^{-}, Mg^{2+}, Na^{+}, and SO_4^{2-} over the long term. Additional strategies must be developed to limit leaching of salts.

The adoption of FS addition to S/S mixtures for concentrated FGD wastewater brines would be positive development for the coal-fired power industry. FS addition can be added directly to the S/S process without requirement of a pre-treatment step. In addition, FS is a waste product from other industries and incorporation of this additive could be considered co-disposal for concentrated FGD wastewater, CFA, and FS. Metals present in the concentrated FGD wastewater, CFA, and FS will all be treated and metal

immobilization enhanced. For example, the CFA in the S/S mixture leaches less metals than non-treated CFA.

LeachXS^{TM} was utilized to model the release of Ca^{2+}, Cl^{-}, Na^{+}, As^{V}, and Se^{VI} in the semi-dynamic tank leaching tests for the scenario of no FS addition. Modeling was very successful for pH and As^{V} and Se^{VI} cumulative release, which added additional evidence for the proposed leaching mechanisms. Se^{VI} release was controlled by the readily soluble phase $CaSeO_4$. As^{V} leaching was successfully modeled utilizing $NaCaAsO_4{\cdot}7.5H_2O$ as the primary immobilization phase. Although the model does not confirm that $NaCaAsO_4{\cdot}7.5H_2O$ was the dominant phase, it confirms that a phase or phases with similar solubility as that modeled for $NaCaAsO_4{\cdot}7.5H_2O$ controlled As release.

Modelling was also successful for Ca^{2+}, Cl^{-}, and Na^{+} at longer leaching times. The model did have some difficulty replicating the “wash-off” effect at low leaching times due to the extreme concentrations of these salts in the S/S solids.

Model utilization in a real scenario for the S/S solid over 20 years indicated that the leachate pH would remain alkaline (pH > 9.0) which greatly benefits immobilization of cationic metals. Ca^{2+}, Cl^{-}, Na^{+}, As, and Se reached their highest leachate concentrations almost immediately and leachate concentrations decreased significantly over time for these elements.

Contact with the salts from concentrated FGD wastewater brines could increase metal leaching from conventional BCFA because of high salt content. This issue is important because the coal-fired power industry is considering several options for concentrated FGD wastewater disposal including direct mixing with CFA with no

pozzonalic reactions and landfilling soluble crystallized salts from FGD wastewater. Both of these options would significantly increase contact between CFA and high salinity leachant. In addition, even if the concentrated brines undergo S/S, the solids will still significantly leach salts. Furthermore, high salt materials for disposal are also being introduced into industry landfills through CFAs impacted by new air emission controls such as injection of $CaBr_2$, $Ca(OH)_2$, Na-based sorbents, and $Na_2CO_3 \cdot NaHCO_3 \cdot 2H_2O$ (trona). Hence, traditional BCFA may be exposed to significant salt concentrations in the future unlike the past.

With regards to cationic metal (Cd^{II}, Cr^{III}, Mn^{II}, Pb^{II}, and Zn^{II}) leaching from BCFA without salt addition, Cd and Mn leaching significantly decreased with increasing pH. Cd and Zn demonstrated amphoteric leaching patterns in regards to pH. Although Zn did demonstrate a slight amphoteric pattern, Zn leaching was higher at low pH compared to high pH. Pb demonstrated low leaching at low and medium pH conditions and moderate leaching at high pH conditions.

Increasing salt addition did not impact Cd, Cr, Mn, and Zn leaching from BCFA at low pH because essentially all of the available cationic metal readily leached regardless of salt addition. Salt addition did significantly increase Pb leaching at low pH due to Cl^- complexation.

Under medium pH conditions, salt addition increased Cd and Mn leaching from BCFA due to Cl^- complexation. $CaCl_2$ addition increased Cr leaching due to competitive cation exchange with Ca^{2+}, while $MgCl_2$ and NaCl did not significantly increase Cr leaching. Moderate salt addition decreased Zn and did not impact Pb leaching at medium

pH due to the low solubility of $PbCl_2$ and Zn hydroxychlorides. For Pb and Zn, leaching only increased at medium pH at the very highest salt addition due to Cl^- complexation overcoming the low solubilities of $PbCl_2$ and Zn hydroxychlorides.

At high pH conditions, salt addition did not increase Cd and Cr leaching from BCFA except at the highest salt addition. The low solubility of Cd and Cr hydroxides at high pH prevented leaching increases with salt addition. However, high Cl^- addition overcame the low solubilities of Cd and Cr hydroxides through Cl^- complexation. Mn leaching increased at high pH only with $MgCl_2$ addition through competitive cation exchange with Mg^{2+}. Pb and Zn leaching decreased at high pH due to increasing precipitation of $PbCl_2$ and Zn hydroxychlorides with increasing Cl^- addition.

In regards to oxyanions, AsO_4^{3-} leaching was the highest at medium pH and lower at low and high pH while SeO_3^{2-} leaching increased with increasing pH. Increasing salt concentrations did no impact Se leaching at low pH likely because of the oxyanion being strongly sorbed to Fe^{III} oxide sorption sites at low pH due to being present as negatively charged species. As leaching did increase at low pH due to anion exchange with Cl^-.

At medium pH, salt addition increased both As and Se leaching due to anion exchange with Cl^-. However, As and Se leaching was also likely impacted by complexation and sorption with the cations (Ca^{2+}, Mg^{2+}, and Na^+) which resulted in $MgCl_2$ addition increasing leaching more than $CaCl_2$ and NaCl addition. Precipitation of As and Se with the cations may also have played a role.

At high pH, both As and Se leaching increased with salt addition. As the BCFA surface becomes more negatively charged at high pH, it is believed that salt addition could

enhance As and Se leaching mainly through compressing the diffuse double layer (DDL) around the BCFA making it easier for the two oxyanions to leach. The leaching results at this pH are also likely impacted by complexation and sorption with the cations as leaching is impacted differently with the addition of the $CaCl_2$, $MgCl_2$, and NaCl.

A surface complexation model was established to model As and Cd leaching at medium pH as these elements has the highest leaching increases with salt addition under the mediaum and high pH conditions which are environmentally relevant for BCFA landfills. The increased As leaching with salt addition at medium pH could be modeled based on: (1) competition between Cl^- and AsO_4^{3-} for hydrous Fe^{III} oxide sorption sites; and (2) complexation and sorption of the cations (Ca^{2+}, Mg^{2+}, and Na^+) with AsO_4^{3-} to CFA surface sites. Modeling of Cd leaching with increasing salt addition at neutral pH indicated that Cd leaching was controlled by (1) Cl^- complexation, and (2) competitive cation exchange for active sites with Ca^{2+}, Mg^{2+}, and Na^+ with Cl^- complexation being the more important process.

It is important for the coal-fired power industry to carefully consider the disposal of high salt materials including concentrated FGD wastewater materials and CFAs impacted by new air emission controls. It would be best to monofill these materials, both concentrated FGD wastewater residuals and new CFAs impacted by air emission controls. These materials should be segregated from traditional BCFA and other coal-combustion residuals (CCRs) that have been landfilled in the past.

5.2 RECOMMENDATIONS

Due to the complexity of the proposed process and potential for significant negative environmental impact upon failure, much additional work needs to be conducted. As mentioned in this work, bituminous coal-fired power plants that utilize forced-oxidation FGDs are the most challenging scenario for ZLD treatment of FGD wastewater with Se^{VI} being the most difficult metal to stabilize. This current work focused on reduction in order to stabilize Se^{VI} in BCFA S/S solids. However, further optimization of mineral formation for BCFA S/S solids is needed including AFm-Se^{VI} formation as observed for immobilization of Se^{VI} in the SCFA S/S solids.

In addition to heavy metal stabilization, work should be conducted on Cl^- immobilization. Due to high solubility, Cl^- is extremely difficult to stabilize. As mentioned in this work, contact with high Cl^- content leachate could increase metal leaching from CFA. The approach to Cl^- stabilization could focus on two processes: (1) formation of low permeability solids, and (2) mineral optimization for maximum formation of AFm-Cl.

A knowledge gap exists on the stability of AFm-Se^{VI} and AFm-Cl phases under environmentally relevant landfill conditions. Although these phases can readily immobilize Se^{VI} and Cl^- under the high pH conditions of S/S, the stability of these phases in S/S solids as the leachate pH decreases over time is not known. Evaluations of the stability of these phases should be conducted including semi-dynamic tank leaching tests (USEPA Method 1315) where the pH has been artificially decreased to simulate various disposal scenarios. In depth characterization of the solids both before and after these tank leaching tests should be conducted. This characterization could be similar to that conducted by Hockley et al.

where the researchers made concentration and mineralogy (XRD analysis) profiles for cement blocks exposed to seawater over the long term (Hockley et al. 1991). This characterization could lead to enhanced mechanistic insight into leaching from S/S solids including processes such as pore refinement and moving boundary layers (Hockley et al. 1991).

The leaching and characterization insight developed from the above described evaluations could be utilized to strengthen the LeachXS^{TM} model for leaching where AFm-Se^{VI} and AFm-Cl are important immobilization phases. The current LeachXS^{TM} model includes AFt-Se phases, but does not include AFm-Se^{VI} and AFm-Cl phases.

The LeachXS^{TM} model could be further enhanced to simulate leachate from a real landfill including disposal scenarios such as disposal (1) with other CCRs, and (2) separately than CCRs. It would also be beneficial for the industry, if the model could simulate extreme weather events such as large scale flooding of the landfill as a worst-case scenario event.

It is also desirable to increase the scale of the leaching experiments to the pilot level. A pilot-scale landfill cell could be installed containing the BCFA S/S solids. Leaching from the cell could be evaluated over a significant time period perhaps 1-2 years to provide realistic leaching data for the industry.

In general, future researchers should consider factors that will be important for the practical application of the S/S process investigated in this study for the coal-fired power industry. Such factors include but are not limited to pumping rheology, minimum and maximum strength requirements, and bleed water production. These factors have been

studied extensively in the U.S. mining industry albeit not for high salt materials and could provide useful insights.

It is also proposed for researchers to investigate strategies for salt reuse form FGD wastewater ZLD residuals. If a concentrated brine was treated economically to a degree that all toxic metals were effectively removed, opportunities for salt reuse could open up including road salt and more importantly chemical feedstocks for the chlor-alkali industry. Although extensive treatment would be required, beneficial us of salt would prevent the accumulation of highly leachable salts in coal-fired power plant industry landfills and provide a potential new revenue stream for the industry.

Further studies should also be conducted on the impact of salt on metal leaching from BCFA. These studies should include molecular spectroscopic studies using advanced techniques such as x-ray absorption spectroscopy to confirm the proposed mechanisms of increased metal mobilization. A greater insight into the impact of salt on metal leaching from CFA and other landfill materials outside of the coal industry is needed as applications of ZLD will only increase in the future for other industries.

REFERENCES

(2016). "Changxing Power Plant Debuts The World's First Forward Osmosis-Based Zero Liquid Discharge Application." 2016, from http://www.wateronline.com/doc/changxing-power-plant-debuts-the-world-s-first-forward-osmosis-based-zero-liquid-discharge-application-0001.

ACAA (2013). 2013 Coal Combustion Product (CCP) Production & Use Survey Report, American Coal Ash Association.

Acosta, J. A., B. Jansen, K. Kalbitz, A. Faz and S. Martínez-Martínez (2011). "Salinity Increases Mobility of Heavy Metals in Soils." Chemosphere **85**(8): 1318-1324.

Akhter, H., L. G. Butler, S. Branz, F. K. Cartledge and M. E. Tittlebaum (1990). "Immobilization of As, Cd, Cr and Pb-Containing Soils by Using Cement or Pozzolanic Fixing Agents." J. Hazard. Mater. **24**: 145-155.

Akhter, H., F. K. Cartledge, A. Roy and M. E. Tittlebaum (1997). "Solidification/Stabilization of Arsenic Salts: Effects of Long Cure Times." J. Hazard. Mater. **52**: 247-264.

Alkhudhiri, A., N. Darwish and N. Hilal (2012). "Membrane Distillation: A Comprehensive Review." Desalination **287**(0): 2-18.

Amrheln, C., J. E. Strong, and P. A. Mosher (1992). "Effect of Deicing Salts on Metal and Organic Matter Mobilization in Roadside Soils." Environmental Science & Technology **26**: 703-709.

Arthur, J. D., B.G. Langhus, and C. Patel (2005). Technical Summary of Oil and Gas Produced Water Treatment Technologies, All Consulting

ASTM (2012). ASTM C618 - 12 Standard Specification for Coal Fly Ash and Raw or Calcined Natural Pozzolan for Use in Concrete.

Bäckström, M., S. Karlsson, L. Bäckman, L. Folkeson and B. Lind (2004). "Mobilisation of Heavy Metals by Deicing Salts in a Roadside Environment." Water Research **38**(3): 720-732.

Balistrieri, L. S. and J. W. Murray (1982). "The Adsorption of Cu, Pb, Zn, and Cd on Goethite from Major Ion Seawater." Geochimica et Cosmochimica Acta **46**(7): 1253-1265.

Balonis, M., B. Lothenbach, G. Le Saout and F. P. Glasser (2010). "Impact of Chloride on the Mineralogy of Hydrated Portland Cement Systems." Cement Concrete Res. **40**(7): 1009-1022.

Basham, K. D., M. Clark, T. France and P. Harrison (2007). What is Fly Ash? Concrete Construction

Batchelor, B. (2006). "Overview of Waste Stabilization with Cement." Waste Manage. **26**: 689–698.

Baur, I. and C. A. Johnson (2003a). "The Solubility of Selenate-AFt ($3CaO{\cdot}Al_2O_3{\cdot}3CaSeO_4{\cdot}37.5H_2O$) and Selenate-AFm ($3CaO{\cdot}Al_2O_3{\cdot}CaSeO_4{\cdot}xH_2O$)." Cement Concrete Res. **33**(11): 1741-1748.

Baur, I. and C. A. Johnson (2003b). "Sorption of Selenite and Selenate to Cement Minerals." Environ. Sci. Technol. **37**(15): 3442-3447.

Bauske, B. and D. Goetz (1993). "Effects of Deicing-Salts on Heavy Metal Mobility Zum Einfluß von Streusalzen auf die Beweglichkeit von Schwermetallen." Acta Hydrochimica et Hydrobiologica **21**(1): 38-42.

Bazarkina, E. F., G. S. Pokrovski, A. V. Zotov and J.-L. Hazemann (2010). "Structure and Stability of Cadmium Chloride Complexes in Hydrothermal Fluids." Chemical Geology **276**(1–2): 1-17.

Belfort, G., R. H. Davis and A. L. Zydney (1994). "The behavior of suspensions and macromolecular solutions in crossflow microfiltration." Journal of Membrane Science **96**(1–2): 1-58.

Berry, M., K. Dombrowski, C. Richardson, R. Chang, E. Borders and B. W. Vosteen (2007). Mercury Control Evaluation of Calcium Bromide Injection into a PRB-Fired Furnance with and SCR. Air Quality VI Conference. Washington, D.C.

Birnin-Yauri, U. A. and F. P. Glasser (1998). "Friedel's Salt, $Ca_2Al(OH)_6(Cl,OH){\cdot}2H_2O$: Its Solid Solutions and Their Role in Chloride Binding." Cement Concrete Res. **28**(12): 1713-1723.

Blanchard, J. M. and M. Murat (1981). "Recovery of Chemicals from Waste Iron Sulfate. A Laboratory Test of the Production of Iron Chloride and/or Electrolytic Iron." Resources and Conservation **6**(1): 21-27.

Blythe, G. and J. Paradis (2008). Impact of Air Emissions Controls on Coal Combustion Products. Palo Alto, California, EPRI.

Boelter, A. M., F. N. Lamming, A. M. Farag, and H. L. Bergman (1992). "Environmental Effects of Saline Oil-Field Discharges on Surface Waters." Environmental Toxicology and Chemistry **11**: 1187-1195.

Bothe Jr, J. V. and P. W. Brown (1999). "The Stabilities of Calcium Arsenates at 23±1°C." J. Hazard. Mater. **69**(2): 197-207.

Bothe, J. V. and P. W. Brown (1999). "Arsenic Immobilization by Calcium Arsenate Formation." Environ. Sci. Technol. **33**(21): 3806-3811.

Camacho L.M., L. D., J. Zhang, J. Li, M. Duke, J. Gomez, and S. Gray (2013). "Advances in Membrane Distillation for Water Desalination and Purification Applications." Water **5**: 94-196.

Carter, N. T. (2010). Energy's Water Demand: Trends, Vulnerabilities, and Management, Congressional Research Service.

Cartiedge, F. K., L. G. Butler, D. Chalasani, H. C. Eaton, F. P. Frey, E. Herrera, M. E. Tittlebaum and S. Yang (1990). "Immobilization Mechanisms in Solidification/Stabilization of Cd and Pb Salts Using Portland Cement Fixing Agents." Environ. Sci. Technol. **6**: 867-873.

Chandel, M. K., L. F. Pratson and R. B. Jackson (2011). "The Potential Impacts of Climate-Change Policy on Freshwater Use in Thermoelectric Power Generation." Energy Policy **39**(10): 6234-6242.

Chapman, C. A. and C. M. Layman (2007). Considerations Impacting the Technology Selection Process for FGD Purge Stream Wastewater Treatment Systems. International Water Conference. Orlando, Florida.

Choi, W.-H., S.-R. Lee and J.-K. Park (2009). "Cement Based Solidification/Stabilization of Arsenic-Contaminated Mine Tailings." Waste Manage. **29**: 1766-1771.

Christensen, T. H. (1984). "Cadmium Soil Sorption at Low Concentrations: I. Effect of time, Cadmium Lad, pH, and Calcium." Water, Air, and Soil Pollution **21**(1-4): 105-114.

Chrysochoou, M., D. Dermatas and X. Meng (2006). "Evaluation of Ettringite and Hydrocalumite Formation for Heavy Metal Immobilization: Literature Review and Experimental Study." J. Hazard. Mater. **136**(1): 20-33.

Coefield, S. (2009). EPA Set to Regulate Wastewater from Coal-Fired Power Plants. Scientific American.

Connor, J. R. (1997). Guide to Improving the Effectiveness of Cement-Based Stabilization/Solidification. Skokie, Illinois, Portland Cement Association.

Connor, J. R. and S. L. Hoeffner (1996). "A Critical Review of Stabilization/Solidification Technology." Critical Reviews in Environmental Science and Technology **28**(4): 397-462.

Cornelis, G., C. A. Johnson, T. V. Gerven and C. Vandecasteele (2008a). "Leaching Mechanisms of Oxyanionic Metalloid and Metal Species in Alkaline Solid Wastes: A Review." Appl. Geochem. **23**(5): 955-976.

Cornelis, G., S. Poppe, T. Van Gerven, E. Van den Broeck, M. Ceulemans and C. Vandecasteele (2008b). "Geochemical Modelling of Arsenic and Selenium Leaching in Alkaline Water Treatment Sludge from the Production of Non-Ferrous Metals." J. Hazard. Mater. **159**(2–3): 271-279.

De Weerdt, K., M. B. Haha, G. Le Saout, K. O. Kjellsen, H. Justnes and B. Lothenbach (2011). "Hydration Mechanisms of Ternary Portland Cements Containing Limestone Powder and Fly Ash." Cement and Concrete Research **41**(3): 279-291.

De Windt, L. and R. Badreddine (2007). "Modelling of Long-Term Dynamic Leaching Tests Applied to Solidified/Stabilised Waste." Waste Management **27**(11): 1638-1647.

Dermatas, D. and X. Meng (2003). "Utilization of Fly Ash for Stabilization/Solidification of Heavy Metal Contaminated Soils." Eng. Geol. **70**(3–4): 377-394.

Detwiler, R. (1997). The Role of Fly Ash Composition in Reducing Alkali-Silica Reaction, Portland Cement Association.

Dhir, R. K., and M.R. Jones (2006). "Development of Chloride Resisting Concrete Using Fly Ash." Fuel **78**: 137-142.

Dixit, S. and J. G. Hering (2003). "Comparison of Arsenic(V) and Arsenic(III) Sorption onto Iron Oxide Minerals: Implications for Arsenic Mobility." Environmental Science & Technology **37**(18): 4182-4189.

Doner, H. E. (1978). "Chloride as a Factor in Mobilities of Ni(II), Cu(II), and Cd(II) in Soil." Soil Science Society of America Journal **42**(6): 882-885.

Du Laing, G., R. De Vos, B. Vandecasteele, E. Lesage, F. M. G. Tack and M. G. Verloo (2008). "Effect of Salinity on Heavy Metal Mobility and Availability in Intertidal Sediments of the Scheldt Estuary." Estuarine, Coastal and Shelf Science **77**(4): 589-602.

Du Laing, G., E. Meers, M. Dewispelaere, B. Vandecasteele, J. Rinklebe, F. M. G. Tack and M. G. Verloo (2009a). "Heavy Metal Mobility in Intertidal Sediments of the Scheldt Estuary: Field Monitoring." Science of The Total Environment **407**(8): 2919-2930.

Du Laing, G., J. Rinklebe, B. Vandecasteele, E. Meers and F. M. G. Tack (2009b). "Trace Metal Behaviour in Estuarine and Riverine Floodplain Soils and Sediments: A Review." Science of The Total Environment **407**(13): 3972-3985.

Du Laing, G., D. Vanthuyne, F. M. G. Tack and M. G. Verloo (2007). "Factors Affecting Metal Mobility and Bioavailability in the Superficial Intertidal Sediment Layer of the Scheldt Estuary." Aquatic Ecosystem Health & Management **10**(1): 33-40.

Duke, F. R. and M. L. Iverson (1958). "Complex Ions in Fused Salts." The Journal of Physical Chemistry **62**(4): 417-418.

Edgar, T. F. (1983). Coal Processing and Pollution Control. Houston, Texas, Gulf Publishing Company.

El-Bourawi, M. S., Z. Ding, R. Maa, and M. Khayet (2006). "A Framework for Better Understanding Membrane Distillation Separation Process." Journal of Membrane Science **285**: 4-29.

Entrekin, S., M. Evans-White, B. Johnson and E. Hagenbuch (2011). "Rapid expansion of natural gas development poses a threat to surface waters." Frontiers in Ecology and the Environment **9**(9): 503-511.

Fatoba, O. O. (2010). Chemical Interactions and Mobility of Species in Fly Ash-Brine Co-Disposal Systems. Doctor of Philosophy in Chemistry, University of the Western Cape.

Feeley Iii, T. J., T. J. Skone, G. J. Stiegel Jr, A. McNemar, M. Nemeth, B. Schimmoller, J. T. Murphy and L. Manfredo (2008). "Water: A Critical Resource in the Thermoelectric Power Industry." Energy **33**(1): 1-11.

Feeley, T. J., A. P. Jones, L. A. Brickett, B. A. O'Palko, C. E. Miller and J. T. Murphy (2009). "An Update on DOE's Phase II and Phase III Mercury Control Technology R&D Program." Fuel Processing Technology **90**(11): 1388-1391.

Fthenakis, V. and H. C. Kim (2010). "Life-Cycle Uses of Water in U.S. Electricity Generation." Renewable and Sustainable Energy Reviews **14**(7): 2039-2048.

Fu, Y., J. Ding, and J. J. Beaudoin (1996). "Corrosion Protection of Reinforcement in Modified High-Alumina Cement Concrete." American Concrete Institute Materials Journal **93-M69**: 609-612.

Garrabrants, A. C., D. S. Kosson, H. A. van der Sloot, F. Sanchez, and O. Hjelmar (2010). Background Information for the Leaching Environmental Assessment Framework (LEAF) Test Methods. USEPA, USEPA.

Garrabrants, A. C., D. S. Kosson, R. DeLapp, P. Kariher, P. F. A. B. Seignette, H. A. van der Sloot, L. Stefanski and M. Baldwin (2012). Interlaboratory Validation of the Leaching Environmental Assessment Framework (LEAF) Method 1314 and Method 1315, United States Environmental Protection Agency.

Garrabrants, A. C., D. S. Kosson, R. DeLapp and H. A. van der Sloot (2014). "Effect of Coal Combustion Fly Ash Use in Concrete on the Mass Transport Release of Constituents of Potential Concern." Chemosphere **103**: 131-139.

Garrabrants, A. C., F. Sanchez and D. S. Kosson (2003). "Leaching Model for a Cement Mortar Exposed to Intermittent Wetting and Drying." AIChE Journal **49**(5): 1317-1333.

Glass, G. K. and N. R. Buenfeld (2000a). "The Influence of Chloride Binding on the Chloride Induced Corrosion Risk in Reinforced Concrete." Corros. Sci. **42**(2): 329-344.

Glass, G. K., B. Reddy and N. R. Buenfeld (2000b). "The Participation of Bound Chloride in Passive Film Breakdown on Steel in Concrete." Corros. Sci. **42**(11): 2013-2021.

Glasser, F. P. (1997). "Fundamental Aspects of Cement Solidification and Stabilisation." J. Hazard. Mater. **52**(2–3): 151-170.

Goñi, S., A. Guerrero and M. S. Hernández (2001). "Spanish LLW and MLW Disposal: Durability of Cemented Materials in (Na, K)Cl Simulated Radioactive Liquid Waste." Waste Manage. **21**(1): 69-77.

Goodarzi, F. and F. E. Huggins (2001). "Monitoring the Species of Arsenic, Chromium and Nickel in Milled Coal, Bottom Ash and Fly Ash from a Pulverized Coal-Fired Power Plant in Western Canada." Journal of Environmental Monitoring **3**(1): 1-6.

Goodarzi, F., F. E. Huggins and H. Sanei (2008). "Assessment of Elements, Speciation of As, Cr, Ni and Emitted Hg for a Canadian Power Plant Burning Bituminous Coal." International Journal of Coal Geology **74**(1): 1-12.

Gryta, M. (2002). "Concentration of NaCl Solution by Membrane Distillation Integrated with Crystallization." Separation Science and Technology **37**(15): 3535–3558.

Gryta, M. (2013). "The Concentration of Geothermal Brines with Iodine Content by Membrane Distillation." Desalination **325**: 16-24.

Guerrero, A., S. Goñi and V. R. Allegro (2009). "Durability of Class C Fly Ash Belite Cement in Simulated Sodium Chloride Radioactive Liquid Waste: Influence of Temperature." J. Hazard. Mater. **162**(2–3): 1099-1102.

Guevara-Riba, A., A. Sahuquillo, R. Rubio and G. Rauret (2005). "Effect of Chloride on Heavy Metal Mobility of Harbour Sediments." Analytical and Bioanalytical Chemistry **382**(2): 353-359.

Halim, C. E. (2004). Investigating the Leaching of Heavy Metals from Cementitious Waste and Contaminated Soil – Assessing the Applicability of Standard Leaching Procedures. Doctor of Philosophy The University of New South Wales.

Halim, C. E., S. A. Short, J. A. Scott, R. Amal and G. Low (2005). "Modelling the Leaching of Pb, Cd, As, and Cr from Cementitious Waste Using PHREEQC." Journal of Hazardous Materials **125**(1–3): 45-61.

Hatje, V., T. E. Payne, D. M. Hill, G. McOrist, G. F. Birch and R. Szymczak (2003). "Kinetics of Trace Element Uptake and Release by Particles in Estuarine Waters: Effects of pH, Salinity, and Particle Loading." Environment International **29**(5): 619-629.

Hickenbottom, K. L., N. T. Hancock, N. R. Hutchings, E. W. Appleton, E. G. Beaudry, P. Xu and T. Y. Cath (2013). "Forward Osmosis Treatment of Drilling Mud and Fracturing Wastewater from Oil and Gas Operations." Desalination **312**(0): 60-66.

Hightower, M. and S. A. Pierce (2008). "The Energy Challenge." Nature **452**: 285-286.

Hockley, D. E. and H. A. Van der Sloot (1991). "Long-Term Processes in a Stabilized Coal-Waste Block Exposed to Seawater." Environmental Science & Technology **25**(8): 1408-1414.

Huang, Y. H., P. K. Peddi, H. Zeng, C. Tang and X. Teng (2013). "Pilot-Scale Demonstration of the Hybrid Zero-Valent Iron Process for Treating Flue-Gas-Desulfurization Wastewater: Part I." Water Science & Technology **67.1**: 16-23.

Huang, Y. H., P. K. Peddi, H. Zeng, C. Tang and X. Teng (2013a). "Pilot-Scale Demonstration of the Hybrid Zero-Valent Iron Process for Treating Flue-Gas-Desulfurization Wastewater: Part I." Water Sci. Technol. **67**: 16 - 23.

Huang, Y. H., P. K. Peddi, H. Zeng, C. Tang and X. Teng (2013b). "Pilot-Scale Demonstration of the Hybrid Zero-Valent Iron Process for Treating Flue-Gas-Desulfurization Wastewater: Part II." Water Sci. Technol. **67**: 239 - 246.

Huffman, G. P., F. E. Huggins, N. Shah and J. Zhao (1994). "Trace Element Transformations in Coal-Fired Power Systems Speciation of Arsenic and Chromium in Coal and Combustion Ash by XAFS spectroscopy." Fuel Processing Technology **39**(1): 47-62.

Huggins, F. E., M. Najih and G. P. Huffman (1999). "Direct Speciation of Chromium in Coal Combustion By-Products by X-ray Absorption Fine-Structure Spectroscopy." Fuel **78**(2): 233-242.

Huggins, F. E., C. L. Senior, P. Chu, K. Ladwig and G. P. Huffman (2007). "Selenium and Arsenic Speciation in Fly Ash from Full-Scale Coal-Burning Utility Plants." Environmental Science & Technology **41**(9): 3284-3289.

Hyks, J., T. Astrup and T. H. Christensen (2009). "Long-Term Leaching from MSWI Air-Pollution-Control Residues: Leaching Characterization and Modeling." Journal of Hazardous Materials **162**(1): 80-91.

Iyer, R. (2002). "The Surface Chemistry of Leaching Coal Fly Ash." Journal of Hazardous Materials **93**(3): 321-329.

Izquierdo, M. and X. Querol (2012). "Leaching Behavior of Elements from Coal Combustion Fly Ash: An Overview." International Journal of Coal Geology **94**(0): 54-66.

Jaffrin, M. Y. (2008). "Dynamic shear-enhanced membrane filtration: A review of rotating disks, rotating membranes and vibrating systems." Journal of Membrane Science **324**(1–2): 7-25.

Jones, D. R. (1995). The Leaching of Major and Trace Elements from Coal Ash. Environmental Aspects of Trace Elements in Coal. D. J. Swaine and F. Goodarzi, Kluwer Academic Publishers**:** 221-262.

Jonte, J. H. and D. S. Martin (1952). "The Solubility of Silver Chloride and the Formation of Complexes in Chloride Solution." Journal of the American Chemical Society **74**(8): 2052-2054.

Kabala, C. and B. R. Singh (2001). "Fractionation and Mobility of Copper, Lead, and Zinc in Soil Profiles in the Vicinity of a Copper Smelter." Journal of environmental Quality **30**: 485–492.

Kameswari, K. S. B., A. G. Bhole and R. Paramasivam (2001). "Evaluation of Solidification/Stabilization (S/S) Process for the Disposal of Arsenic-Bearing Sludges in Landfill Sites." Environ. Eng. Sci. **18**: 167-176.

Kamon, M., T. Katsumi and Y. Sano (2000). "MSW Fly Ash Stabilized with Coal Ash for Geotechnical Application." J. Hazard. Mater. **76**: 265-283.

Kaplan, D. I., K. Roberts, J. Coates, M. Siegfried, and S. Serkiz (2008). Saltstone and Concrete Interactions with Radionuclides: Sorption (Kd), Desorption, and Reduction Capacity Measurements. U. S. D. o. Energy. Savannah River Site, Aiken, South Carolina, United States Department of Energy.

Kargbo, D. M., R. G. Wilhelm, and D. J. Campbell (2010). "Natural Gas Plays in the Marcellus Shale: Challenges and Potential Opportunities." Environmental Science & Technology **44**: 5679–5684.

Keller, I. R. B. (2002). The Immobilisation of Heavy Metals and Metalloids in Cement Stabilised Wastes: A Study Focusing on the Selenium Oxyanions SeO_3^{2-} and SeO_4^{2-}. Doctor of Philosophy, Swiss Federal Institute of Technology.

Keon, N. E., C. H. Swartz, D. J. Brabander, C. Harvey and H. F. Hemond (2001). "Validation of an Arsenic Sequential Extraction Method for Evaluating Mobility in Sediments." Environmental Science & Technology **35**(13): 2778-2784.

Kharaka, Y. K. and I. Barnes (1973). SOLMNEQ: Solution-mineral equilibrium computations**:** 88.

Khattak, R. A., A. L. Page and W. M. Jarrell (1989). "Mechanism of Native Manganese Release in Salt-Treated Soils." Soil Science Society of America Journal **53**(3): 701-705.

Kim, A. G. and G. Kazonich (2004). "The Silicate/Non-Silicate Sistribution of Metals in Fly Ash and its Effect on Solubility." Fuel **83**(17–18): 2285-2292.

Kinniburgh, D. and D. Cooper. (2010). "PhreePlot - Creating Graphical Output with PHREEQC." Retrieved August 20, 2016, 2016, from http://www.phreeplot.org/.

Koch, H. and S. Vögele (2009). "Dynamic Modelling of Water Demand, Water Availability and Adaptation Strategies for Power Plants to Global Change." Ecological Economics **68**(7): 2031-2039.

Kosson, D. S., H. A. van der Sloot, A. C. Garrabrants and P. F. A. B. Seignette (2014). Leaching Test Relationships, Laboratory-to-Field Comparisons and Recommendations for Leaching Evaluation using the Leaching Environmental Assessment Framework (LEAF), USEPA.

Kumpienem, J., A. Lagerkvist, and C. Maurice (2007). "Stabilization of Pb- and Cu-Contaminated Soil using Coal Fly Ash and Peat." Environmental Pollution **145**: 365-373.

Kumpienem, J., A. Lagerkvist and C. Maurice (2007). "Stabilization of Pb- and Cu-Contaminated Soil using Coal Fly Ash and Peat." Environ. Pollut. **145**: 365-373.

Lampris, C. (2013). Solidification/Stabilisation of Air Pollution Control Residues from Municipal Solid Waste Incineration. PhD, Imperial College London.

Lampris, C., J. A. Stegemann and C. R. Cheeseman (2009). "Solidification/Stabilisation of Air Pollution Control Residues Using Portland Cement: Physical Properties and Chloride Leaching." Waste Management **29**(3): 1067-1075.

Langen, T. A., M. Twiss, T. Young, K. Janoyan, J. C. Stager, J. Osso, H. Prutzman, and B. Green (2006). Environmental Impacts of Winter Road Management at the Cascade Lakes and Chapel Pond. Potsdam, New York, Clarkson Center for the Environment.

Layman, C. M. (2013). Navigating the New Steam Electric Power Effluent Limitation Guidelines. International Water Conference. Orlando, Florida**:** 174-187.

Li, X. D., C. S. Poona, H. Suna, I. M. C. Lob and D. W. Kirk (2001). "Heavy Metal Speciation and Leaching Behaviors in Cement Based Solidified/Stabilized Waste Materials." J. Hazard. Mater. **A82**: 215–230.

Libuś, Z. and H. Tiałowska (1975). "Stability and Nature of Complexes of the type MCl+ in Aqueous Solution (M=Mn, Co, Ni, and Zn)." Journal of Solution Chemistry **4**(12): 1011-1022.

Liu, W., S. J. Borg, D. Testemale, B. Etschmann, J.-L. Hazemann and J. Brugger (2011). "Speciation and Thermodynamic Properties for Cobalt Chloride Complexes in Hydrothermal Fluids at 35–440°C and 600bar: An In-Situ XAS Study." Geochimica et Cosmochimica Acta **75**(5): 1227-1248.

Liu, W., A. Migdisov and A. E. Williams-Jones (2012). "The Stability of Aqueous Nickel(II) Chloride Complexes in Hydrothermal Solutions: Results of UV–Visible Spectroscopic Experiments." Geochimica et Cosmochimica Acta **94**: 276-290.

Lombardi, M., T. Mangialardi, L. Piga, and P. Sirini (1998). "Mechanical and Leaching Properties of Cement Solidied Hospital Solid Waste Incinerator Fly Ash." Waste Management **18**: 99 - 106.

Lores, E. M. and J. R. Pennock (1998). "The Effect of Salinity on Binding of Cd, Cr, Cu and Zn to Dissolved Organic Matter." Chemosphere **37**(5): 861-874.

Luo, J., L. Ding, Y. Wan and M. Y. Jaffrin (2012). "Threshold flux for shear-enhanced nanofiltration: Experimental observation in dairy wastewater treatment." Journal of Membrane Science **409–410**(0): 276-284.

Luo, J., Z. Zhu, L. Ding, O. Bals, Y. Wan, M. Y. Jaffrin and E. Vorobiev (2013). "Flux behavior in clarification of chicory juice by high-shear membrane filtration: Evidence for threshold flux." Journal of Membrane Science **435**(0): 120-129.

Lützenkirchen, J. (1997). "Ionic Strength Effects on Cation Sorption to Oxides: Macroscopic Observations and Their Significance in Microscopic Interpretation." Journal of Colloid and Interface Science **195**(1): 149-155.

Macknick, J., R. Newmark, G. Heath and K. C. Hallett (2012). "Operational Water Consumption and Withdrawal Factors for Electricity Generating Technologies: A Review of Existing Literature." Environmental Research Letters **7**: 1-10.

Mahlaba, J. S. (2006a). Evaluation of Paste Technology to Co-Dispose of Ash and Brines Sasol Synfuels Complex. Master's Degree, University of the Witwatersrand.

Mahlaba, J. S., E. P. Kearsley, and R. A. Kruger (2011a). "Physical, Chemical, and Mineralogical Characteristics of Hydraulically Disposed Fine Coal Fly Ash from SASOL Synfuels." Minerals Engineering.

Mahlaba, J. S., E. P. Kearsley, R. A. Kruger, and P. C. Pretorius (2011b). "Evaluation of Workability and Strength Development of Fly Ash Pastes Prepared with Industrial Brines Rich in SO_4^{2-} and Cl^- to Expand Brine Utilization." Minerals Engineering **24**: 1077-1081.

Mahlaba, J. S., E.P. Kearsley, and R. A. Kruger (2011c). "Effect of Fly Ash Characteristics on the Behavior of Paste Prepared Under Varied Brine Conditions." Minerals Engineering **24**: 1077-1081.

Mahlaba, J. S., P. C. Pretorius, and M. P. Augustyn (2006b). Influence of Admixtures on Paste Behaviour and the Role of Surface Area on Remobilization. 11th International Seminar on Thickened Tailings and Paste. Botswana.

Malviya, R. and R. Chaudhary (2006). "Leaching Behavior and Immobilization of Heavy Metals in Solidified/Stabilized Products." Journal of Hazardous Materials **137**(1): 207-217.

Mangialardi, T., A. E. Paolini, A. Polettini, and P. Sirini (1999). "Optimization of the Solidification/Stabilization Process of MSW Fly Ash in Cementitious Matrices." Journal of Hazardous Materials **B70**: 53-70.

Marcus, Y. (1991). "Thermodynamics of Solvation of Ions. Part 5.-Gibbs Free Energy of Hydration at 298.15 K." Journal of the Chemical Society, Faraday Transactions **87**(18): 2995-2999.

Martinez-Diez, L., and F.J. Florido-Diaz (2001). "Desalination of Brines by Membrane Distillation." Desalination **137**: 267-273.

Masue, Y., R. H. Loeppert and T. A. Kramer (2007). "Arsenate and Arsenite Adsorption and Desorption Behavior on Coprecipitated Aluminum:Iron Hydroxides." Environmental Science & Technology **41**(3): 837-842.

Matschei, T., B. Lothenbach and F. P. Glasser (2007). "The AFm Phase in Portland cement." Cement Concrete Res. **37**(2): 118-130.

McGinnis, R. L., N. T. Hancock, M. S. Nowosielski-Slepowron and G. D. McGurgan (2013). "Pilot Demonstration of the NH_3/CO_2 Forward Osmosis Desalination Process on High Salinity Brines." Desalination **312**(0): 67-74.

McWhinney, H. G., D. L. Cocke, K. Balke and J. Dale Ortego (1990). "An Investigation of Mercury Solidification and Stabilization in Portland Cement Using X-Ray Photoelectron Spectroscopy and Energy Dispersive Spectroscopy." Cement Concrete Res. **20**(1): 79-91.

Meeussen, J. C. L. (2003). "ORCHESTRA: An Object-Oriented Framework for Implementing Chemical Equilibrium Models." Environmental Science & Technology **37**(6): 1175-1182.

Mi, B. and M. Elimelech (2013). "Silica Scaling and Scaling Reversibility in Forward Osmosis." Desalination **312**(0): 75-81.

Mickley, M. (2008). Survey of High Recovery and Zero Liquid Discharge Technologies for Water Utilities. W. R. Foundation. Alexandria, Virginia, Water Reuse Foundation.

Miller, J., H. Akhter, F. K. Cartledge and M. McLearn (2000). "Treatment of Arsenic-Contaminated Soils. II: Treatability Study and Remediation." J. Environ. Eng. **126**: 1004-1012.

Millward, G. E. and Y. P. Liu (2003). "Modelling Metal Desorption Kinetics in Estuaries." Science of The Total Environment **314–316**(0): 613-623.

Mohapatra, R. and S. B. Kanungo (1997). "Physico-Chemical Characteristics of Fly Ash Samples from Thermal Power Plants of Orissa." Indian Journal of Engineering & Materials Sciences **4**: 271-281.

Moon, D. H., D. Dermatas and N. Menounou (2004). "Arsenic Immobilization by Calcium–Arsenic Precipitates in Lime Treated Soils." Sci. Total Environ. **330**: 171–185.

Moon, D. H., D. G. Grubb and T. L. Reilly (2009). "Stabilization/Solidification of Selenium-Impacted Soils using Portland Cement and Cement Kiln Dust." J. Hazard. Mater. **168**: 944–951.

Moon, D. H., M. Waznea, I. Yoon and D. G. Grubba (2008). "Assessment of Cement Kiln Dust (CKD) for Stabilization/Solidification (S/S) of Arsenic Contaminated Soils." J. Hazard. Mater. **159**: 512-518.

Narukawa, T., A. Takatsu, K. Chiba, K. W. Riley and D. H. French (2005). "Investigation on Chemical Species of Arsenic, Selenium and Antimony in Fly Ash from Coal Fuel Thermal Power Stations." Journal of Environmental Monitoring **7**(12): 1342-1348.

Nelson, S. S., D. R. Yongek and M. E. Barber (2009). "Effects of Road Salts on Heavy Metal Mobility in Two Eastern Washington Soils." Journal of Environmental Engineering **135**: 505-510.

NETL (2009). Impact of Drought on U.S. Steam Electric Power Plant Cooling Water Intakes and Related Water Resource Management Issues, National Energy Technology Laboratory.

Nishimura, T. and R. Hata (2007). "Chemistry of the Ca–Se(IV)–H_2O and Ca–Se(VI)–H_2O Systems at 25 °C." Hydrometallurgy **89**(3–4): 346-356.

Nishimura, T., R. Hata and F. Hasegawa (2009). "Chemistry of the M (M=Fe, Ca, Ba)-Se-H_2O Systems at 25 °C " Molecules **2009**(14).

Nishimura, T. and R. G. Robins (1998). "A Re-evaluation of the Solubility and Stability Regions of Calcium Arsenites and Calcium Arsenates in Aqueous Solution at 25°C." Miner. Process. Extr. Metall. Rev. **18**(3-4): 283-308.

Norrström, A. C. (2005). "Metal Mobility by De-Icing Salt from an Infiltration Trench for Highway Runoff." Applied Geochemistry **20**(10): 1907-1919.

Norrström, A. C. and G. Jacks (1998). "Concentration and Fractionation of Heavy Metals in Roadside Soils Receiving De-Icing Salts." Science of The Total Environment **218**(2–3): 161-174.

Novotny, E. V., and H. G. Stefan (2010). "Projections of Chloride Concentrations in Urban Lakes Receiving Road De-icing Salt." Water, Air, & Soil Pollution **211**: 261-271.

Paalman, M. A. A., C. H. Van Der Weijden and J. P. G. Loch (1994). "Sorption of Cadmium on Suspended Matter Under Estuarine Conditions; Competition and Complexation with Major Sea-Water Ions." Water, Air, and Soil Pollution **73**(1): 49-60.

Page, C. L. and Ø. Vennesland (1983). "Pore Solution Composition and Chloride Binding Capacity of Silica-Fume Cement Pastes." Matériaux et Construction **16**(1): 19-25.

Pakzadeh, B., J. E. Renew and J. Wos (2014). Demonstration Development Project: Vortex-Based Antifouling Membrane System Treating Flue Gas Desulfurization Wastewater. Palo Alto, California, Electric Power Research Institute.

Palfy, P., E. Vircikova and L. Molnar (1999). "Processing of Arsenic Waste by Precipitation and Solidification." Waste Manage. **19**: 55-59.

Pan, P. and N. J. Susak (1989). "Co(II)-Chloride and -Bromide Complexes in Aqueous Solutions Up to 5 M NaX and 90°C: Spectrophotometric Study and Geological Implications." Geochimica et Cosmochimica Acta **53**(2): 327-341.

Papadakis, V. G. (2000). "Effect of Fly Ash on Portland Cement Systems: Part II. High-Calcium Fly Ash." Cement and Concrete Research **30**(10): 1647-1654.

Paria, S. and P. K. Yuet (2006). "Solidification-Stabilization of Organic and Inorganic Contaminants Using Portland Cement: A Literature Review." Environ. Rev. **14**: 217-255.

Parkhurst, D. L. and C. A. J. Appelo (1999). User's Guide to PHREEQC (Version 2)— A Computer Program for Speciation, Batch-Reaction, One-Dimensional Transport, and Inverse Geochemical Calculations, USGS.

Parkhurst, D. L. and C. A. J. Appelo (2013). Description of Input and Examples for PHREEQC Version 3: A Computer Program for Speciation, Batch-Reaction, One-Dimensional Transport, and Inverse Geochemical Calculations. Techniques and Methods. Reston, VA**:** 519.

Pereira, C. F., M. Rodriguez-Piñero and J. Vale (2001). "Solidification/Stabilization of Electric Arc Furnace Dust Using Coal Fly Ash Analysis of the Stabilization Process." J. Hazard. Mater. **B82**: 183-195.

Pérez-González, A., A. M. Urtiaga, R. Ibáñez and I. Ortiz (2012). "State of the Art and Review on the Treatment Technologies of Water Reverse Osmosis Concentrates." Water Research **46**(2): 267-283.

Peulon, S. and D. Lincot (1998). "Mechanistic Study of Cathodic Elecfrodeposition of Zinc Oxide and Zinc Hydroxychioride Films from Oxygenated Aqueous Zinc Chloride Solutions." Journal of the Electrochemical Society **145**(3): 864-874.

Phillip, W. A., J. Yong , and M. Elimelech (2010). "Reverse Draw Solute Permeation in Forward Osmosis: Modeling and Experiments." Environmental Science & Technology **44**: 5170–5176.

Pickering, W. F. (1986). "Metal Ion Speciation — Soils and Sediments (A Review)." Ore Geology Reviews **1**(1): 83-146.

Pierrard, J. C., J. Rimbault and M. Aplincourt (2002). "Experimental Study and Modelling of Lead Solubility as a Function of pH in Mixtures of Ground Waters and Cement Waters." Water Research **36**(4): 879-890.

PSU (2009). Shaping Proposed Changes to Pennsylvania's Total Dissolved Solids Standard, Penn State University - College of Agricultural Sciences, Agricultural Research and Cooperative Extension.

Qian, G., Y. Cao, P. Chui and J. Tay (2006). "Utilization of MSWI Fly Ash for Stabilization/Solidification of Industrial Waste Sludge." J. Hazard. Mater. **B129**: 274-281.

Ramgobeen, D. (2010). "Preparation and Testing of Chloride & Sulphate Containing Minerals from Industrial Wastes", Solidification/Stabilisation of Chloride & Sulphate ions from APC Residues with Calcium Aluminate Cements. Master's Degree, University College of London.

Rapin, J.-P., G. Renaudinb, E. Elkaimc and M. Francoisa (2002). "Structural Transition of Friedel's Salt $3CaO{\cdot}Al_2O_3{\cdot}CaCl_2{\cdot}10H_2O$ Studied by Synchrotron Powder Diffraction." Cement and Concrete Research **32**: 513-519.

Reddy, B., G. K. Glass, P. J. Lim and N. R. Buenfeld (2002). "On the Corrosion Risk Presented by Chloride Bound in Concrete." Cement Concrete Comp. **24**(1): 1-5.

Reddy, B. R., D. N. Priya, S. V. Rao, and P. Radhika (2005). "Solvent Extraction and Separation of Cd(II), Ni(II) and Co(II) from Chloride Leach Liquors of Spent Ni–Cd Batteries Using Commercial Organo-Phosphorus Extractants." Hydrometallurgy **77**: 253 – 261.

Reichle, R. A., K. G. McCurdy and L. G. Helpler (1975). "Zinc Hydroxide: Solubility Product and Hydroxy-Complex Stability Constants from 12.5-75 ^{o}C." Canadian Journal of Chemistry **53**: 3841-3845.

Renaudina, G., F. Kubelb, J.-P. Riverac and M. Francoisa (1999). "Structural Phase Transition and High Temperature Phase Structure of Friedels Salt, $3CaO{\cdot}Al_2O_3{\cdot}CaCl_2{\cdot}10H_2O$." Cement Concrete Res. **29**: 1937–1942.

Renew, J. E., C. Acharya, A. Capelouto, K. Jenkins and K. Hendershot (2016a). Long-Term Evaluation of a 50-GPM Vibratory Shear Enhanced Process Membrane Filtration System for Treatment of Flue Gas Desulfurization Wastewater. 2016 International Water Conference. San Antonio, Texas.

Renew, J. E., C.-H. Huang, B. Burns and M. Carrasquillo (2014). Immobilization of Heavy Metals by Solidification / Stabilization in Co-Disposed Coal Fly Ash and Concentrated Flue Gas Desulfurization Wastewater Brines. Power Plant Pollutant Control "MEGA" Symposium. Baltimore, Maryland.

Renew, J. E., C.-H. Huang, S. E. Burns, M. Carrasquillo, W. Sun and K. M. Ellison (2016b). "Immobilization of Heavy Metals by Solidification/Stabilization of Co-Disposed Flue Gas Desulfurization Brine and Coal Fly Ash." Energy & Fuels **30**: 5042-5051.

Reynolds, J. E. and E. L. Coltrinari (1981). Chloride Leach Process for Recovering Metal Values in the Presence of Arsenic, Hazen Research, Inc. **4,244,735**.

Richard, F. C. and A. C. M. Bourg (1991). "Aqueous Geochemistry of Chromium: A Review." Water Res. **25**(7): 807-816.

Rio, S. and A. Delebarre (2003). "Removal of Mercury in Aqueous Solution by Fluidized Bed Plant Fly Ash." Fuel **82**(2): 153-159.

Roy, W. R. and P. M. Berger (2011). "Geochemical Controls of Coal Fly Ash Leachate pH." Coal Combustion and Gasification Products **3**: 63-66.

Santos, S., G. Ungureanu, R. Boaventura and C. Botelho (2015). "Selenium Contaminated Waters: An Overview of Analytical Methods, Treatment Options and Recent Advances in Sorption Methods." Science of The Total Environment **521–522**: 246-260.

Scanlon, B. R., I. Duncan and R. C. Reedy (2013). "Drought and the Water–Energy Nexus in Texas." Environmental Research Letters **8**: 1-14.

Schiopu, N., L. Tiruta-Barna, E. Jayr, J. Méhu and P. Moszkowicz (2009). "Modelling and Simulation of Concrete Leaching Under Outdoor Exposure Conditions." Science of The Total Environment **407**(5): 1613-1630.

Séby, F., M. Potin-Gautier, E. Giffaut, G. Borge and O. F. X. Donard (2001). "A Critical Review of Thermodynamic Data for Selenium Species at 25°C." Chemical Geology **171**(3–4): 173-194.

Seignette, P., A. Garrabrants, D. Kosson and H. van der Sloot (2014). LeachXS Pro User's Guide Version 2.0.0.

Senanayake, G. a. D. M. M. (1998). "Speciation and Reduction Potentials of Metal Ions in Concentrated Chloride and Sulfate Solutions Relevant to Processing Base Metal Sulfides." Metallurgical Transactions B **19B**: 37-45.

Shaffer, D. L., J. R. Werber, H. Jaramillo, S. Lin and M. Elimelech (2015). "Forward Osmosis: Where Are We Now?" Desalination **356**: 271-284.

Sinadinovic, D., G. Kamberovic, and A. Sutic (1997). "Leaching Kinetics of Lead from Lead (II) Sulphate in Aqueous Calcium Chloride and Magnesium Chloride Solutions." Hydrometallurgy **47**: 137-147.

Singh, M., and M. Gart (1999). "Cementitious Binder from Fly Ash and Other Industrial Wastes." Cement and Concrete Research **29**: 309–314.

Singh, T. S., K. K. Pant (2006). "Solidification/Stabilization of Arsenic Containing Solid Wastes Using Portland Cement, Fly Ash and Polymeric Materials." Journal of Hazardous Materials **B131**: 29–36.

Sirkar, K. K., and L. Song (2009). Pilot-Scale Studies for Direct Contact Membrane Distillation-Based Desalination Process. U.S. Department of the Interior Bureau of Reclamation, U.S. Department of the Interior Bureau of Reclamation.

Solem-Tishmack, J. K. and G. J. McCarthy (1995). "High-Calcium Combustion By-Products: Engineering Properties, Ettringite Formation, and Potential Application in Solidification and Stabilization of Selenium and Boron." Cement Concrete Res. **25**: 658-670.

Sovacool, B. K. and K. E. Sovacool (2009). "Identifying Future Electricity–Water Tradeoffs in the United States." Energy Policy **37**(7): 2763-2773.

Spang, E. S., W. R. Moomaw, K. S. Gallagher, P. H. Kirshen and D. H. Marks (2014). "Multiple Metrics for Quantifying the Intensity of Water Consumption of Energy Production." Environmental Research Letters **9**: 1-8.

Stanmore, B. R. and D. W. Page (1992). "Yield Stresses and Sedimentation in Dense Flyash Slurries." Powder Technology **72**(2): 167-175.

Stone, M. L., C. Rae, F. F. Stewart and A. D. Wilson (2013). "Switchable Polarity Solvents as Draw Solutes for Forward Osmosis." Desalination **312**(0): 124-129.

Su, C. and R. D. Ludwig (2005). "Treatment of Hexavalent Chromium in Chromite Ore Processing Solid Waste Using a Mixed Reductant Solution of Ferrous Sulfate and Sodium Dithionite." Environ. Sci. Technol. **39**: 6208-6216.

Su, D. C. and J. W. C. Wong (2003). "Chemical Speciation and Phytoavailability of Zn, Cu, Ni and Cd in Soil Amended with Fly Ash-Stabilized Sewage Sludge." Environ. Int. **29**: 895– 900.

Su, T. and J. Wang (2011). "Modeling Batch Leaching Behavior of Arsenic and Selenium from Bituminous Coal Fly Ashes." Chemosphere **85**(8): 1368-1374.

Suryavanshi, A. K., J. D. Scantlebury and S. B. Lyon (1996a). "Mechanism of Friedel's Salt Formation in Cements Rich in Tri-Calcium Aluminate." Cement Concrete Res. **26**(5): 717-727.

Suryavanshi, A. K. and R. N. Swamy (1996b). "Stability of Friedel's Salt in Carbonated Concrete Structural Elements." Cement Concrete Res. **26**(5): 729-741.

Talbot, R. W., M. A. Anderson and A. W. Andren (1978). "Qualitative Model of Heterogeneous Equilibriums in a Fly Ash Pond." Environ. Sci. Technol. **12**(9): 1056-1062.

Terzano, R., M. Spagnuolo, L. Medici, B. Vekemans, L. Vincze, K. Janssens and P. Ruggiero (2005). "Copper Stabilization by Zeolite Synthesis in Polluted Soils Treated with Coal Fly Ash." Environ. Sci. Technol. **39**: 6280-6287.

Teutli-Sequeira, A., M. Solache-Ríos and M. T. Olguín (2009). "Influence of Na^{+}, Ca^{2+}, $Mg^{2+}$and NH_4^{+} on the sorption behavior of Cd^{2+} from aqueous solutions by a Mexican Zeolitic Material." Hydrometallurgy **97**(1–2): 46-52.

Tian, Y., B. Etschmann, W. Liu, S. Borg, Y. Mei, D. Testemale, B. O'Neill, N. Rae, D. M. Sherman, Y. Ngothai, B. Johannessen, C. Glover and J. Brugger (2012a). "Speciation of Nickel (II) Chloride Complexes in Hydrothermal Fluids: In Situ XAS Study." Chemical Geology **334**(0): 345-363.

Tian, Y., B. Etschmann, W. Liu, S. J. Borg, Y. Mei, D. Testemale, B. O'Neill, N. Rae, D. M. Sherman, Y. Ngothai, B. Johannessen, C. Glover and J. Brugger (2012b). "Speciation of Nickel (II) Chloride Complexes in Hydrothermal Fluids: In Situ XAS Study." Chemical Geology **334**(0): 345-363.

Tiruta-Barna, L. (2008). "Using PHREEQC for Modelling and Simulation of Dynamic Leaching Tests and Scenarios." Journal of Hazardous Materials **157**(2–3): 525-533.

Tiruta-Barna, L., Z. Rethy and R. Barna (2005). "Release Dynamic Process Identification for a Cement Based Material in Various Leaching Conditions. Part II. Modelling the Release Dynamics for Different Leaching Conditions." Journal of Environmental Management **74**(2): 127-139.

Tong, T. and M. Elimelech (2016). "The Global Rise of Zero Liquid Discharge for Wastewater Management: Drivers, Technologies, and Future Directions." Environmental Science & Technology **50**(13): 6846-6855.

Truesdell, A. H., B. F. Jones and G. Survey (1973). WATEQ, a Computer Program for Calculating Chemical Equilibria of Natural Waters, U.S. Department of the Interior, Geological Survey.

Tyler, L. D. and M. B. McBride (1982). "Mobility and Extractability of Cadmium, Copper, Nickel, and Zinc in Organic and Mineral Soil Columns." Soil Science **134**(3): 198-205.

USCB. (2014). "2014 National Population Projections." Retrieved 14 June 2015, 2015, from http://www.census.gov/population/projections/data/national/2014.html.

USDOE (2006). Energy Demands on Water Resources: Report to Congress on the Interdependency of Energy and Water, United States Department of Energy.

USDOE (2013). U.S. Energy Sector Vulnerabilities to Climate Change and Extreme Weather, United States Department of Energy.

USDOE (2014). The Water-Energy Nexus: Challenges and Opportunities, United States Department of Energy.

USEIA (2015a). Annual Energy Outlook 2015 with Projections to 2014, United States Energy Information Administration.

USEIA. (2015b). "Coal Explained - Coal Prices and Outlook." from http://www.eia.gov/Energyexplained/index.cfm?page=coal_prices.

USEPA (1992a). Method 1311 - Toxicity Characteristic Leaching Procedure

USEPA (1992b). USEPA Method 3005A - Acid Digestion of Waters for Total Recoverable or Dissolved Metals for Analysis by FLAA or ICP Spectroscopy.

USEPA (1993). Method 300.0 Determination of Inorganic Anions by Ion Chromatography, USEPA.

USEPA (1994a). Method 200.8 - Determination of Trace Elements in Waters and Wastes by Inductively Coupled Plasma - Mass Spectrometry. USEPA.

USEPA (1994b). Sample Preparation Procedure for Spectrochemical Determination of Total Recoverable Elements. USEPA.

USEPA (1996a). Acid Digestion of Sediments, Sludges, and Soils.

USEPA (1996b). Method 3052 - Microwave Assisted Acid Digestion of Siliceous and Organically Based Matrices.

USEPA (2007). Method 6020a - Inductively Coupled Plasma Mass Spectrometry.

USEPA (2009). Steam Electric Power Generation Point Source Category: Final Detailed Study Report. USEPA. Washington, DC.

USEPA (2012). "Method 1313 - Liquid-Solid Partitioning as a Function of Extract pH Using a Parallel Batch Extraction Procedure."

USEPA (2013). "Method 1315 - Mass Transfer Rates of Constituents in Monolithic or Compacted Granular Materials Using a Semi-Dynamic Tank Leaching Procedure."

USEPA (2015). Effluent Limitations Guidelines and Standards for the Steam Electric Power Generating Point Source Category; Final Rule 40 CFR Part 423 U. S. E. P. Agency. Federal Register.

USGS (1998). Estimated Use of Water in the United States in 1995, United States Geological Survey

USGS (2004). Estimated Use of Water in the United States in 2000, United States Geological Survey.

USGS (2014). Treatise on Geochemistry, Oxford: Elsevier.

Usman, A. R. A., Y. Kuzyakov and K. Stahr (2005). "Effect of Immobilizing Substances and Salinity on Heavy Metals Availability to Wheat Grown on Sewage Sludge-Contaminated Soil." Soil and Sediment Contamination: An International Journal **14**(4): 329-344.

Valls, S. and E. Vazquez (2002). "Leaching Properties of Stabilised/Solidified Cement-Admixtures-Sewage Sludges Systems." Waste Manage. **22**: 37-45.

van der Hoek, E. E. and R. N. J. Comans (1996). "Modeling Arsenic and Selenium Leaching from Acidic Fly Ash by Sorption on Iron (Hydr)oxide in the Fly Ash Matrix." Environmental Science & Technology **30**(2): 517-523.

van der Sloot, H. A., A. van Zomeren, J. C. L. Meeussen, P. Seignette and R. Bleijerveld (2007). "Test Method Selection, Validation Against Field Data, and Predictive Modelling for Impact Evaluation of Stabilised Waste Disposal." Journal of Hazardous Materials **141**(2): 354-369.

van der Sloot, H. A. and A. Zomeren (2012). "Characterisation Leaching Tests and Associated Geochemical Speciation Modelling to Assess Long Term Release Behaviour from Extractive Wastes." Mine Water and the Environment **31**(2): 92-103.

Voglar, G. E. and D. Leštan (2011). "Efficiency Modeling of Solidification/Stabilization of Multi-Metal Contaminated Industrial Soil Using Cement and Additives." Journal of Hazardous Materials **192**(2): 753-762.

Wang, J., H. Ban, X. Teng, H. Wang and K. Ladwig (2006). "Impacts of pH and Ammonia on the Leaching of Cu(II) and Cd(II) from Coal Fly Ash." Chemosphere **64**(11): 1892-1898.

Wang, J., X. Teng, H. Wang and H. Ban (2004). "Characterizing the Metal Adsorption Capability of a Class F Coal Fly Ash." Environmental Science & Technology **38**(24): 6710-6715.

Wang, J., T. Wang, J. G. Burken, C. C. Chusuei, H. Ban, K. Ladwig and C. P. Huang (2008). "Adsorption of Arsenic(V) Onto Fly Ash: A Speciation-Based Approach." Chemosphere **72**(3): 381-388.

Wang, S. and C. Vipulanandan (2000). "Solidification/Stabilization of Cr(VI) with Cement Leachability and XRD Analyses." Cement Concrete Res.(30): 385-389.

Wang, T. (2007a). The Leaching Behavior of Arsenic, Selenium and Other Trace Elements in Coal Fly Ash. Doctoral, Missouri University of Science and Technology.

Wang, T. (2007b). The Leaching Behavior of Arsenic, Selenium and Other Trace Elements in Coal Fly Ash. Doctoral Missouri University of Science and Technology.

Wang, T., J. Wang, J. G. Burken, H. Ban and K. Ladwig (2007). "The Leaching Characteristics of Selenium from Coal Fly Ashes." Journal of Environmental Quality **36**: 1784-1792.

Wang, T., J. Wang, Y. Tang, H. Shi and K. Ladwig (2009). "Leaching Characteristics of Arsenic and Selenium from Coal Fly Ash: Role of Calcium." Energ. Fuel. **23**(6): 2959-2966.

Winand, R. (1991). "Chloride Hydrometallurgy." Hydrometallurgy **27**: 285-316.

Wingenfelder, U., C. Hansen, G. Furrer and R. Schulin (2005). "Removal of Heavy Metals from Mine Waters by Natural Zeolites." Environmental Science & Technology **39**(12): 4606-4613.

Winkel, L., A. Johnson, M. Lenz, T. Grundl, O.X. Leupin, M. Amini, and L. Charlet (2012). "Environmental Selenium Research – from Microscopic Processes to Global Understanding." Environmental Science & Technology **46** 571–579.

Wu, Y., Y. Chi, H. Bai, G. Qian, Y. Cao, J. Zhou, Y. Xu, Q. Liu, Z. P. Xu and S. Qiao (2010). "Effective Removal of Selenate from Aqueous Solutions by the Friedel Phase." J. Hazard. Mater. **176**(1–3): 193-198.

Xiong, H. (2006). "Estimation of Medium Effects on Equilibrium Constants in Moderate and High Ionic Strength Solutions at Elevated Temperatures by Using Specific Interaction Theory (SIT): Interaction Coefficients Involving Cl, OH^- and Ac^- up to 200°C and 400 bars." Geochemical Transactions **7**(4).

Yeboah, N. N. N., C. R. Shearer, S. E. Burns and K. E. Kurtis (2014). "Characterization of Biomass and High Carbon Content Coal Ash for Productive Reuse Applications." Fuel **116**: 438-447.

Yilmaz, O., K. Unlu and E. Cokca (2003). "Solidification/Stabilization of Hazardous Wastes Containing Metals and Organic Contaminants." J. ENVIRON. ENG.(129): 366-376.

Yudovich, Y. E. and M. P. Ketris (2005). "Arsenic in Coal: A Review." International Journal of Coal Geology **61**(3–4): 141-196.

Zhang, J. and P. L. Bishop (2002). "Stabilization/Solidification (S/S) of Mercury-Containing Wastes Using Reactivated Carbon and Portland Cement." J. Hazard. Mater. **B92**: 199–212.

Zhang, M. and E. J. Reardon (2003). "Removal of B, Cr, Mo, and Se from Wastewater by Incorporation into Hydrocalumite and Ettringite." Environ. Sci. Technol. **37**: 2947-2952.